**IMPERIAL COLLEGE OF SCIENCE, TECHNOLOGY AND MEDICINE**
**University of London**

# UPDATING STRUCTURAL DYNAMICS MODELS USING FREQUENCY RESPONSE DATA

by

**Wilhelmina Josefine Visser**

A thesis submitted to the University of London
for the degree of Doctor of Philosophy

Department of Mechanical Engineering
Imperial College of Science, Technology and Medicine
London SW7

September 1992

*Of making many books there is tw end, and much study wearies the body. Here is the conclusion of the matter: Fear God and keep His commandments, for this is the whole duty of man.*

*Ecclesiastes 12:12b,13*

# ABSTRACT

Structural dynamics model updating has been defined as the adjustment of an existing analytical model using experimental data such that the model more accurately reflects the dynamic behaviour of the structure.

The aim of the present work was to develop a practical approach for updating structural dynamics models. This was achieved by critical investigation of existing methods and by exploring new techniques. Many of the recently-developed updating techniques were classified and presented in a consistent notation. Location and subsequent updating of modelling errors were investigated using (i) modal data and (ii) frequency response function (FRF) data.

Limitations of model updating using modal data were verified and illustrated by employing the error matrix method. A new procedure was proposed and various mode expansion techniques to overcome experimental coordinate incompleteness were compared. Despite numerical improvements to the error matrix procedure, updating using modal data remained far from being satisfactory.

Particular attention was given to an updating technique using measured frequency response functions (FRFs) directly: the Response Function Method (RFM). Analytically-generated test cases and experimental data for a free-free beam showed that the RFM can locate modelling errors in the realistic case of noisy and incomplete experimental data. Application of statistical analysis tools proved to be successful in obtaining more reliable error estimates.

The RFM was further developed to include updating of damping matrices although some reasoned assumptions about the form of the damping should be made. Recommendations were made for appropriate measurement sites and frequency points selection. Coordinate expansion of experimental FRF data by new receptance column expansion techniques and model reduction were also addressed. Locating structural joint modelling errors was investigated and the benefits of a new approach introducing additional elements in the FE model at joints were demonstrated. Finally, a recommended strategy for updating structural dynamics models was presented.

# ACKNOWLEDGEMENTS

I would like to express my gratitude to my supervisors, Prof. D. J. Ewins and Dr. M. Imregun, for their valuable advice, interest, and encouragement throughout this project.

I also would like to thank my past and present colleagues of the Imperial College Dynamics Section who by their enthusiasm, encouragement and their useful (and sometimes not so useful) discussions provided insight into related fields of interest and an enjoyable working environment.

I am grateful to both the Science and Engineering Research Council and the Defence Research Agency (formerly the Royal Aerospace Establishment, Farnborough) for their financial support provided for this project. I especially would like to acknowledge Dr. M. Nash (DRA) for the informative discussions and Dr. G. Skingle (DRA) for providing the experimental data for the experimental case study on the 3-bay truss structure.

Special thanks are due to my parents, and also to Wim, Sandra, Marianne and Vicky, for all their love and support during the course of this work, especially during the last few months. Without them this thesis would not have been completed.

# NOMENCLATURE

## Basic Terms, Dimensions and Subscripts

| | |
|---|---|
| $x, y, z$ | translational degrees of freedom/coordinates |
| $\theta_x, \theta_y, \theta_z$ | rotational degrees of freedom/coordinates |
| $N$ | total number of degrees of freedom/coordinates |
| $n$ | number of primary/master/measured DOFs (also denoted by subscript $_1$) |
| $s$ | number of secondary/slave/unmeasured DOFs (also denoted by subscript $_2$) |
| $m$ | number of included/effective modes |
| $r, q$ | current mode number |
| $L$ | number of correlated mode pairs |
| $N_f$ | number of frequency points |
| $i, j, k, l$ | integers |
| $\omega$; $f$ | frequency of vibration (in $rad.s^{-1}$; Hz) |
| $i$ | $\sqrt{-1}$ |

## Matrices, Vectors and Scalars

| | |
|---|---|
| $[\ ]$ | matrix |
| $\{\ \}$ | column vector |
| $[\ \ ]$ | diagonal matrix |
| $[\ ]^T$; $\{\ \}^T$ | transpose of a matrix; vector (i.e. row vector) |
| $[I]$ | identity matrix |
| $[0]$ | null matrix |
| $[\ ]^{-1}$ | inverse of a matrix |
| $[\ ]^+$ | generalised/pseudo inverse of a matrix |
| $[\ ]^*$ | complex conjugate of a matrix |
| $[U], [V]$ | matrices of left and right singular vectors |
| $[\Sigma]$ | rectangular matrix of singular values |
| $[S]$ | sensitivity matrix |
| $[T]$ | transformation matrix |
| $[A^D]$ | deleted matrix |
| $[A^E]$ | expanded matrix |
| $[A^R]$ | reduced matrix |
| $\|\ \|$ | norm of a matrix/vector |
| $\varepsilon$ | value of a norm/error/perturbation |

## Spatial and Modelling Properties

| | |
|---|---|
| $[M]$ | mass matrix |
| $[K]$ | stiffness matrix |
| $[D]$ | damping matrix |
| $[M_A]$; . . | analytical/theoretical/predicted/FE mass; . . . matrix |
| $[M_X]$; . . | experimentally derived/test mass; . . . matrix |
| $[\Delta M]=[M_X]-[M_A]$; . . | mass; . . . error/modification matrix |
| $[M_U]=[M_A]+[AM]$; . . | updated/refined/improved mass; . . matrix |
| $N_m$ | total number of mass elements |
| $N_k$ | total number of stiffness elements |
| $N_d$ | total number of damping elements |

## Modal and Frequency Response Properties

| | |
|---|---|
| $\omega_r$ | natural frequency of $r^{th}$ mode ($rad.s^{-1}$) |
| $\eta_r$ | structural damping loss factor of $r^{th}$ mode |
| $m_r$ | modal/effective mass of $r^{th}$ mode |
| $k_r$ | modal/effective stiffness of $r^{th}$ mode |
| $[\lambda_r]$ | eigenvalue matrix |
| $[\psi]$ | unit-normalised mode shape/eigenvector matrix |
| $[\phi]$ | mass-normalised mode shape/eigenvector matrix |
| $\{\psi\}_r$; $\{\phi\}_r$ | $r^{th}$ mode shape/eigenvector |
| $\psi_{jr}$; $\phi_{jr}$ | $j^{th}$ element of $r^{th}$ mode shape/eigenvector |
| $[\alpha(\omega)]$ | receptance matrix |
| $[Z(\omega)]$ | dynamic stiffness matrix |
| $\alpha_{jk}(\omega) = (x_j/f_k)_{f_l=0;\, l=1,n;\, l\neq k}$ | individual receptance element between coordinates j and k (response at coordinate j due to excitation at coordinate k) |
| ${}_rA_{jk} = \phi_{jr}\,\phi_{kr}$ | modal constant |
| $[R]$ | residual matrix |

## Standard Abbreviations

| | |
|---|---|
| DOF(s) | degree(s) of freedom |
| EMM | error matrix method |
| FE | finite element |
| FRF | frequency response function |
| MAC | modal assurance criterion |
| COMAC | coordinate modal assurance criterion |
| RFM | response function method |
| SVD | singular value decomposition |

# TABLE OF CONTENTS


ABSTRACT I
ACKNOWLEDGEMENTS II
NOMENCLATURE III

## CHAPTER 1 - INTRODUCTION

1.1 BACKGROUND
1.2 THE ANALYTICAL APPROACH
1.3 THE EXPERIMENTAL APPROACH
1.4 CORRELATION AND UPDATING
1.5 SCOPE OF THESIS

## CHAPTER 2 - LITERATURE REVIEW

2.1 INTRODUCTION 8
2.2 TECHNIQUES FOR COMPARISON AND CORRELATION 8
2.2.1 Direct comparisons 8
2.2.2 The modal assurance criterion (MAC) 9
2.2.3 The coordinate modal assurance criterion (COMAC) 9
2.2.4 Ortbogonality methods 10
2.2.5 Energy comparisons and force balance 10
2.3 SIZE AND MESH INCOMPATIBILITY 11
2.3.1 Model reduction 11
2.3.2 Coordinate expansion 12
2.4 MODEL UPDATING METHODS USING MODAL DATA 14
2.4.1 Methods using Lagrange multipliers 15
2.4.2 Direct method based on matrix perturbation 17
2.4.3 Error matrix methods 17
2.4.4 Matrix mixing methods 19
2.4.5 Methods based on force balance 19
2.4.6 Methods based on orthogonality 21
2.4.7 Statistics and sensitivity methods 22
2.4.8 Energy methods 24
2.4.9 Updating based on control methods 24
2.5 MODEL UPDATING METHODS USING RESPONSE DATA 25
2.5.1 A direct updating technique using FRF data 25
2.5.2 Techniques based on minimising response equation errors 26
2.5.3 Updating methods using time domain data 27
2.6 CONCLUDING REMARKS 28

## CHAPTER 3-UPDATING USING MODAL DATA, THE EMM

3.1 INTRODUCTION 30
3.2 THE ERROR MATRIX METHOD 31
3.2.1 Theory 31
3.2.2 Case studies on a 10 DOF system 31
3.3 AN IMPROVED PROCEDURE FOR THE EMM 34
3.3.1 Theory 34
3.3.2 Case studies on a 10 DOF system 35
3.4 THE GARTEUR III EXERCISE 37
3.5 CONCLUDING REMARKS 40

## CHAPTER 4 - EXPANDING MEASURED MODE SHAPES


4.1 INTRODUCTION 41
4.2 THEORETICAL BACKGROUND 41
4.2.1 The Inverse Reduction Method 41
4.2.2 The Modal Transformation Expansion Method 42
4.3 CASE STUDIES 44
4.3.1 Test cases 44
4.3.2 Summary of results 49
4.4 MODEL UPDATING USING EXPANDED MODES 52
4.4.1 The GARTEUR III exercise 52
4.4.2 Discussion on expanded data and the orthogonality condition 56
4.5 CONCLUDING REMARKS 58


## CHAPTER 5 - UPDATING USING FRF DATA; THE RFM


5.1 INTRODUCTION 59
5.2 THEORY 59
5.3 COORDINATE INCOMPLETENESS 61
5.4 UNIQUENESS OF THE SOLUTION 62
5.5 CASE STUDIES ON AN 8 DOF SYSTEM 63
5.5.1 The 8 DOF system 63
5.5.2 Updating using complete data from the experimental model 64
5.5.3 Incomplete experimental data 65
5.5.4 Frequency points selection 68
5.5.5 Noisy experimental data 69
5.6. CASE STUDIES ON A FREE-FREE BEAM 71
5.6.1 The free-free beam 71
5.6.2 Noise-free experimental FRF data 72
5.6.3 Noisy experimental FRF data 75
5.6.4 The effect of excitation direction 77
5.6.5 The effect of reduced number of coordinates 78
5.6.6 The effect of coordinate mismatch 80
5.7 THE GARTEUR III EXERCISE 81
5.8 CONVERGENCE CRITERIA 84
5.9 CONCLUDING REMARKS 86


## CHAPTER 6 - UPDATING USING COMPLEX FRF DATA


6.1 INTRODUCTION 88
6.2 THEORETICAL BACKGROUND 88
6.3 CASE STUDIES ON A FREE-FREE BEAM 90
6.4 USING MEASURED FRF DATA 92
6.5. CONCLUDING REMARKS 95

## CHAPTER 7 - COMPUTATIONAL ASPECTS OF THE RFM


7.1 INTRODUCTION 96
7.2 RFM SOLUTION IMPROVEMENTS 96
7.2.1 Iterative refinement %
7.2.2 Balancing the solution matrices 97
7.2.3. Recommendations 101
7.3 FREQUENCY POINT SELECTION FOR THE RFM 101
7.3.1 Basic Equations 101
7.3.2 Noise-free 2 DOF test cases 104
7.3.3 2 DOF test cases with noise 107
7.3.4 Substitution of unmeasured data with analytical counterparts 109
7.3.5 Recommendations 111
7.4 COMPUTATIONAL CONSIDERATIONS 112
7.4.1 Least-squares solution 112
7.4.2 Receptance matrix calculations 113
7.4.3 The uniqueness of the updated model 114
7.4.4 Recommendations 124
7.5 CONCLUDING REMARKS 124


## CHAPTER 8 - COORDINATE INCOMPATIBILITY


8.1 INTRODUCTION 126
8.2 RECEPTANCE COLUMN COORDINATE EXPANSION METHODS 127
8.2.1 The inverse-reduction method 127
8.2.2 Using analytical mode shapes 127
8.3 COMPARISON OF COORDINATE EXPANSION METHODS 129
8.4 EXPANDED EXPERIMENTAL COORDINATES IN THE RFM 132
8.4.1 2 DOF test case 132
8.4.2 Beam test cases 134
8.5 REDUCED ANALYTICAL COORDINATES IN THE RFM 136
8.6 CONCLUDING REMARKS 139


## CHAPTER 9 - UPDATING OF STRUCTURAL JOINTS


9.1 INTRODUCTION 141
9.2 PROPOSED JOINT UPDATING PROCEDURE 143
9.3 CASE STUDIES ON A FRAME STRUCTURE 145
9.3.1 The 2D frame models 145
9.3.2 Joint discontinuity 146
9.3.3 Joint stiffness modelling errors 150
9.3.4 Discussion 154
9.4 APPLICATION OF THE JOINT UPDATING PROCEDURE 154
9.4.1 The analytical frame model 154
9.4.2 Joint discontinuity 155
9.4.3 Joint stiffness modelling errors 158
9.4.4 Discussion 162
9.5 CONCLUDING REMARKS 163

## CHAPTER 10 - EXPERIMENTAL CASE STUDY


10.1 THE 3-BAY TRUSS STRUCTURE 164
10.2 EXPERIMENTAL DATA 164
10.3 THE FINITE ELEMENT MODEL 165
10.4 CORRELATION BETWEEN EXPERIMENTAL AND FE DATA 166
10.5 SIMULATED UPDATING CASE STUDIES 172
10.6 MODEL UPDATING USING MEASURED FRF DATA 173
10.6.1 Direct use of the experimental data 173
10.6.2 Employing regenerated experimental data 175
10.6.3 Error location using the RFM 176
10.6.4 Updating the FE model 177
10.6.4 Discussion 178
10.7. CONCLUDING REMARKS 181


## CHAPTER 11 - CONCLUSIONS AND SUGGESTIONS


11.1 CONCLUSIONS 183
11.1.1 Introduction 183
11.1.2 Updating using modal data 183
11.1.3 Updating using frequency response data 184
11.2 RECOMMENDED UPDATING STRATEGY 186
11.3 SUMMARY OF CONTRIBUTIONS OF PRESENT WORK 189
11.4 SUGGESTIONS FOR FURTHER STUDIES 190
11.5 CLOSURE 191


## APPENDICES


A THE RESPONSE FUNCTION METHOD 192
B ILLUSTRATIONS OF REDUCED COORDINATES IN THE RFM 196
C THE 3-BAY TRUSS STRUCTURE 204
D 3-BAY TRUSS STRUCTURE - RFM RESULTS 208


## REFERENCES

# LIST OF FIGURES


**Fig. 1.1:** Overview of analytical and experimental models 5

**Fig. 3.1:** *Experimental* and analytical 10 DOF systems 32
**Fig. 3.2:** Error matrices for a 10 DOF systems 33
**Fig. 3.3:** MAC and COMAC values for updated 10 DOF models using the EMM and the improved error matrix procedure (EMM'), test case b. 36
**Fig. 3.4:** The GARTEUR structure 37
**Fig. 3.5:** GARTEUR III MAC and COMAC values 38
**Fig. 3.6:** GARTEUR III, standard EMM error location (leading diagonal values) 39
**Fig. 3.7:** GARTEUR III, improved error matrix procedure (EMM') error location 39
**Fig. 3.8:** GARTEUR III, updated natural frequencies against *experimental* ones 39
**Fig. 3.9:** Modelling errors of the GARTEUR III exercise 40

**Fig. 4.1:** Mode shape coordinate expansion of a 10 DOF system 45
**Fig. 4.2:** Mode shape coordinate expansion of a 100 DOF system 46
**Fig. 4.3:** Mode shape coordinate expansion of a clamped beam 47
**Fig. 4.4:** Mode shape coordinate expansion of a frame structure 48
**Fig. 4.5:** Mode shape coordinate expansion discrepancies 51
**Fig. 4.6:** GARTEUR III, error location results by EMM using inverse reduction expanded *experimental* mode shapes 53
**Fig. 4.7:** GARTEUR III, error location results by EMM' using inverse reduction expanded *experimental* mode shapes 53
**Fig. 4.8:** GARTEUR III, error location results by EMM using modal transformation expanded *experimental* mode shapes 53
**Fig. 4.9:** GARTEUR III, error location results by EMM' using modal transformation expanded *experimental* mode shapes 54
**Fig. 4.10:** GARTEUR III, updated natural frequencies against *experimental* ones for four different updating procedures 55
**Fig. 4.11:** Mass orthogonality for the frame example 57

**Fig. 5.1:** The 8 DOF system 63
Fig. 5.2: Receptance FRF $\alpha_{66}$ obtained from the *experimental* and analytical models of the 8 DOF system 64
**Fig. 5.3:** Receptance FRF a66 obtained from the *experimental* and updated analytical models of the 8 DOF system 65
**Fig. 5.4:** Receptance FRF a66 obtained from the *experimental* and updated analytical models of the 8 DOF system using Cl constraints 66
**Fig. 5.5:** Convergence towards the unique solution using C2 constraints 67
**Fig. 5.6:** Variation of p-values with level of noise 70
**Fig. 5.7:** 8 DOF models, standard deviation of p-values against noise level 71
**Fig. 5.8:** 8 DOF models, mean p-values against noise level 71
**Fig. 5.9:** FE model of the uniform beam 72
**Fig. 5.10:** Receptance FRF $\alpha_{5y5y}$ obtained from the *experimental* and analytical beam models 72
**Fig. 5.11:** pvalues for an incomplete *experimental beam* model 73
**Fig. 5.12:** Receptance FRF $\alpha_{5y5y}$ obtained from the *experimental* and updated analytical beam models 73
**Fig. 5.13:** Receptance FRF $\alpha_{5z5z}$ obtained from the *experimental* and updated analytical beam models 74
Fig. 5.14: A 2 DOF system with x and y directions decoupled 74
Fig. 5.15: p-values for an incomplete *experimental* model with 3% noise 76
Fig. 5.16: pvalues for an incomplete *experimental* model with 6% noise 77

| | | |
|---|---|---|
| **Fig. 5.17:** | p-values for an incomplete ***experimental*** model **with** 10% noise | 77 |
| **Fig. 5.18:** | pvalues obtained for excitation in Y direction and excitation in Z direction | 78 |
| **Fig. 5.19:** | pvalues obtained for excitation in Y direction and excitation in Z direction for an incomplete ***experimental*** model with 3% noise | 78 |
| **Fig. 5.20:** | pvalues for an incomplete ***experimental*** model with 3% noise (correspondence factor 7.8%) | 79 |
| **Fig. 5.21:** | Ap for each iteration for incomplete ***experimental beam*** models with 3% noise | 79 |
| **Fig. 5.22:** | pvalues for an incomplete ***experimental*** model with 3% noise (15 ***experimental points*** on beam edge - model mismatch) | 80 |
| **Fig. 5.23:** | **Receptance FRF** $\alpha_{31,31}$ obtained from the ***experimental*** and analytical GARTEUR models | 81 |
| **Fig. 5.24:** | Indication of unstable elements on the GARTEUR structure | 82 |
| **Fig. 5.25:** | Mean p-value to standard deviation ratio for GARTEUR III | 83 |
| **Fig. 5.26:** | **Receptance FRF** $\alpha_{31,31}$ obtained from the ***experimental*** and updated analytical GARTEUR models | 84 |
| **Fig. 5.27:** | Typical variations in the sum of the percentages difference squared | 85 |
| **Fig. 6.1:** | pvalues for incomplete complex ***experimental data*** with 3% noise (simultaneous error on real and imaginary parts) | 90 |
| **Fig. 6.2:** | pvalues for incomplete complex ***experimental data*** **with** 3% noise (independent error on real and imaginary part) | 91 |
| **Fig. 6.3.:** | Experimental set-up | 92 |
| **Fig. 6.4:** | pvalues using **the** real part of measured **FRF** data | 93 |
| Fig. 6.5: | Comparison of the measured, analytical and updated analytical receptance **FRF** | 93 |
| Fig. 6.6: | pvalues using measured **FRF** data | 94 |
| Fig. 6.7: | The effect of an exponential window on lightly damped response data | 94 |
| Fig. 7.1: | Balancing of RFM system matrices | 98 |
| Fig. 7.2: | The sum of the percentage differences squared for 4 beam examples | 99 |
| Fig. 7.3: | the RPM applied to an incomplete complex ***experimental*** beam example with independent noise on **real** and imaginary parts, 3% and 10% respectively | 100 |
| Fig. 7.4: | SDGF and 2 **DOF** systems | 103 |
| Fig. 7.5: | 2 **DOF** test case, **+20%** k2 error | 105 |
| Fig. 7.6: | 2 DOF test case, **+20%** ml error | 106 |
| Fig. 7.7: | 2 DOF test case, **+20%** $m_2$ error | 106 |
| Fig. 7.8: | 2 **DOF** test case, **+20%** k2 error, noisy ***experimental data*** | 108 |
| **Fig. 7.9:** | **2 DOF** test case, **+20%** k2 error, constant noise value on the ***experimental data*** | 109 |
| **Fig. 7.10:** | **2 DOF** test case, **+20%** k2 error, 100% **error** on ***expanded experimental data*** | 110 |
| **Fig. 7.11:** | Comparison of **RFM** CPU time per iteration for calculating analytical **receptance** matrix by dynamic stiffness inversion or modal summation | 113 |
| **Fig. 7.12:** | Comparison of ***experimental and*** updated mceptance curves obtained from one **RFM** run only | 115 |
| **Fig. 7.13:** | Comparison of ***experimental*** and updated mceptance curves obtained using one **RFM** run only for an increasing number of frequency points selected | 117 |
| **Fig. 7.14:** | Standard deviation against the number of frequency points for the beam example with 10% random noise | 118 |
| **Fig. 7.15:** | ***Experimental*** and updated receptance curves using all- and selected pvalues | 120 |
| Fig. 7.16: | Standard deviation against the number of runs for **the** beam example with 10% random noise | 121 |
| Fig. 7.17: | Number of modelling errors located for the beam example with 10% random noise, for an increasing number of **RFM** runs | 121 |
| Fig. 7.18: | Updated and ***experimental*** receptance curves, for an increasing number of RPM runs | 122 |

**Fig. 8.1:** Expanded cross receptance, $\alpha_{5y1\theta z}$, for a correspondence factor of 16.7% obtained from the inverse reduction expansion technique 130

**Fig. 8.2:** Expanded cross receptance $5y1\theta_z$ for a correspondence factor of 17% obtained from the modal expansion technique 130

**Fig. 8.3:** Expanded receptances for a correspondence factor of 7.8% obtained from the inverse reduction expansion technique 131

**Fig. 8.4:** Expanded receptances for a correspondence factor of 7.8% obtained from the expansion technique using modal data 132

**Fig. 8.5:** RFM applied to update a 2 DOF system using expanded *experimental data* 133

**Fig. 9.1:** Joint examples and typical FE models 142

**Fig. 9.2:** Updating of joints, options.(i), (ii) and (iii) 144

**Fig. 9.3:** 2D frame models 146

**Fig. 9.4:** RFM results for a discontinuity at joint J1 in the *experimental* model 148

**Fig. 9.5:** RFM results for a discontinuity at joint J1 in the analytical model 149

**Fig. 9.6:** RFM results for a joint modelling error, kj=O. 1, at join J1 in the *experimental model* 151

**Fig. 9.7:** RFM results for a joint modelling error, kj=0.001, at joint J1 in the *experimental* model 152

**Fig. 9.8:** RFM results for a joint modelling error, kj=10, at joint J1 in the *experimental* model 153

**Fig. 9.9:** The analytical frame model with additional joint elements. 155

**Fig. 9.10:** RFM results using the proposed joint updating strategy for a discontinuity at joint J1 in the *experimental* model 156

**Fig. 9.11:** RFM results using the proposed joint updating strategy for a discontinuity at joint J1 in the analytical model 157

**Fig. 9.12:** RFM results using the proposed joint updating strategy for a joint modelling error, kj=O.l, at joint J1 in the *experimental* model 159

**Fig. 9.13:** RFM results using the proposed joint updating strategy for a joint modelling error, kj=0.001, at joint J1 in the *experimental* model 160

**Fig. 9.14:** RFM results using the proposed joint updating strategy for a joint modelling error, kj=lO, at joint J1 in the *experimental* model 161

**Fig. 10.1:** The 3-bay truss structure 164

**Fig. 10.2:** The FE model of the 3-bay truss structure 166

**Fig. 10.3:** 3-bay truss structure experimental and analytical receptance FRF $\alpha_{J4zJ4z}$ 167

**Fig. 10.4:** 3-bay truss structure MAC values between various experimental data sets 169

**Fig. 10.5:** 3-bay truss structure MAC values between experimental and analytical data 170

**Fig. 10.6:** Natural frequency comparison of the 3-bay truss structure 170

**Fig. 10.7:** 3-bay truss structure COMAC values between experimental and FE data 171

**Fig. 10.8:** 3-bay truss structure COMAC values between various experimental data sets 172

**Fig. 10.9:** Experimental and regenerated receptance FRF $\alpha_{J4zJ4z}$ for the 3-bay truss structure 175

**Fig. 10.10:** Locations of modelling errors in the FE model of the 3-bay truss structure 176

**Fig. 10.11:** Indicated modelling errors in the FE model of the 3-bay truss structure 177

**Fig. 10.12:** 3-bay truss structure experimental, analytical and updated analytical receptance FRF mm $\alpha_{J4zJ4z}$ 178

**Fig. 10.13:** Reciprocal experimental receptance curves of the 3-bay truss structure 179


# LIST OF TABLES


**Table 1.1:** Stages in analytical model updating 6

**Table 3.1:** Maximum errors in a 10 DOF system located using EMM and the improved EMM procedure (EMM') 35

**Table 5.1:** GARTEUR III, p-values. 83

# CHAPTER 1

# INTRODUCTION

## 1.1 BACKGROUND

Vibration phenomena have always been a cause of concern to engineers, even more so today as structures are becoming lighter and more flexible due to increased demands for efficiency, speed, safety and comfort. The effects of vibration present major hazards and operating limitations ranging from discomfort (including noise), malfunction, reduced performance, early breakdown and structural failure which, in the worst case, can be catastrophic. It is clear that a thorough understanding of the vibration levels encountered in service is essential. Hence, accurate mathematical models are required to describe the vibration characteristics of structures, which subsequently can be used for design purposes to limit the negative effect of vibrations.

The earliest main contributions to the theoretical understanding of the vibration phenomenon were made in the late 1600s by Newton and Leibnitz. Newton's laws define first principles of interaction of forces between and/or on bodies for both statics and dynamics. Later, significant contributions were made by, among others, Bernoulli (1732), who used Bessel functions to describe modes of continuous systems, Kirchhoff (1850), on the theory of plate vibration, Rayleigh (1877), on the theory of sound, and Love (1926), who worked on the mathematical theory of elasticity which is used as the basis of today's vibration analysis. Earlier this century major contributions to the theoretical understanding of vibration phenomena were made by Den Hartog [1], Bishop and Johnson [2] and Timoshenko [3].

Today, the study of the dynamic behaviour of a structure can be divided into two separate activities, namely analytical predictions and vibration tests. For simple structures, such as beams and plates, good analytical predictions using closed form solutions can be easily found in various reference books and tables (such as Blevins [4]) or lumped parameter systems can be used to describe the dynamic behaviour. For more complex structures the most widely used analytical tool is the Finite Element (FE) method, modal testing and analysis being the experimental counterpart. Due to different limitations and

assumptions, each approach has its own advantages and shortcomings. Both techniques are described in sections 1.2 and 1.3.

## 1.2 THE ANALYTICAL APPROACH

The Finite Element method assumes that a continuous structure can be discretised by describing it as an assembly of finite (discrete) elements, each with a number of boundary points which are commonly referred to as nodes.

Any structure can theoretically be divided into very small elements such that a good approximation of the displacement shape (or stress field) can be obtained for each element using second- or third-order shape functions. To obtain continuity across element boundaries; displacement or stress approaches employ the following three arguments (i) equilibrium, (ii) compatibility and (iii) the constitutive laws, while energy approaches rely on the principal of virtual work equating internal work to external work. Subsequently, the individual elements can be assembled and the acquired set of simultaneous equations solved. In its early days (1960s) the Finite Element techniques found their main application in the area of stress analysis, but the benefit of FE methods for dynamic analysis was soon recognised.

For structural dynamic analysis, element mass, stiffness and damping matrices are generated first and then assembled into the global system matrices; [MA], $[K_A]$ and [DA]. The mass and stiffness matrices are easily defined in terms of spatial and material properties of the system. The damping, however, is not so easily modelled and the damping matrix is usually omitted from the system, although it is possible to assume proportional damping in a simplified representation. In most cases, dynamic analysis is carried out assuming an undamped system giving the modal properties; the natural frequencies $\omega_{Ar}$ and corresponding eigenvectors $\{\phi_A\}_r$. The modal solution can subsequently be used to calculate frequency response levels for the structure under study.

Element system matrices have been developed for many simple structures, such as beams, plates, shells and bricks. Most general-purpose FE packages have a wide range of choice of element types, and the user must select the appropriate elements for the structure under investigation and its particular application. Further theoretical background and practical implementation of the FE method are given in various text books, such as by Cook [5], Bathe [6] and Zienkiewicz [7].

The FE method is extensively used in industry as it can produce a good representation of a true structure. However, one must bear in mind that, due to limitations in the FE method, an FE model is always an approximation of the structure under study. Especially for complicated structures, approximations can lead to errors being introduced into the FE model. Inaccuracies and errors in an FE model can arise due to:

(1) inaccurate estimation of the physical properties of the structure;
(2) discretisation errors of distributed parameters due to faulty assumptions in individual element shape functions and/or a poor quality mesh;
(3) poor approximation of boundary conditions;
(4) inadequate modelling of joints;
(5) introduction of additional inaccuracies during the solution phase such as the reduction of large models to a smaller size; and
(6) computational errors which are mainly due to rounding off.

These approximations can - depending on the operator and, to a lesser extent, on the package used - lead to a wide range of results if the same structure is analysed by different analysts, as indicated by the DYNAS survey [8]. Therefore, there is a need to verify and validate FE models if accurate predictions are sought.

## 1.3 THE EXPERIMENTAL APPROACH

The experimental approach relies on extracting the vibration characteristics of a structure from measurements. It consists of two steps, (i) taking the measurements and (ii) analysing the measured data. In the last two decades substantial progress has been made in the experimental approach thanks to continued development of modal analysis techniques, the benefits of better data-acquisition and measurement equipment as well as advances in computing hardware and software.

Excitation of the structure under study can be by either single- or multi-point input. The structure can be excited in various ways: (i) by a short impulse, (ii) by applying a stepped sine excitation over the frequency range of interest, (iii) using white noise or pseudo random noise. The driving force is in most cases applied by a shaker or, in the case of impact testing, by an instrumented hammer. The response is measured at one or more points by accelerometers which are connected to a data acquisition device, usually an FFT analyser.

Subsequent modal analysis of the stored measured data, or modal identification, is carried out to obtain the modal properties of the system. Various techniques have been extensively developed and ranging from single-degree-of-freedom curve fits (as proposed in 1947 by Kennedy and Pancu [9]) to global multi-degrees-of-freedom curve fits. The theoretical background of these methods and practical aspects of vibration measurement techniques are discussed by Ewins [10].

Vibration measurements are taken directly from a physical structure, without any assumptions about the structure, and as such they are considered to be more reliable than their FE counterparts. However, limitations and errors in the experimental approach can occur due to:

(1) experimental errors due to noise, the application of windows and filters;
(2) the assumption of linear response while there can also be non-linear structural response and/or non-linearities in the measurement system;
(3) poor modal analysis of experimental data, resulting in either under-analysis, not all modes are identified or, on the other hand, over-analysis, leading to false modes;
(4) limited number of measured degrees of freedom due to physical inaccessibility and/or equipment limitations;
(5) not all modes of interest being excited e.g. due to excitation at a node,
(6) difficulty in measuring rotational degrees of freedom.

A variation in experimental results can also be obtained, depending on the experimental set-up and operator, as highlighted by the SAMM survey [11].

## 1.4 CORRELATION AND UPDATING

Both the analytical and experimental approaches to vibration analysis effectively assume that the vibration characteristics of continuous systems can be described by a mathematical model possessing a limited number of coordinates and modes, which is a valid assumption within a given frequency range. **Fig 1.1** gives an overview of the analytical and experimental routes to various vibration data sets. Note that modal analysis of measured data to obtain a theoretical description of the structure under study is also referred to as model- or system identification. An FE model can be compared to its experimentally-derived counterparts at any one level a-e in **Fig. 1.1.** Analytical versus experimental model comparisons are also referred to as model correlation, validation or verification.

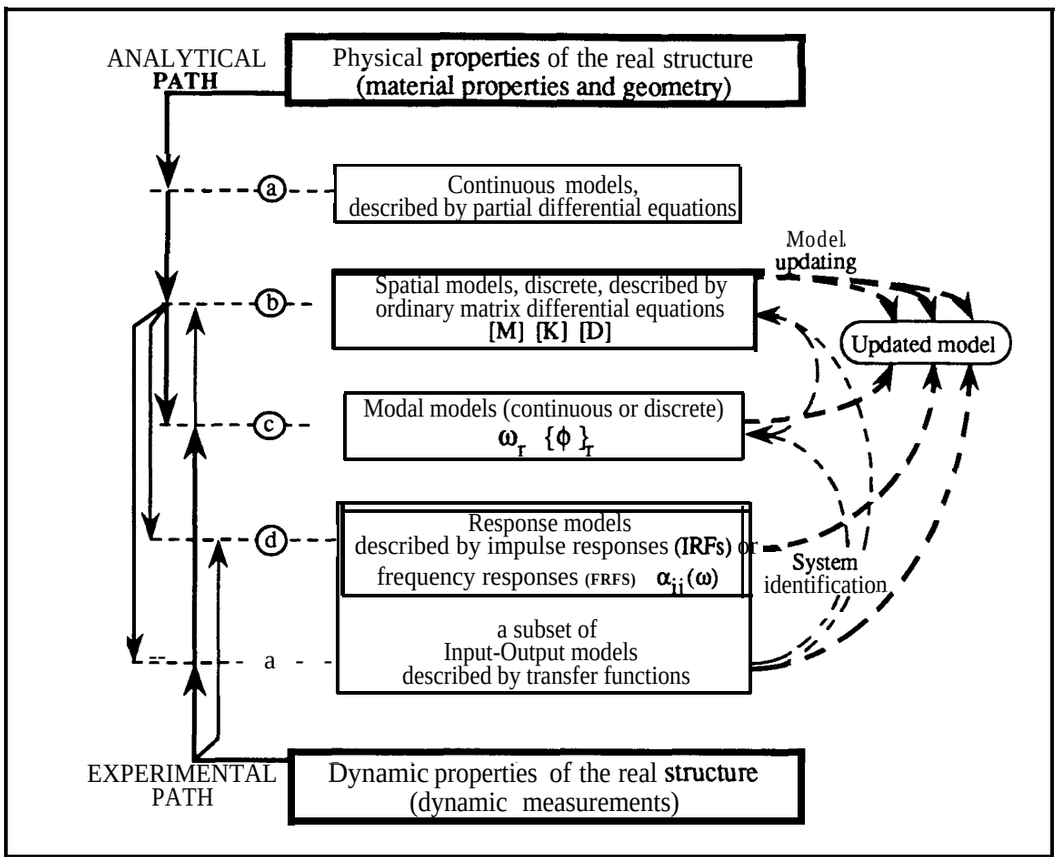


**Fig. 1.1:** Overview of analytical and experimental models

Model updating can be defined as the adjustment of an existing analytical model which represents the structure under study, using experimental data, so that it more accurately reflects the dynamic behaviour of that structure. This is represented graphically in **Fig. 1.1** where a combination of analytical and experimental data are used to generate an updated model. Model updating is also on occasions referred to as model adjustment, alignment, correction or refinement. It is not to be confused with model optimisation or modification which aims to change the structure under study to achieve a pre-set required response behaviour under operating conditions.

It is generally believed that more confidence can be placed on experimental data as measurements are taken on the true structure. Therefore, the analytical model of a structure is usually updated on the strength of the experimental model. One can identify at least six criteria of increasing complexity which a ***good*** model ought to satisfy. For each of these levels of correctness, the updated model has to reproduce:

(i) the modal properties at measured points;
(ii) the measured frequency response functions;
(iii) the modal properties at unmeasured points for measured modes;

(iv) the unmeasured frequency response functions;
(v) (i-iv) and the correct connectivities;
(vi) the *correct* model.

The difference between criteria (v) and (vi) is that for criterion (v) a limited (measured) frequency range is considered while for (vi) the model satisfies all criteria for frequencies beyond the measured frequency range. A perfect model, i.e. one that correctly represents the structure for all frequencies and applications, is a contradiction in terms. A very detailed model can approach reality. However, if the model is too detailed it defeats its own purpose, namely: to have a simple and easy-to-handle tool for theoretical predictions. Hence, the purpose(s) of the model and the objectives of the model updating exercise are to be determined prior to updating. The criteria (i)-(vi) can also be set out in tabular form providing a schematic overview of the various stages in model updating.

| freq. range→ / ↓ coordinates | measured (limited) | | measured+ unmeasured |
|---|---|---|---|
| | modal properties | frequency response data | modal properties + frequency response data |
| measured (incomplete) | i | iii | vi (*unique model*) |
| measured + unmeasured (complete) | ii | iv | |
| connectivities | v | | |

**Table 1.1: Stages** in analytical model updating

Structural dynamics model updating can be divided into two steps: (i) locating the errors and (ii) correcting them. Most diffkulties are encountered in the first step, or localisation. The difficulties in locating the errors arise due to:

(i) insufficient experimental modes;
(ii) insufficient experimental coordinates;
(iii) size and mesh incompatibility of the experimental and FE models;
(iv) experimental and other random and systematic errors (as discussed in sections 1.2 and 1.3).

## 1.5 SCOPE OF THESIS

Although the requirements for model updating are well understood, and many methods of updating have been suggested in recent years, a logical updating strategy applicable to real structures is still largely unavailable. As there is an obvious need for reliable analytical models and therefore for a reliable updating approach, the main objective of this project is to develop a robust and practical updating strategy applicable to real engineering structures.

In order to reach this goal three distinct steps have been identified, namely:

(i) to carry out a literature survey of previous work, with the aims of (a) obtaining an overview of existing methods (b) envisaging advantages and disadvantages of the various methods, and (c) identifying problems encountered during updating;

(ii) to select promising techniques and to investigate them in more detail with a view to develop an updating method capable of addressing the problems encountered during practical implementation; and

(iii) to propose an updating strategy based on the experience gained in (i) and (ii).

Chapter 2 of this thesis contains an extensive literature review of previous work in a consistent format and notation. Chapter 3 presents an investigation of one of the model updating techniques using modal data - the error matrix method (EMM) - and the advantages and disadvantages of using modal data are discussed. An improved procedure is proposed. A comparison of various mode shape expansion techniques is presented in chapter 4. Chapter 5 focuses on an updating method which uses frequency response data directly, the response function method (RFM). As the RFM has numerous advantages over the EMM and indeed other methods using modal data, further work concentrates on this technique. Suggestions for improvements to increase the success of the RFM are made. Chapter 6 presents a case study illustrating the practical use of the RFM in the case of damping and true experimental data. Chapter 7 considers some computational aspects of the RFM and coordinate incompatibility is addressed in chapter 8. Two receptance column coordinate expansion techniques are proposed and their application within the RFM is investigated. The implications of analytical model coordinate reduction on the RFM is also addressed. Chapter 9 considers practical implementation of the RFM in more detail by addressing problems introduced by the updating of structural joints and suggests possible remedies. Chapter 10 is devoted to an experimental case study of a 3-bay truss structure and, finally, a recommended updating strategy is proposed and the main conclusions of this research are presented in chapter 11.

# CHAPTER 2

# LITERATURE REVIEW

## 2.1 INTRODUCTION

There is a growing interest in updating analytical mass and stiffness matrices using measured data as confidence in experimental data has increased due to advances in measurement and analysis techniques. In recent years many updating methods have been proposed and this chapter offers a review of the current literature. The purpose of this chapter is threefold:

(i) to present a number of state-of-the-art model updating techniques in a consistent and unified notation,
(ii) to identify potential difficulties the methods must address,
(iii) to suggest new avenues for research.

## 2.2 TECHNIQUES FOR COMPARISON AND CORRELATION

Before updating an analytical model, it is good practice to compare the experimental and analytical data sets to obtain some insight as to whether both sets are in reasonable agreement so that updating is at all possible. In almost all cases the experimental data set is incomplete as measurements are taken at selected locations in selected coordinate directions and only a limited number of modes can be identified.

### 2.2.1 Direct comparisons

The most common method of comparing natural frequencies from two different models is to plot experimental values against analytical ones for all available modes. The points of the resulting curve should lie on a straight line of slope 1 for perfectly correlated data. A systematic derivation suggests a consistent error (e.g. in material properties) while a large random scatter suggests poor correlation.

Mode shapes can also be compared in the same fashion by plotting analytical mode shapes against experimental ones. For perfectly correlated modes, the points should lie on a straight line of slope 1. The slope of the best straight line through the data points of two correlated modes is also defined as the modal scale factor (MSF)[10]:

$$MSF(\phi_A,\phi_X) = \frac{\{\phi_A\}^T\{\phi_X\}^*}{\{\phi_A\}^T\{\phi_A\}^*} \tag{1}$$

Frequency response functions are normally compared directly by overlaying several on the same frame.

### 2.2.2 The modal assurance criterion (MAC)

The modal assurance criterion (MAC), which is also known as mode shape correlation coefficient (MCC), between analytical mode i and experimental mode j is defined as [12]:

$$MAC(\phi_{iA},\phi_{jX}) = \frac{|\{\phi_A\}_i^T\{\phi_X\}_j^*|^2}{\{\phi_A\}_i^T\{\phi_A\}_i^*\{\phi_X\}_j^T\{\phi_X\}_j^*} \tag{2}$$

A MAC value close to 1 suggests that the two modes are well correlated and a value close to 0 indicates uncorrelated modes.

### 2.2.3 The coordinate modal assurance criterion (COMAC)

The COMAC is based on the same idea as the MAC but in this case an indication of the correlation between the two models for a given common coordinate is obtained [13]. The COMAC for coordinate i is defined as:

$$COMAC(i) = \frac{\left(\sum_{r=1}^{L} |(\psi_A)_{ir}(\psi_X)_{ir}^*|\right)^2}{\sum_{r=1}^{L}(\psi_A)_{ir}^2 \sum_{r=1}^{L}(\psi_X)_{ir}^{*\,2}} \tag{3}$$

where L is the total number of correlated mode pairs as indicated by the MAC values. Again, a value close to 1 suggests good correlation.

### 2.2.4 Orthogonality methods

The most common methods of comparison based on the property of modal orthogonality are the cross orthogonality method:

$$[COM_{A,X}] = [\phi_A]^T[M_A][\phi_X] \tag{4}$$

and the mixed orthogonality check:

$$[MOC_{A,X}] = [\phi_X]^T[M_A][\phi_X] \tag{5}$$

techniques [14-16]. For perfect correlation, the leading diagonal elements of the orthogonality matrix must all be equal to 1 while the off-diagonal ones should remain 0.

### 2.2.5 Energy comparisons and force balance

The kinetic and potential energies stored in each mode for both experimental and finite element models can be computed using the following expressions [17]:

$$\text{KINETIC ENERGY} = 1/2\,\{\dot{\phi}\}_r^T\,[M]\,\{\dot{\phi}\}_r$$

$$\text{POTENTIAL ENERGY} = 1/2\,\{\phi\}_r^T\,[K]\,\{\phi\}_r \tag{6}$$

A force balance [15,18] can be obtained by comparing modal forces:

$$\{F_X\}_r = [K_A]\,\{\phi_X\}_r$$
$$\{F_A\}_r = [K_A]\,\{\phi_A\}_r \tag{7}$$

where r is the mode number.

Another possibility is to determine a force error vector by using mixed experimental and FE data [19,20]:

$$\left([K_A] - \omega_{Xr}^2 [M_A]\right)\{\phi_X\}_r = \{\Delta F\}_r \tag{8}$$

The energy comparison and force balance techniques are not as widely used as MAC and COMAC.

## 2.3 SIZE AND MESH INCOMPATIBILITY

In most practical cases, the number of coordinates defining the finite element model exceeds by far the number of measured coordinates. Also, measurement coordinates are often not the same as finite element master coordinates, some coordinates being too difficult to measure (e.g. rotations) or physically inaccessible (e.g. internal coordinates). As most updating techniques require a one-to-one correspondence between the two data sets, there are two possible avenues to explore:

(i) reducing the finite element model by choosing the measured degrees of freedom as masters, or

(ii) expanding the measured data so that they are the same size as their finite element counterparts.

### 2.3.1 Model reduction

Reducing the size of the analytical model can be achieved using a matrix condensation technique, various formulations of which can be found in [21-26]. These techniques rely on choosing a number of coordinates as masters and expressing the initial mass and stiffness matrices in terms of these coordinates only. Hence, the order of these matrices is reduced to the number of masters selected. The two main approaches are dynamic condensation where the correct stiffness properties are retained while the inertia properties are approximated and static condensation where the situation is reversed. A comparison of the various reduction techniques is given in [27,28]. In most cases the choice is limited to the reduction technique(s) implemented in the finite element package used.

The most popular reduction technique is the dynamic condensation due to Guyan [21]:

$$[M^R] = [M_{11}] - [M_{12}]\,[K_{22}]^{-1}\,[K_{21}] - [K_{12}]\,[K_{22}]^{-1}\,[M_{21}] + [K_{12}]\,[K_{22}]^{-1}\,[M_{22}]\,[K_{22}]^{-1}\,[K_{21}]$$

$$[K^R] = [K_{11}] - [K_{12}]\,[K_{22}]^{-1}\,[K_{21}] \tag{9}$$

where subscript 1 denotes master or measured DOF(s) and subscript 2 denotes slave or unmeasured DOF(s). It should be borne in mind that reduction techniques such as Guyan's were formulated in order to be able to obtain the eigensolution of large matrix eigen-equations and not for model updating purposes. Hence it is not surprising to discover that the problem of model updating is further compounded by several additional problems due to model reduction. The choice of master coordinates is of paramount importance to the success of the reduction and one should refrain from choosing coordinates as masters because they happen to coincide with the measurement coordinates.

Some significant disadvantages of reduction are that:

(i) the measurement points often are not the best points to choose as masters as they are always on the surface of the structure while for dynamic condensation it is vital to select masters corresponding to large inertia properties;

(ii) there may not be enough measurement coordinates to be used as masters;

(iii) all reduction techniques yield system matrices where the connectivity of the original model is lost and thus the physical representation of the original model disappears; and

(iv) the reduction introduces extra inaccuracies since it is only an approximation of the full model.

### 2.3.2 Coordinate expansion

An easy way to fulfil the requirement of coordinate compatibility is to substitute the unmeasured coordinates by their analytical counterparts. This approach is closely related to updating using matrix mixing methods which is discussed in section 2.4.4, but can be used in most updating methods. It can be regarded as a form of coordinate expansion and has the advantage that it does not require additional computations. However, this substitution can lead to unstable solutions and erroneous results, especially in direct (non-iterative) updating techniques, and hence some mode shape coordinate expansion

techniques have been proposed for use during updating. To date there exist at least four possible approaches to expand the measured mode shapes to the size of the analytical ones.

(i) The inverse reduction method, also known as 'Ridder's method, [25], makes use of the analytical mass and stiffness matrices and is defined as follows:

$$\left\{ \begin{bmatrix} K_{11} & K_{12} \\ K_{21} & K_{22} \end{bmatrix}_A - \omega_X^2 \begin{bmatrix} M_{11} & M_{12} \\ M_{21} & M_{22} \end{bmatrix}_A \right\} \begin{Bmatrix} \phi_1 \\ \phi_2 \end{Bmatrix}_X = \begin{Bmatrix} 0 \\ 0 \end{Bmatrix}$$

where $\{\phi_{1X}\}$ is the measured part of the eigenvector while $\{\phi_{2X}\}$ is the unknown part. Rearranging the lower matrix equation gives:

$$\{\phi_{X2}^E\} = -([K_{22}]_A - \omega_X^2[M_{22}]_A])^{-1}([K_{21}] - \omega_X^2[M_{21}])\{\phi_{X1}\} \qquad (10)$$

Alternative derivations of an expression for $\{\phi_{2X}\}$ can be obtained by rearranging the upper matrix equation or by using both equations to find an expression for the expanded set of coordinates. This technique has the disadvantage of relying on knowledge of the analytical mass and stiffness matrices and therefore errors in the analytical system matrices will influence the quality of the expanded measured coordinates directly.

(ii) O'Callahan et al [29] suggest that the rotational degrees of freedom for the experimental data set can be derived from those given by the analytical eigensolution. Assuming that each measured mode shape can be expressed as a linear combination of the analytical mode shape, and by rearrangement of the equation obtained the expanded mode is defined as (see chapter 4):

$$\begin{Bmatrix} \phi_1 \\ \phi_2 \end{Bmatrix}_X^E = \begin{bmatrix} \phi_{11} \\ \phi_{21} \end{bmatrix}_A [\phi_{11}]_A^{-1} \{\phi_1\}_X \qquad (11)$$

A similar formulation has been proposed by Lipkins and Vandeurzen [30] to obtain smoothed expanded measured data. Smoothing is achieved by selecting fewer analytical modes for expansion (m) than there are measured coordinates (n), thus $[\phi_{11}]_{nxm}$ is overdetermined and a generalised inverse returns a least squares solution which smoothes

combinations of analytical and experimental modal data [26] A comparison of these variations is presented by Gysin in [31].

(iii) The experimental modes can also be expanded by interpolation of the measured coordinates using spline fits [32,33]. One advantage of using interpolation is that there is no need for an analytical model. At the same time this is also a disadvantage as there are no further data to rely on to verify the quality of the expansion. Another shortcoming of the interpolation method is that the expanded modes become less accurate as the ratio of unknown to known information increases. This restriction equally applies to the previous two expansion methods but to a lesser extent.

(iv) Recently, another expansion method using the analytical mode shapes and the MAC matrix has been suggested by Lieven and Ewins [34]. For a number of correlated mode pairs the analytical modes are scaled to match the corresponding experimental modes and the expanded coordinates are calculated as follows:

$$[\phi_{2_X}] = [\phi_{21}\ \phi_{22}]_A\,[MAC_{X,A}]^T \tag{12}$$

For model updating employing response data coordinate incompatibility has largely been ignored and either reduced models, with all its disadvantages, are used or the missing coordinates are substituted by their analytical counterparts. Response data coordinate incompatibility is addressed in this thesis in chapter 8, where, for the first time, two receptance column expansion techniques are proposed and the application to model updating is investigated.

## 2.4 MODEL UPDATING METHODS USING MODAL DATA

In recent years, many methods to improve the quality of analytical models using experimental data have been proposed and this process is often referred to as model updating. The 1985 report by Dornier [18] contains an extensive literature study and offers a comparative study of some of the main methods. Similar comparisons can also be found in refs. [35,36]. Recent literature reviews have been published by Ibrahim and Saafen [37], Ceasar [38] and Heylen and Sas [39]. The purpose of this section is to present some of the most commonly used model updating techniques in a unified and consistent notation.

### 2.4.1 Methods using Lagrange multipliers

The method proposed by Baruch [40] assumes that the mass matrix is correct and updates the stiffness matrix by minimising the *distance:*

$$\varepsilon = \|[K_A]^{-0.5}([K_U] - [K_A])[K_A]^{-0.5}\| \tag{13a}$$

between the updated and the analytical stiffness matrices using Lagrange multipliers. Applying the following constraint equations:

$$[K_U] - [K_U]^T = 0$$

$$[\phi_X]^T[K_U][\phi_X] - [\omega_X^2] = 0$$

the updated stiffness matrix can be obtained as:

$$[K_U] = [K_A] + [\Delta K]$$

where

$$[\Delta K] = -[K_A][\phi_X][\phi_X]^T[M_A] - [M_A][\phi_X][\phi_X]^T[K_A] + [M_A][\phi_X][\phi_X]^T[K_A][\phi_X][\phi_X]^T[M_A] + [M_A][\phi_X][\omega_X^2][\phi_X]^T[M_A] \tag{13b}$$

Berman [41] uses the same approach to update the mass matrix by minimising:

$$\varepsilon = \|[M_A]^{-0.5}([M_U] - [M_A])[M_A]^{-0.5}\| \tag{14a}$$

using Lagrange multipliers and the orthogonality condition as the constraint equation. The updated mass matrix is obtained as:

$$[M_U] = [M_A] + [\Delta M]$$

where

$$[\Delta M] = [M_A][\phi_X]1([\phi_X]^T[M_A][\phi_X])^{-1}\left([I] - [\phi_X]^T[M_A][\phi_X]\right)([\phi_X]^T[M_A][\phi_X])^{-1}[\phi_X]^T[M_A] \tag{14b}$$

For the updated stiffness matrix there are two additional constraint equations, namely the eigenvalue equation and the symmetry condition, and the updated stiffness matrix is defined as:

$$[K_U] = [K_A] + [\Delta K] + [\Delta K]^T$$

where

$$[AK] = 0.5[M_U][\phi_X]\left([\phi_X]^T[K_A][\phi_X] + [\omega_X^2]\right)[\phi_X]^T[M_U] - [K_A][\phi_X][\phi_X]^T[M_U] \quad (14c)$$

Ceasar [42] uses the same approach as Berman by applying the same three constraints but also includes the preservation of the system's total mass and that of the interface forces. A more detailed formulation of the problem is considered at the expense of increased computational effort and applicability to small and banded matrices only.

Similar updating techniques with different Lagrange multipliers have been proposed by Wei [43] and O'callahan and Chou [44]. It has since been suggested that these methods are applicable to special cases only [45]. A detailed review of methods based on Lagrange multipliers is given in [38].

Likewise, Beattie and Smith [46,47], minimise the following equation, assuming the mass matrix is correct:

$$\varepsilon = \|[M_A]^{-0.5}([K_U] - [K_A])[M_A]^{-0.5}\| \quad (15a)$$

subject to $[K_U][\phi_X] = [M_U][\phi_X][\omega_X^2]$ and $[K] = [K]^T$ giving:

$$[AK] = [M_A][\phi_X][\omega_X^2][\phi_X]^T[M_A] - [K_A][\phi_X]([\phi_X]^T[K_A][\phi_X])^{-1}[\phi_X]^T[K_A] \quad (15b)$$

which is comparable to equation 14c. This is solved using algorithms based on multiple variable secant methods for non-linear system optimisation. The use of these additional techniques is demonstrated in [48].

### 2.4.2 Direct method based on matrix perturbation

Chen, Kuo and Garba [49] define the updated mass and stiffness matrices as:

$$[M_U] = [M_A] + [\Delta M]$$

$$[K_U] = [K_A] + [\Delta K]$$

using matrix perturbation theory to obtain:

$$[\Delta M]=[M_A][\phi_A]\left(2[\,I\,]-[\phi_A]^T[M_A][\phi_X] - [\phi_A]^T[M_A][\phi_A]\right)[\phi_A]^T[M_A] \qquad (16a)$$

$$[\Delta K] = [M_A][\phi_A]\left(2[\diagdown\omega_{A\diagdown}^2]+2[\diagdown\omega_{A\diagdown}][\diagdown\omega_{X\diagdown}]-[\phi_A]^T[K_A][\phi_X]-[\phi_A]^T[K_A][\phi_A]\right)[\phi_A]^T[M_A] \qquad (16b)$$

A modified version of this method [18] includes a procedure to update the damping matrix.

### 2.4.3 Error matrix methods

The error matrix between two experimental and analytical matrices is defined as follows:

$$[\Delta S] = [S_x] - [S_A]$$

where [S] can be the stiffness or the mass matrix.

The error matrix method (EMM) proposed by Sidhu and Ewins [50] is defined as:

$$[AK] \cong [K_A]\{[K_A]^{-1} - [K_X]^{-1}\}[K_A] \qquad (17a)$$

where [AK] is assumed to be a small matrix such that $\lim_{n\to\infty}$ [AK]" = [O]. Although in a mathematical sense this requirement has no meaning, it evolved from the assumption that

second order terms are negligible. Thus, the error matrix method is a first order approximation and is only valid for small modelling errors.

Estimating the two pseudo-flexibility matrices using modal data yields:

$$[AK] \cong [K_A]\{ [\phi_A][\omega_A^2]^{-1}[\phi_A]^T - [\phi_X][\omega_X^2]^{-1}[\phi_X]^T\} [K_A] \tag{17b}$$

$$[AM] \cong [M_A] \{[\phi_A][\phi_A]^T - [\phi_X][\phi_X]^T\} [M_A] \tag{17c}$$

Further work on the error matrix method was carried out by He and Ewins [51] and Ewins et al [52]. Some of the publications focusing around the error matrix method include a number of case studies where the success of the method is discussed when applied to a practical example [53-55]. Recent advances on the error matrix method are presented in [56].

A modified version of the error matrix method [57] defines the stiffness error matrix as:

$$[\Delta K] = (([\phi_X][\omega_X^2]^{-1}[\phi_X]^T)^+ - ([\phi_A][\omega_A^2]^{-1}[\phi_A])^+ \tag{18}$$

and uses the singular value decomposition technique (SVD) [58] to calculate the inverse of the pseudo flexibility matrices resulting from correlated experimental and analytical modes. The obvious advantage of this approach is that the analytical system matrices are not required. Especially for large systems, most FE packages do not assemble the full system matrices and accessing the system matrices can be difficult.

Gaukroger [59] obtains a slightly different formulation by including the orthogonality condition:

$$[\Delta K] = \left[[I] - [K_A]\sum_{r=1}^{m}\left(\{\phi_{Xr}\}\omega_{Xr}^{-2}\{\phi_{Xr}\}^T - \{\phi_{Ar}\}\omega_{Ar}^{-2}\{\phi_{Ar}\}^T\right)\right]^{-1} [K_A] - [K_A] \tag{19a}$$

$$[\Delta M] = \left[[I] - [M_A]\sum_{r=1}^{m}\left(\{\phi_{Xr}\}\{\phi_{Xr}\}^T - \{\phi_{Ar}\}\{\phi_{Ar}\}^T\right)\right]^{-1}[M_A] - [M_A] \tag{19b}$$

Brown [32] makes use of vector space theory to obtain further error matrix formulations which depend on the chosen projection of the matrices used. The final expressions are quite similar to the basic formulation of the error matrix method.

Brown [60] also proposes an error location method based on non-zero values of matrix [A] defined as

$$[\Delta] = 0.5\,(2\,[M_A]\,[\phi_X]\,[\omega_X^2]^{-1}\,[\phi_X]^T\,[M_A] - [K_A]\,[\phi_X]\,[\phi_X]^T\,[M_A] - [M_A]\,[\phi_X]\,[\phi_X]^T\,[K_A]) \quad (20)$$

where a large element Aij indicates the location of the error. This matrix-cursor type formulation identifies both mass and stiffness errors concurrently but it cannot distinguish between the two.

### 2.4.4 Matrix mixing methods

The matrix mixing technique used by Link [61] and Caesar [62], combines the experimental mode shapes with the analytical ones to obtain a complete eigenvector set:

$$[K_U]^{-1} = [K_A]^{-1} + ([K_{X\text{-incomplete}}]^{-1} - [K_{A\text{-incomplete}}]^{-1})$$

$$= [K_A]^{-1} + ([\phi_X][\omega_X^2]^{-1}[\phi_X]^T - [\phi_A][\omega_A^2]^{-1}[\phi_A]^T) \quad (21)$$

where the pseudo inverses are also obtained using correlated experimental and analytical modes. A similar approach is used for the mass matrix. The rank deficient matrices can be inverted using the SVD technique. Also, the similarity of this technique and those proposed by Gaukroger and by Lieven should be noted.

### 2.4.5 Methods based on force balance

The dynamic force balance approach taken by Berger, Chaquin and Ohayon [63] assumes that the analytical mass matrix is correct and uses the force balance of the analytical system matrices and the measured modes for error location. For mode r:

$$([K_A] + [\Delta K] - \omega_{Xr}^{-2}[M_A]) \begin{Bmatrix} \phi_{X2} \\ \phi_{X1} \end{Bmatrix}_r = \begin{Bmatrix} 0 \\ F \end{Bmatrix}_r \tag{22}$$

where: $[AK] = \sum_{j=1}^{nxn} pj\ Kj$ and $\{F\}$ is the resultant force vector.

The unknown error coefficients pj can be found either by minimising $\sum_{r=1}^{m}\{F\}_r$ or by iterating for $p_j$.

This method is further developed on a substructure basis [64]. Likewise, Link [65, 66] updates by minimisation of the output error (force residual) using a weighted least squares solution or Bayesian approach.

A similar approach was used by Fisette et al [67] and further developed by Ibrahim et al [68] to obtain a direct method, the so called two-response method, with emphasis on the uniqueness of the solution. The technique is based on the use of any two normal modes and defines the updated matrices as:

$$[K_U] = \Sigma\, a_i\, [K_i]$$
$$[M_U] = \Sigma\, b_i\, [M_i]$$

where $a_i$ and $b_i$ are the unknowns. For experimental mode r the updated matrices which include all $[K_i]$ and $[M_i]$ must satisfy:

$$([K_U] - \omega_r^2[M_U])\{\phi_X\}_r = 0 \tag{23a}$$

substitution gives:

$$[A]_r\{a\}_r = [B]_r\{b\}_r \tag{23b}$$

where $\{a\}$ and $\{b\}$ are vectors containing the unknown $a_i$'s and $b_i$'s respectively, and

$$[A]_r = \left[\{[K_1]\{\phi_X\}_r\}\ \{[K_2]\{\phi_X\}_r\}\ \ldots\right]$$
$$[B]_r = \left[\{\omega_r^2\,[M_1]\{\phi_X\}_r\}\ \{\omega_r^2\,[M_2]\{\phi_X\}_r\}\ \ldots\right] \tag{23c}$$

Similarly, for experimental mode q: $[A]_q\{a\}_q = [B]_q\{b\}_q$

For a unique solution

$$\{a\}_r = \{a\}_q$$
$$\{b\}_r = \{b\}_q \tag{23d}$$

In practical cases a unique solution may not exist and a correlation coefficient determining a uniqueness factor between the two vector sets {a} and {b} is defined in order to be able to select the *most unique* solution (although a mathematician might justifiably argue that is either unique or it is not!) from which the updated system matrices are calculated. Each eigenvalue and corresponding eigenvector obtained by rearranging (23c) into an eigenvalue problem represents a possible solution. For realistic applications this method is found to be of limited success [69].

### 2.4.6 Methods based on orthogonality

The possible use of the orthogonality equations to improve stiffness and mass characteristics of an FE model was first noted by Berman and Flannely in one of the earliest publications concerning systematic use of incomplete measured data [70].

Later, Niedbal et al [71] proposed to rearrange the modal orthogonality equations to obtain:

$$[A]\{b\} = \{B\} \tag{24a}$$

where the unknown vector {b} contains the elements of the updated mass and stiffness matrices while vector {B} contains O's and l's (or O's and h's for mass-normalised eigenvectors). The matrix [A] is defined in terms of the experimental eigenvector elements

$$[A] = \begin{bmatrix} \phi_{11}^2 & 2\phi_{11}\phi_{21} & 2\phi_{11}\phi_{31} & \cdot\cdot & \phi_{n1}^2 \\ \phi_{11}\phi_{12} & \phi_{11}\phi_{21}+\phi_{22}\phi_{11} & \phi_{12}\phi_{31}+\phi_{32}\phi_{11} & \cdot\cdot & \phi_{n1}\phi_{n2} \\ \cdot & \cdot & \cdot & \cdot\cdot & \cdot \\ \cdot & \cdot & \cdot & \cdot\cdot & \cdot \\ \phi_{1m}^2 & 2\phi_{1m}\phi_{2m} & \cdot & \cdot\cdot & \phi_{nm}^2 \end{bmatrix}_X \tag{24b}$$

The above set of linear equations (24a) is then solved for vector {b} using a least squares approximation. This method requires the connectivities of the analytical model only and it

then identifies values for the updated system matrices. A similar approach, referred to as the eigendynamic constraint method, was suggested by To et al [45]. The use of complete eigenvectors is of paramount importance for success of these methods. More recently Nobari et al [72] have derived a new modal-based updating technique analogous to component mode synthesis analysis, a formulation which could also be derived from an eigendynamic constraint approach. An additional feature of this modified approach lies in its applicability to incomplete experimental data.

Creamer and Junkins [73] use a combination of analytical modal data and experimental frequency response data to find model normalisation factors and subsequently to update the system matrices using the orthogonality conditions.

### 2.4.7 Statistics and sensitivity methods

Collins et al [74], in one of the earliest updating publications, used statistics as the basis for updating. The variance associated with the structural parameters is minimised in order to determine those which reproduce the measured modal properties, measurement errors also being included as known uncertainties. This technique was further developed into a sensitivity-type of analysis where an iterative process to determine the structural parameters capable of reproducing measured modal data is employed. Chen and Wada [75] introduced a similar approach for both correlation and updating purposes.

In recent years, sensitivity based methods have increased in popularity due to their ability to reproduce the correct measured natural frequencies and mode shapes. Almost all sensitivity based methods compute a sensitivity matrix [S] by considering the partial derivatives of modal parameters with respect to structural parameters via a truncated Taylor's expansion. The resulting matrix equation is of the form:

$$\{\Delta w\} = [\,S\,]\{\Delta p\} \tag{25}$$

where the elements of { Ap} are the unknown changes in structural elements and { Aw }represents the changes in modal data required , e.g.:

$$\{\Delta w\} = \{\{\Delta\phi_1\}^T, \{\Delta\phi_2\}^T, \{\Delta\phi_3\}^T, \ldots, \{\Delta\phi_m\}^T, \{\Delta\omega_1^2, \text{---}, \Delta\omega_m^2\}^T\}^T \tag{26}$$

The matrix equation (25) is solved for the unknown vector { Ap }, and subsequently { Ap} is used to update the analytical mass and stiffness matrices. A new eigensolution is calculated and the process is repeated until the target modal properties are obtained. It should be noted that the formulation of the sensitivity matrix is based on a Taylor expansion and hence the method is an approximate one. It is customary to retain the first term only in the series [76] (first order sensitivity method) but some researchers also consider the effect of including the second order term (second order sensitivity method).

The sensitivity methods differ in the selection of parameters and the definition of the optimisation constraints (natural frequencies and mode shapes, orthogonality conditions). For the parameter selection the options can be: (i) elements of the [M] and [K] matrices [77], (ii) sub domain matrices [77] or macro elements [78] or (iii) geometric and material properties used as input data to the FE model [79-81]. Lallement and Zhang [82] discuss some of the difficulties related to sensitivity analysis. Janter et al [83] offer a comparison of the interpretability, controllability and compatibility of the sensitivity techniques but all these techniques are CPU intensive as a new eigensolution has to be computed for each iteration.

The sensitivity based methods seem to provide us with an updated analytical model capable of recreating (some of) the measured modes but if applied directly they have the disadvantage of modifying the most sensitive element rather than that in error. It is therefore recommended to localise the error first and allow for changes in the associated elements only. Heylen and Janter [84] use MAC and Spatial-MAC calculations to locate modelling errors. It has also been suggested to include a MAC sensitivity equation in the analysis [85, 86]. User controllability can be incorporated by applying weighting factors and upper and lower bounds on adjustments [87,88].

Dascotte and Vanhonacker [89] also considers the sensitivity approach in combination with confidence estimations on the experimental data and illustrates the relative merits of this method when applied to a practical example [90]. Slater et al [91] use statistical analysis on mode shape difference vectors to localise the errors which can then be corrected using a sensitivity approach. Chen [20] also combines statistical considerations with other updating methods to achieve an optimally corrected model.

### 2.4.8 Energy methods

Roy et al [92,93] derive a set of linear equations comparing the sum of predicted potential and kinetic energies (see equation (6)) for each part of the structure with its experimental counterpart calculated using measured modal masses and stiffnesses. The objective function is minimised employing a least-squares approach or a weighted least squares-approach with error bounds on parameters associated with parts which are updated.

Ladeveze and Reynier [94] also adopt an energy approach, using kinematic constraints, stress-strain equations and the constitutive equations to derive an updating technique. Unfortunately, the method is presented mathematically without adequate explanation for symbols used. As usual, the published examples give good results and the technique appears to be very promising.

### 2.4.9 Updating based on control methods

Minas and Inman, defining the analytical model in a state-space system, adapt commonly-used control techniques such as eigenstructure assignment and pole placement methods to the updating problem [95,96]. The updated stiffness and damping matrices are defined as:

$$[D_U]=[D_A] - [B][G][T_{\dot{x}}] \text{ and } [K_U]=[K_A] - [B][G][T_x] \qquad (27a)$$

where B = constant coefficient feedback matrix
$T_x$ = position measurement transformation matrix (linking measured coordinates to analytical ones)
$T_{\dot{x}}$ = velocity measurement transformation matrix (linking measured coordinates to analytical ones)
G = a closed loop gain matrix to be calculated.

[B] [G] is defined as:

$$[B][G] = -[[M_A][\phi_X][\omega_X^4]+[D_A][\phi_X][\omega_X^2]+[K_A][\phi_X]][[\dot{x}][\phi_X][\omega_X^2]+[x][\phi_X]]^{-1} \qquad (27b)$$

and the gain matrix is calculated iteratively, assigning initial values to [B] $[\dot{x}]$ and $[x]$. The objective function is set to achieve a symmetric updated model:

$$J = \| [B][G][\dot{x}] + [\dot{x}]^T[G]^T[B]^T \| + \| [B][G][x] + [x]^T[G]^T[B]^T \| \qquad (27c)$$

Note that throughout their derivation Minas and Inman include transformation matrices linking measured coordinates to analytical ones. In theory, these transformation matrices should be incorporated in all methods discussed in this chapter. However, most methods assume direct one-to-one correspondence of the measured coordinates with their analytical counterparts.

A similar approach to construct symmetric matrix coefficients is also suggested in[97] with emphasis on updating analytical systems exhibiting rigid body modes. The technique can be labelled as an inverse method, since it requires the solution of an inverse eigensolution problem.

Likewise, Zimmerman and Widengren demonstrate the use of additional constraints and a symmetric eigenstructure assignment method [98].

## 2.5 MODEL UPDATING METHODS USING RESPONSE DATA

The updating methods reviewed so far make use of modal data only and hence frequency response functions (FRF) measurements are not used directly since they have to be analysed first to obtain the required modal data. Historically, this was the most natural way of comparing analytical and experimental models since the former was readily available in modal form. Recently, some methods have been proposed to use response data directly.

### 2.5.1 A direct updating technique using FRF data

Unlike Creamer and Junkins [73], who use experimental frequency response data indirectly to update the system, Lin and Ewins [99] proposed a technique which makes direct use of the measured FRF data. After some algebra, their formulation is reduced to:

$$[\alpha_A(\omega)]\,[\Delta Z(\omega)]\,\{\alpha_X(\omega)\}_i = \{\alpha_A(\omega)\}_i - \{\alpha_X(\omega)\}_i \tag{28a}$$

which can be rewritten as:

$$[A(\omega)]\,\{p\} = \{\Delta\alpha(\omega)\} \tag{28b}$$

where matrix [A(o)] and vector $\{\Delta\alpha(\omega)\}$ are known in terms of measured and/or predicted response properties and the elements of vector $\{p\}$ indicate the position of the error in the original system matrices. It should be noted that [A(o)] and $\{\Delta\alpha(\omega)\}$ can be formed using any combination of discrete FRF data and the system is overdetermined.

### 2.5.2 Techniques based on minimising response equation errors

The frequency response equation error techniques are based on the basic equation of motion:

$$([K_U] - \omega^2[M_U])\,\{u_X(\omega)\}_r = \{F_X(\omega)\} \tag{29}$$

Response equation error updating methods are equivalent to force balance methods employing modal data (see section 2.4.5). Various approaches using response equation error have been proposed:

(i) Natke [100] derives two methods distinguishing between an input and an output residual vector to be minimised using a weighted least squares approach.

(ii) Using the frequency response functions directly without having to have a priori knowledge of the analytical system matrices bring us into the area of structure identification rather than that of updating. A technique for identification using a frequency filter based on least squares solution has been suggested by Mottershead [101]. This technique has also been applied to improve reduced finite element models [102] and is closely related to equation error approaches.

(iii) Friswell and Penny [103], based on the approach proposed by Mottershead, develop an equation error algorithm via Taylor expansion of the updated system matrices with reference to the analytical system. The coordinate incompleteness is overcome by a

$$[\alpha_A(\omega)]\,[\Delta Z(\omega)]\,\{\alpha_X(\omega)\}_i = \{\alpha_A(\omega)\}_i - \{\alpha_X(\omega)\}_i \tag{28a}$$

which can be rewritten as:

$$[A(\omega)]\,\{p\} = \{\Delta\alpha(\omega)\} \tag{28b}$$

where matrix [A(o)] and vector $\{\Delta\alpha(\omega)\}$ are known in terms of measured and/or predicted response properties and the elements of vector $\{p\}$ indicate the position of the error in the original system matrices. It should be noted that [A(o)] and $\{\Delta\alpha(\omega)\}$ can be formed using any combination of discrete FRF data and the system is overdetermined.

### 2.5.2 Techniques based on minimising response equation errors

The frequency response equation error techniques are based on the basic equation of motion:

$$([K_U] - \omega^2[M_U])\,\{u_X(\omega)\}_r = \{F_X(\omega)\} \tag{29}$$

Response equation error updating methods are equivalent to force balance methods employing modal data (see section 2.4.5). Various approaches using response equation error have been proposed:

(i) Natke [100] derives two methods distinguishing between an input and an output residual vector to be minimised using a weighted least squares approach.

(ii) Using the frequency response functions directly without having to have a priori knowledge of the analytical system matrices bring us into the area of structure identification rather than that of updating. A technique for identification using a frequency filter based on least squares solution has been suggested by Mottershead [101]. This technique has also been applied to improve reduced finite element models [102] and is closely related to equation error approaches.

(iii) Friswell and Penny [103], based on the approach proposed by Mottershead, develop an equation error algorithm via Taylor expansion of the updated system matrices with reference to the analytical system. The coordinate incompleteness is overcome by a

dynamic reduction, the so called zero$^{th}$ order modal transformation technique [104], of the analytical system to the measured coordinates. The updating parameters are confined to a few physical properties only.

(iv) Larsson and Sas [105] also use Taylor expansion of the dynamic stiffness matrix coupled with a modified equation error approach. Their formulation is similar to equation (28a) of section 2.5.1. One immediate advantage seems to be the use of a reduced system which is obtained by deleting the unmeasured coordinates from the analytical receptance matrix which is inverted again to obtain an dynamic-equivalent reduced dynamic stiffness matrix.

(v) Conti and Donley [106] update the full FE model using response data by minimising the residual error between the analytical and experimental response. To overcome coordinate incompatibility the analytical system is reduced to the size of the experimental data set using one of 4 proposed reduction techniques. The same transformation is applied to the sub-domain matrices to be updated.

(vi) Ibrahim et al [107] use an approach similar to their normal mode formulation (section 2.4.5). The equation error set of linear equations is rearranged into an eigenvalue problem which yields *the unique* solution. The advantage over the modal approach is that, the final updating values can be scaled appropriately due to the surplus of data.

### 2.5.3 Updating methods using time domain data

The area of updating using time domain data remains largely unaddressed. The equation error formulations used in frequency and modal domain methods (equations (22) and (29)) are in principle applicable to time domain data. Time domain methods will have similar advantages to their frequency domain counterparts in that no modal analysis of the measured data is required. However, they will lack the direct link between model and dynamic response as is obvious in updating techniques using modal data or frequency response data. More importantly, simultaneous measurement of displacement, velocity and acceleration is required, which, in practice, is very difficult, if not impossible. Another drawback is that damping predictions cannot be made in the time domain.

## 2.6 CONCLUDING REMARKS

Although a vast amount of research has been dedicated to the area of model updating, results so far suggest that the problem remains largely unsolved and a very substantial amount of work is still needed. The sheer volume of techniques proposed and the number of variations tried also suggest that this research field is far from reaching maturity. In any case, the only successful updating exercises seem to be those for which the errors are known in advance by the researchers.

(i) Although some publications [39,108,109] comment upon the uniqueness aspect of the updating problem, in most cases the solution seems to depend on the chosen parameters and constraints and the particular updating technique employed.

(ii) On a more philosophical note, the expectations from the model updating process are not formulated very clearly in the sense that a well-updated model is not or ***cannot be*** defined concisely: the maximum allowable discrepancies between the two models and their relationship to measurement accuracy need to be investigated further.

(iii) Some of the current literature seems to be dealing with ***treasure-hunt*** style updating problems where a number of elements in the ***so-called*** experimental model are modified and the assumption of one-to-one correspondence between the two models is made. In practical cases, sources of error are often in boundary conditions and/or structural joints and hence the idea of finding the ***modified*** elements is far from being realistic.

(iv) It seems that error predictions using modal based updating methods of section 2.4 depend largely on the reduction or expansion technique used and there is little agreement between the various methods suggested.

(v) Sensitivity-based methods seem quite promising in the sense that they reproduce the desired modal properties. Some of the serious limitations lie in the fact that: (a) the most sensitive element (rather than that in error) is changed and (b) knowledge of the element mass and stiffness matrices as well as those of the sub domains which constitute the model is required. The latter would in turn necessitate a different (and much more tedious) modelling route for finite element analyses, a hardly realistic proposition when the size of the finite element model is large.

(vi) The recently-proposed FRF-based methods are perhaps even more promising since each individual FRF measurement contains information on out-of-range modes as well as on those within the frequency range of interest and it is possible to specify measurement and excitation points to ensure maximum efficiency. Another advantage may well lie in the direct use of raw measured data, thus eliminating lengthy modal analysis procedures.

(vii) The use of true experimental data is rather an exception, almost all reported cases dealing with theoretically-generated data only. Some of the anticipated additional difficulties -which will render the formulation of a successful model updating process even more elusive than it is now- are listed below.

- Mapping problem. The test coordinate grid is very often different from the finite element mesh. Indeed, it would be very expensive, if at all possible, to measure at all finite element nodes and in all co-ordinate directions. Also, there may be some physical constraints on the actual structure rendering some points totally inaccessible.

- Effect of damping and complex modes. Experimental and analytical data sets are incompatible due to the fact that the analytical model usually yields real undamped modes while the modal tests lead to complex modes with damping. Often the normal mode approach is used in which case the complex modes are *converted* to real ones [79,110-112].

- Experimental and modal analysis errors. It is often conveniently ignored that the measured data also contain systematic and random errors. Also the reliability of analysed data may further be put into question by inaccuracies introduced during modal analyses, computational or superfluous modes being one of the side effects of some curve-fitting techniques employed.

- Algebraic manipulation of noise-polluted matrices can give rise to large errors, especially during inversion [113].

# CHAPTER 3

# UPDATING USING MODAL DATA; THE ERROR MATRIX METHOD

## 3.1 INTRODUCTION

The purpose of this chapter is to explore some of the advantages and disadvantages of model updating using modal data with the error matrix method.

The most obvious disadvantage of using modal properties is that the measured response data are not used directly but have to be transformed into modal data via modal analysis. Modal analysis, despite advancements on the various analysis techniques, introduces additional inaccuracies into the experimental data set. A few typical examples of such error are:

(i) inherent assumptions in the modal analysis techniques (e.g. linearity);
(ii) operator misjudgement; and
(iii) introducing superfluous modes and/or omitting modes.

Modal analysis also takes time, a valuable commodity, and the experimental modes obtained are complex while their analytical counterparts from the FE model are real undamped modes. The experimental modes are usually ***converted*** into real modes although this is not a prerequisite for the error matrix method which can deal with complex modal data.

However, one of the advantages of using the experimental modal data is that it gives a relatively easy platform for comparison purposes. As vibration properties are usually defined in terms of natural frequencies and mode shapes, it follows that early updating methods were based on modal data. We will now focus on one modal-based updating technique, the error matrix method (EMM), to illustrate difficulties encountered during model updating on a few numerical case studies.

## 3.2 THE ERROR MATRIX METHOD

### 3.2.1 Theory

The standard error matrix method, first proposed by Sidhu and Ewins [50], is summarised as follows:

The stiffness error matrix is defined as: $[AK] = [K_X] - [K_A]$ (la)

and hence: $$[K_X] = [K_A] + [\Delta K] \quad \text{(lb)}$$

Inverting both sides of equation (lb) and using the binomial matrix expansion under the assumption that [AK] is a *small* matrix such that $\lim_{n\to\infty} [\Delta K]^n = [0]$:

$$[K_X]^{-1} = [K_A]^{-1} - [K_A]^{-1}[\Delta K]\,[K_A]^{-1} + [K_A]^{-2}[\Delta K]^2\,[K_A]^{-1} - \ldots\ldots \quad (2)$$

retaining the first-order term only and rearranging gives:

$$[\Delta K] \cong [K_A]\,\{\,[K_A]^{-1} - [K_X]^{-1}\,\}\,[K_A] \quad (3)$$

As $[K_X]$ is unknown, both the experimental and analytical flexibility matrices are expressed using correlated modes to generate pseudo-flexibility matrices, and hence:

$$[AK] \cong [K_A]\,\{[\phi_A][\omega_A^2]^{-1}[\phi_A]^T - [\phi_X][\omega_X^2]^{-1}[\phi_X]^T\}\,[K_A] \quad (4a)$$

Similarly for [AM]:.

$$[AM] \cong [M_A]\,\{[\phi_A]\,1\,[\phi_A]^T - [\phi_X][\phi_X]^T\}\,[M_A] \quad (4b)$$

### 3.2.2 Case studies on a 10 DOF system

The 10 DOF lumped parameter system of **Fig. 3.1,** was employed to investigate the effectiveness of the EMM. The experimental data were simulated using an analytical model, changing $m_7$ and $k_3$ as indicated in **Fig. 3.1.** Note that from here on italics are

*used* to distinguish between simulated experimental data and **measured experimental data. Three** noise-free *experimental data* sets were considered:

(a) 10 modes at 10 coordinates (complete *experimental* model),

(b) 5 modes at 10 coordinates (mode-incomplete *experimental* model),

(c) 5 modes at 5 coordinates (coordinate- and mode-incomplete *experimental* model).

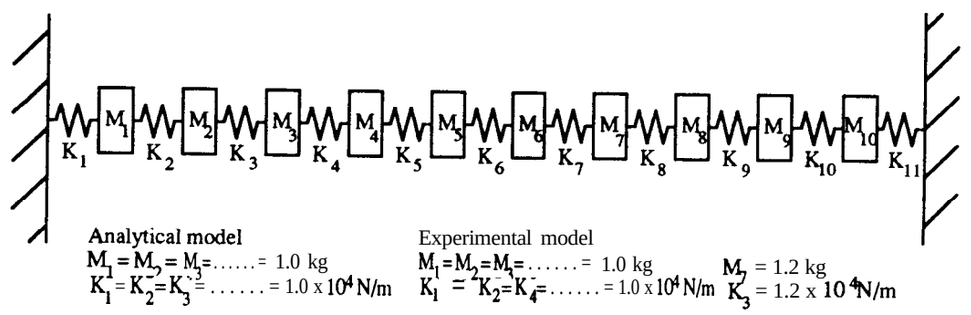


**Fig. 3.1:** *Experimental* and analytical 10 DOF systems

In test case (a), the unrealistic situation of a fully-measured system, the EMM located the errors correctly. The error matrices, normalised with respect to the maximum error, are shown in **Fig. 3.2a**. Despite a full experimental model and no added noise, the located errors had discrepancies of 15% for mass and 17% for stiffness error values when compared with the reference values. However, the updated natural frequencies and mode shapes compared very well to their *experimental* counterparts. The discrepancy arose due to the first order approximation in the derivation of the error matrix equation.

The error matrices for case (b) also indicated the modelling errors at the correct positions. However, mass-related modelling errors appeared in the stiffness error matrix and vice versa, and spurious modelling errors also emerged. Results for case (b) were better than those of case (c), where *experimental data* were both coordinate- and mode- incomplete. For test cases (c) a **Guyan** reduced analytical model was used to ensure coordinate compatibility and the two initial modelling errors were spread through the error matrices. The main disadvantages of model reduction **are** that (i) the connectivities of the original model are lost and (ii) extra inaccuracies are introduced, especially as the experimental coordinates are often not suitable to be chosen as masters. The combined effect of (i) and (ii) is clearly shown in **Fig. 3.2c**.

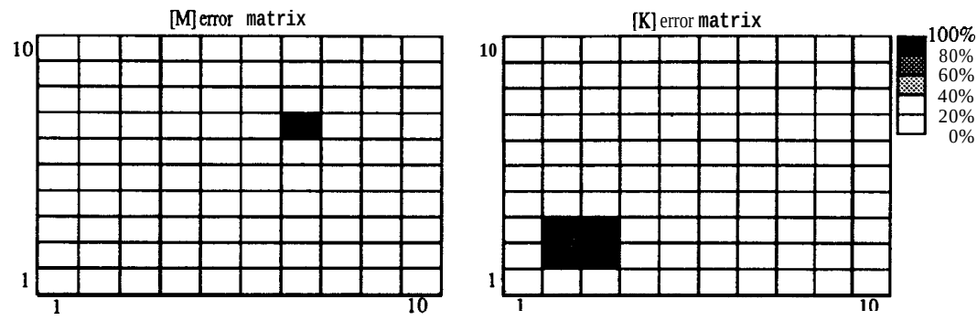


(a) Test case a, ***experimental*** system fully known

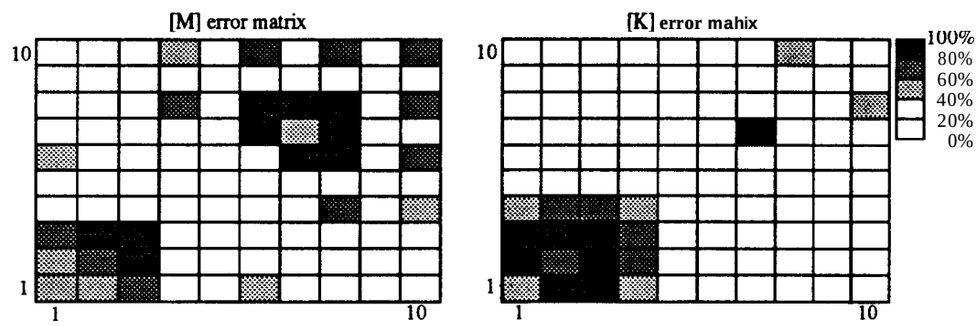


(b) Test case b, 5 modes ***measured*** at 10 coordinates

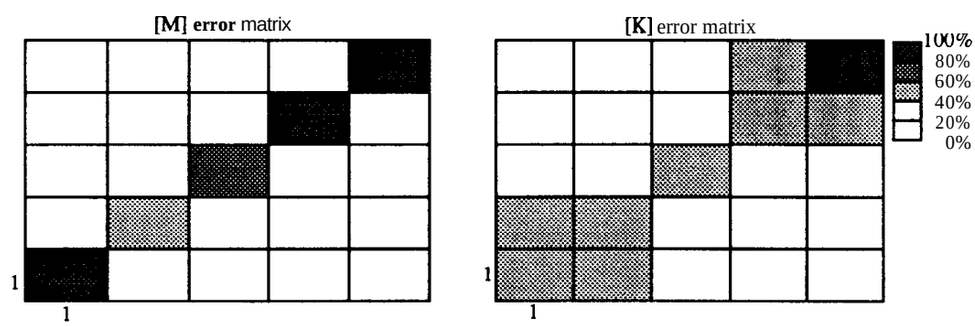


(c) test case c, 5 modes ***measured*** at 5 coordinates

**Fig. 3.2:** Error matrices for a 10 DOF systems

The updated modal solution for case (b) gave improved natural frequencies, MAC and COMAC values for the first 5 modes. The natural frequencies of the higher, ***unmeasured,*** modes were similar to those of the original analytical model but the MAC and COMAC values, especially for modes 9 and 10 decreased. For case (c) the error location was not very successful, although the MAC and COMAC values between the 5 updated analytical and ***experimental*** modes improved. However, differences in natural frequencies between ***experimental*** and updated models were similar to, or even worse than, the differences prior to updating.

## 3.3 AN IMPROVED PROCEDURE FOR THE EMM

As indicated in case (a), the EMM can be successful in error location but even for a fully-measured noise-free system the magnitude of the predicted errors are not necessarily correct. The numerical accuracy of the EMM formulation can be improved by including second-order terms of the binomial matrix expansion given in equation (2), but this would increase the computational effort substantially. An alternative approach to improve the EMM is suggested below.

### 3.3.1 Theory

Rearranging the following identity,

$$[[A] + [B]] = [A]^{-1} - [[A]+[B]]^{-1}[B][A]^{-1} \tag{5}$$

one obtains:

$$[B] = [[A]+[B]]\,[[A]^{-1} - [[A]+[B]]^{-1}]\,[A] \tag{6}$$

Letting: $[A] = [K_A]$

and $[[A]+[B]] = [K_X]$ **(7)**

yields:

$$[AK] = [K_x]\,[\,[K_A]^{-1} - [K_X]^{-1}]\,[K_A] \tag{8}$$

which is identical in form to equation **(3).** However, equation (3) is an approximation derived from perturbation theory while equation (8) is exact. From equation **(8):**

$$[\Delta K] = [K_X]\,[K_A]^{-1}[K_A] - [K_X]\,[K_X]^{-1}\,[K_A] = [K_X] - [K_A]$$

Substituting $[K_X]$ in equation (8) by $[K_A]+[\Delta K]$ one obtains:

$$[AK] = [K_A][[K_A]^{-1} - [K_X]^{-1}]\,[K_A] + [\Delta K]\,[[K_A]^{-1} - [K_X]^{-1}]\,[K_A] \tag{9}$$

Now, a new error matrix, [AK'], can be obtained by substituting the first estimate of [AK] from the standard error matrix method (equation (3)), i.e.:

$$[\Delta K] = [K_A]\,[[K_A]^{-1} - [K_X]^{-1}]\,[K_A]$$

into equation (9), to obtain:

$$[\Delta K'] = [\Delta K] + [\Delta K]\,\{\,[K_A]^{-1} - [K_X]^{-1}\,\}\,[K_A] \qquad (10a)$$

Calculation of [AK'] will require very little extra computational effort as it only involves one extra matrix multiplication.

Similarly: $$[\Delta M'] = [\Delta M] + [\Delta M]\,\{\,[M_A]^{-1} - [M_X]^{-1}\,\}\,[M_A] \qquad (10b)$$

### 3.3.2 Case studies on a 10 DOF system

The previous 3 cases of the 10 DOF lumped parameter system of section 3.2.2 were used to compare the improved error matrix procedure (EMM') with the standard error matrix method (EMM). The indicated errors for test case (a) are given in **Table 3.1.**

| | true error | EMM | EMM' |
|---|---|---|---|
| $\Delta K_{max}$ | 0.20000 | 0.16667 (17%) (15%) | 0.19544 (2.8%) (2.4%) |

**Table 3.1:** Maximum errors in a 10 DOF system located using EMM and the improved EMM procedure (EMM')

**Table 3.1** clearly shows that the new error matrix procedure gave improved numerical values (less than 3% discrepancy) compared to the standard error matrix method (17% and 15% discrepancy). Comparing the updated model natural frequencies with their *experimental* counterparts it was found that the maximum discrepancy was less than 1% at mode 10 compared with 4% at mode 10 for the standard EMM. All MAC and COMAC values of the updated mode shapes of case (a) were between 0.996 and 1.000 for the EMM and equal to 1.000 for the improved procedure. Hence for this test case the advancement with respect to updated mode shapes was not very significant.

For case (b) both methods again showed similar trends in error localisation: the new procedure located the maximum stiffness error at the correct position (coordinate 3) but substantial additional errors also appeared at the mass error locations. The standard method, on the other hand, also indicated correctly an error at coordinate 3 but the maximum error was shown erroneously at coordinate 7.

Considering the first 5 natural frequencies of the updated model, the maximum discrepancies compared with the *measured* modes were 1% and 3% for mode 5 for the improved and standard error matrix method respectively. Although the natural frequency improvement was noticeable, only a minor improvement in mode shapes was observed as shown in **Fig. 3.3.**

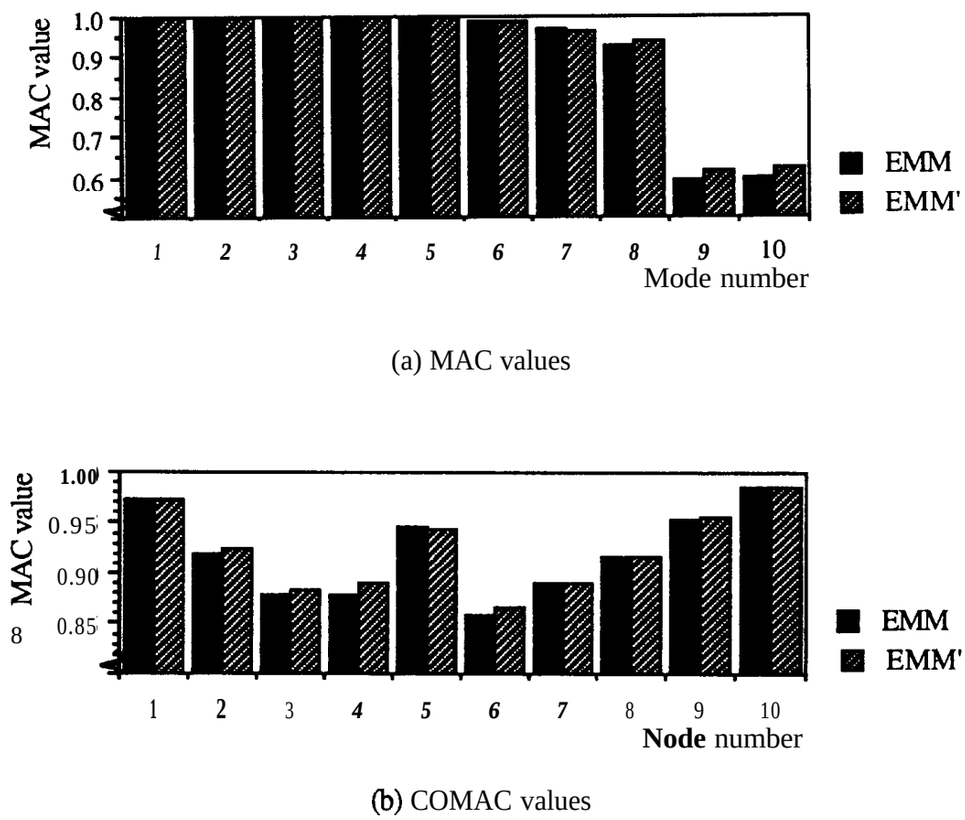


**Fig. 3.3:** MAC and COMAC values for updated 10 DOF models using the EMM and the improved error matrix procedure (EMM'), test case b.

The new procedure did not improve the location aspect of the error matrix method for case (c) where, due to the Guyan reduction, the modelling errors were spread over many coordinates. And, as for case (b), the updated natural frequencies obtained using the

improved error matrix procedure were closer to the *experimental* frequencies than those obtained using the standard EMM. For both error matrix procedures the MAC and COMAC values improved substantially after updating to values similar to those obtained for the first 5 modes of case (b), slightly better numerical results were again obtained for EMM' compared to the standard EMM .

Both methods should be used with caution in the case of coordinate incompleteness because of the spreading of errors as a result of the Guyan reduction. The limitations of the Error Matrix Method using Guyan reduced matrices, are common to all updating techniques using modal data, with the possible exception of the sensitivity methods (section 2.4.7), indicating the necessity for mode expansion (Chapter 4).

## 3.4 THE GARTEUR III EXERCISE

The GARTEUR exercises play an important role to examine and compare the effectiveness of updating techniques developed by the various organisations represented in the GARTEUR (Group for Aeronautical Research and Technology in Europe). The second test case considered here is the third GARTEUR exercise which consists of a grounded 2D frame structure **(Fig 3.4).**

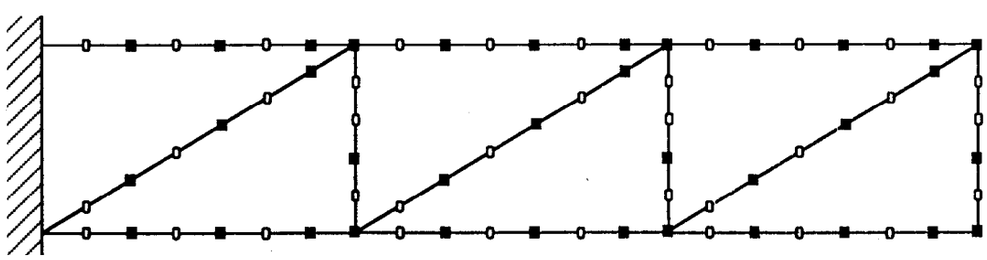

**Fig. 3.4:** The GARTEUR structure

The complete 2D model consisted of 72 nodes resulting in 144 translational (x, y) and 72 rotational (9,) degrees of freedom. The same basic model was used to derive the *experimental* data but some unknown changes had been made to the cross sectional area and second moment of area of some of the elements The *experimental* data, with 10% of random noise applied to the mode shapes and 3% to the natural frequencies, consisted of the first 10 modes with shapes *measured* in the x and y directions of the 36 nodes indicated by ■ in **Fig. 3.4.**

The correlated mode shape MAC and COMAC values of the raw data are given in **Fig. 3.5.** The COMAC plot shows that the erroneous areas can be mainly expected in the first bay. Both the standard error matrix method and the improved error matrix procedure were applied using a Guyan reduced analytical model.

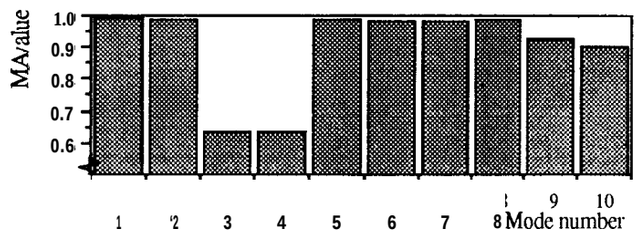


(a) MAC values

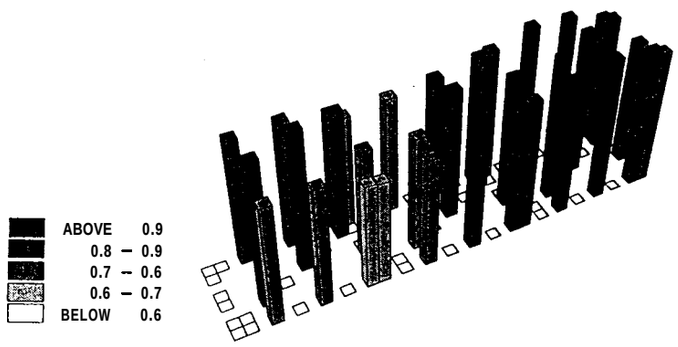


(b) COMAC values

**Fig. 3.5:** GARTEUR III MAC and COMAC values

A global indication of errors was obtained by taking the mean error matrix values in the x and y directions of each node (on the leading diagonal of the error matrices) and these were superimposed on a grid plot of the GARTEUR structure **(Figs. 3.6** and 3.7). A very similar error location pattern can be observed for results obtained by EMM **(Fig.3.6)** and EMM' **(Fig. 3.7)** . The errors indicated by the EMM had spread out more and were smaller compared with the errors obtained using the new error matrix procedure (EMM') which were more localised and considerably larger in size at certain coordinates.

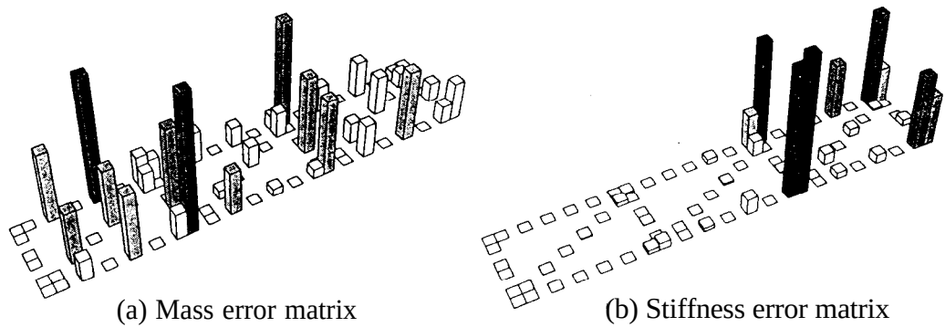

(a) Mass error matrix (b) Stiffness error matrix

**Fig. 3.6:** GARTEUR III, standard EMM error location (leading diagonal values)

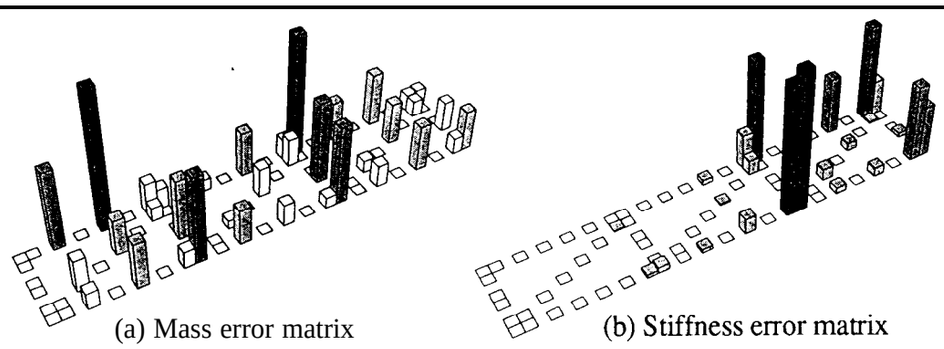

(a) Mass error matrix (b) Stiffness error matrix

**Fig. 3.7:** GARTEUR III, improved error matrix procedure (EMM') error location

Comparing the updated modal solutions to their *experimental* counterparts, the natural frequency correlation and MAC values were, unfortunately, worse than before the updating process **(Fig. 3.8)** and the COMAC values were only marginally better than before. This is an indication that the error matrix algorithms are probably not suited to large noise-polluted incomplete models.

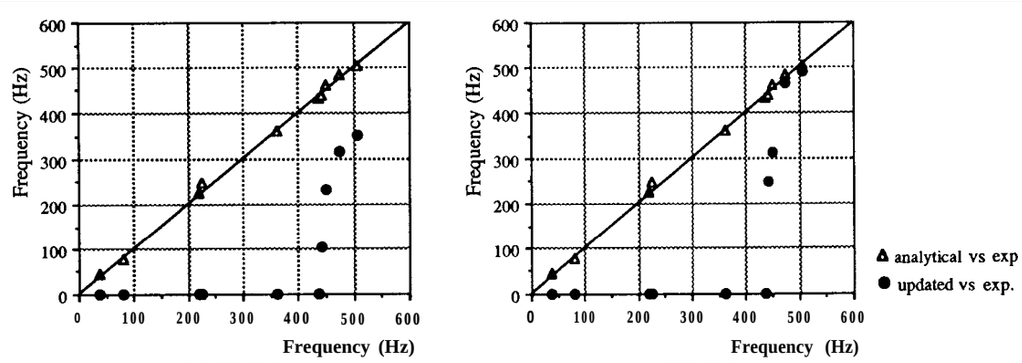


(a) EMM (b) EMM

**Fig. 3.8:** GARTEUR III, updated natural frequencies against *experimental* ones

The true errors, shown in Fig. 3.9, reaffirm that neither the error matrix method nor the improved error matrix procedure was very successful in error location. This was most likely due to the adverse effects of the Guyan reduction of the analytical matrices necessary to obtain the correct analytical system size. The high percentage noise applied to the *experimental* data also had adverse effects.

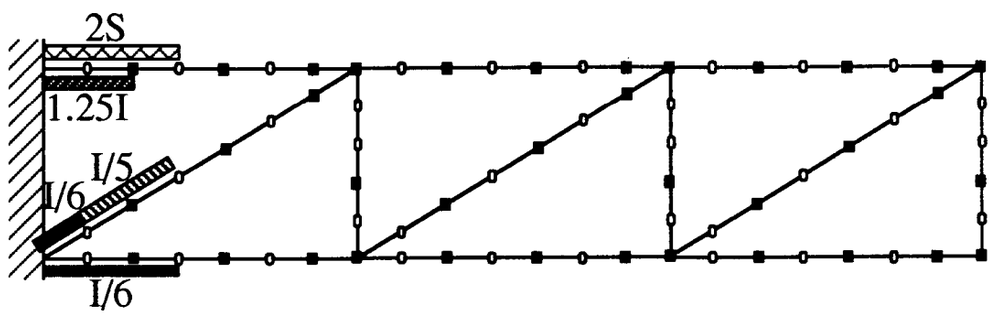


Fig. 3.9: Modelling errors of the GARTEUR III exercise

## 3.5 CONCLUDING REMARKS

In this chapter an updating technique using modal data, namely the Error Matrix Method (EMM), has been used to illustrate some of the difficulties encountered during updating.

An improved EMM procedure, derived from a mathematical identity rather than perturbation theory, is proposed. It requires only one extra matrix multiplication in addition to the standard EMM. The new error matrix procedure (EMM') gives numerically better results for the unrealistic case of complete *experimental* models but for cases of incomplete experimental data, the improvements are negligible since there are inherent difficulties within the basic algorithm. The numerical study of a larger system confirmed the above findings.

The main conclusion in this chapter is the inadequacy of the error matrix method. Although more successful case studies are reported in published literature results seem to be both analyst- and case-dependent. If the limitations derive from the reduction process, coordinate expansion is probably a possible way of overcoming some of the difficulties due to Guyan reduction.

# CHAPTER 4

# EXPANDING MEASURED MODE SHAPES

## 4.1 INTRODUCTION

One of the most common problems in updating FE models is the coordinate incompleteness of the experimental model, which can be due to (i) difficulties in the measurement of rotations and/or (ii) physically inaccessible coordinates (e.g. internal coordinates) and/or (iii) the size of the FE model bearing in mind that measuring many coordinates is expensive and time-consuming. Most updating techniques require both data sets to be expressed in the same coordinate system. There are two possibilities to overcome coordinate incompatibility: either by model reduction, choosing the measured coordinates as masters in the FE model, or by mode shape expansion, expanding the experimental modes to all FE coordinates. As was shown in chapter 3, the main disadvantages of model reduction are that (i) the connectivities of the original model are lost, and (ii) extra inaccuracies are introduced, especially as the experimental coordinates are often not the best points to choose as masters. Therefore, experimental mode shape coordinate expansion is considered the next logical step.

Two methods of mode expansion are investigated in this chapter. The method which appears to be most commonly used is the inverse reduction technique[25], which uses the analytical mass and stiffness matrices to expand the incomplete mode shapes obtained in a typical modal test. Another method recently proposed [29,30] expands the experimental mode shapes on the basis of the analytical ones. These two methods are considered to be the most promising of the four mentioned in chapter 2, and therefore they will be investigated in some more detail.

## 4.2 THEORETICAL BACKGROUND

### 4.2.1 The Inverse Reduction Method

**The** inverse reduction technique starts from the basic equation:

# CHAPTER 4

# EXPANDING MEASURED MODE SHAPES

## 4.1 INTRODUCTION

One of the most common problems in updating FE models is the coordinate incompleteness of the experimental model, which can be due to (i) difficulties in the measurement of rotations and/or (ii) physically inaccessible coordinates (e.g. internal coordinates) and/or (iii) the size of the FE model bearing in mind that measuring many coordinates is expensive and time-consuming. Most updating techniques require both data sets to be expressed in the same coordinate system. There are two possibilities to overcome coordinate incompatibility: either by model reduction, choosing the measured coordinates as masters in the FE model, or by mode shape expansion, expanding the experimental modes to all FE coordinates. As was shown in chapter 3, the main disadvantages of model reduction are that (i) the connectivities of the original model are lost, and (ii) extra inaccuracies are introduced, especially as the experimental coordinates are often not the best points to choose as masters. Therefore, experimental mode shape coordinate expansion is considered the next logical step.

Two methods of mode expansion are investigated in this chapter. The method which appears to be most commonly used is the inverse reduction technique[25], which uses the analytical mass and stiffness matrices to expand the incomplete mode shapes obtained in a typical modal test. Another method recently proposed [29,30] expands the experimental mode shapes on the basis of the analytical ones. These two methods are considered to be the most promising of the four mentioned in chapter 2, and therefore they will be investigated in some more detail.

## 4.2 THEORETICAL BACKGROUND

### 4.2.1 The Inverse Reduction Method

The inverse reduction technique starts from the basic equation:

$$[[K_X] - \omega_X^2 [M_X]]\{\phi_X\}=0 \tag{1}$$

As the experimental mass and stiffness matrices are unknown, they are replaced by the analytical system matrices. The coordinates are rearranged such that the measured coordinates are in the top part of the matrix equation (subscript 1):

$$\left[ \begin{bmatrix} K_{11} & K_{12} \\ K_{21} & K_{22} \end{bmatrix}_A - \omega_X^2 \begin{bmatrix} M_{11} & M_{12} \\ M_{21} & M_{22} \end{bmatrix}_A \right]_{NxN} \begin{Bmatrix} \phi_1 \\ \phi_2 \end{Bmatrix}_X = \begin{Bmatrix} 0 \\ 0 \end{Bmatrix} \tag{2}$$

If one assumes that errors are predominantly in the measured coordinates, the lower matrix equation will be more correct. Rearranging the lower matrix equation gives the following expression for the unmeasured coordinates:

$$\{\phi_{2X}\}_{(N-n)x1} =$$

$$-[[K_{22_A}] - \omega_X^2 [M_{22_A}]]^{-1}_{(N-n)x(N-n)} [[K_{21_A}] - \omega_X^2[M_{21_A}]]_{(N-n)xn} \{\phi_{1X}\}_{nx1} \tag{3}$$

The inverse reduction method is also known as 'Kidder's method', 'physical expansion method' or 'dynamic expansion'.

### 4.2.2 The Modal Transformation Expansion Method

The second expansion technique uses the analytical mode shapes rather than the analytical system matrices. It is assumed that each experimental mode can be expressed as a linear combination of the analytical mode shapes:

$$\{\phi_X\} = [\phi_A]\{\gamma\} \tag{4}$$

This can be considered a valid assumption as the modes of the analytical model are describing the same subspace as the true structure if there are enough degrees of freedom in the analytical model.

The matrices can be rearranged such that the known measured coordinates are contained in the top part of the matrix equation:

$$\begin{Bmatrix} \phi_{1_X} \\ \phi_{2_X} \end{Bmatrix}_{Nx1} = \begin{bmatrix} \phi_{11} & \phi_{12} \\ \phi_{21} & \phi_{22} \end{bmatrix}_{A_{NxN}} \begin{Bmatrix} \gamma_1 \\ \gamma_2 \end{Bmatrix}_{Nx1} \tag{5}$$

Alternatively $\{\phi_{1_X}\}$ can be expressed by $[\phi_{11}]\{\gamma_1\}$, so it is possible to proceed by setting $\{\gamma_2\} = \{0\}$. This has the effect of assuming that the higher analytical modes contribute little to the lower experimental modes and equation (5) becomes:

$$\begin{Bmatrix} \phi_{1_X} \\ \phi_{2_X} \end{Bmatrix}_{Nx1} \cong \begin{bmatrix} \phi_{11_A} \\ \phi_{21_A} \end{bmatrix}_{Nxm} \{\gamma_1\} \tag{6}$$

$\{\gamma_1\}$ can then be found from the known coordinates:

$$\{\gamma_1\}_{mx1} = [\phi_{11_A}]^+_{nxm} \{\phi_{1_X}\}_{nxl} \tag{7}$$

Provided the inverse of $[\phi_{11}]$ exists:

$$\begin{Bmatrix} \phi^E_X \end{Bmatrix}_{Nx1} = \begin{bmatrix} \phi_{11} \\ \phi_{21_A} \end{bmatrix} \begin{bmatrix} \phi_{11_A} \end{bmatrix}^+_{nxm} \begin{Bmatrix} \phi_{1_X} \end{Bmatrix}_{nx1} \tag{8}$$

where: N = number of analytical coordinates;
n = number of measured coordinates; and
m = number of modes used for expansion.

If n is greater than m, the system is overdetermined and either the generalised inverse or the SVD inversion technique can be used to invert $[\phi_{11}]$. For an overdetermined system, the expanded experimental mode shapes will be smoothed if the regenerated measured coordinates are retained after expansion. This method is referred to as the modal transformation method where the transformation matrix is based on the experimental and

analytical mode shapes as described in equation (8). Expanding several modes simultaneously:

$$\left[\{\phi^{E}_{1_X}\} \ldots \{\phi^{E}_{m_{x_X}}\}\right]_{Nxm_x} = \begin{bmatrix}\phi_{11_A}\\ \phi_{21_A}\end{bmatrix}\left[\{\gamma_1\}\ \{\gamma_2\} \cdots \{\gamma_{m_x}\}\right]_{nxmx} = \begin{bmatrix}\phi_{11_A}\\ \phi_{21_A}\end{bmatrix}[T] \quad (9)$$

Alternative derivations of the modal transformation method are known as 'SEREP' [26]. SEREP is defined as:

$$[\phi]_{X_{Nxm_x}} = [\phi]_{Nxm}[\phi]^{+}_{nxm}[\phi_{11}]_{X_{nxm_x}} = [T'][\phi_{11}]_{X_{nxm_x}} \quad (10)$$

where [T'] can be calculated using (i) analytical modal data only, (ii) experimental modal data only or (iii) a combination of the two modal data sets. Of these three number (i), FE based SEREP, is shown to be most reliable [53]. For the FE based SEREP equation (10) is the same as equation (9).

## 4.3 CASE STUDIES

### 4.3.1 Test cases

Four test cases of increasing complexity were used to investigate the various aspects of the two expansion techniques:

(a) a 10-DOF lumped parameter model **(Fig. 4.1)**, to investigate the importance of mode selection and the various inversion techniques;
(b) a 100-DOF lumped parameter model **(Fig. 4.2)**, to investigate the effect of a small measured-to-unmeasured coordinates ratio;
(c) a 2D clamped beam **(Fig. 4.3)**, to investigate the behaviour of expanded rotational coordinates; and
(d) a 3D frame **(Fig. 4.4)**, representing a typical engineering structure.

For each structure various incomplete experimental data sets, i.e. with different correspondence factors, were expanded using the two methods under investigation. The correspondence factor is defined as the ratio of unmeasured coordinates to the total number of (analytical) coordinates. For each test case the expanded mode shapes

were compared with their true counterparts by visual comparison and by calculation of MAC values. Typical examples for each test case and various are also shown in **Figs. 4.1-4.4.**

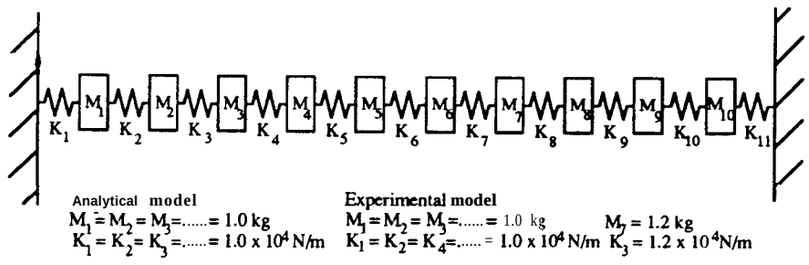


(a) Analytical and experimental models

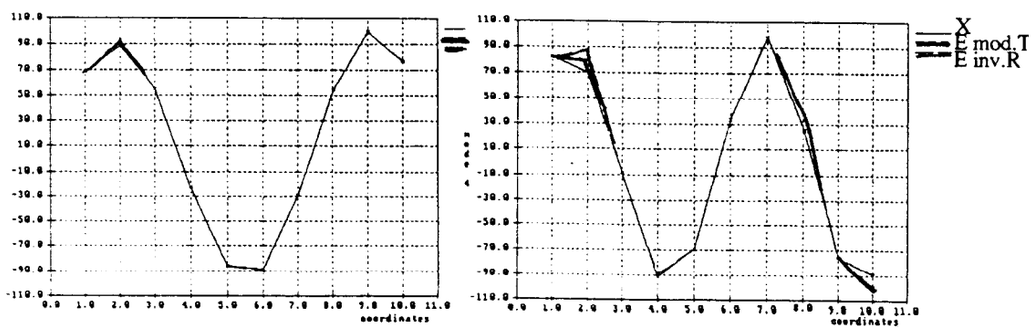


mode **3** mode **4**

(b) Expanded mode shapes for a correspondence factor of 50%

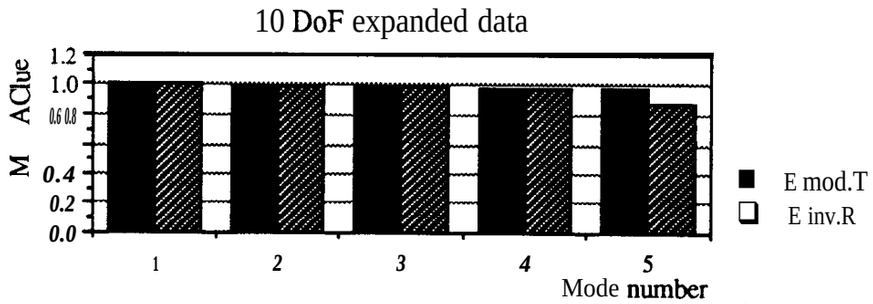


(c) Typical MAC values of expanded mode with true *experimental* counterpart

**Fig. 4.1:** Mode shape coordinate expansion of a 10 DOF system

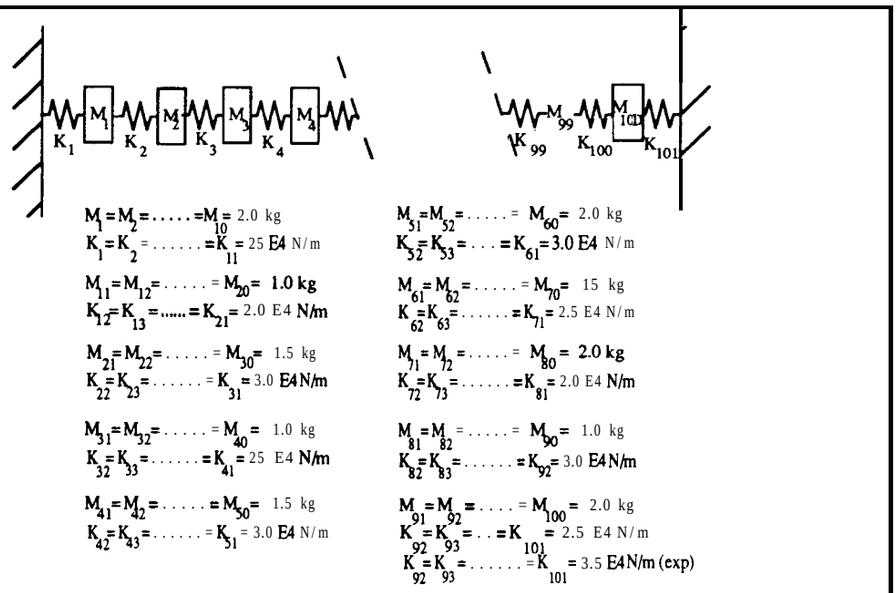


(a) Analytical and experimental models

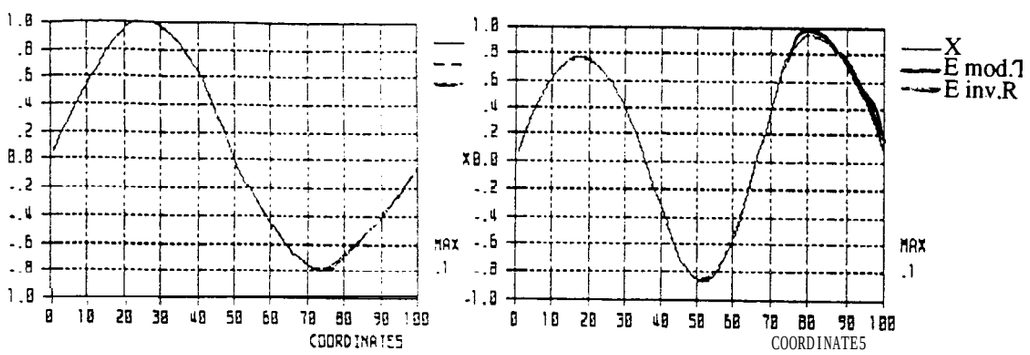


mode 2 mode 3

(b) Expanded mode shapes for a correspondence factor of 5%

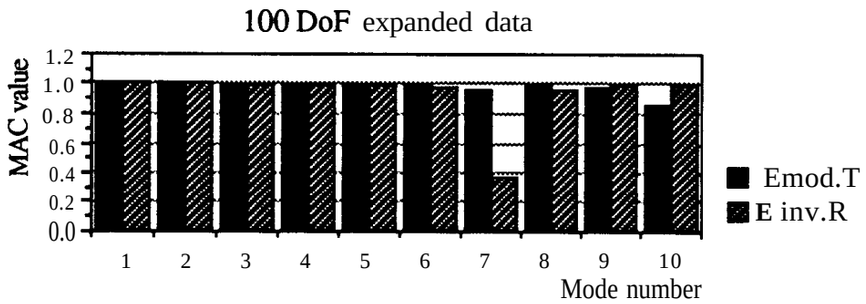


(c) Typical MAC values of expanded mode with true *experimental* counterpart

Fig. 4.2: Mode shape coordinate expansion of a 100 DOF system

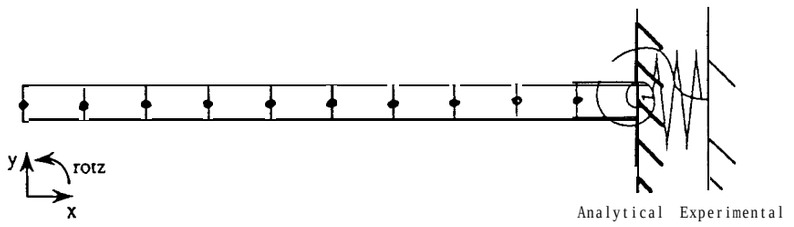


(a) Analytical and experimental models

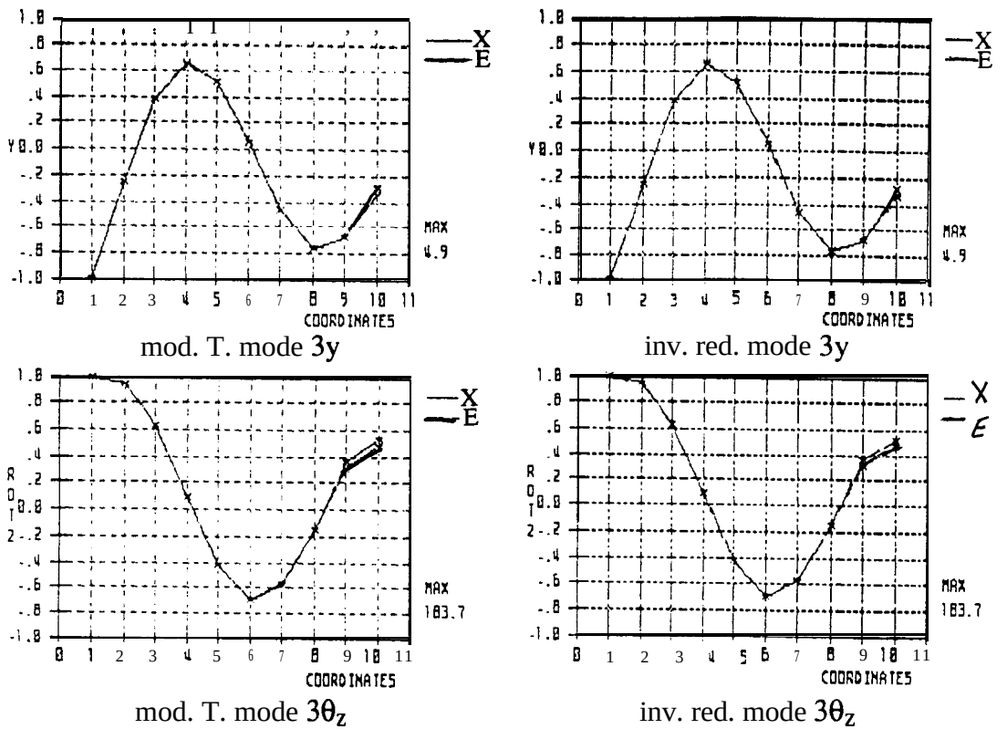


(b) Expanded mode shapes for a correspondence factor of 21.2%
(measured coordinates 5-x, 1 -y, 1-θz)

clamped beam example

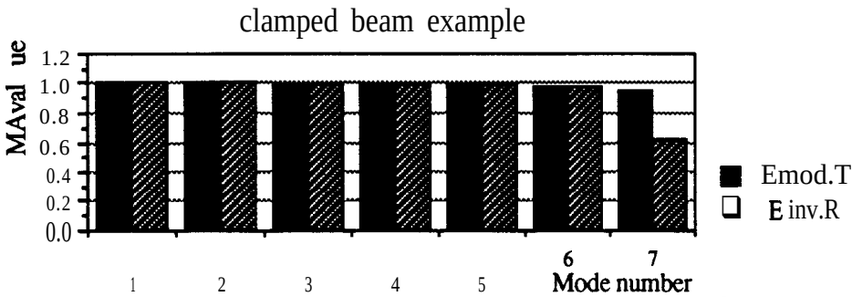


(c) Typical MAC values of expanded mode with true *experimental* counterpart

**Fig. 4.3:** Mode shape coordinate expansion of a clamped beam

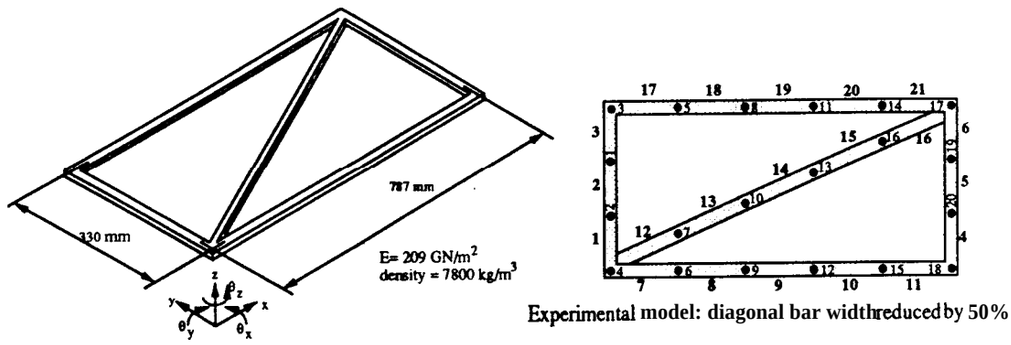


(a) Analytical and experimental models

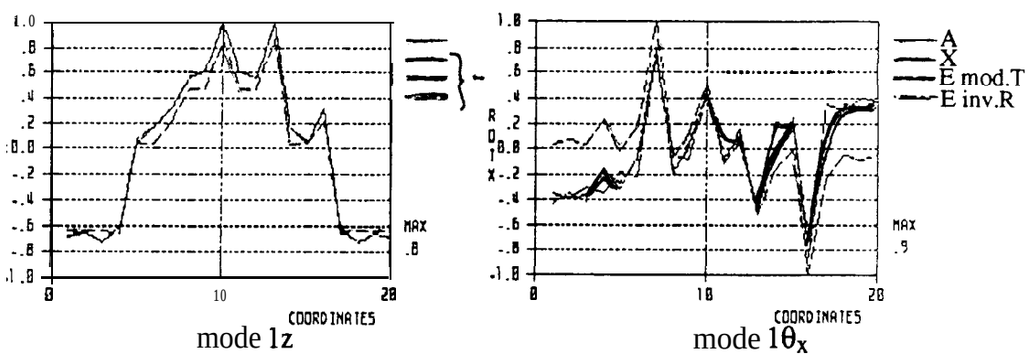


(b) Expanded mode shapes for a correspondence factor of 27.5%

frame expanded modes

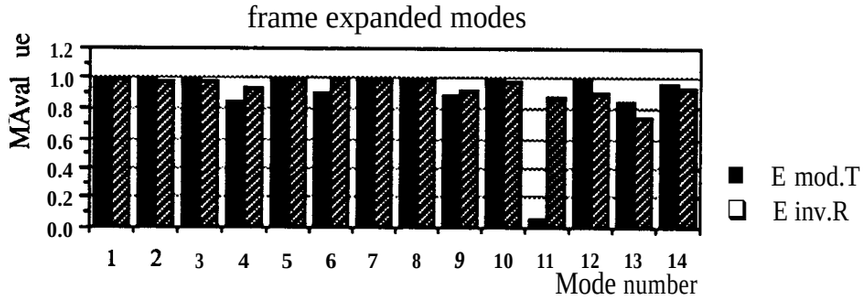


(c) Typical MAC values of expanded mode with true *experimental* counterpart

**Fig. 4.4:** Mode shape coordinate expansion of a frame structure

As can be seen from **Figs. 4.1-4.4,** both expansion techniques can produce well-expanded modes. As numerous test cases were carried out it is appropriate to give a summary of the results rather than showing all expanded modes and comparisons which can be found in [114].

### 4.3.2 Summary of results

For both methods the quality of the expansion depends on the selection of experimental coordinates and, to some extent, on the imposed modelling errors. The modal transformation technique also involves choosing the appropriate mode shapes to be included in the transformation matrix. For both techniques the selection of experimental coordinates influences the success of expansion, but other effects, such as a reduction in the number of measured coordinates, are more pronounced for the modal transformation method. The following observations on selecting experimental coordinates for successful expansion can be made:

(i) one must measure as many coordinates as possible, and at positions coinciding with nodes on the analytical model: an obvious point;
(ii) for numerical stability of the expansion technique, the measurement coordinates should include those with the largest deflections (which, in any case, is good experimental practice); and,
(iii) it is important for more complex structures to select experimental coordinates at each part of the structure with a dynamic response that is unique to that part.

It should also be noted that, in general, expanded rotational degrees of freedom show more discrepancies from their true counterparts than expanded translational degrees of freedom. This is mainly due to the lack of measured rotational degrees of freedom and the problem can be greatly reduced if one or more rotational degrees of freedom are included in the experimental coordinate set. However, it is difficult to measure rotational degrees of freedom in practice.

Successful expansion by the modal transformation method also depends on mode selection and recommendations for this process are as follows:

(i) the number of analytical modes selected must be smaller than the number of experimental coordinates in order to obtain an overdetermined matrix equation. The selected set of analytical modes can result in a numerically unstable inversion, but this can be overcome by reducing the number of modes used and/or by reselecting;
(ii) for each experimental mode to be expanded a corresponding analytical mode must be included in the mode selection;

(iii) if two analytical modes have a high correlation with one another, e.g. due to coordinate aliasing, they should not both be included in the same mode selection; and,

(iv) for the higher modes, best results are obtained if some lower and some higher modes (than the one to be expanded) are included in the mode selection.

Visual comparison of the (animated) mode shapes before and after expansion will show obvious expansion errors in the form of discontinuities and differences in the nodal line patterns. There are some additional criteria which can be used for the modal transformation expansion method. These are:

(i) the matrix inversion must be good (easily verified by checking the total sum of the elements $[\phi_{11}][\phi_{11}]^{-1}$);

(ii) inspection of $\{\gamma\}$ values: general guidelines being (a) the $\gamma$ value corresponding to the correlated analytical mode should be greater than 0.5 for a MSF of approximately 1 between the experimental and analytical correlated modes, and (b) $\gamma$ values should not be greater than 1.5. High values of $\gamma$, greater than 1.5, are most likely due to numerical instabilities in the inversion process. The case of all the values of $\gamma$ less than 0.5 can be (a) because there is no correlated analytical mode for the experimental mode included in the analytical mode selection (see mode selection) or (b) due to the mode selection causing an unstable inversion which can be a result of coordinate aliasing, especially when higher modes are included; and,

(iii) the MAC value between the measured coordinates of a mode shape and the reproduced coordinates of the expanded set of that mode should be, depending on the amount of experimental noise, greater than, say, 0.9. This MAC value also indicates the amount of smoothing.

For the modal transformation expansion approach, the generalised inverse gave comparable or negligibly improved by comparison with the SVD inversion when calculating the inverse of a numerically stable overdetermined matrix and requires less CPU time. However, the SVD inversion gave far better results for numerically ill-conditioned overdetermined matrices and it also provided a check on the number of small singular values representing the rank of the matrix which, for this application, can be used as an indication of the quality of the mode selection.

Comparing the inverse reduction method with the modal transformation technique, it was found that more computational effort was required as a matrix inversion is necessary for each experimental mode shape while a careful analytical mode shape selection in the latter

method can expand several experimental modes at once. The expanded modes obtained showed discontinuities at locations of analytical modelling error and these expansion errors were also larger than for the modal transformation technique. For the latter method a larger region of the structure was affected i.e. the discrepancies were spread **(Fig.** 4.5(a)).

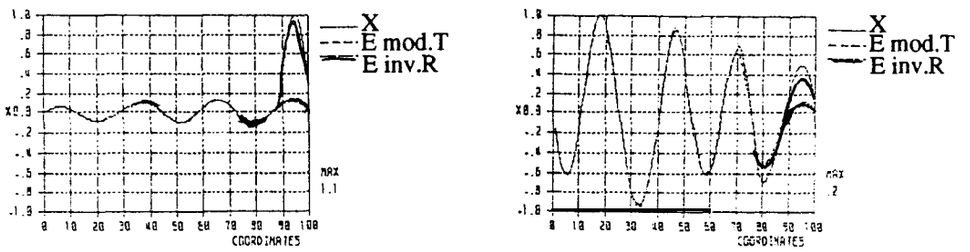


mode 7 mode 8

(a) 100 DOF example mode 8,

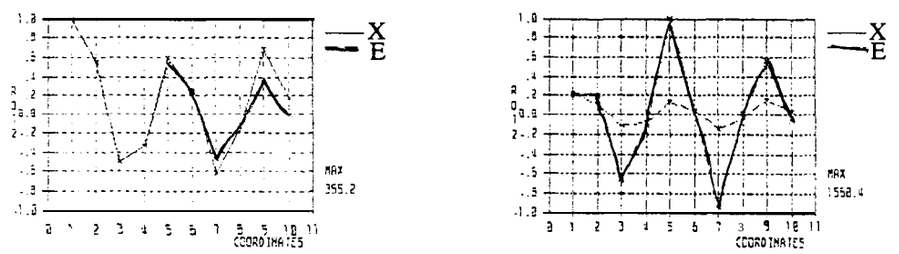


modal transformation method inverse reduction method

(b) Clamped beam example mode 7 θz

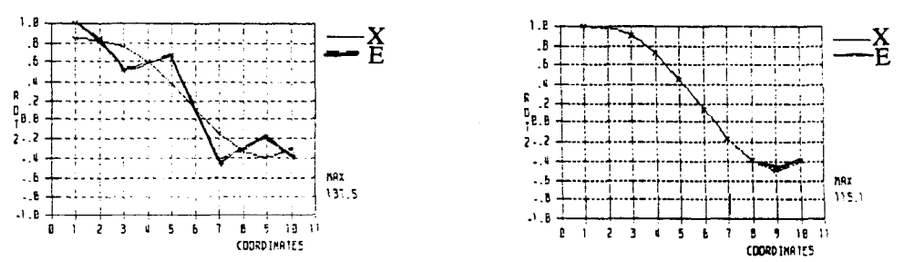


modal transformation method inverse reduction method

(c) Clamped beam example mode 2 θz

**Fig. 4.5:** Mode shape coordinate expansion discrepancies

The expanded mode shape error for both techniques usually occurs at the place(s) of the analytical modelling error(s), unless the number of experimental coordinates is insufficient. In that case errors are likely to occur at the region(s) where the number of measured coordinate(s) is/are most sparse. However, in most cases, the error between expanded and true experimental modes is not as large as the difference between the analytical and true experimental modes. Both methods produce comparable and generally well-expanded mode shapes, but both can at times produce poorly-expanded modes **(Fig. 4.5).** The difference between the two expansion methods is case-dependent and within each case can also vary for different modes as indicated by the MAC values in **Fig. 4.1c-4.4c**. Which expansion method to use should be based on whether the application for the expanded modes is more sensitive to large local errors or to smaller spread out errors.

Although both expansion techniques can produce well-expanded modes for most cases, if one of the mode shapes is expanded badly it should ideally not be included in a subsequent updating process. The main disadvantages of the inverse reduction technique are that (i) there are no checks to verify correctness of the expansion, apart from visual inspection and (ii) there is no smoothing of the measured coordinates in case of noisy experimental data. The main advantage, compared with the modal transformation method, is that there are no decisions to be made. As a result, the inverse reduction technique is the most favoured in practice.

## 4.4 MODEL UPDATING USING EXPANDED MODES

### 4.4.1 The GARTEUR III exercise

The two expansion methods were applied to the *experimental* data of the GARTEUR III structure introduced in chapter 3. Error location results using both the standard and improved error matrix procedures are given in **Figs. 4.6-4.9.**

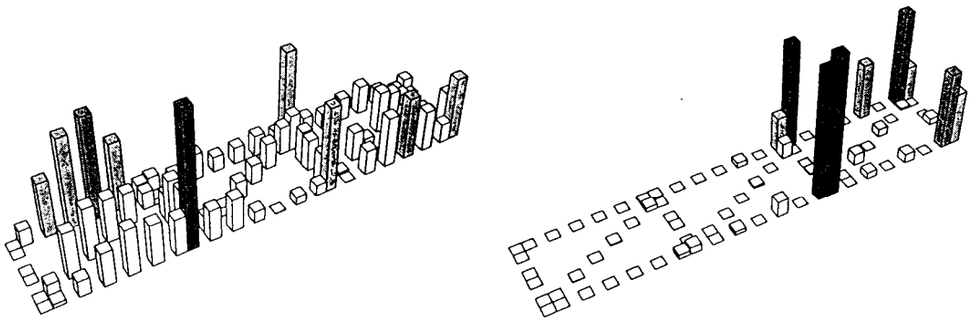

(a) Mass errors (b) Stiffness errors

**Fig. 4.6:** GARTEUR III, error location results by EMM using inverse reduction expanded *experimental* mode shapes

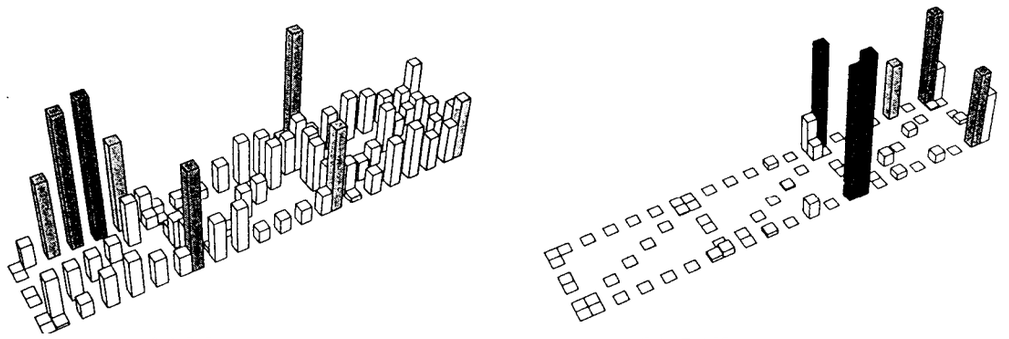

(a) Mass errors (b) Stiffness errors

**Fig. 4.7:** GARTEUR III, error location results by EMM' using inverse reduction expanded *experimental* mode shapes

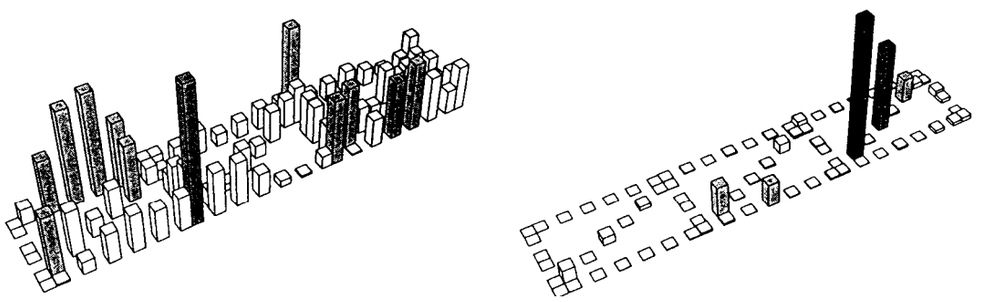

(a) Mass errors (b) Stiffness errors

**Fig. 4.8:** GARTEUR III, error location results by EMM using modal transformation expanded *experimental* mode shapes

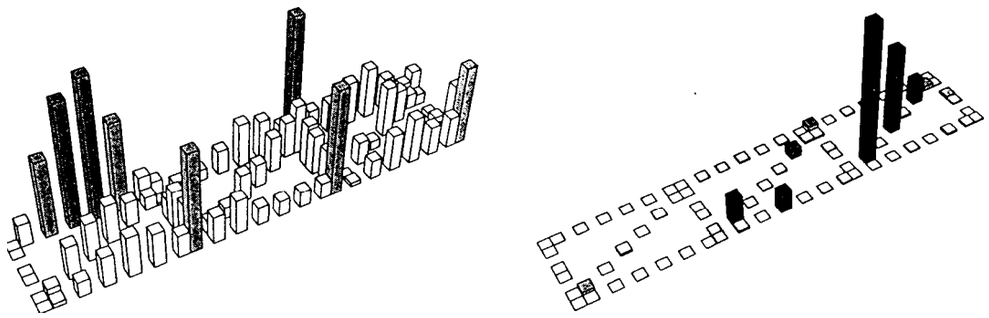

(a) Mass errors (b) Stiffness errors

**Fig. 4.9:** GARTEUR III, error location results by EMM' using modal transformation expanded *experimental* mode shapes

Referring to the true errors introduced, as shown in **Fig. 3.9,** the error location results shown in **Fig. 4.6-4.9** were again not successful: in particular the indicated stiffness errors bore little resemblance to the expected error locations. The mass error matrices predicted the correct location among some spurious ones. Comparing the four different error location procedures for this example; the modal transformation coordinate expanded *experimental* data and the improved error matrix procedure gave the best results for error location purposes.

The analytical model was updated using the four sets of error matrices illustrated in **Fig. 4.6-4.9. The** updated natural frequencies are compared to the experimental ones in **Fig. 4.10.** For each of the four procedures employing expanded data the updated natural frequencies were substantially better than those obtained for the Guyan reduced model cases **(Fig. 3.8).** However the updated system MAC and COMAC values did not exhibit improvements compared with those obtained between the original FE model and their experimental counterparts. From an updating point of view, the inverse reduction method expanded experimental data and the standard EMM gave the best results in this case.

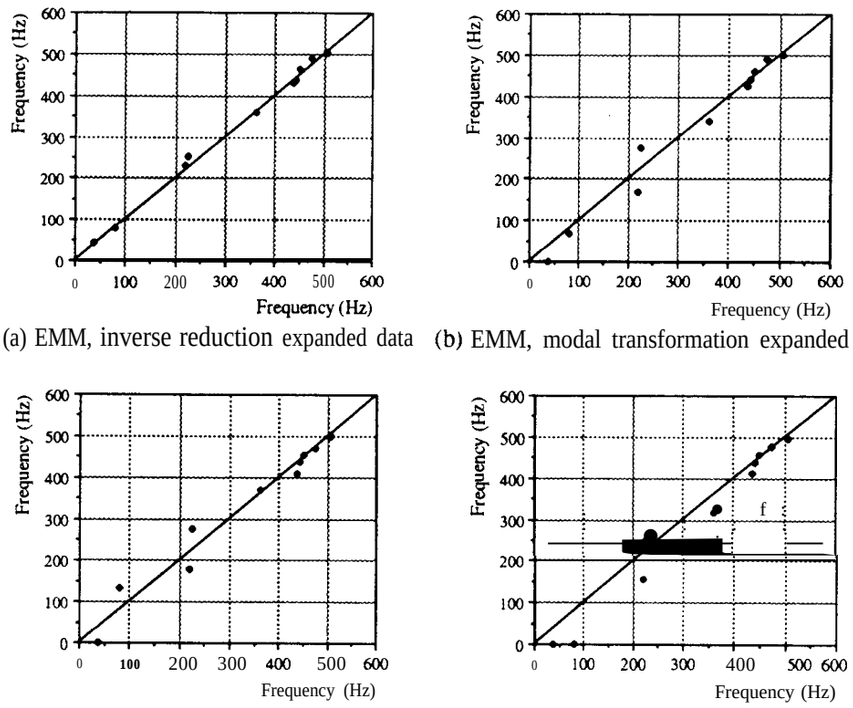


(a) EMM, inverse reduction expanded data (b) EMM, modal transformation expanded data

(c) EMM', inverse reduction expanded data (d) EMM', modal transformation expanded data

**Fig. 4.10:** GARTEUR III, updated natural frequencies against ***experimental*** ones for four different updating procedures

The reason that the updating results were far from satisfactory was likely due to the relatively high percentage of noise applied to the ***experimental*** data. In particular 3% noise on the natural frequencies is high. The adverse effects of this noise are most significant for the stiffness error matrix which is calculated using the pseudo flexibility matrix:

$$[K]^{-1} = [\phi_X]\,[\omega_X^2]^{-1}\,[\phi_X]^T.$$

Lieven [56] suggests that the accuracy of experimental data should be to 4 significant figures for mode shapes and 6 significant figures for natural frequencies for successful updating using the EMM. However, the GARTEUR III data were supplied "as is" and could not be changed to suit the updating method. In most practical applications the updating problem can not be altered, although in some cases it might be possible to acquire a better experimental data set by additional measurements (improved accuracy, more measured coordinates).

It must be pointed out that, although the GARTEUR III exercise results were far from adequate, both the EMM and the expansion techniques are case-dependent and have been used successfully on some practical examples [56].

### 4.4.2 Discussion on expanded data and the orthogonality condition

Most methods for checking the validity of the expanded mode shapes to date have not considered the orthogonality of the expanded modal data with respect to the experimental model. Measured mode shapes are mass-normalised modes. Do the expanded modes satisfy the orthogonality condition? Are the expanded modes also mass-normalised with respect to the experimental system? These are important requirements if the expanded modes are to be used for updating techniques based on this property.

For mass-normalised modes the orthogonality equations are:

$$[\phi_X]^T[M_X][\phi_X] = [I]$$

and

$$[\phi_X]^T[K_X][\phi_X] = [\omega_X^2] \qquad (11)$$

The error matrix method indirectly incorporates orthogonality conditions as it makes use of the pseudo inverses, since these are derived from the orthogonality condition (equation (10):

$$[M_X]^{-1} = [\phi_A][\phi_A]^T \text{ and } [K_X]^{-1} = [\phi_X][\omega_X^2]^{-1}[\phi_X]^T \qquad (12)$$

Thus, if the expanded mode shapes are not orthogonal to the experimental mass and stiffness matrices, errors are introduced in the updating process.

To verify whether the deviation from the orthogonality condition of expanded modes is significant, $[\phi_X^E]^T[M_X][\phi_X^E]$ and $[\phi_X^E]^T[K_X][\phi_X^E]$ were calculated for various test cases of section 4.3.1. A typical example, the orthogonality of expanded *experimental* modal data with respect to the *experimental* mass matrix of the frame model, is shown in **Fig. 4.11.** This shows that, in this particular case, there are considerable discrepancies for (badly) expanded mode 11; there is a large peak on the leading diagonal and also significant values at off diagonal elements which should be zero.

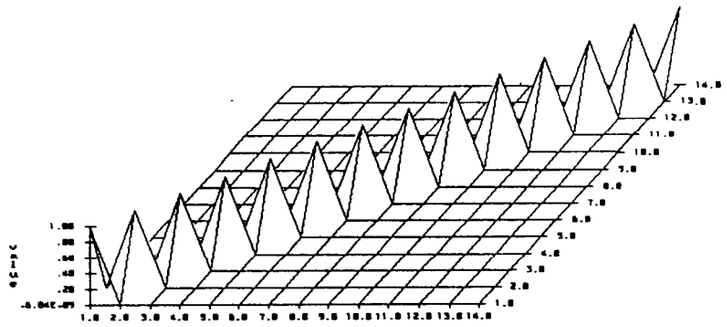

(a) *experimental* modal data and the experimental mass matrix

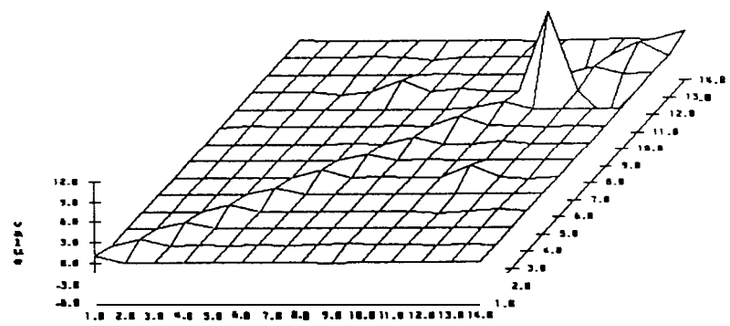

(b) expanded modal data and the experimental mass matrix

**Fig. 4.11:** Mass orthogonality for the frame example

As expected, errors in the expanded mode shapes orthogonality matrix depended on the quality of the expanded mode(s). And, since the expansion methods are case-dependent, the achieved orthogonality is also case-dependent. Considering several test cases and comparing the orthogonality of expanded data obtained by the two expansion methods investigated in this chapter, neither shows overall better orthogonality. Discrepancies are case-dependent, and are mainly influenced by the closeness of the analytical model to the experimental model and the quality of the expansion. The quality of expansion, as discussed before, also depends on the ratio of measured to unmeasured coordinates, the mode selection (for the modal transformation expansion method) and the quality of measurements. In the test cases noise-free *experimental* data were used. Noise on the experimental data, such as for the GARTEUR III exercise, will compound the problem.

Thus, for both expansion techniques, the expanded set is not orthogonal with respect to the system matrices. In real-life updating problems the experimental system matrices are unknown and there can be no check on the orthogonality of the expanded modes.

Therefore it is advised to use more than one set of expanded data in case of employing an updating technique based on orthogonality. And, if possible, a combination of updating techniques should be employed to verify results.

## 4.5 CONCLUDING REMARKS

In this chapter it is shown that well-expanded modes can be obtained by both the inverse reduction technique and the modal transformation method. A number of suggestions on coordinate and mode shape selection are made for successful and reliable expansion.

The modal transformation method, as compared with the inverse reduction technique, shows no discontinuities in the mode shapes, noise is smoothed, the error is generally smaller although more spread out and it is less CPU intensive. The main advantage of the inverse reduction technique is that there are no decisions to be made, in contrast to the modal transformation method where the analytical mode selection is of vital importance to the success of the method. Therefore, despite the success of the modal transformation method, in practice, the inverse reduction technique is the most favoured.

The expansion techniques were applied to the GARTEUR III exercise, using both the standard EMM and the improved procedure suggested in chapter 3. Best error location results were obtained using modal transformation coordinate-expanded *experimental* data and the improved error matrix procedure. From an updating point of view, best results were obtained using the inverse reduction method expanded experimental data and the standard error matrix method.

The importance of orthogonality of the expanded experimental modes in case of employing an updating technique based on this property is pointed out. It is shown that for both expansion techniques the expanded set is not orthogonal with respect to the experimental system matrices. Discrepancies are case-dependent, and are mainly influenced by the closeness of the analytical model to the experimental model.

# CHAPTER 5

# UPDATING USING FRF DATA; THE RESPONSE FUNCTION METHOD

## 5.1 INTRODUCTION

Most updating methods proposed in recent years rely on analysing the frequency response data to obtain modal data, a process which inevitably introduces inaccuracies and errors over and above those already present in the measured (FRF) data. They also use a finite (and small) number of modes, which results in the formulation of an underdetermined problem in most cases. Some additional shortcomings were illustrated using the error matrix method in chapters 3 and 4.

In this chapter the response function method (RFM), an updating technique using frequency response function data, is investigated. The basic theory of this updating technique was recently presented by Lin [99]. Updating using frequency response data overcomes both the problem caused by insufficient data, as measured data can be acquired at any number of frequency points, and the problem of introducing additional inaccuracies from modal analysis, as the measured FRF data are used directly. Another advantage of using FRF data directly is that no pairing or matching of mode shapes is required, and problems normally associated with close modes do not occur.

## 5.2 THEORY

Consider the mathematical identity:

$$[[A]+[B]]^{-1}_{NxN} = [A]^{-1}_{NxN} - [[A]+[B]]^{-1}_{NxN}[B]_{NxN}[A]^{-1}_{NxN} \qquad (1)$$

Let $[A] = [Z_A(\omega)]$

and $[A]+[B] = [Z_X(\omega)]$,

where: $[Z_X(\omega)] = [Z_A(\omega)] + [\Delta Z(\omega)]$

and assuming that both [A] and [A+B] are non singular, we can write:

$$[Z_X(\omega)]^{-1}_{NxN} = [Z_A(\omega)]^{-1}_{NxN} - [Z_X(\omega)]^{-1}_{NxN} [[Z_X(\omega)]-[Z_A(\omega)]]_{NxN} [Z_A(\omega)]^{-1}_{NxN} \quad (2)$$

Equation (2) is valid irrespective of the size of the modelling errors or other differences between the analytical and experimental models. Only at resonance frequencies, where $[Z_A(\omega)]$ and/or $[Z_X(\omega)]$ are singular, equation (2) is invalid. Equation (2) can be rewritten in a more convenient form:

$$[\alpha_X(\omega)]_{NxN} [[Z_X(\omega)] - [Z_A(\omega)]]_{NxN} [\alpha_A(\omega)]_{NxN} = [\alpha_X(\omega)]_{NxN} - [\alpha_A(\omega)]_{NxN} \quad (3a)$$

Transposing (3a) gives:

$$[\alpha_A(\omega)]_{NxN} [\Delta Z(\omega)]_{NxN} [\alpha_X(\omega)]_{NxN} = [\alpha_A(\omega)]_{NxN} - [\alpha_X(\omega)]_{NxN} \quad (3b)$$

Taking the $i^{th}$ column of both sides of equation (3b):

$$[\alpha_A(\omega)]_{NxN} [\Delta Z(\omega)]_{NxN} \{\alpha_X(\omega)\}_{i_{Nx1}} = \{\{\alpha_A(\omega)\}_i - \{\alpha_X(\omega)\}_i\}_{Nx1}$$

or:

$$[\alpha_A(\omega)]_{NxN} [[\Delta K] - \omega^2[\Delta M]]_{NxN} \{\alpha_X(\omega)\}_{i_{Nx1}} = \{\{\alpha_A(\omega)\}_i - \{\alpha_X(\omega)\}_i\}_{Nx1} \quad (4)$$

Using the symmetry of the system matrices, as shown in appendix A, equation (4) can be rewritten as:

$$[C(\omega)]_{NxN(N+1)} \{p\}_{N(N+1)} = \{\Delta\alpha(\omega)\}_N \quad (5)$$

where the elements of matrix [C(o)] and those of vector $\{\Delta\alpha(\omega)\}$ are known in terms of analytical and measured FRFs, elements of the analytical mass and stiffness matrices and the excitation frequency. The elements of the unknown vector $\{p\}$, the so-called "p-values", indicate both the amount and the location of the error(s) in the analytical mass and stiffness matrices. By stacking the matrix equation (5) for a number ($N_f$) of different

excitation frequencies the system becomes overdetermined and can be solved for vector $\{p\}$, as $\{p\}$ is independent of $\omega$:

$$\begin{bmatrix} [C(\omega_1)] \\ [C(\omega_2)] \\ [C(\omega_3)] \\ \cdot \\ \cdot \\ \cdot \end{bmatrix} \{p\} = \begin{bmatrix} \{\Delta\alpha(\omega_1)\} \\ \{\Delta\alpha(\omega_2)\} \\ \{\Delta\alpha(\omega_3)\} \\ \cdot \\ \cdot \\ \cdot \end{bmatrix} \tag{6}$$

Taking a structure with N degrees of freedom yields a maximum of N (N+1) unknowns when both the mass and stiffness matrices are symmetrical. Assuming that a full column of the FRF matrix can be measured, equation (5) will lead to N equations at each frequency point; hence the minimum requirement for the solution is the knowledge of any column (or row) of the FRF matrix at (N+1) frequency points since there are N(N+1) unknowns. It should also be noted that the problem can become overdetermined since, in general, there are more than (N+1) frequency points within the range of interest, in which case a least-squares solution can be used to determine the p-values.

## 5.3 COORDINATE INCOMPLETENESS

Many of the coordinates specified in the analytical model cannot be measured because of various restrictions on the test structure and, in common with other updating techniques, the resulting incompleteness of measured data gives rise to a number of difficulties. Usual ways to deal with this problem are to reduce the size of the analytical model or to expand the experimental one. A different approach will be adopted here. The s unmeasured (missing) response functions, which are elements of the receptance FRF vector, $\{\alpha_x(\omega)\}$, in equation (4), can be replaced by their analytical counterparts and the corresponding rows are deleted from equation (5). The minimum required number of frequency points is now given by the number of unknowns, N(N+1), divided by the number of measured coordinates, n = N-s. In other words, even when some of the required response functions cannot be measured, equations (4) and (5) can still be solved in an iterative fashion by substituting the required but unmeasured FRF values in $\{\alpha_x(\omega)\}$ with their (updated) analytical counterparts until a degree of convergence is reached.

## 5.4 UNIQUENESS OF THE SOLUTION

In the case of coordinate incompleteness, a non-unique solution will almost certainly be obtained if all elements of the system matrices are updated simultaneously. Additional constraints, taking into account physical connectivities, can be introduced by forcing the null elements to remain zero in order to limit the number of possible solutions. These will be called Cl constraints. This approach relies on the connectivities in the analytical matrices being correct, an assumption which must be investigated further.

To further reduce the possibility of a non-unique solution even more constraints may be required. These constraints, which will be called C2 constraints, can be introduced by considering the mass and stiffness matrices of individual finite elements. Since the p-values indicate both the location and the amount of the error(s), the error matrices can be written as a linear combination of the element mass and stiffness matrices,

$$[\Delta M] = \sum_{i=1}^{N_m} p_i [M_e]$$

$$[\Delta K] = \sum_{i=1}^{N_k} p_i [K_e] \qquad (7)$$

where the $\sum$ sign denotes matrix building. It should be noted that C2 constraints include Cl constraints. This approach has, in most cases, the added advantage of reducing the number of unknowns to be determined, and the minimum required number of frequency points is now $(N_k + N_m) / n$.

Yet further constraints can be introduced by using macro-elements - that is, several finite elements which describe a distinct part of the structure grouped together into one element - or by updating the physical parameters used in the definition of the FE model. However, it is considered that the latter constraints limit the ability of the updating method to identify local modelling errors in the analytical model. The choice of parameters is of vital importance to the success of any updating technique, as it reflects inherent assumptions about the correctness of the model. The RFM can have several solutions due to the choice of updating parameters involved. However, it is considered more important that for a certain choice in parameters, bearing in mind the inherent limitations of these updating parameters, a single (unique) set of p-values are obtained which reflect the modelling errors correctly.

## 5.5 CASE STUDIES ON AN 8 DOF SYSTEM

### 5.5.1 The 8 DOF system

An 8-DOF lumped parameter system, shown in **Fig. 5.1,** was employed to investigate the use of the FRF-based updating technique for a number of test cases. It should be noted that the mass matrix for this system is not diagonal, an uncharacteristic feature of such simple systems. The ***experimental*** model was provided by a version of the basic system in which there was a 30% increase in the value of $k_3$ and a 25% increase in that of $I_3$. A typical receptance FRF, $\alpha_{66}$, computed for both models over the 10-100Hz frequency range is plotted in **Fig. 5.2.**

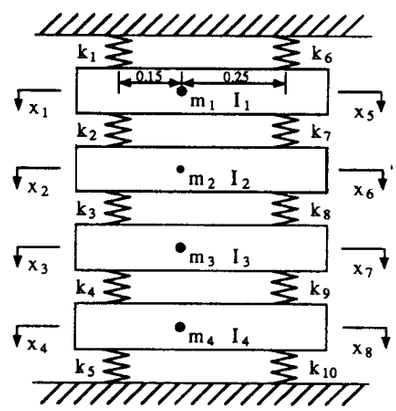


| | | | |
|---|---|---|---|
| $I_1$ = 5.0 kgm$^2$ | $m_1$ = 1.0 kg | $k_1$ = 1.0 MN/m | $k_6$ = 1.8 MN/m |
| $I_2$ = 1.0 kgm$^2$ | $m_2$ = 2.0 kg | $k_2$ = 1.5 MN/m | $k_7$ = 1.0 MN/m |
| $I_3$ = 4.0 kgm$^2$ | $m_3$ = 3.0 kg | $k_3$ = 1.5 MN/m | $k_8$ = 3.0 MN/m |
| $I_4$ = 1.24 kgm$^2$ | $m_4$ = 6.0 kg | $k_4$ = 3.0 MN/m | $k_9$ = 1.5 MN/m |
| | | $k_5$ = 1.9 MN/m | $k_{10}$ = 2.5 MN/m |

**Fig. 5.1:** The 8 DOF system

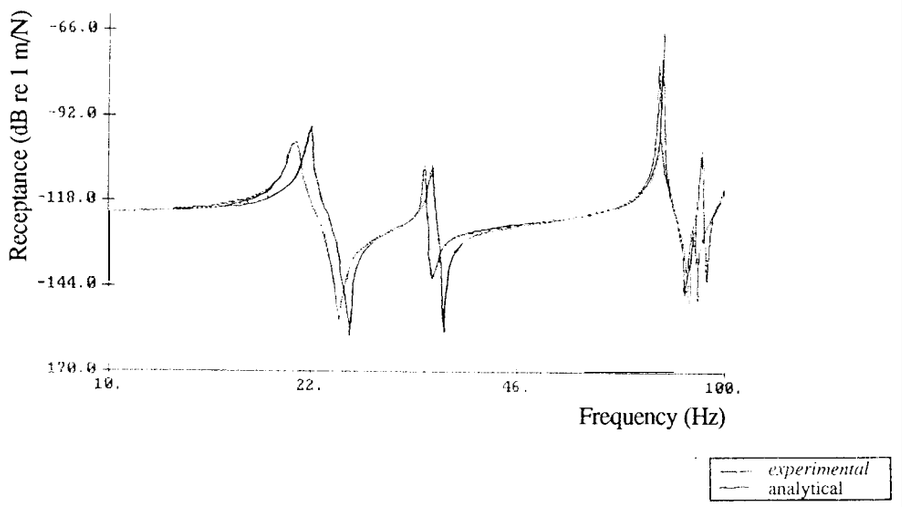


**Fig. 5.2:** Receptance FRF $\alpha_{66}$ obtained from the *experimental* and analytical models of the 8 DOF system

### 5.5.2 Updating using complete data from the *experimental* model

At first it was assumed that all required FRFs, that is to say an entire column of $[\alpha_X]$, were *measured. The* following three cases were investigated:

(i) no constraints, i.e. 8x(8+1)=72 unknowns and a minimum of 72/8 = 9 frequency points;

(ii) Cl constraints, i.e. 26 unknowns and 26/8 = 4 frequency points required; and

(iii) C2 constraints, i.e. 18 unknowns and 18/8 = 3 frequency points required.

In all three cases, the natural frequencies, system matrices and frequency response functions of the analytical model were updated correctly in the sense that they matched those of the *experimental* model. A receptance FRF ($\alpha_{66}$) obtained from the updated analytical model is shown in **Fig. 5.3.** Also plotted in the same figure is the *measured* receptance FRF $\alpha_{66}$, which was seen to be identical to the updated one within the frequency range considered (0- 100Hz) and beyond.

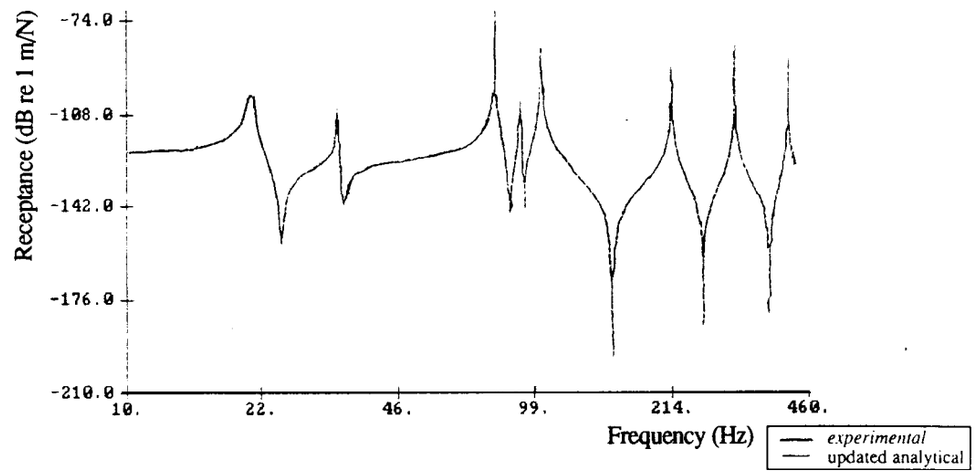


**Fig. 5.3:** Receptance FRF $\alpha_{66}$ obtained from the ***experimental*** and updated analytical models of the 8 DOF system (complete ***experimental*** model, unique updated model)

### 5.5.3 Incomplete *experimental* data

The incomplete data from the ***experimental*** model consisted of 4 FRFs only which were ***measured*** at coordinates 1, 3, 6, and 8. Twenty points were selected from the ***measured*** frequency range and the convergence criterion, defined by the relative percentage difference between measured and updated analytical FRFs at the selected frequency points, was taken as 1%.

Convergence was obtained after 8 iterations using Cl constraints. However, a closer inspection showed that the mass and stiffness matrices of the updated system did not correspond to those used to create the ***experimental*** data, although good agreement was reached at the FRF level **(Fig. 5.4).** Further runs, where different numbers/combinations of frequency points were used, produced different updated system matrices which, in turn, all gave the ***correct*** frequency response functions. Clearly, in each case, the updated model was not unique.

The number of ***measured*** FRFs was then increased to 5, 6 and finally to 7. As before, each case yielded different system matrices but gave satisfactory agreement between FRFs. Elements of the updated mass and stiffness matrices corresponding to the unmeasured points were observed to exhibit large errors. As the number of measured coordinates was increased, these errors were found to decrease: over 100% error for 4 ***measured*** points, 50% for 5, 18% for 6 and 5% for 7 points, thus converging to the

unique solution which was eventually obtained using a complete vector of *experimental* FRFs.

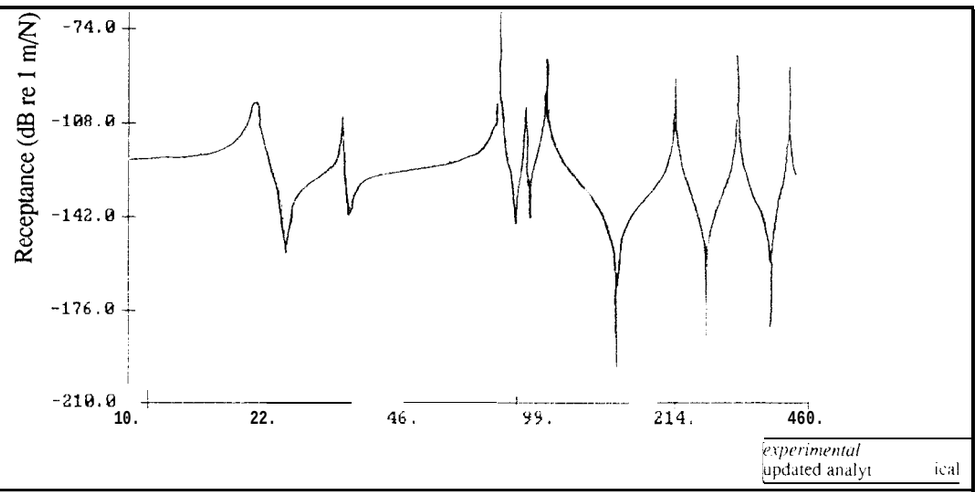


**Fig. 5.4:** Receptance FRF $\alpha_{66}$ obtained from the *experimental* and updated analytical models of the 8 DOF system using Cl constraints (incomplete *experimental* model, non-unique updated model)

If the modifications are confined to the mass or the stiffness matrix errors only, as opposed to errors occurring simultaneously in both mass and stiffness matrices, 6 iterations were required to reach convergence when 4 *measured* FRFs were used. In these special cases the updated mass (or stiffness matrix) was found to be unique.

Next, **C2** constraints were applied to limit the number of possible solutions when both the mass and stiffness matrices were modified. Eighteen parameters ($I_1, m_1, I_2, m_2, \ldots,$ $k_1, k_2, \ldots, k_9$ and $k_{10}$) were selected to form equation (6), thus reducing the number of unknowns from 26 to 18. However, as before, a non-unique solution, with small differences (between 0-2% on the p-values) as compared with the expected model, was obtained in the sense that several sets of updated matrices produce the *correct* FRFs. This was thought to be due to the fact that both $k_5$ and $k_6$, which were used as independent updating parameters, did not have a measurement points directly at one of their nodes. Although this is not a fundamental requirement, $k_5$ and $k_6$ were less sensitive for updating purposes when employing the selected 4 *measured* FRFs. To overcome this problem macro elements were formed by grouping $k_1$ with $k_6$ and $k_5$ with $k_{10}$, thus reducing the number of unknowns from 18 to 16. Convergence was achieved within 5 iterations using 7 frequency points **(Fig. 5.5).** Also, the solution seemed to be unique since further runs using different set of frequency points yielded the same mass and stiffness matrices for the updated system.

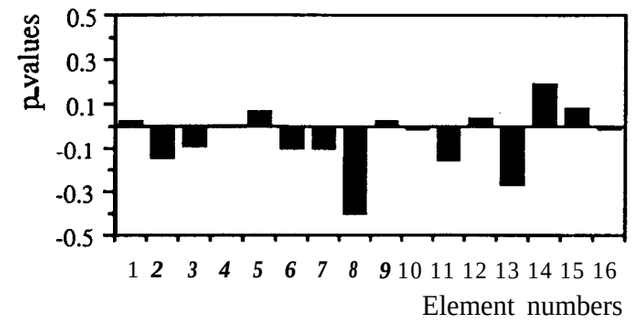


(a) p-values after 1 iteration

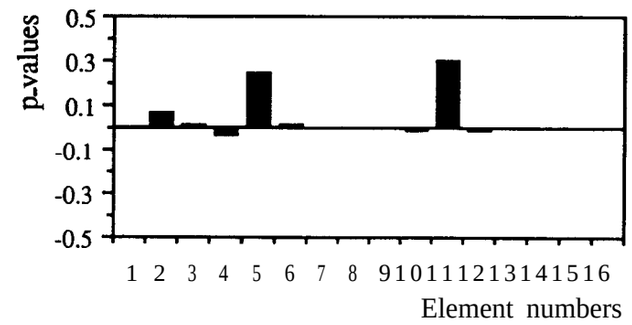


(b) p-values after 3 iterations

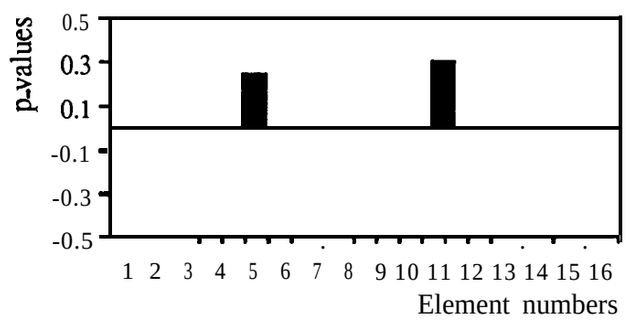


(c) p-values after 5 iterations

**Fig. 5.5:** Convergence towards the unique solution using C2 constraints

At this stage, it must be noted that, although elements which did not have a measurement point associated with them were less sensitive, by adding an extra convergence criterion which ensures convergence of the p-values (see section 5.5.4) the correct updated model was obtained even in the case of 18 unknowns. Using the additional criterion more iterations were needed to reach convergence than when a single convergence criterion, based on the difference between experimental and updated receptance values, was used. To ensure rapid convergence and improved solution stability, the recommended minimum number of measurement coordinates is at least one per finite element.

### 5.5.4 Frequency points selection

During the investigation it was discovered that, unless the experimental model was complete, the choice of frequency points for the updating procedure had a marked influence on the speed of convergence and on the accuracy of the final solution. Hence, a preliminary investigation into the best selection of frequency points should be conducted using the incomplete noise-free *experimental* model of the previous section. In all cases the frequency points were selected randomly in a specified frequency range and were kept constant throughout the iterations. In this particular case, the maximum number of iterations was set to 30 and two convergence criteria were used:

(i) the absolute value of the consecutive difference in the p-values between iterations should be less than 1% to ensure the stability of the solution; and

(ii) the consecutive percentage difference between measured and regenerated FRFs should be constant This is implemented by monitoring the sum of the percentages difference squared:

$$SPDS = \sum_{k=1}^{nfpts} \sum_{j=1}^{ncor_x} \left( \frac{\alpha_{x_{ij}}(\omega_k) - \alpha_{u_j}(\omega_k)}{\alpha_{x_{ij}}(\omega_k)} x100 \right)^2 \qquad (7)$$

The use of more frequency points and from a wider frequency range improved the rate of convergence, although it was also observed that too many frequency points in the selection can in some cases increase the number of iterations to reach convergence. When the minimum required number of frequency points was used, no convergence was obtained except for the full 10- 100 Hz frequency range. This shortcoming was remedied by using more frequency points. By observation of the various test cases it was deduced that the recommended number of frequency points to be used is at least twice the minimum requirement in case of noise-free incomplete experimental data. It is anticipated that in case of noisy experimental data more frequency points will be required to overcome the expected adverse effects of noise.

It was also noticed that large fluctuations in the p-values usually occurred (-5,5) during the first few iterations, although convergence could still be achieved. A maximum change of 50% (Ap = 0.5) was allowed between iterations to ensure solution stability. However, in some cases, p-values of -1.0 were obtained during the first few iterations which meant the corresponding element was deleted from the updated matrices, resulting

in numerical instability and jeopardising convergence. In most cases this problem was cured by using a new selection of frequency points.

If a frequency point was selected in the immediate vicinity of a resonance, the inversion of matrix [C] becomes prone to ill-conditioning. The discrepancies between various sets of results obtained using different frequency points could, perhaps, be explained in the light of this observation (computational aspects and frequency point selection are addressed in more detail in chapter 7).

It was also observed that selecting points at higher frequencies gave best results and quicker convergence. Selecting points close to the first natural frequency gave a maximum percentage error compared to the true value of the non-zero p-values of 40% , while around mode 2 this was reduced to 0.4%. Selecting points around modes 3 and 4 the percentage error is even smaller. This is thought to be due to the fact that individual stiffness (k) and mass ($\omega^2 m$) elements of the system matrices were about the same order of magnitude at these frequencies, which ensured better numerical stability.

### 5.5.5 Noisy *experimen tal* data

The case where measured FRFs contain a certain amount of noise, a feature inherently present in all measured data, was also investigated. The *experimental* FRFs of the 8 DOF system were polluted by adding between 1% and 12% random noise in the following way:

$$\alpha_{x_{ij}}(\omega_k) = (1 + r \times n\%)\, \alpha_{x_{ij}}(\omega_k)) \tag{8}$$

where r is equal to a random value between -1 and 1. The RFM was repeated for 4 different sets, A-D, of randomly selected frequency points in the 10-100 Hz range in order to check the repeatability of the solution in the case of polluted experimental FRF data. The number of frequency points selected was increased to 30 to compensate for the expected adverse effects of the random noise.

The number of iterations required to achieve convergence was seen to increase with increasing levels of noise; averages of 9 iterations for 0% noise, 12 iterations for 4% noise and 16 for 12% noise were recorded. For the extreme case of 20% noise no convergence was obtained in 30 iterations for 2 of the 4 frequency point sets. In the last

case, although the error was located, its magnitude was not predicted correctly due to noise.

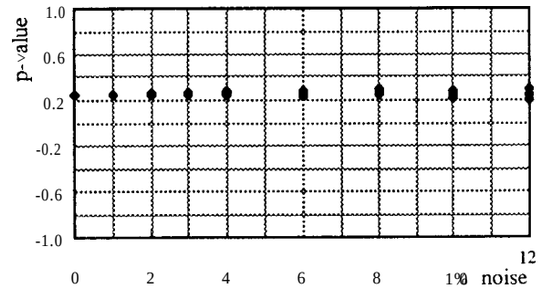


(a) Element 5, correct p-value = 0.25

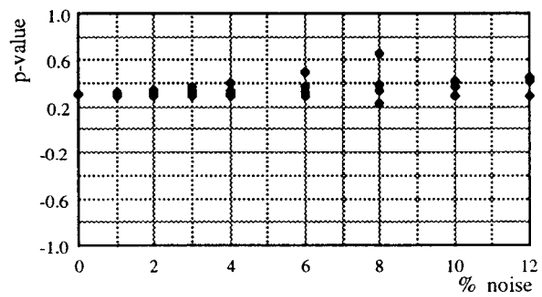


(b) Element 11, correct p-value = 0.30

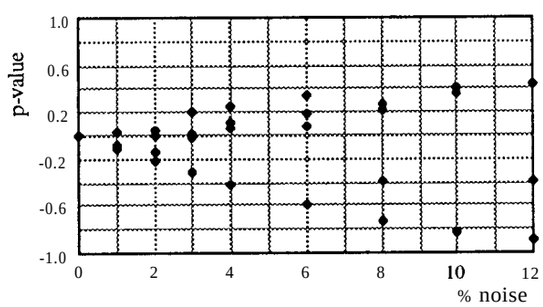


(c) Element 2, correct p-value = 0.0

**Fig. 5.6:** Variation of p-values with level of noise (4 cases, A-D)

p-values versus noise levels for elements 5 and 11, which were modified by 25% and 30% respectively, are plotted in **Fig. 5.6** for all four test cases (A-D). As expected, p-values diverged from the correct values (0.25 for element 5 and 0.30 for element 11) as noise levels increased. This was verified by the plot of the standard deviations with respect to the true p-value **(Fig. 5.7).** However, in all cases a good indication of the size and location of the error was obtained. The remaining p-values for the unmodified elements also showed trends similar to elements 5 and 11, but the corresponding p-values were either small in comparison (for most elements) or inconsistent in size and magnitude

when collective results from tests A-D were considered. The latter observation is illustrated in **Fig. 5.6c** where p values for element 2, for which the largest errors were incorrectly predicted, are plotted.

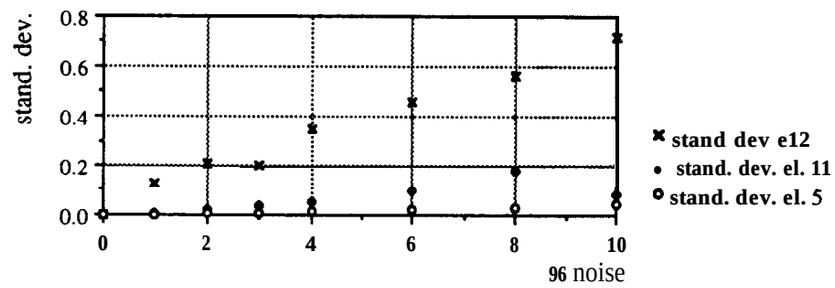


**Fig. 5.7: 8** DOF models, standard deviation of p-values against noise level

p-values found for sets A-D were averaged in order to determine whether discrepancies from one set to the next were randomly distributed about the expected p-values such that the mean values could predict the correct p-values. The mean p-values obtained from sets A-D are plotted in **Fig. 5.8.** The same procedure was repeated for a number of further runs with other frequency point selections and it was found that the averaging technique can be used successfully for error location when dealing with noisy experimental data.

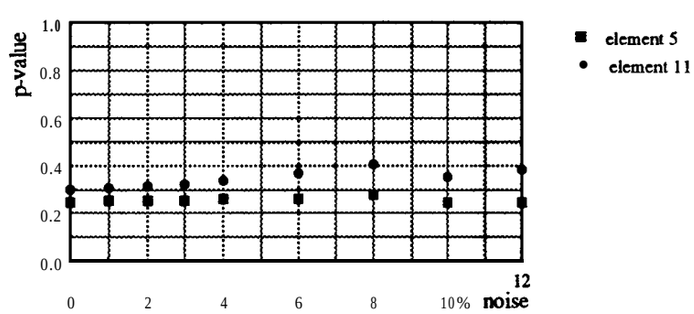


**Fig. 5.8: 8** DOF models, mean p-values against noise level

## 5.6. CASE STUDIES ON A FREE-FREE BEAM

### 5.6.1 The free-free beam

The second example was based on a free-free steel beam of dimensions 25.4 mm x 31.75 mm x 1400 mm which was considered to be a simple but representative engineering structure. The *experimental* data were simulated using a uniform beam model and the

FRF data for this beam were obtained via a Finite Element model (consisting of 14 3D beam elements) for both Y and Z directions at an excitation point 400 mm away from one end. Six known errors were introduced to the analytical Finite Element model, also consisting of 14 3D beam elements, as shown in **Fig. 5.9**. A typical FRF obtained from the analytical model with known errors is plotted in **Fig. 5.10** together with the *experimental curve* representing the correct uniform beam.

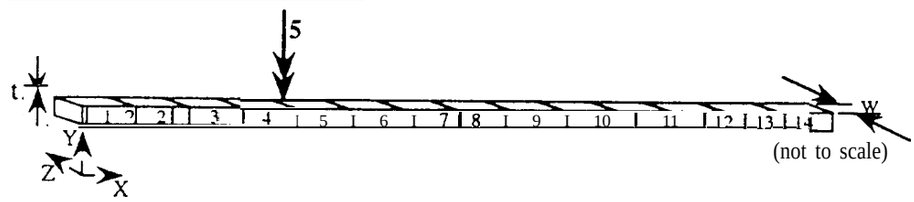


Fig. la FE model of the uniform beam with following errors: element 2 t' = 1.1 t
element 3 w' = 0.8 w
element 6 t' = 1.5 t
element 10 E'=1.2E
element 11 t' = 1.3 t
element 14 p' = 0.7ρ

**Fig. 5.9:** FE model of the uniform beam

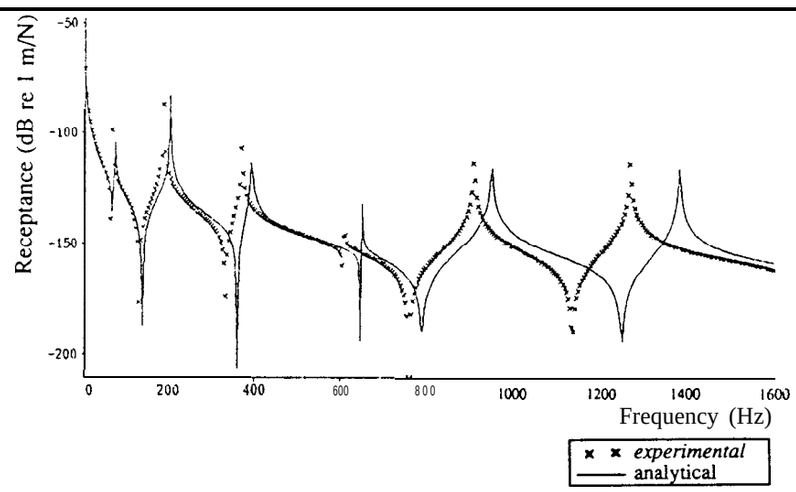


**Fig. 5.10:** Receptance FRF $\alpha_{5y5y}$ obtained from the *experimental* and analytical beam models

### 5.6.2 Noise-free *experimental* FRF data

Two initial test cases were carried out using noise-free FRF data: in the first case, all elements of the FRF vector (rotations as well as translations) were assumed to be known while in the second case it was assumed that measurements were made in the Y direction

only (i.e. a correspondence factor of 16.7%). The first case converged in 2 iterations only while the second one required 12 iterations but both cases yielded very similar p-values which are shown in **Fig. 5.11.**

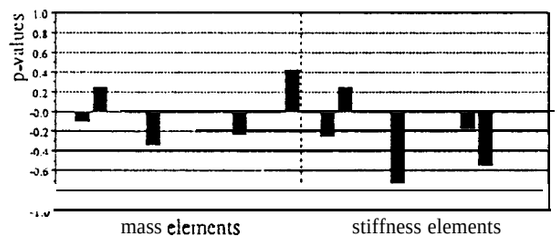


**Fig. 5.11:** p-values for an incomplete *experimental beam* model

All elements in error were correctly identified. The computed p-values were used to update the model in spite of the fact that a change in thickness affects both the inertia and the mass in the mass matrices and that the stiffness matrices are sensitive to both elastic modulus and thickness changes. In other words, the errors were not linear combinations of individual finite elements. Nevertheless, a plot of one of the FRFs of the updated model plotted together with the *experimental* one **(Fig. 5.12.)** showed a favourable comparison.

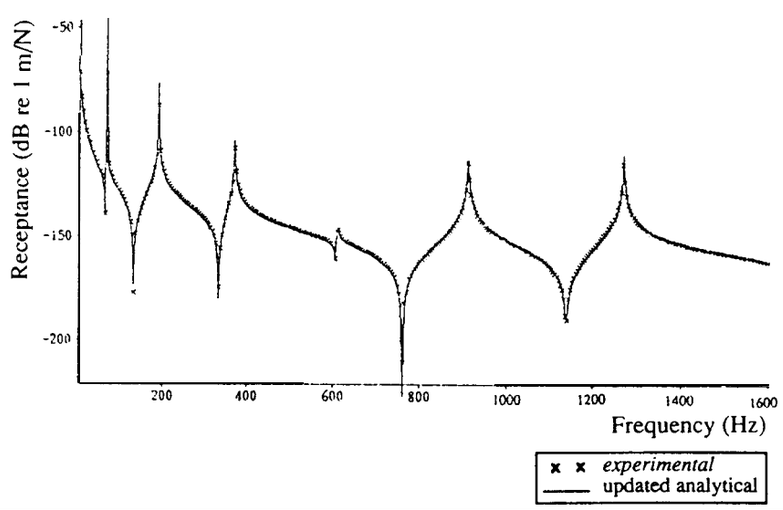


**Fig. 5.12:** Receptance FRF $\alpha_{5y5y}$ obtained from the *experimental* and updated analytical beam models

Note that in this case the model was corrected using a receptance column for excitation in the y direction only. The objective of the RFM is minimisation of the difference in frequency response between the ***experimental*** and updated models for a certain excitation point. In the beam example, no improvements were achieved for excitation in the other directions because only receptance curves for response in the y-direction were measured and the response directions in a simple beam model are decoupled. This was clearly shown by comparing a typical ***experimental analytical*** and updated FRFs for excitation in the z direction (Fig. 5.13) which indicated that care must be taken how the p-values are used to update a model.

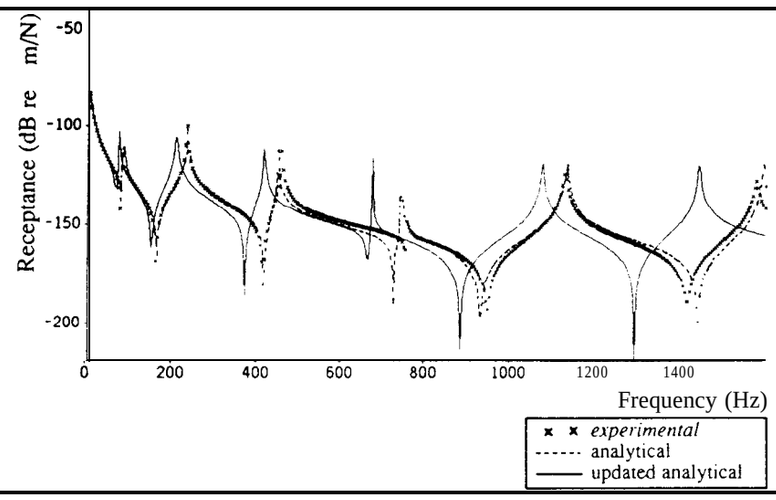


Fig. 5.13: Receptance FRF $\alpha_{5z5z}$ obtained from the ***experimental*** and updated analytical beam models.

A simple 2 DOF example, as shown in Fig. 5.14, demonstrated this problem further. Due to decoupling of x and y, element $k_2$ cannot be updated if only $\alpha_1$ of the experimental model is ***measured***. In general, if a set of ***experimental*** receptance data used in the RFM is insensitive to an analytical modelling error, this error cannot be detected using the given ***experimental*** data set. However, most modelling errors will affect the frequency response for several directions, and therefore the RFM can, in most cases, locate the modelling errors using a single receptance column.

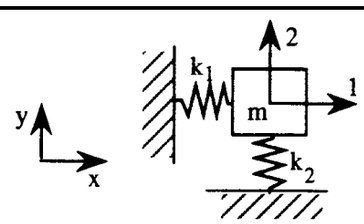


Fig. 5.14: 2 DOF system, x and y directions decoupled

### 5.6.3 Noisy *experimental* FRF data

In the case of incomplete FRF data with added noise, many sets of p-values can be obtained by choosing a different selections of frequency points and hence the solution is not unique. The number of frequency points used in any one set, $N_f$, is important for the convergence of the solution. As shown in section 5.3, the minimum number of frequency points which must be used is the ratio of the number of p-values to be calculated to the number of measurement points available. The adverse effects of coordinate incompleteness and noise can be partly offset by choosing more frequency points than the required minimum, but there is a cut-off point beyond which additional frequency points give no added benefit while increasing the CPU time for each run as the analytical receptance matrix needs to be calculated for each frequency point selected and each iteration. Furthermore, too many frequency points in the selection can substantially increase the number of iterations to reach convergence. It was observed that a 4 to 8 times overdetermined system produced the best convergence characteristics while locating the errors reasonably accurately. However, due to the surplus of *experimental* data it is possible to repeat the RFM using various sets of frequency points, each yielding a set of p-values. The scatter and repeatability of these p-values can then be investigated using some statistical analysis tools to help to identify the most reliable results.

3% noise was added to simulated FRF data of the uniform beam and six different sets of p-values were obtained. The computed p-values together with their mean, standard deviation and mean-to-standard deviation ratio are shown in **Fig. 5.15.** As can be seen from **Fig. 5.15c**, the mean-to-standard deviation ratio clearly identified the elements in error.

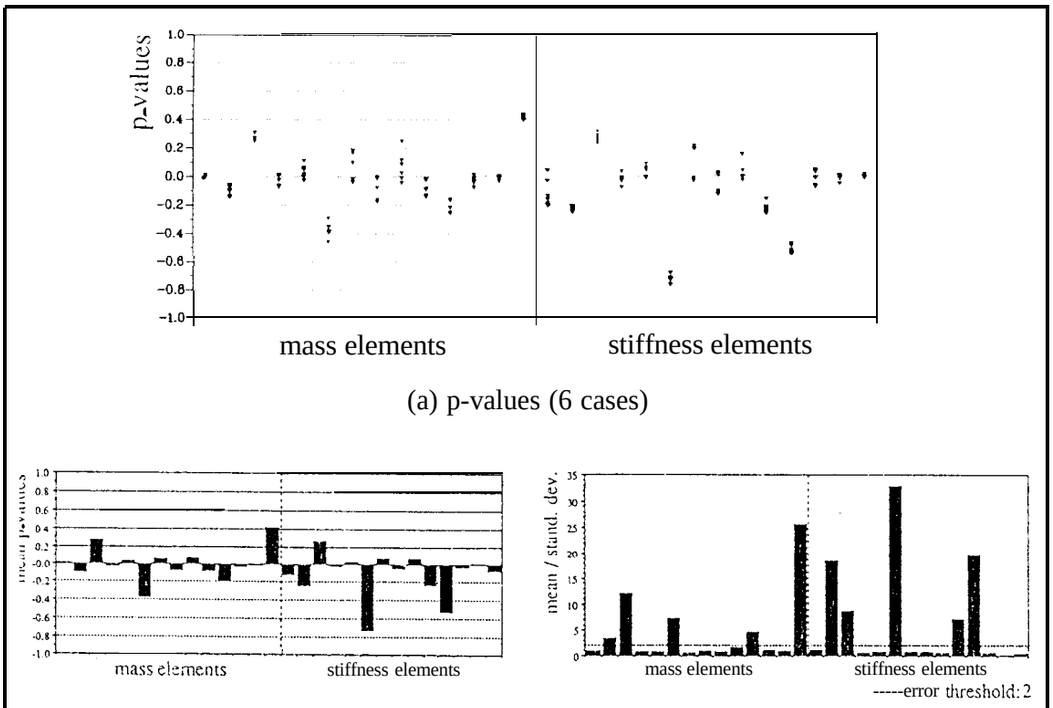


(a) p-values (6 cases)

(b) Mean p-values

(c) Mean p-value to standard deviation ratio

**Fig. 5.15:** p-values for an incomplete *experimental* model with 3% noise

A further case, this time with 6% added noise, is illustrated in **Fig. 5.16.** The average standard deviation of the p-values increased from less than 0.002 for no noise and 0.05 for 3% noise to 0.10 for 6%. Although the scatter of the p-values increased, the mean-to-standard deviation ratio still identified the elements in error. A mean-to-standard deviation ratio greater than 2 indicated the presence of an error if the scatter in p-values is small. In the case of 10% added noise **(Fig. 5.17)**, the average standard deviation was 0.19. Using an error threshold of 1, all elements in error were identified, apart from $m_2$, the smallest mass element change ($p(m_2)$=0.09).

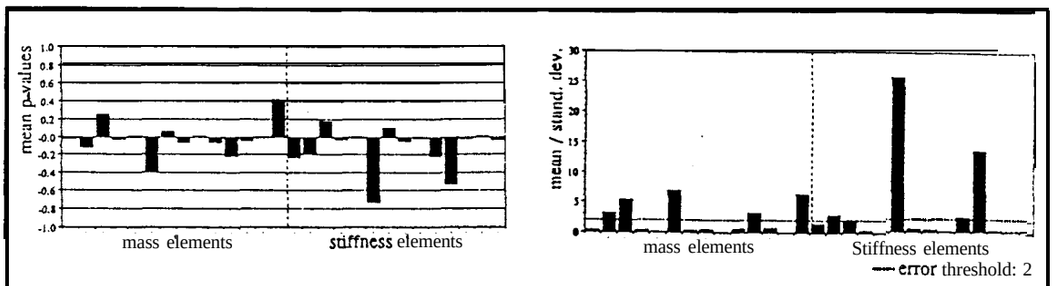


(a) Mean p-values (b) Mean p-value to standard deviation ratio

Fig. 5.16: p-values for an incomplete *experimental* model with 6% noise

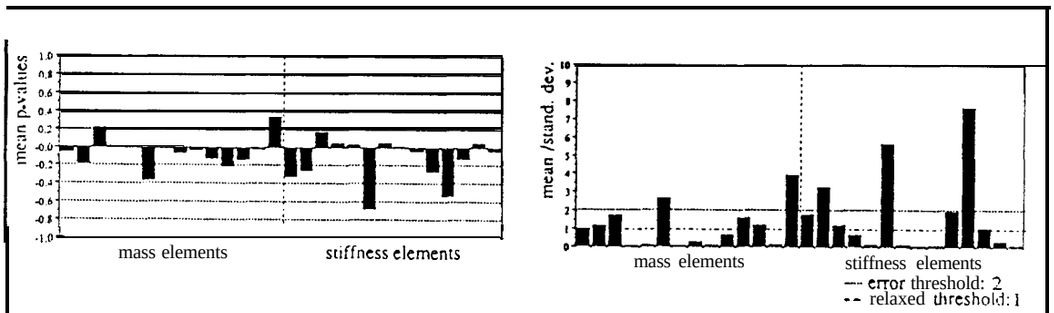


(a) Mean p-values (b) Mean p-value to standard deviation ratio

Fig. 5.17: p-values for an incomplete *experimental* model with 10% noise

### 5.6.4 The effect of excitation direction

To illustrate the effect of the excitation direction, some of the earlier cases were repeated for an excitation in the **z** direction, assuming that the **FRFs** were *measured* in the z direction instead of the y direction. The p-values obtained for the y and **z** excitations for the noise-free case are shown in Fig. 5.18. All mass errors had identical values but there were discrepancies in the magnitudes of the stiffness errors. This was not a surprising result since the p-values are linear modification factors for each element and as such they indicate the location of the errors and reflect an approximation of the modelling error but do not represent their actual magnitude. Results for the 3% noise case are plotted in **Fig. 5.19** and it is immediately seen that one of the errors was not located. The missing error corresponded to the smallest thickness change in the y direction and had a relatively small effect on the frequency response functions in the **z** direction.

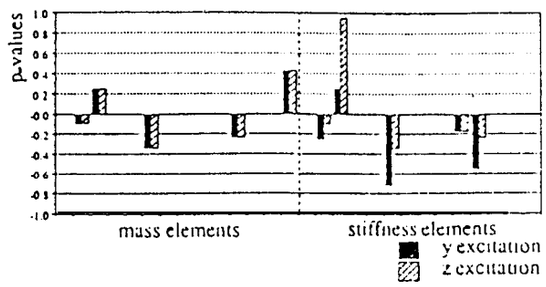


Fig. **5.18: p-values** obtained for excitation in **y** direction and excitation in **z** direction

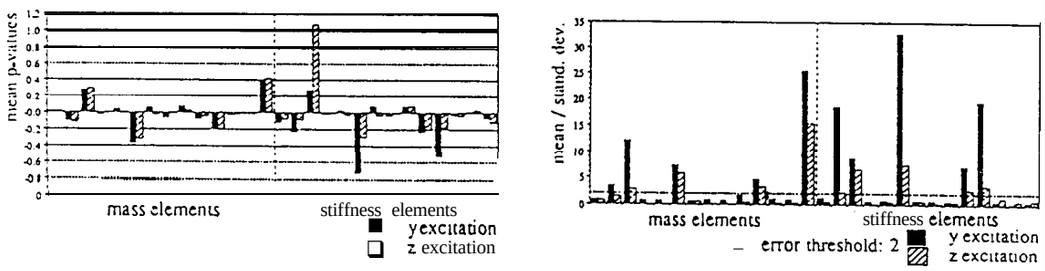


(a) Mean p-values (b) Mean p-value to standard deviation ratio

**Fig. 5.19:** p-values obtained for excitation in y direction and excitation in z direction for an incomplete *experimental* model with 3% noise

It is interesting to note that if data from two or more excitation directions are available, the error location process can be repeated for each direction and a comparison of the p-values should provide very useful information about the reliability of the error location process. In the case of zooming into erroneous elements by allocating additional p-values to individual element matrix elements, it is likely that concurrent use of FRF data from various excitation directions will be desirable and probably even essential.

### 5.6.5 The effect of reduced number of coordinates

Next the number of measurement sites was reduced from 15 to 7, i.e. a correspondence factor of 7.8% In this case, convergence was not so easily achieved: the average standard deviation increased to 0.20 for 3% noise and only the largest errors - namely, those in $m_6, m_{14}, k_6, k_{10}$ and $k_{11}$ - were detected (see **Fig. 5.20).** As only 7 out of 90 DOFs were known, and 5 (with p-values greater or equal to 0.22) out of a total of 10 elements in error were identified, this can be considered a satisfactory result.

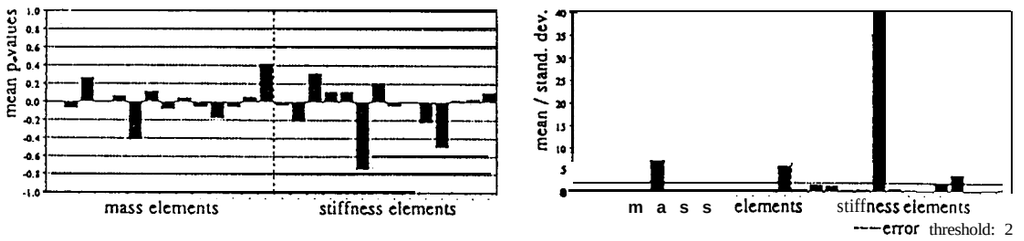


(a) Mean p-values (b) Mean p-value to standard deviation ratio

**Fig.** 5.20: p-values for an incomplete *experimental* model with 3% noise (correspondence factor 7.8%)

On reducing the number of measurement sites even further, to 5 only, the success rate (that is, the ratio of runs that converged to a solution to the total number of runs) dropped even further and the average standard deviation became 0.44. This was expected as the solution became increasingly unstable due to the reduced number of measurement sites. This can be observed in **Fig. 5.21:** changes in p values between iterations became more and more erratic until convergence was not achieved at all **(Fig. 5.21c**).

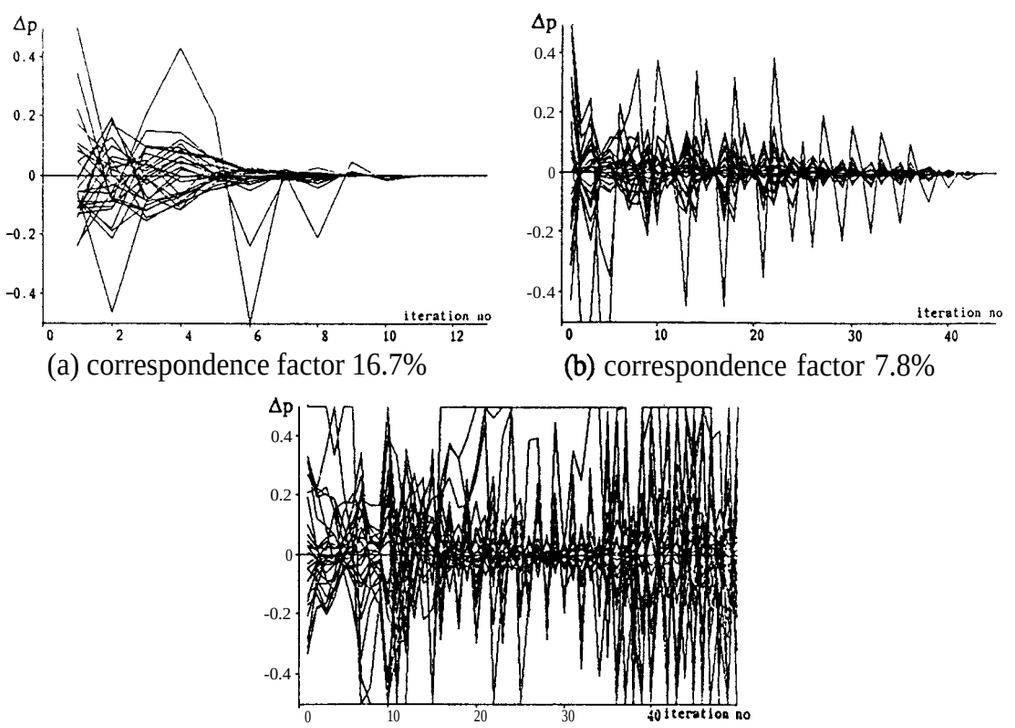


(a) correspondence factor 16.7% (b) correspondence factor 7.8%

(c) correspondence factor 5.6% (no convergence)

**Fig. 5.21:** Ap for each iteration for incomplete*experimental* beam models with 3% noise

### 5.6.6 The effect of coordinate mismatch

In the previous case studies it was assumed that the ***experimental*** FRFs were measured coordinates corresponding exactly to their analytical counterparts. In reality, coordinate mismatch often occurs: even for a simple beam, the measurement points will be on surface and not on the neutral axis, as was assumed so far. Therefore, a third FE model was set up to investigate the effect of this type of coordinate mismatch.

The third FE model consists of 168 24 DOF brick elements and 15 Y coordinates were assumed to be ***measured*** at one of the surfaces. Due to Guyan reduction of the FE model and differing finite element assumptions between beam and brick elements, extra discrepancies were inherently introduced in addition to the 3% noise which, as before, was randomly distributed over the ***experimental*** FRFs. An average of 14 iterations were required to reach convergence and the average standard deviation was 0.07. Six sets of p values were computed and, using the mean-to-standard deviation ratio and an error threshold of 2, all elements in error were identified **(Fig. 5.22).** However, for no apparent reason, an extra element, namely $k_8$, was also identified as being erroneous. The mean p-value of $k_8$ was relatively small at 0.074, and the resulting updated frequency response functions compared very well with corresponding experimental FRFs.

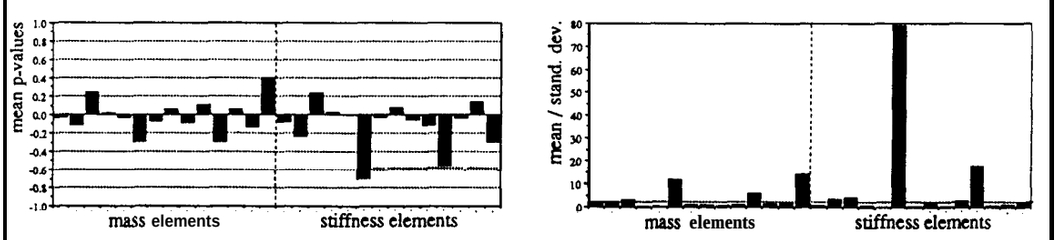


(a) Mean p-values (b) Mean p-value to standard deviation ratio

**Fig. 5.22:** p-values for an incomplete ***experimental*** model with 3% noise (15 ***experimental*** points on beam edge - model mismatch)

Due to the mixture of elements used, namely 3D brick elements for the ***experimental*** and 3D beam elements for the analytical model, each with different assumed shape functions additional modelling discrepancies were introduced. This phenomenon was of increasing significance for higher frequencies. The objective of model updating is to obtain an updated model with improved physical significance and Mottershead[115] emphasises

that one should not correct modelling errors due to model discretisation and element shape functions. However, the author of this thesis would like to point out that if this phenomenon has a significant influence over the frequency range of interest then the original analytical FE model can already be considered to be erroneous. The FE analyst should ensure that the FE mesh selected has "converged", i.e. such that mesh refinement gives no substantial changes in response in the frequency range considered.

## 5.7 THE GARTEUR III EXERCISE

The GARTEUR III exercise, first introduced in chapter 3, was also used as a RFM case study. Some initial difficulties in obtaining independent *experimental* data from other sources emphasise the importance of good communications between experimental&s and analysts. To overcome these difficulties the *experimental* and analytical data were generated by a common route.

The *experimental* **FRFs** were generated with 3% random added noise at 72 known coordinates, according to the modelling mismatches indicated in Fig. 3.9. A comparison of an *experimental* and analytical receptance curve is given in **Fig. 5.23.**

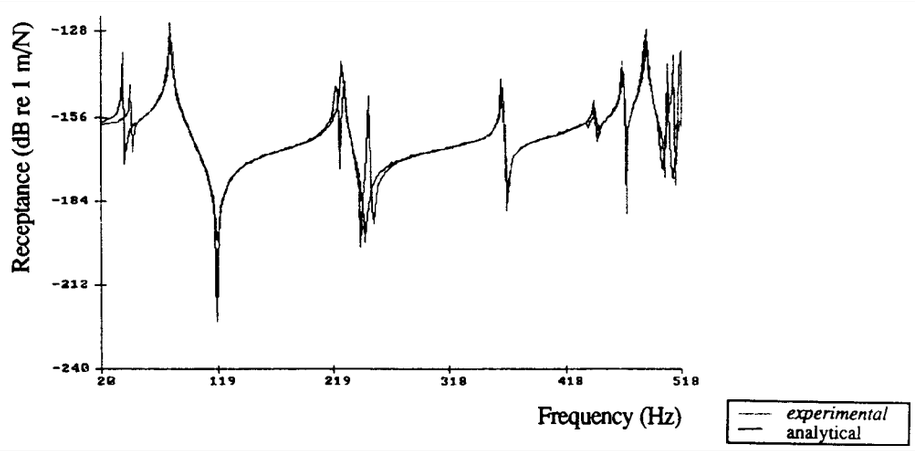


**Fig. 5.23:** Receptance FRF $\alpha_{31,31}$ obtained from the *experimental* and analytical **GARTEUR** models

Several runs were started but no convergence was obtained within 50 iterations. It is observed that certain elements (indicated in **Fig. 5.24)** were very unstable and their associated p-values tended to diverge. This phenomenon can occur either because some elements are insensitive (changes in the element mass and stiffness have no significant

appropriate rows makes the element unstable. One possible solution to eliminate elements which appear to be unstable from the updating process, is to assume that these elements are without error, an assumption which is not necessarily true. Another approach, as suggested in section 5.53, is to group unstable elements with their neighbouring elements thus forming macro elements and obtaining an averaged p-value. The latter option still enables some localisation of modelling errors in unstable elements and hence this approach is generally more applicable. Therefore the unstable elements for the GARTEUR model were grouped together with the adjoining elements

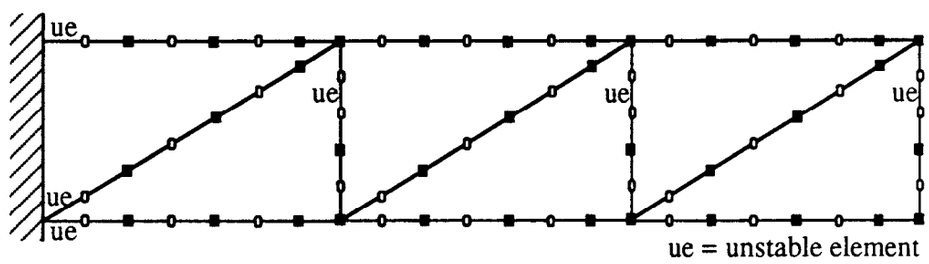


**Fig. 5.24:** Indication of unstable elements on the GARTEUR structure

Although convergence of all the p-values was still not obtained, the solution appeared to be more stable than before. The sum of the percentage difference squared at the selected frequency points (equation (7)) was used to monitor the behaviour of the RFM. Out of a total of 10 runs using different frequency point selections 6 runs were selected on the basis of the largest decrease in the sum of percentage differences squared. The mean-to-standard deviation ratio of the p-values at the iteration number for which this sum was a minimum are given in **Fig. 5.25.**

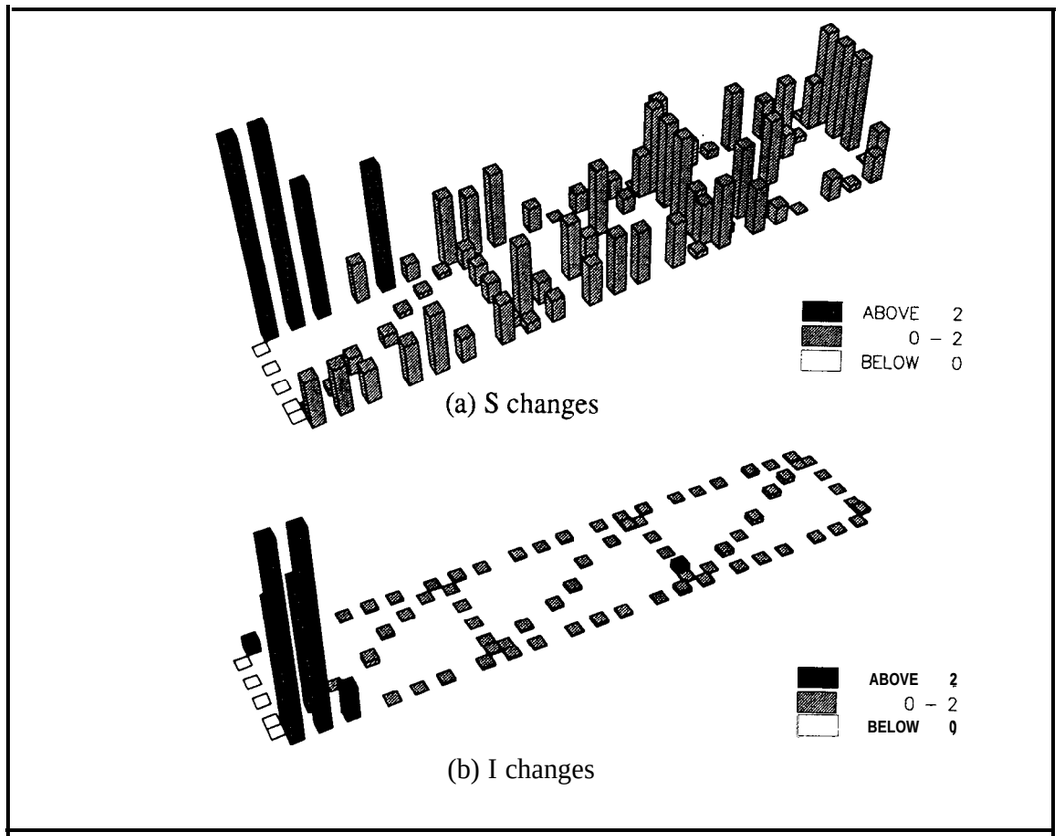


**Fig. 5.25:** Mean p-value to standard deviation ratio for GARTEUR III

Despite the difficulties reported above the results obtained were fairly encouraging, one element in error was not identified and two were incorrectly identified as erroneous but both additional p-values were small (see **Table 5.1).** Calculating the updated FRF and comparing this with the *experimental* one led to good agreement **(Fig. 5.25).**

| S changes | | I changes | |
|---|---|---|---|
| mean p-value RFM | true p-value | mean p-value RFM | true p-value |
| 1.31 | 1.00 | 0.33 | 0.25 |
| 1.31 | 1.00 | 0.33 | 0.25 |
| 1.18 | 1.00 | -0.85 | -0.83 |
| 0.22 | 0.00 | -0.82 | -0.83 |
| | | -0.82 | -0.83 |
| | | -0.82 | -0.83 |
| | | -0.82 | -0.80 |
| | | 0.00 | -0.80 |
| | | -0.29 | 0.00 |

**Table 5.1:** GARTEUR III, p-values.

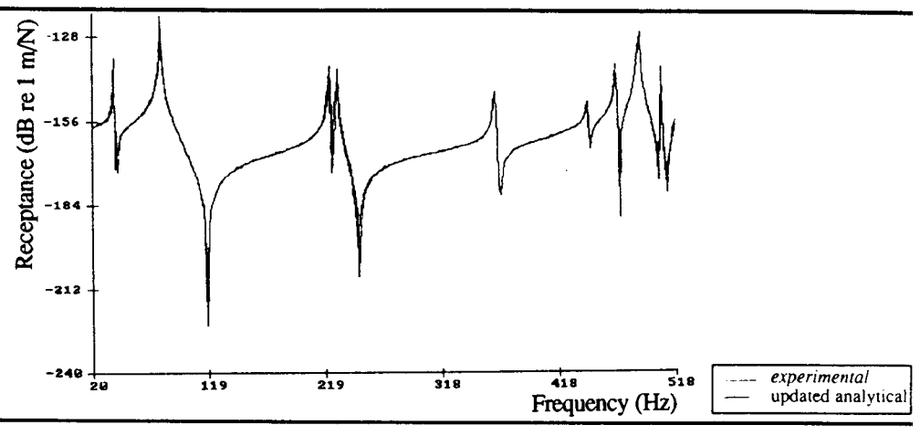


**Fig.** 5.26: Receptance FRF $\alpha_{31,31}$ obtained from the ***experimental*** and updated analytical GARTEUR models

Although these results were not a perfect unique solution, which cannot be achieved in case of incomplete noisy experimental data, they were very good compared to the results obtained using the error matrix methods (chapters 3 and 4).

## 5.8 CONVERGENCE CRITERIA

The convergence criterion is based either on the absolute or the relative difference between two successive p-values during the iteration process. The computation time was found to be very sensitive to this difference and a relative difference between two successive p-values of 0.1% was used for the beam case studies and the GARTEUR III exercise. Using a much smaller value results in numerous extra iterations without an added benefit, especially when the accuracy of the measured FRFs and the requirements of the updated model are considered. To reduce computation time further, an individual p-value which has satisfied this convergence criterion can be assumed to remain constant for all subsequent iterations.

The sum of the squared percentage differences between experimental and updated FRFs for the selected frequency points was also used as a convergence check in order to stop the iteration process when there were no further improvements from one iteration to the next. However, convergence should not be sought under this criterion unless all p-values show a satisfactory degree of convergence or only those p-values which have converged are included in the statistical analysis. **Fig. 5.27** shows typical variations in the sum of the percentage difference squared for case studies on the beam example (3% random added noise 15, 7, 5 measurement points).

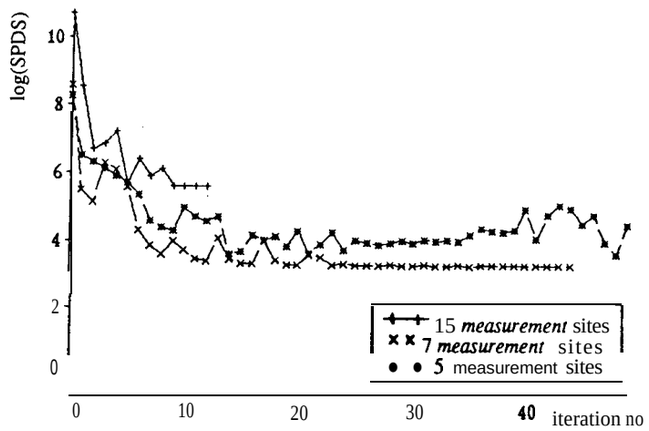


**Fig. 5.27:** Typical variations in the sum of the percentages difference squared

It was observed that usually, for the test cases carried out, convergence was not achieved if the sum of the differences squared exceeded the initial value for that run, unless this occurred during the first few (2 or 3) iterations when p-values can change erratically, giving rise to considerable changes in the FRFs. Comparing the drop in the sum of the percentage difference squared before and after the first iteration can be used as an indication for convergence, where a small drop suggests that it is unlikely to reach convergence and a large drop implies a good solution. Unfortunately however, the latter does not guarantee convergence.

Computation time can be reduced by analysing sets of p-values after a fixed number of iterations, e.g. for the 3% noise beam test case of section 56.3, all elements in error were identified after 8 or more iterations. However, best results are obtained if p-values of converging solutions only are included in the selection of sets. Generally, it is impossible to predict convergence until it has indeed been reached, especially for unstable solutions which can be due, for example, to noisy data or to a reduced number of measurement sites. Secondly, the speed of convergence is case-dependent. Therefore, a convergence criterion based on a fixed number of iterations is not recommended.

If, however, convergence is not reached after several frequency point selections, the statistical analysis applied to the p-values at the minimum of the sum of the percentage differences squared can give satisfactory results. This procedure can also be used in addition to the final p-values for converging test cases, where the most reliable results are those with the smallest average standard deviation.

Considering the relative importance of each of the p-values, one ought to bear in mind that the reliability of resulting p-values depends on the sensitivity of the experimental FRF data employed to changes in that element. Some element changes will have little influence on the resulting receptances corresponding to the measured data set in comparison with changes in other elements. The p-values of those elements are therefore ineffective for model updating purposes

## 5.9 CONCLUDING REMARKS

In this chapter the Response Function Method, an FRF-based updating technique, is introduced. The use of the RFM was investigated in some detail on a number of case studies: an 8 DOF lumped parameter model, a free-free beam model with known modelling errors and the GARTEUR III exercise. Satisfactory results were obtained, even in the case of noisy incomplete experimental data.

Although the number of possible solutions can be reduced dramatically using various constraints, it should be remembered that in the general case, where the experimental model is incomplete and contains noise, the updated model is not unique .

In the general case, modelling errors cannot be expressed as a linear combination of the individual element mass and stiffness matrices; hence the attempt to model the error in each element by a single p-value is only an approximation. This technique is useful for error location but not necessarily for updating.

In common with many other updating techniques, the incompleteness of the experimental model remains a major problem while correcting the analytical model using the RFM. The problem is overcome by substitution of the missing coordinates by their (updated) analytical counterparts and is also addressed on a statistical basis (thanks to the plentiful data) by considering several sets of possible solutions for various frequency point sets. It has been demonstrated that the updating procedure can be applied successfully in the presence of noise by judicious use of the ratio of mean to standard deviation of the p-values for error location.

As expected, noise on the measured FRF data has an adverse effect on error location since it tends to make the solution process unstable and it increases the scatter of the p-

values. A reduced number of measurement sites and model mismatch also have adverse effects.

It is recommended that the number of frequency points used for updating should be 4-8 times the minimum requirement to make the system of equations numerically stable and to reduce the adverse effects of noisy and incomplete experimental data. P-values can be unstable either because the system is insensitive to changes in particular elements, or because the solution process makes it unstable. The latter occurs especially when the number of measurement coordinates is too small in the vicinity of the corresponding element. It is therefore recommended that at least one coordinate per element should have an FRF associated with it. This can always be achieved by grouping elements together.

# CHAPTER 6

# UPDATING USING COMPLEX FRF DATA

## 6.1 INTRODUCTION

Vibration test data are always complex due to the inherent damping mechanism(s) dissipating energy in any vibrating system. Damping can be modelled as viscous, structural or Coulomb damping. Most FE models yield mass and stiffness system matrices only and damping is either ignored completely or some form of proportional damping is added at a later stage. As the objective of model updating is to obtain a correct analytical model, the identification of damping matrices also needs to be addressed. In updating analytical models using modal data, complex mode shapes can lead to many incompatibility problems. Some updating techniques are extended to include some form of damping identification, but real experimental mode shapes are usually required and this necessitates the conversion of the measured complex modes into real ones, thereby introducing additional inaccuracies. Updating techniques using FRF data should also include the complex nature of measured data to identify system damping matrices. In this chapter the RFM is extended to deal with complex experimental data and the derivation of a damping matrix is discussed.

## 6.2 THEORETICAL BACKGROUND

As previously, let us assume that modelling errors can be expressed as linear combinations of the individual element mass and stiffness matrices

$$[\Delta M] = \sum_{i=1}^{N_m} p_i [ M_{el}$$

$$[\Delta K] = \sum_{i=1}^{N_k} p_i [K_{e1} \qquad (1)$$

All practical structures exhibit a certain amount of damping and hence all measured frequency response data are complex. If we assume structural damping, the RFM (see chapter 5 equation (4)) can be written as:

$$[\alpha_A(\omega)]_{NxN}\,[-\omega^2\,[\Delta M] + [\Delta K] + i\,[\Delta D]\,]_{NxN}\{\alpha_X(\omega)\}_{i_{Nx1}} = \{\{\alpha_A(\omega)\}_i - \{\alpha_X(\omega)\}_i\}_{Nx1} \qquad (2)$$

with

$$[\Delta D] = \sum_{i=1}^{N_d} p_i\,[\,D_e\ 1 \qquad (3)$$

Rearranging equation (2) now gives:

$$[C(\omega)]_{Nx(N_m+N_k+N_h)}\ \{p\}_{(N_m+N_k+N_h)} = \{\Delta\alpha(\omega)\}_N \qquad (4)$$

As the p-values are always real numbers, equation (4) can be separated into its real and imaginary parts and the resulting equation rearranged as:

$$[C(\omega)]_{(2\ x\ P\ x\ N)\ x\ (N_m+N_k+N_h)}\{p\}_{(N_m+N_k+N_h)} = \{B(\omega)\}_{2\ x\ P\ x\ N} \qquad (5)$$

where P is the number of frequency points used.

In most cases, the finite element model is undamped and hence individual element damping matrices are not available. Nevertheless, a form of proportional damping i.e.:

$$[\,D_e\,] = \text{constant x}\ [\,K_e\,] \qquad (6)$$

can be assumed as a starting point. This form of proportional damping also allows for variations in damping values over the structure. For a more refined description of the damping; this can be assumed to be a linear combination of mass and stiffness element matrices and as such there will be 2 additional p-values associated with each finite element. This will increase the number of unknowns substantially and as the damping is most difficult to measure accurately in experiments, the added benefit of the finer description of the damping is likely to be lost.

## 6.3 CASE STUDIES ON A FREE-FREE BEAM

The initial individual element damping matrices were formed using proportional damping and the constant in equation (6) was taken as 1%. The *experimental* FRFs were generated via modal summation including a damping term.

Initially, it was decided to introduce 3% error simultaneously on both real and imaginary parts of the experimental FRFs and six sets of p-values were computed for six different sets of frequency points. The results are summarised in Fig. 6.1.

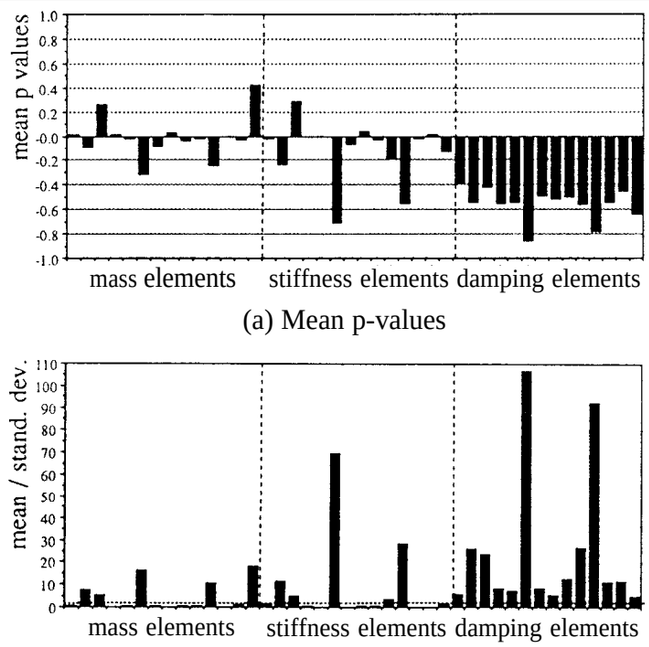


(a) Mean p-values

(b) Mean p-value to standard deviation ratio

Fig. 6.1: p-values for incomplete complex *experimental* data with 3% noise (simultaneous error on real and imaginary parts)

Also, it was decided to change the pattern of the imposed noise and 3% error was introduced independently on the real and imaginary parts of the FRFs and the same set of calculations were repeated. The results are summarised in Fig 6.2. Both sets of results were in agreement and furthermore the errors were located with good accuracy. (However, further calculations, not reported here, showed that the success of the method is dependent on the selection of the frequency points, a matter which will be explored in detail in chapter 7.) The resulting p-values suggested that the initial value of damping was too high since the average p-value for damping elements was about -0.5, indicating

that the initial estimate ought to be corrected by (l+p) = 0.5 which gave a damping constant of 0.5x.01=0.005. Also note that local variations in damping due to the modelling errors were reflected correctly in the damping p-values.

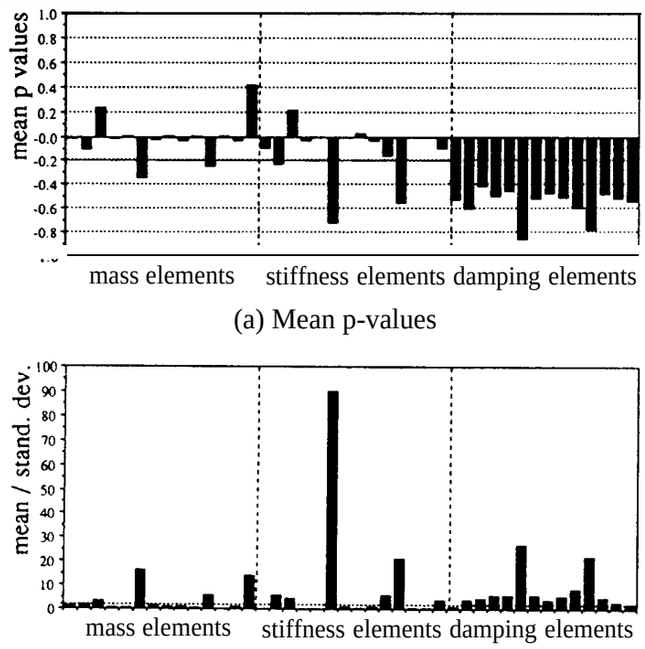


(a) Mean p-values

(b) Mean p-value to standard deviation ratio

**Fig. 6.2:** p-values for incomplete complex experimental data with **3%** noise (independent error on real and imaginary part)

In practice, the imaginary part of the FRF data is measured with less accuracy than the real part of the FRF data. Increasing the noise on the imaginary part caused the RFM to become less stable and convergence was not so easily reached. The main reason for this trend is that the p-values associated with the mass and stiffness elements converge faster and these are subsequently omitted from the iterative process while the RFM continues to identify modelling errors using the p-values associated with damping elements only. Hence at this stage the identified p-values for the damping elements may well include some updating values which are due to other modelling errors. That damping elements converge last is due to damping being of second order importance for off-resonance FRF data.

In cases of reasonable initial damping assumptions and moderate noise on the imaginary parts of the experimental FRF data, the damping matrix can be identified using the RFM, a feature illustrated above on the beam example. For more complex structures, the main

source of damping will be in the joints. In such cases, it will be reasonable to reduce the number of unknowns by specifying one damping p-value for each distinct continuous part of the structure (a macro damping element) and one p-value for each of the joints. As joints are often a major source of modelling errors and introduce some additional problems in model updating, the updating of joints will be investigated in detail in chapter 9.

It should also be noted that the introduction of noise to analytically-generated data by a random percentage error over the FRF is far from being realistic and merits research in its own right. Recently some initial numerical case studies of noise introduced by vibration measurement were presented by Jung [78].

## 6.4 USING MEASURED FRF DATA

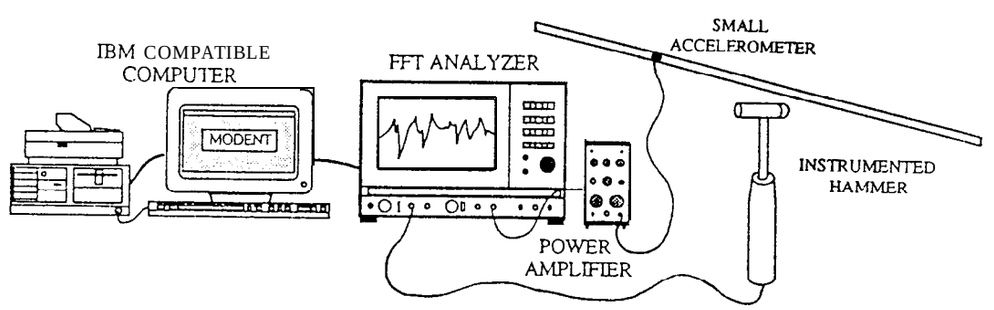


Fig. 6.3.: Experimental set-up

As shown in Fig. 6.3, the FRFs of the uniform beam were obtained via impact testing using a PCB hammer and a B&K accelerometer. The beam was freely suspended and an accelerometer was attached to a point at 400 mm from one end. Baseband inertances were obtained for a frequency range up to 1.6 kHz at 15 points in the y direction.

The p-values were first computed for real FRF data by setting the imaginary part of the measured FRF to zero. This was considered to be a justifiable approximation because of the light damping in the system and the selection of FRF data away from resonance peaks. Results from six independent runs are given in Fig. 6.4 from which it can be seen that mass errors in elements 2, 6, 11 and 14; and stiffness errors in elements 2,6,

10 and 11 were successfully located. However, fictitious errors in elements 8 and 10 were also suggested and the relatively small error in element 3 was not detected. This is in agreement with results presented in section 5.6.6 where model mismatch, as is present here, was simulated.

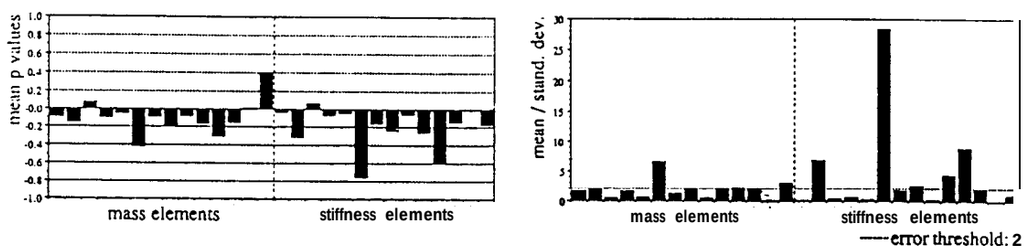


(a) Mean p-values (b) Mean p-value to standard deviation ratio

**Fig. 6.4:** p-values using the real part of measured FRF data

The updated FRF is plotted in **Fig. 6.5** together with the experimental and initial FRFs. In spite of the moderate success of the error location process, the mean p-values reflected the modelling errors with reasonable accuracy and it was immediately seen that the updated FRF is much closer to the measured FRF than the initial one.

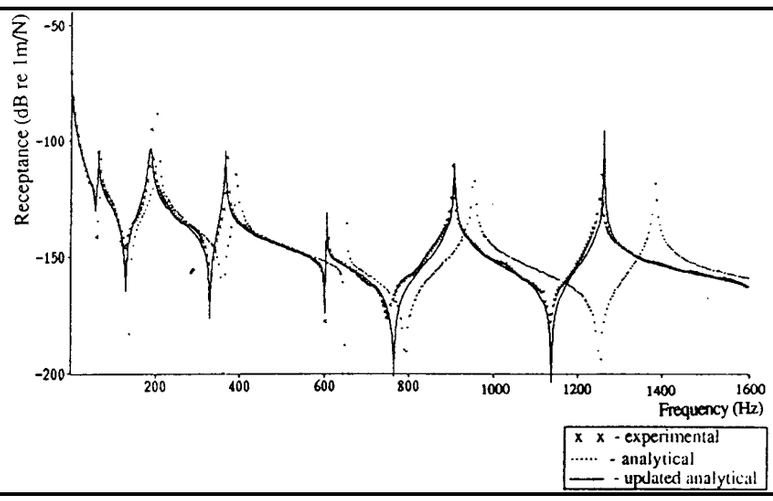


**Fig. 6.5:** Comparison of the measured, analytical and updated analytical receptance FRF $\alpha_{5y5y}$

It was then decided to use both the real and imaginary parts of the FRF and results after six runs are given in **Fig. 6.6. The** error location was not very successful in the sense that, in addition to the true errors, several fictitious ones were also indicated. The problem was traced to non-convergence of the damping p-values. This is perhaps not a

surprising result in view of the simplicity of the damping model used and the amount of *electronic* damping introduced during the signal processing stage of the measurements. The electronic damping was mainly caused by the exponential window applied to the measured displacement. The exponential window was applied to overcome leakage, a common signal processing problem associated with impact testing on lightly damped structures as, to satisfy periodic behaviour for correct Fourier transformations, the response must die away by the end of the sample time **(Fig.** 6.7).

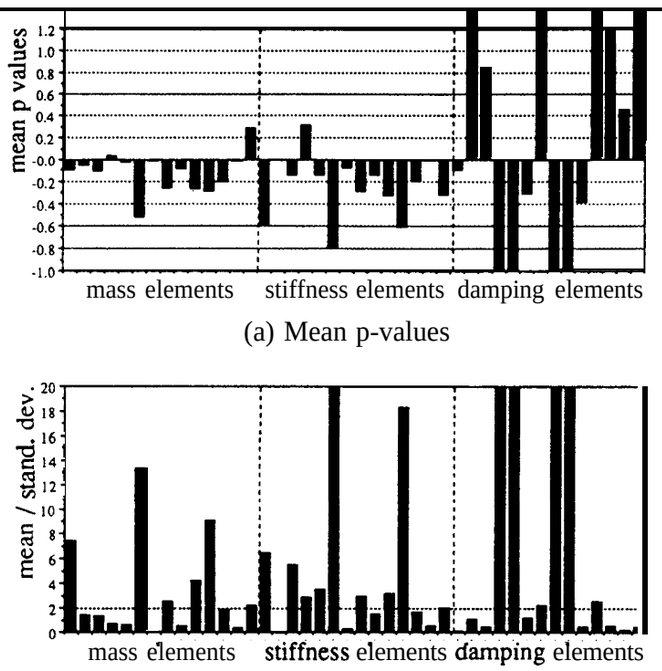


(a) Mean p-values

(b) Mean p-value to standard deviation ratio

**Fig. 6.6:** p-values using measured FRF data

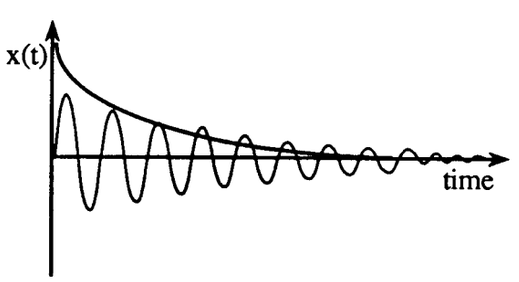


**Fig. 6.7: The** effect of an exponential window on lightly damped response data

As damping of the FRF data is of second order importance, experimental noise tends to drown the damping contributions of the **FRFs.** Other experimental errors can arise due to

(i) other signal processing errors, such as averaging which overcomes random error but not bias error(s), (ii) measurement equipment; such as the mounting effect of the accelerometer, (iii) the repeatability of the measurement, manually hitting at the same spot several times and (iv) measurement noise. Also, as mentioned previously, the fact that measurement coordinates are on the beam surface while the FE model coordinates are along its neutral axis, has an adverse effect on the RFM too.

Results obtained by setting the imaginary part of the FRF to zero (Fig. 6.4) were reasonable, while those obtained by retaining both real and imaginary parts of the FRF data were not so satisfactory. Good initial assumptions about the damping present in the structure and accurate (less noisy) measurement response data are required for successful identification of the damping matrix.

## 6.5. CONCLUDING REMARKS

The use of the Response Function Method in the case of complex experimental data has been investigated for the case of the free-free beam example of chapter 5 using both simulated and measured FRF data to update an initial analytical model.

Complex FRF data with noise, simulated or measured, make the convergence process slow and often numerically unstable. However, in the case of lightly damped structures, an acceptable solution can be found by setting the imaginary part of the FRF to zero.

Good initial assumptions about the damping present in the structure and accurate measured response data are required to identify a damping matrix successfully.

The results obtained indicate the necessity of further investigation on the convergence of the RFM in the case of *difficult* FRF data and on methods of stabilising the solution process. These issues will be addressed in the next chapter.

# CHAPTER 7

# COMPUTATIONAL ASPECTS OF THE RFM

## 7.1 INTRODUCTION

The basic methodology of the RFM and the use of statistical analysis tools in the case of incomplete noisy experimental data has been demonstrated in chapters 5 and 6. It has been found that for certain test cases the solution process can become unstable, reducing the success rate of the various runs of the RFM. This proves to be a significant problem when complex experimental FRFs are used, i.e. when damping is included, but can also be due to noise, an insufficient number of measurement sites and/or model mismatch. Therefore, methods to stabilise the solution process need to be addressed. Possible solutions are: (i) improvement of the solution procedure, e.g. balancing the final set of equations just prior to inversion, and (ii) improving the frequency point selection. This chapter evaluates these options together with some other computational considerations of the RFM

## 7.2 RFM SOLUTION IMPROVEMENTS

To improve the RFM solution procedure for each iteration there are various avenues to be explored. The free-free steel beam of dimensions 25.4 x 31.75 x 1400 mm, with a finite element model consisting of 14 3D beam elements, as introduced in chapter 5 **Fig. 5.8,** was considered again. The *experimental* data consisted of a numerical simulation of an incomplete receptance column with 3% random added noise. Four test cases (2 cases without damping and 2 cases with proportional damping) were used to evaluate the effectiveness of the proposed procedures.

### 7.2.1 Iterative refinement

To solve the overdetermined system of linear equations of the RFM, $[C](p)=\{\Delta\alpha\}$, a pseudo-inverse (i.e. SVD or generalised inverse) of [C] is used, which yields an approximate solution for the p-values. To check whether any non-convergence is

encountered due to numerical errors while inverting [C], a residual is calculated. The residual (r} is defined as:

$$\{r\} = \{\Delta\alpha\} - [C]\{p\} \tag{1}$$

where {p} is calculated from $[C]\{p\}=\{\Delta\alpha\}$.

This residual can subsequently be used in an iterative refinement technique to improve the solution. The following algorithm [116] is applied for each iteration within the 4 test cases:

(i) calculate $\{p\}_1$ from $[C]\{p\}=\{\Delta\alpha\}$
(ii) calculate the residual as $\{r\}_1=\{\Delta\alpha\}-[C]\{p\}_1$
(iii) calculate $\{p\}_2=[C]^{-1}\{r\}_1$
(iv) $\{p\} = \{p\}_1+\{p\}_2$
(v) repeat from (ii) till $\|\{p\}_{n-1}-\{p\}_n\| <$ tolerance

At all stages during the 4 examples the residual appeared to be small, and the results demonstrated that the iterative refinement algorithm gave no further improvement to the solution: both the number of iterations to reach convergence and the final p-values were the same with and without this iterative refinement. As the system is several times overdetermined, and an optimum least squares solution for each iteration is already obtained, including the iterative refinement just adds to the CPU time required without any apparent additional benefit to the quality of the solution.

### 7.2.2 Balancing the solution matrices

A second possibility of improving the solution process can be by balancing the system matrices. Various balancing options were considered as follows (see **Fig. 7.1):**

(i) No balancing, as in chapters 5 and 6.
(ii) Balancing all mass-related elements in [C] with respect to the maximum mass-related value; all stiffness-related elements with respect the maximum stiffness related value and similarly for damping elements, if any. This ensures that each element type carries equal weight in the updating process. The balancing is achieved by multiplying the appropriate rows with a constant, defined as $Bc_{Mel}, Bc_{Kel}, Bc_{Del}$ respectively **(Fig. 7.1).**
**(iii)** Balancing each row in [C] to a maximum element value of 1.0 by multiplying each row with constant $Bc_{Ri}$. Now, for each selected frequency point, the

corresponding experimental value has the same confidence. Without this type of balancing, the order of importance can vary substantially between rows, depending on the frequency point selected and its associated response levels.

(iv) Using a combination of (ii) and (iii).

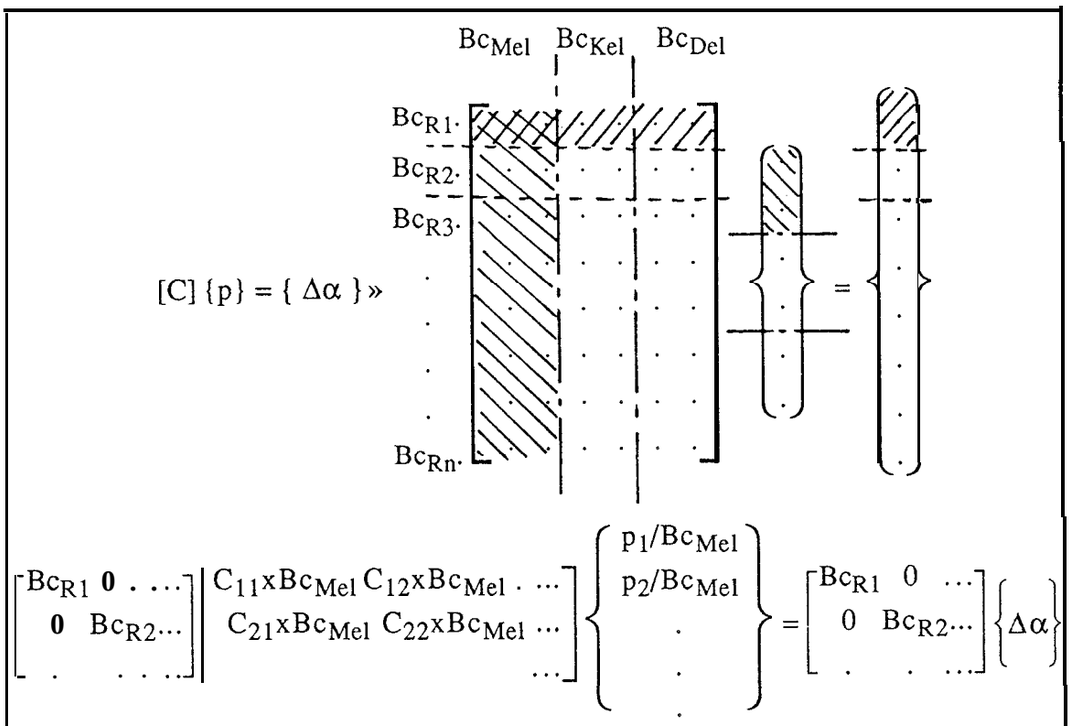


**Fig. 7.1:** Balancing of RFM system matrices

Comparisons of the sum of the percentage differences squared:

$$SPDS = \sum_{k=1}^{nfpts} \sum_{j=1}^{ncor_x} \left( \frac{\alpha_{x_{ij}}(\omega_k) - \alpha_{u_j}(\omega_k)}{\alpha_{x_{ij}}(\omega_k)} x100 \right)^2$$

for the frequency points selected for each of the four examples using the four possible balancing approaches are given in **Fig. 7.2.** The starting and end values of the sum of the percentage differences squared for the four test cases, and the average standard deviation for mass and stiffness p-values, using the various balancing options, are given in **Table. 7.1.**

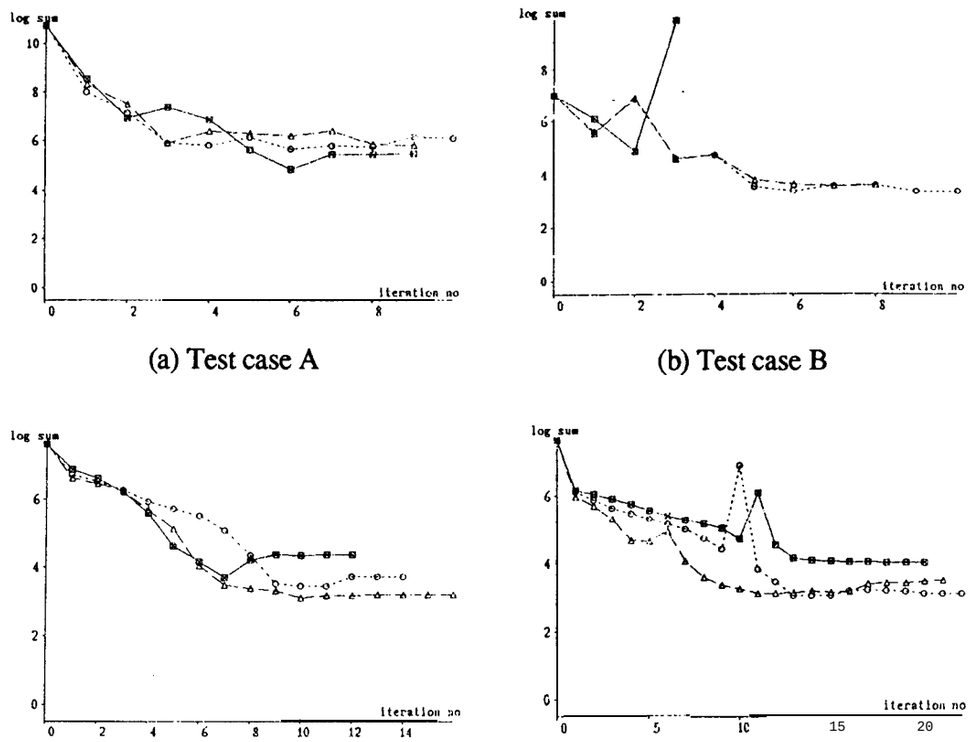


**Fig. 7.2: The** sum of the percentage differences squared for 4 beam examples
□ no balancing - option (i). x balancing option (ii), A option (iii), o option (iv)

| case | SPDS | SPDS end no bal. (i) | SPDS end (ii) | SPDS end (iii) | SPDS end(iv) |
|---|---|---|---|---|---|
| A | $0.6 \times 10^{11}$ | $0.3 \times 10^{6}$ | $0.3 \times 10^{6}$ | $0.6 \times 10^{6}$ | $0.4 \times 10^{6}$ |
| B | $0.1 \times 10^{8}$ | $0.7 \times 10^{10}$ | $0.7 \times 10^{10}$ | $0.4 \times 10^{4}$ | $0.2 \times 10^{4}$ |
| C | $0.4 \times 10^{8}$ | $0.2 \times 10^{5}$ | $0.2 \times 10^{5}$ | $0.2 \times 10^{4}$ | $0.5 \times 10^{4}$ |
| D | $0.4 \times 10^{8}$ | $0.1 \times 10^{5}$ | $0.1 \times 10^{5}$ | $0.3 \times 10^{4}$ | $0.1 \times 10^{4}$ |
| mean of the standard deviation of final p-values | | 0.054 | 0.054 | 0.027 | 0.021 |

**Table 7.1:** Comparison of results using various balancing options

As can be seen from **Table 7.1,** option (iv) gave better results, in most cases, when compared with the other options and also provided the most stable process **(Fig. 7.2).**

Using the beam example without damping another 10 sets of results were computed using different random frequency point selections. Without balancing, 4 convergent and 6 non-convergent solutions were obtained while including balancing option (iv) resulted in 9 converging solutions, with equal or better results. This was also verified on a complex *experimental* data-set with 3% random noise on the real part and 10% random noise on the imaginary part of the FRFs. This test case did not generate an adequate solution using the standard RFM, while, as shown in **Fig. 7.3,** good results were obtained when balancing was included.

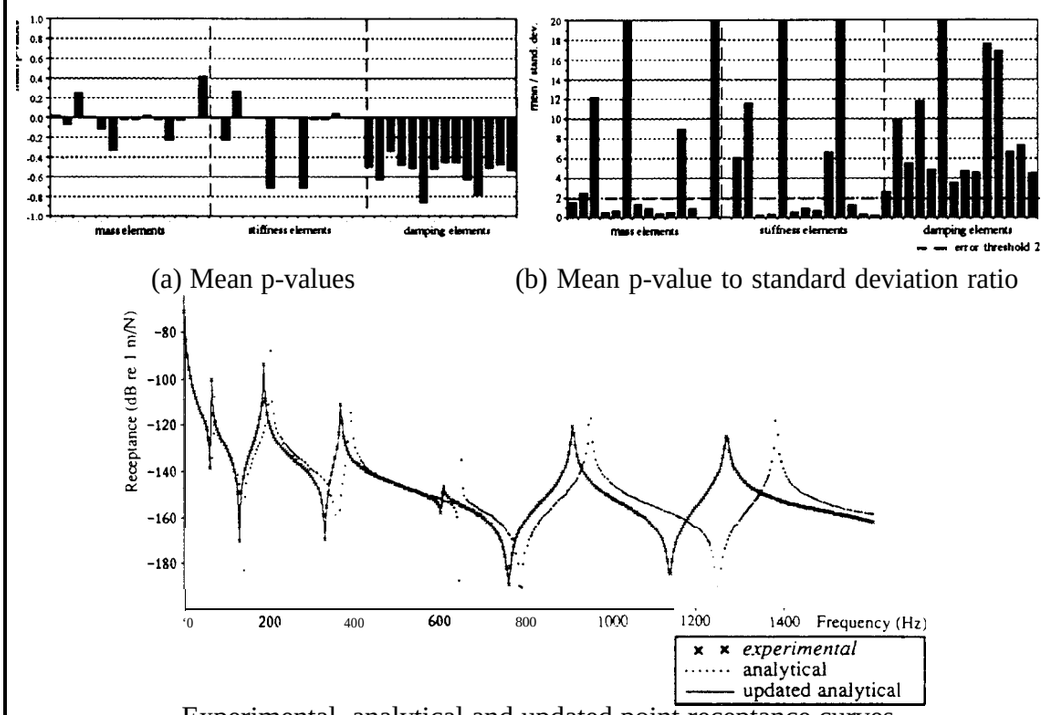


(a) Mean p-values (b) Mean p-value to standard deviation ratio

(c) Experimental, analytical and updated point receptance curves

**Fig. 7.3:** the RFM applied to an incomplete complex *experimental beam* example with independent noise on real and imaginary parts, 3% and 10% respectively

Balancing the system matrices can be compared to weighting as used in Bayesian optimisation model updating approaches. The difference here lies in the fact that weighting matrices aims to reflect the estimated distribution of confidence in the measured data based either on the variance or on engineering judgement while for balancing option (iv) no such presumptions are made. The aim of balancing is to simply maximise

numerical stability by reflecting equal importance with respect to element type and measured data for each FRF data point selected.

### 7.2.3. Recommendations

The inclusion of an iterative refinement algorithm to the solution process increases the CPU time required without additional benefit to the resulting p-values. Therefore, the use of such a refinement is not recommended.

In contrast it has been shown that balancing the matrices can be beneficial to the convergence of the solution. Hence, it is recommended that such a procedure should be included as a standard feature of the solution process.

## 7.3 FREQUENCY POINT SELECTION FOR THE RFM

This section investigates the rationale of the frequency point selection, and endeavours to answer the following questions:

- "Why do results for some frequency point selections converge and others diverge or become rank-deficient?;
- "Which frequency points are most likely to give good results?;
- "Is it possible to converge to a wrong solution?".

Some of these questions have been partly answered by the experience gained from the numerous test cases already reported. However, as there are many variables to consider, it is perhaps appropriate to consider some simple 1 and 2 DOF systems.

### 7.3.1 Basic Equations

**SDOF system**

Consider an undamped SDOF lumped mass-spring system **(Fig. 7.4a)**. For this:

$$[\alpha(\omega)] = [Z(\omega)]^{-1} = \left[[K] - \omega^2[M]\right]^{-1} = \frac{1}{k \quad \omega^2 m} \qquad (1)$$

The basic RFM applied to this case is:

$$\alpha_A(\omega) - \alpha_X(\omega) = \alpha_X(\omega)\, \Delta Z(\omega)\, \alpha_A(\omega) \tag{2}$$

which becomes:

$$AZ(o) = \frac{\alpha_A(\omega) - \alpha_X(\omega)}{\alpha_X(\omega)\, \alpha_A(\omega)} \tag{3}$$

In the derivation of the RFM it was already stated that there exists no solution if the receptance matrix [a] is singular: that is, at anti-resonance or resonance frequencies. However for a SDOF case, other problems might arise if:

(i) $\Delta\alpha(\omega) = a,(w) - a,(o) = 0$, hence $\Delta Z=0$, indicating $\Delta k - \omega^2 \Delta m = 0$ (4a)

(ii) $\alpha_X(\omega) >> \alpha_A(\omega)$, then $AZ(o) = \dfrac{-\alpha_X(\omega)}{\alpha_X(\omega)\, \alpha_A(\omega)} \approx \dfrac{-1}{\alpha_A(\omega)}$ (4b)

(iii) $\alpha_A(\omega) >> \alpha_X(\omega)$, then $\Delta Z(\omega) = \dfrac{\alpha_A(\omega)}{\alpha_X(\omega)\, \alpha_A(\omega)} \approx \dfrac{1}{\alpha_X(\omega)}$ (4c)

These three categories can, clearly, lead to erroneous results. Categories (i) and (iii) should be treated with caution as, in the limit, the resulting p-values depend on the experimental receptance value only, which contains experimental noise. Of course, the detriment of random errors in the experimental data can be overcome by selecting enough frequency points to make an overdetermined system and thus to obtain an averaged p-value. This will also be beneficial to overcome problems due to poor frequency point selection, as the chance that all randomly-selected frequency points have receptance values falling in the same categories (i), (ii) or (iii) must be small.

(a) a SDOF system (b) a 2 DOF system

**Fig. 7.4**: SDOF and 2 DOF systems

## 2 DOF system

As a SDOF system has no anti-resonances, an alternative 2 DOF system **(Fig. lb)** is considered. Assuming that only $\alpha_{11}$ is measured and using a single frequency point, the RFM is determinate if there is just one element in error. The RFM gives the following expressions for a single modelling error only (see appendix A, equation (A10)):

$$\text{if } p_{m_2} = p_{k_1} = p_{k_2} = 0 \qquad p_{m_1} = \frac{\alpha_{11_A}(\omega) - \alpha_{11_X}(\omega)}{-\omega^2\, \alpha_{11_X}(\omega)\, m_1\, \alpha_{11_A}(\omega)} \tag{5a}$$

$$\text{if } p_{m_1} = p_{k_1} = p_{k_2} = 0 \qquad p_{m_2} = \frac{\alpha_{11_A}(\omega) - \alpha_{11_X}(\omega)}{-\omega^2\, \alpha_{12_X}(\omega)\, m_2\, \alpha_{12_A}(\omega)} \tag{5b}$$

$$\text{if } p_{m_1} = p_{m_2} = p_{k_2} = 0 \qquad p_{k_1} = \frac{\alpha_{11_A}(\omega) - \alpha_{11_X}(\omega)}{\alpha_{11_X}(\omega)\, k_1\, \alpha_{11_A}(\omega)} \tag{5c}$$

$$\text{if } p_{m_1} = p_{m_2} = p_{k_1} = 0 \qquad p_{k_2} = \frac{\alpha_{11_A}(\omega) - \alpha_{11_X}(\omega)}{(\alpha_{11_X}(\omega) - \alpha_{12_X}(\omega))\, k_1\, (\alpha_{11_A}(\omega) - \alpha_{12_A}(\omega))} \tag{5d}$$

Equations (5) illustrate, that there again exists no solution at anti-resonance or at natural frequencies. With reference to the three categories which possibly yield erroneous results as identified previously (equation (4)) , only in case of ml- or $k_1$-modelling errors will the same problems be encountered. For modelling errors in $m_2$ or $k_2$, the categories (ii) and (iii) become more compounded as the unmeasured coordinate is also included in the

equation. This illustrates that the RFM is case-dependent on the particular analytical model to be updated and the modelling error(s) to be identified.

### 7.3.2 Noise-free 2 DOF test cases

In the 2 DOF test cases only one element was in error at a time and hence a determinate system was achieved using a single value of $\alpha_{11}$ during any one RFM run. The first test case had a **+20%** error in the value of $k_2$ of the analytical model, and a comparison of the receptance curves is shown in **Fig. 7.5a**. A frequency range from 30 to 80 Hz in steps of 0.5 Hz was considered and, assuming $\alpha_{11}$ only was *measured,* each frequency point was used consecutively to find $p_{k_2}$. **Fig. 7.5b** shows the variation in p-values obtained and **Fig. 7.5c** displays the number of iterations to reach convergence. A correct **p**-value of -0.2 was identified over the entire frequency range except around the experimental resonances. In this case, data points selected around the regions of the *experimental* anti-resonances, the analytical resonances and analytical anti-resonances had no significant adverse effects on the RFM. Employing data points around the experimental resonances or below the first resonance showed that it is possible to obtain erroneous p-values if the experimental data are incomplete, even if there is no experimental noise *and the* error location is known. For a complete experimental data set, the correct p-vale was obtained in 1 iteration, independent of frequency point selection.

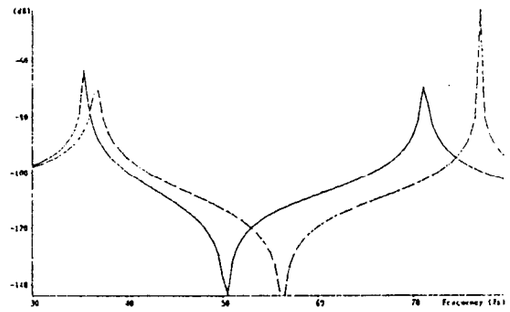

(a) Receptance curves $\alpha_{11}$

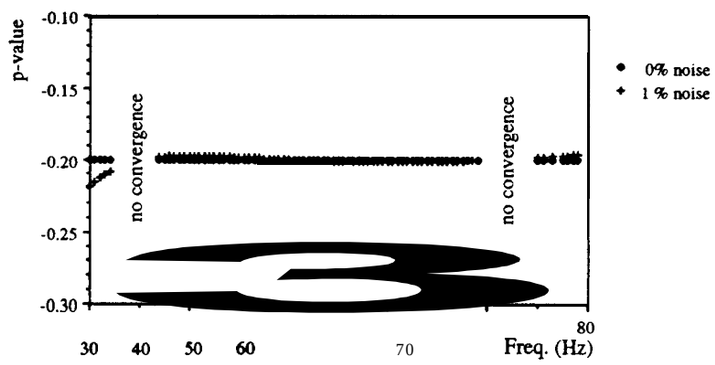


(b) p-value against frequency point selected

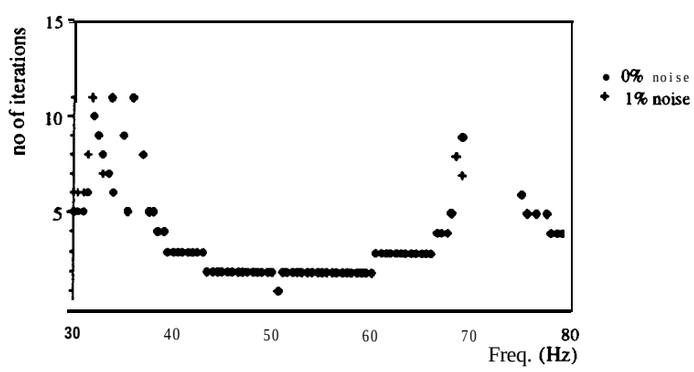


(c) Number of iterations against frequency point selected

**Fig. 7.5: 2** DOF test case, **+20%** $k_2$ error

These results were compared with results obtained for a **+20%** change in $m_1$ and subsequently in $m_2$ of the analytical model, as shown in **Figs. 7.6** and 7.7. For a change in ml, the correct p-values were obtained irrespective of frequency point selected. The effects of frequency point selection observed for a change in $m_2$ were similar to those for a change in $k_2$. This suggested that the location of the measurement point on the structure under study is important, and that improved success in error location can be

achieved if the measurement points are directly at the element in error. However, as error locations are generally unknown, this will be difficult to achieve in practice. Careful thought before measurement is suggested, as many errors **will** occur at or near joints, and so an adequate number of measurement sites will be required in those regions. For a $k_1$ modelling error the RFM shows the same behaviour with respect to the frequency point selection as for a $m_1$ modelling error, as expected by inspection of equations (5a) and (5c).

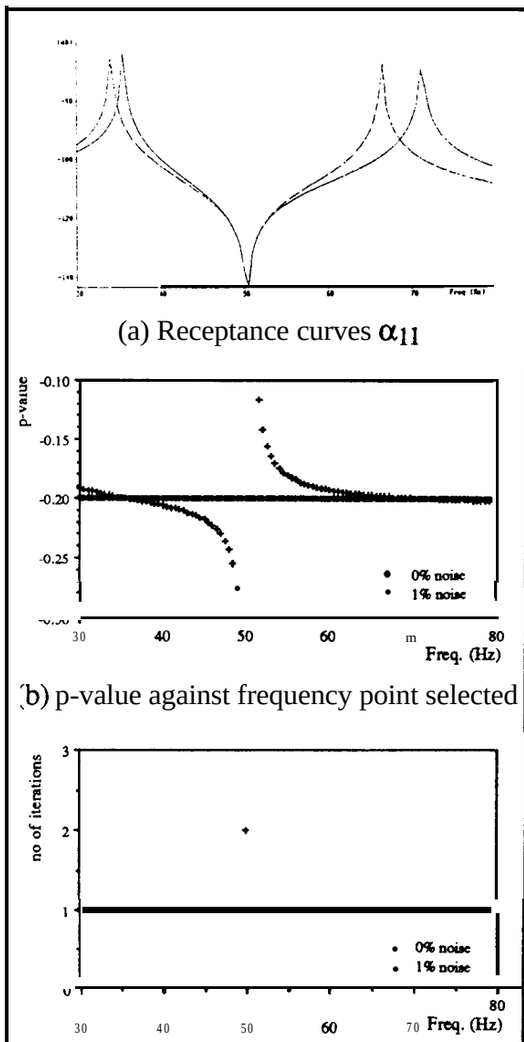


(a) Receptance curves $\alpha_{11}$

(b) p-value against frequency point selected

(c) Number of iterations against frequency point selected

**Fig.** 7.6: 2 DOF test case. **+20% $m_1$** error

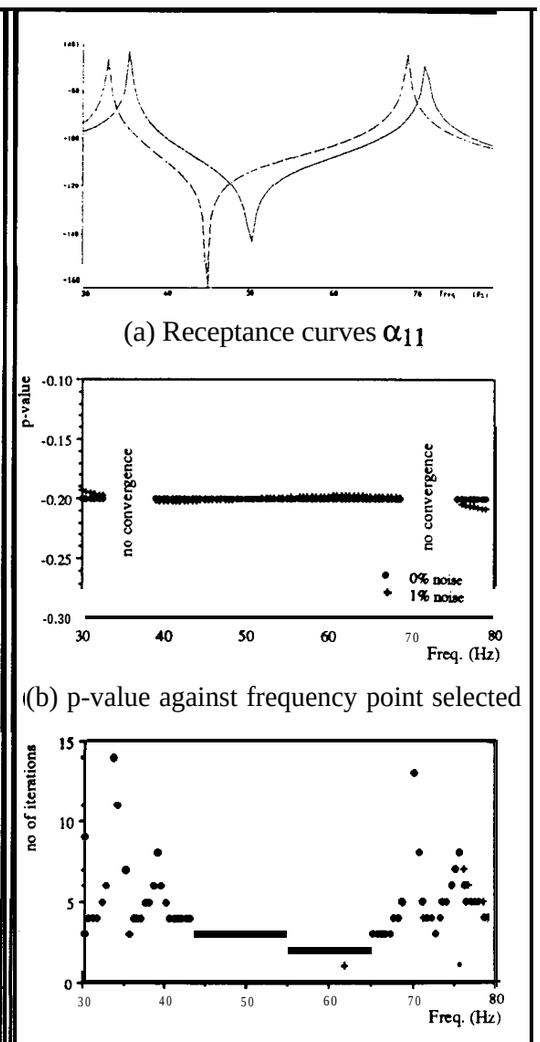


(a) Receptance curves $\alpha_{11}$

(b) p-value against frequency point selected

(c) Number of iterations against frequency point selected

**Fig.** 7.7: 2 DOF test case, **+20% $m_2$** error

It appears that from the categories (i) - (iii) identified in section 2.1, only (ii) represented a real problem for noise-free data. As there was no noise on the simulated ***experimental*** data, category (i) was acceptable and category (iii) did not pose any difficulties as, after

the first iteration, the analytical receptance curve was updated using the identified p-value and the analytical resonance shifted away from that particular frequency point.

### 7.3.3 2 DOF test cases with noise

The effect of noise was investigated for each test case, again assuming that only $\alpha_{11}$ was measured. A constant percentage, 1%, of bias error was added to each *experimental* receptance value, $\alpha_{Xn}(\omega) = 1.01\ \alpha_X(\omega)$. The effect of bias on p-values is also shown in **Figs. 7.5-7.7**. The effect of bias was worst below the first resonance, and hence this frequency range should be avoided. If the solution converges, the effect of the *experimental* error was smallest for frequency points closer to resonances when the resulting error in the p-values was a minimum. The error in the p-values due to the bias on the *experimental* receptance value increased as the percentage difference between *experimental* and analytical receptances decreased, as in that case $\Delta\alpha$ became dominated by the *experimental* error. This was especially noticeable for a +20% change in $m_1$, where the analytical and *experimental* anti-resonance for $\alpha_{11}$ coincided: here, the solution stopped after 1 iteration and an incorrect p-value was obtained. In this test case, even for a complete *experimental* receptance column with 1% added bias, an incorrect p-value was obtained from the RFM for a frequency point near the anti-resonance.

**Fig. 7.8** shows the effect of various percentages of bias on p-values against frequency point selected. As expected, a higher *experimental* error resulted in a less accurate p-value. It was also noticed that the frequency range around *experimental* resonances for which no convergence was obtained became wider.

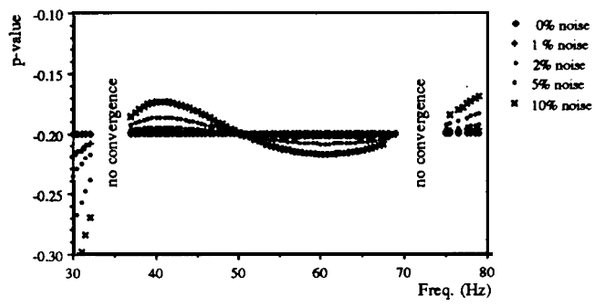


(a) p-value against frequency point selected

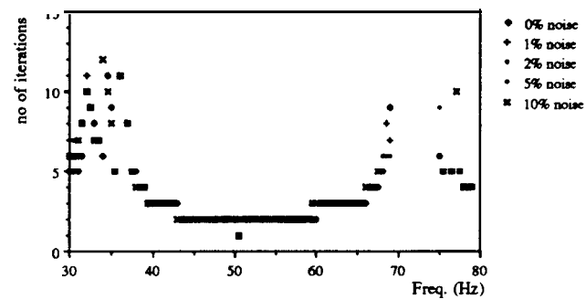


(b) Number of iterations against frequency point selected

**Fig. 7.8: 2** DOF test case, **+20%** $k_2$ error, noisy experimental data

A constant error value added to the ***experimental*** receptance curve was also investigated **(Fig. 7.9).** This showed that the two largest p-value errors occurred below the first resonance and above the second resonance, and these frequency ranges should be excluded from the frequency point selection. However, in practice, the measurement frequency range will never include all modes, therefore the frequency range above the highest mode is automatically avoided. As expected, substantial errors in the p-values were also experienced when frequencies close to the anti-resonance, where the effect of the added noise was more significant, were used.

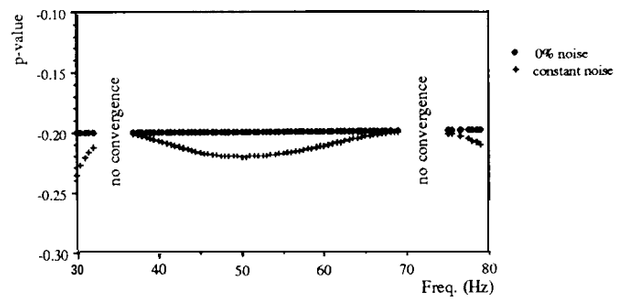


(a) p-value against frequency point selected

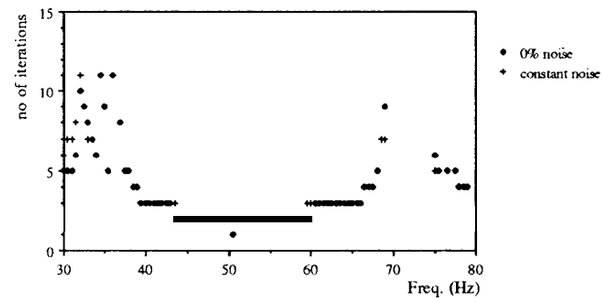


(b) Number of iterations against frequency point selected

**Fig. 7.9: 2** DOF test case, +20% $k_2$ error, constant bias error on the *experimental* data

### 7.3.4 Substitution of unmeasured data with analytical counterparts

For the 2 DOF test cases, the coordinate incompleteness of the *experimental* model will only affect changes in p-values for modelling errors in $m_2$ and $k_2$ as can be seen from equations (5). Equations (5) also show that a complete column of noise-free *experimental* data gives perfect results, independent of frequency point selection and modelling errors. Assuming that it is possible to "coordinate-expand" an incomplete experimental data set to the size of the analytical model, the added benefit of employing expanded data to the solution process of the RFM is explored. Supposing that expanded experimental data can be achieved, there are two possibilities of implementing the expanded set in the RFM: (i) to assume that the experimental receptance column is correct and to solve the problem without deleting rows during the solution process, or (ii) to use the expanded receptance values as a better alternative to substitution with the analytical counterparts, i.e. to delete the rows for which the corresponding *experimental* receptance is unmeasured as in the case of analytical receptance substitution. The two approaches were applied to a problem

with a 20% modelling error in $k_2$ assuming no noise on the ***measured*** data and a 100% error on the actual receptance value for the unmeasured receptance values to simulate ***expanded*** data. The results are shown in **Fig. 7.10.**

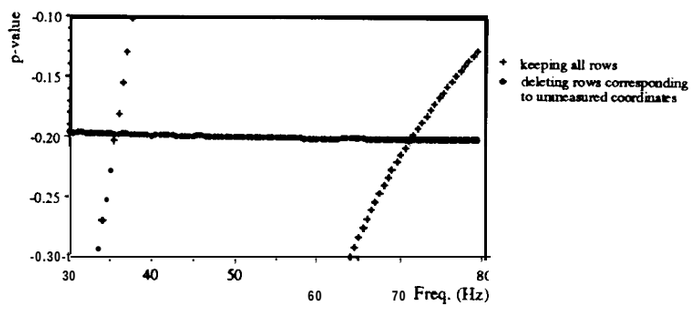


(a) p-value against frequency

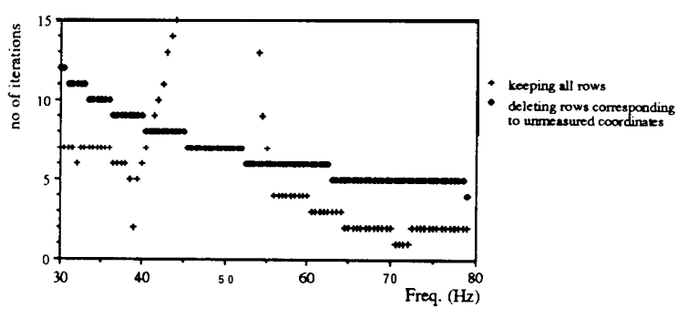


(b) Number of iterations against frequency point selected

**Fig. 7.10: 2** DOF test case, **+20%** $k_2$ error, 100% error on ***expanded experimental*** data

From **Fig. 7.10** it is observed that while an expanded $\alpha_{12}$ was used, better results were achieved if the row of $\Delta\alpha$ corresponding to the unmeasured degree of freedom was deleted. Better results, in terms of number of iterations and p-value accuracy, were obtained for case (i), keeping all rows, only when frequency points close to the experimental resonances were selected for updating. Deleting the rows corresponding to unmeasured coordinates for case (ii), good p-values were obtained independent of the frequency point selection. Thus, the use of expanded coordinates should be to substitute missing coordinates in the rows retained in the RFM only and not to increase the number of linear equations for each frequency point selected. Using expanded data there is no region of non-convergence around the experimental resonances. Also, it should be noted that the results were not so satisfactory around the anti resonance, the frequencies of which changes from one FRF to the next. This feature will cause less difficulties for

systems with more DOFs. These results emphasise the significance of coordinate incompleteness and point towards the possible benefits of coordinate-expansion of experimental receptance data. Coordinate incompleteness is considered in more detail in chapter 8.

### 7.3.5 Recommendations

Frequency point selection has an influence on the success of the RFM. There are 3 categories which may lead to erroneous results; (i) $\Delta\alpha(\omega) = 0$, (ii) $\alpha_X(\omega) >> \alpha_A(\omega)$ and (iii) $\alpha_A(\omega) >> \alpha_X(\omega)$. The effect of frequency point selection depends on the modelling error, measurements taken directly at the point(s) of errors will identify a modelling error more easily.

It is shown that points at frequencies in the vicinity of the experimental resonances should be avoided, while experimental anti-resonances present less of a problem unless the analytical and experimental anti-resonances coincide, which is very unlikely in practice. Frequency points around analytical resonances and anti-resonances have a less distinct effect on the final results.

It is recommended that frequency points below the first mode be avoided in the frequency point selection. In general, for given data sets, better results are obtained for frequency points with larger differences between experimental and analytical receptance values, as the effect of the noise on the experimental data becomes less dominant for larger differences.

If all coordinates are measured, very good results are obtained, almost independent of the frequency points selected. This result indicates the adverse effect of the substitution of the unmeasured coordinates by their analytical counterparts. The use of expanded data is investigated and it is observed that, assuming an expanded set for all unmeasured coordinates can be obtained, the rows of Act corresponding to unmeasured degrees of freedom should still be deleted. Thus, expanded FRF values are used to substitute missing coordinates in the rows retained in the RFM and not to increase the number of linear equations for each frequency point selected.

Notwithstanding the results of this investigation, one must bear in mind that the success of the RFM is very case-dependent and, secondly, that many of the adverse effects resulting from experimental coordinate incompleteness and noise are greatly reduced by,

unlike the 2 DOF examples used here, selecting more frequency points than the minimum required to obtain overdetermined systems of equations,.

## 7.4 COMPUTATIONAL CONSIDERATIONS

### 7.4.1 Least-squares solution

The RFM consists of a set of overdetermined algebraic equations of the form $[C]\{p\} = \{\Delta\alpha\}$, which is to be solved for $\{p\}$. A least-squares solution can be obtained using (i) the generalised inverse, also known as the Moore-Penrose generalised inverse, or (ii) the Singular Value Decomposition (SVD), a special technique of obtaining a generalised inverse with some additional features.

The basic equation for the generalised inverse of an Nxn matrix [C] where N > n is defined as:

$$[C]^{+}_{Nxn} = ([C]^{T}[C])^{-1}_{nxn}\,[C]^{T}_{Nxn} \tag{6}$$

The SVD approach is defined as follows:

decompose [C] as:

$$[C]_{Nxn} = [U]_{NxN}\,[\Sigma]_{Nxn}\,[V]^{T}_{nxn} \tag{7}$$

where [U] and [V] are orthogonal matrices and the diagonal matrix $[\Sigma]$ contains the singular values of matrix [C]. Hence:

$$[C]^{+}_{Nxn} = [V]_{nxn}\,[\Sigma]^{-1}_{Nxn}\,[U]^{T}_{NxN} \tag{8}$$

where $[\Sigma]^{-1}$ consist of the inverse of the non-zero singular values.

There are many publications which explain the theoretical background and discuss the suitability of these techniques to modal analysis and related topics [58,117,118] and so only the main points of interest are mentioned here. Although the singular value decomposition method is CPU-intensive (it involves two eigensolutions) and requires more storage space, it is a very reliable method and $[\Sigma]$ gives a direct indication of the

rank of the system matrix [C]. If memory space and CPU time are limited then the generalised inverse provides a good alternative. In that case, it is recommended to include a check on the inversion. A combination of the two techniques, where $([C]^T [C])^{-1}$ of the generalised inverse approach is computed using the SVD method, reduces both memory space required and CPU time compared with using the SVD method only and also provides a direct check for rank deficiency of [C].

### 7.4.2 Receptance matrix calculations

The rectangular matrix [C] includes the full receptance matrix $[\alpha_A]$ at each frequency point selected, and for each subsequent iteration the full updated receptance matrix, $[\alpha_U]$, is required. The receptance matrix can be calculated either (i) by inversion of the analytical dynamic stiffness matrix or (ii) by obtaining the modal solution and then using this in a subsequent modal summation. Now, if only a few frequency points are required, the first option will take less CPU time, but as the number of frequency points increases; the CPU time increases approximately proportionally with respect to the number of frequency points, in contrast with the modal summation approach here the incremental CPU time is very small **(Fig. 7.11). The** actual CPU time depends on the computing facilities used, the size of the analytical system and the number of frequency points selected. As the FE model is large in most cases, usually resulting in a small ratio of measured to unmeasured coordinates, and measured data also contain noise, more frequency points are required and the modal summation approach will generally be most CPU-cost-effective.

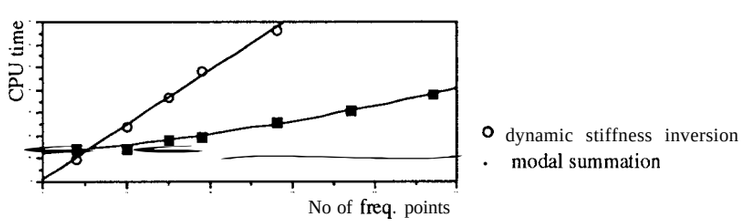


**Fig. 7.11:** Comparison of RFM CPU time per iteration for calculating analytical receptance matrix by dynamic stiffness inversion or modal summation

To use the modal summation approach, a complete eigensolution of the updated system is required during each iteration. There are various eigensolution techniques which can be used [8,119]. For large systems the computation of the complete eigensolution is computationally expensive and if only a limited frequency range is of interest a partial eigensolution, such as the subspace iteration method, can be used to represent the analytical system adequately. The contributions of the higher modes towards receptance

values in the lower frequency range decreases quadratically as the difference in excitation frequency and natural frequency increases. Care should be taken that enough modes are included in the modal summation, the actual number of modes required to satisfactorily represent the FRF over the frequency range of interest is case-dependent. A constant residual term can be calculated using:

$$[\alpha_A(o)] = [\alpha_{Aic}(o)] + [R] \tag{9a}$$

and

$$[\alpha_A(o)] = \left[ [K] + i[D] \right]^{-1} \tag{9b}$$

where:

$$[\alpha_{Aic}(o)] = [\phi]_{Nxm} \left[ \omega_r^2 + i\eta_r\omega_r^2 \right]_{mxm}^{-1} [\phi]_{mxN}^T$$

Thus:

$$[\alpha_A(\omega)] = [\phi]_{Nxm} \left[ \omega_r^2 - \omega^2 + i\eta_r\omega_r^2 \right]_{mxm}^{-1} [\phi]_{mxN}^T + [R] \tag{10}$$

### 7.4.3 The uniqueness of the updated model

In chapter 5 it was already established that the RFM does not produce a unique solution for a selected set of updating parameters due to noise on the experimental data. It has been shown in various test cases employing overdetermined systems, and subsequent use of statistical analysis tools, that the elements in error can be located. A combination of this error location procedure and the mean p-values obtained is then used to update the system. However, for some applications the only requirement might be to regenerate the measured FRFs using a mathematical model. Then the question arises: “Is one RFM run, i.e. the p-values obtained from one set of frequency points, sufficient to regenerate the measured FRFs?". The beam example with 15 *measured* coordinates in the y direction with 10% added random noise was used for 4 alternative RFM runs employing 10 and 15 frequency points. In **Fig. 7.12,** regenerated FRFs using the p-values obtained are plotted with their *experimental* counterparts. Note that although 10% added noise polluted *experimental* data were used, noise-free *experimental* data are plotted here.

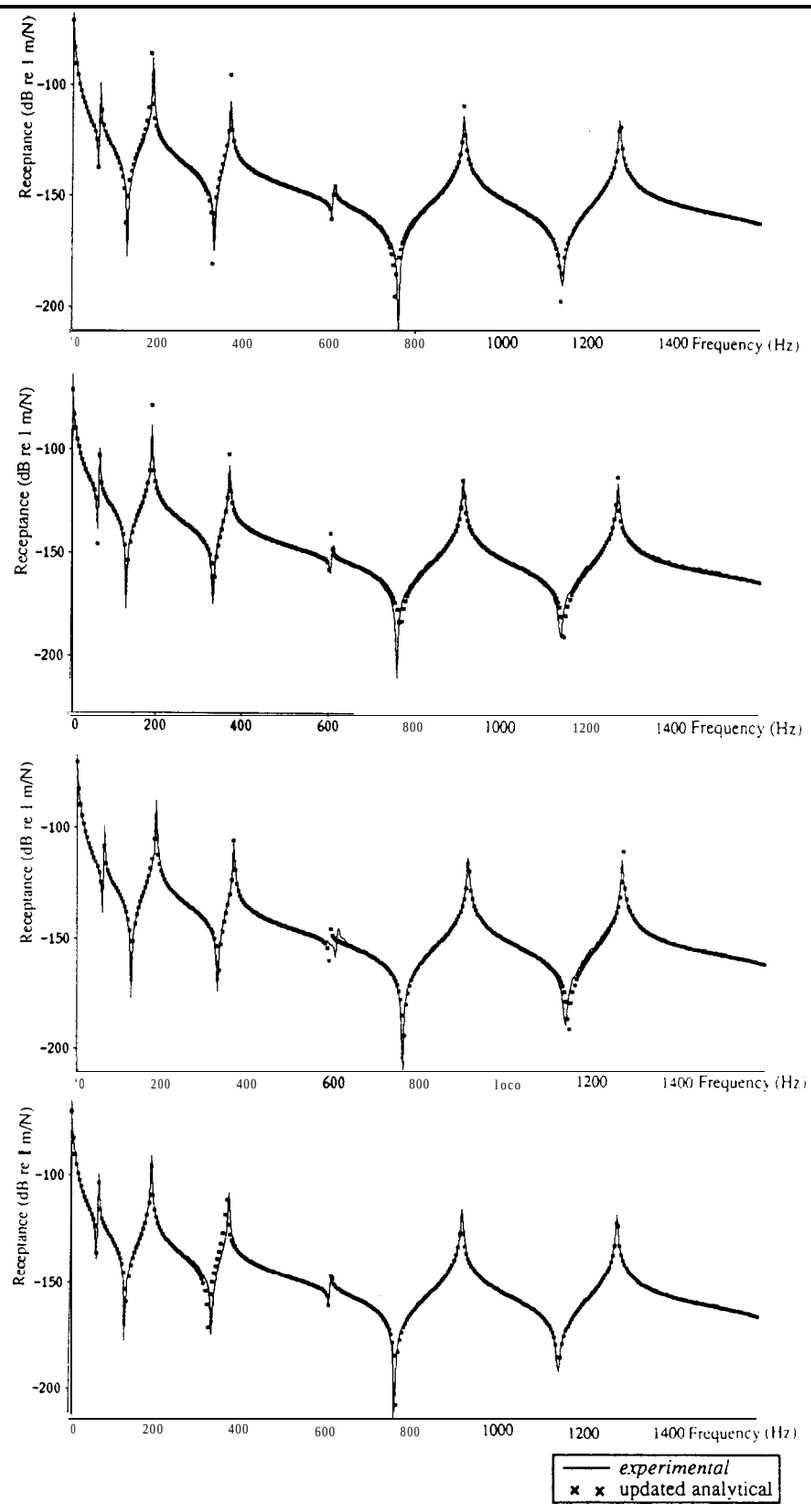


**Fig. 7.12:** Comparison of *experimental* and updated receptance curves obtained from one RFM run only

Despite fairly large variations in resulting p-values, the updated **FRFs** compared very well with the *experimental* ones, within the frequency range of interest. However, unless there is a specific application where regenerated **FRFs** only are of interest, in the opinion of the author it is of more value to identify where the modelling errors are and to obtain insight into the physical meaning of the modelling errors rather than using a black-box approach just to regenerate **FRFs.**

As was illustrated with the beam example in chapter 5, a number of fairly substantial errors of various origins can be located adequately, and the updated receptance curves compared well to their measured counterpart Returning to the question of uniqueness of the updated model, the effect of choosing more frequency points is considered next. The updated **FRFs** beyond the frequency range of interest were also inspected **(Fig. 7.13).**

The benefit in selecting more frequency points in the RFM to regenerate the **FRFs** within the frequency range of interest appeared not very significant as it could not be detected by visual inspection. The sum of the percentages difference squared between the *experimental* and the updated receptance curves (SPDS) for the O-1600 Hz frequency range were compared. It was observed that for a limited number of frequency points, in this case 15, the SPDS, which reflects the quality of the updated curve, can vary substantially. Selecting an increased number of frequency points the quality of the updated receptance curves was more consistent and the SPDS compared to the better SPDS values obtained using 15 frequency points. It is clear from **Fig. 7.13,** that beyond the frequency range used for updating (0- 1600 Hz in this case) there is no added benefit in choosing more frequency points.

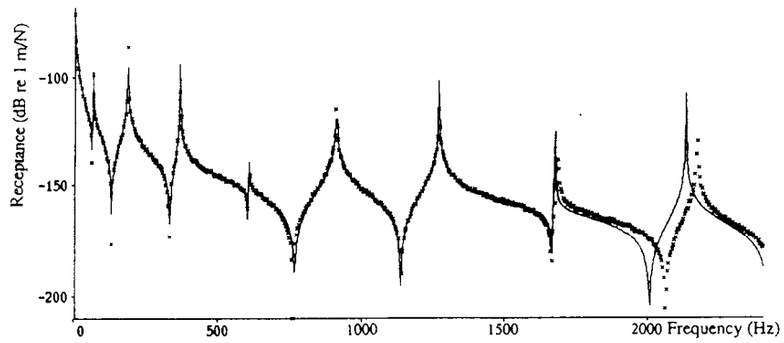


(a) 15 frequency points

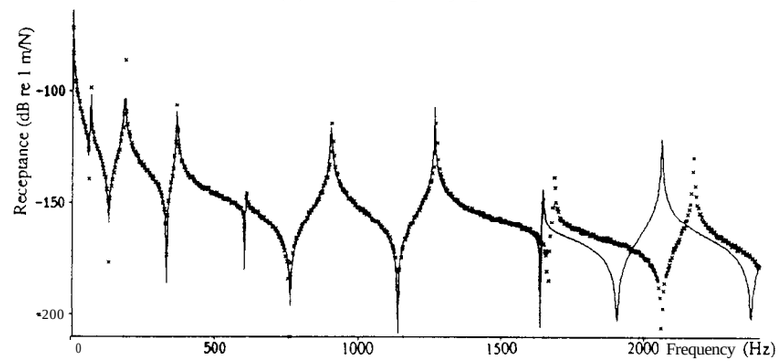


(b) 30 frequency points

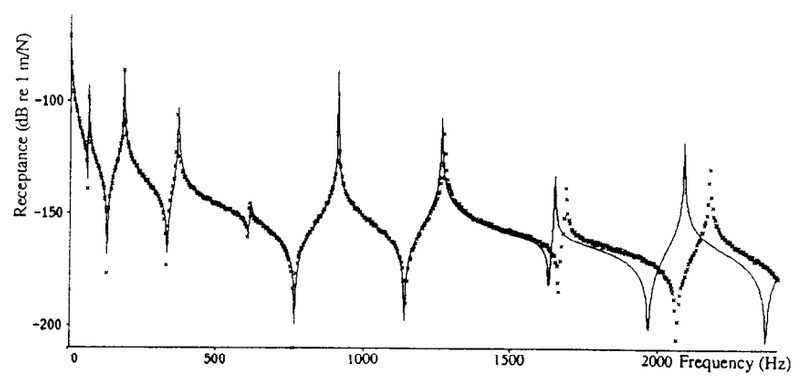


(c) 90 frequency points

× × *experimental*
updated analytical

**Fig. 7.13:** Comparison of ***experimental*** and updated receptance curves obtained using one RFM run only for an increasing number of frequency points selected

The standard deviation (obtained from 2 runs only), as compared with the ideal p-values for an increasing number of frequency points, is shown in **Fig. 7.14. A** simple curve fit suggest a decrease in standard deviation as the number of frequency points increases, as is to be expected from a statistical point of view. This also verified the observation on the consistency of the updated receptance curves. The number of iterations to reach

convergence, which varies between frequency points sets, was on average approximately the same and hence there is no additional benefit in increasing the number of frequency points to decrease CPU time.

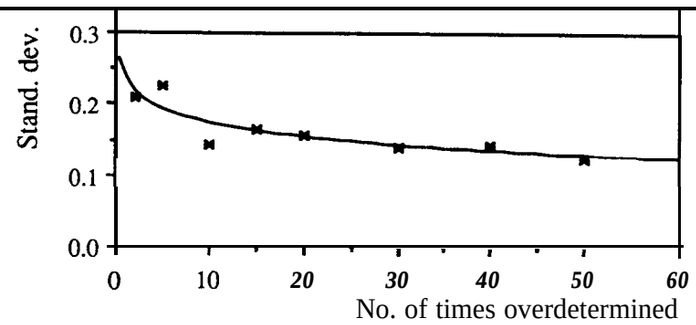


**Fig. 7.14:** Standard deviation against the number of frequency points for the beam example with 10% random noise

Of course, the ability to regenerate the measured FRFs depends to a large extent on the capability of the original FE model and updating parameters to represent the structure under study. If there are fundamental differences between the structure and the FE model it is unlikely that the model can ever represent the structure satisfactorily. Similarly, localised response variations cannot be represented adequately if too coarse an FE model is used. So far, a reasonable comparison between FE model and structure has been assumed. The adverse effects of model mismatch were illustrated in section 5.6 and local effects, in particular due to structural joints, are discussed in more detail in chapter 9. Apart from these fairly general comments, no guidelines of maximum allowable discrepancies for which the RFM will work are included here. The use of some maximum relative Euclidean norm based on the error matrices and the original FE system matrices to define a maximum allowable error is, in the opinion of the author, unrealistic as this bounds the unknown quantity to be identified. It would be more realistic to define a numerical variable based on the measured receptances in comparison with the FE model equivalent values, i.e. based on $\|\{\Delta\alpha\}\|$. Although this scalar would give some indication of feasibility, it is not investigated in more detail on the basis that it is an over simplification of a very complex problem. The ability of the RFM to update successfully depends on:

(i) the structure under study
(ii) the quality and quantity of the experimental data,
(ii) the FE model chosen to represent the structure,
(iv) the updating parameters selected,
(v) the type, location and spread of modelling errors.

Two situations where a norm based on $\|\{\Delta\alpha\}\|$ will probably fail to indicate whether RFM updating will be successful are:

(i) in case of one substantial modelling error at a specific location in the model resulting in a large Euclidean norm while the RFM can be applied successfully; and,

(ii) an approved $\|\{\Delta\alpha\}\|$ but due to too few badly measured receptance curves and a very coarse FE model failure to update the FE model using the RFM.

In **Fig. 7.15** the updated point receptance curves using 6 RFM runs of 15 frequency points are compared with the updated receptance curves using 3 runs with 30 frequency points, using both all the mean p-vales and the mean p-values of the erroneous elements only. All updated receptance curves shown here are of comparable quality. It is noteworthy that using all mean p-values to calculate the updated system gives better results than using the mean p-values of the indicated erroneous elements only.

Above 1600 Hz the best results were obtained using the mean p-values from 6 runs **(Fig. 7.15b**). For error location, both data sets located 7 modelling errors correctly, but when 3 runs of 30 points were used, 4 additional modelling errors were indicated. Hence, if the main objective is error location, it is beneficial to carry out more RFM runs. In all the examples of previous chapters 6 RFM runs produced adequate results. Statistically, more reliable results are obtained for an increased number of data sets, each data set consisting of p-values obtained from a RFM run, provided that the chosen p-values are able to approximate the actual modelling error. More runs are especially beneficial if the standard deviation of the p-values is high due to (i) noise, (ii) a high ratio of unmeasured-to-measured coordinates and/or (iii) model mismatch. The number of RFM runs required can be determined from the standard deviation of the p-values. The variation in the average standard deviation by including another set of p-values from an additional RFM run must be negligible. In this case 6 runs appeared to be sufficient **(Fig. 7.16a**). One advantage of carrying out more runs is that, as anticipated for an increasing number of runs, the mean p-values approximate the expected p-values better than if less RFM runs are carried out **(Fig. 7.16b**).

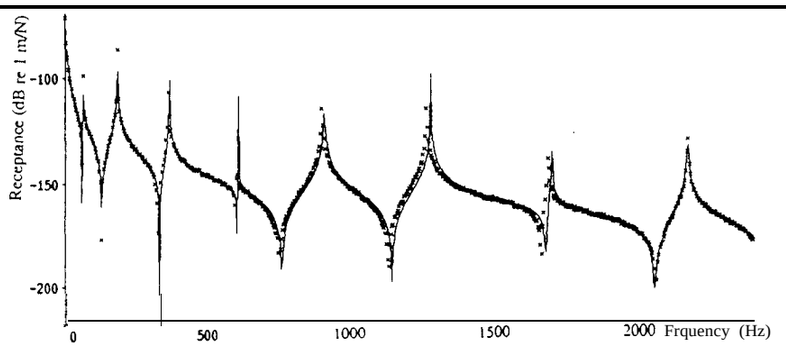


(a) 15 frequency points all mean p-values

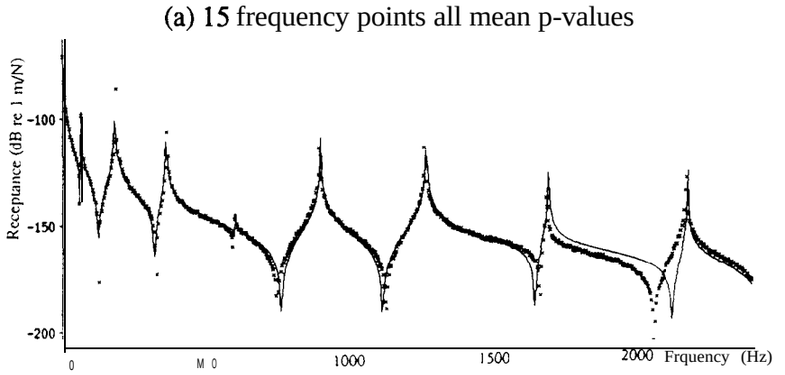


(b) 15 frequency points selected mean p-values

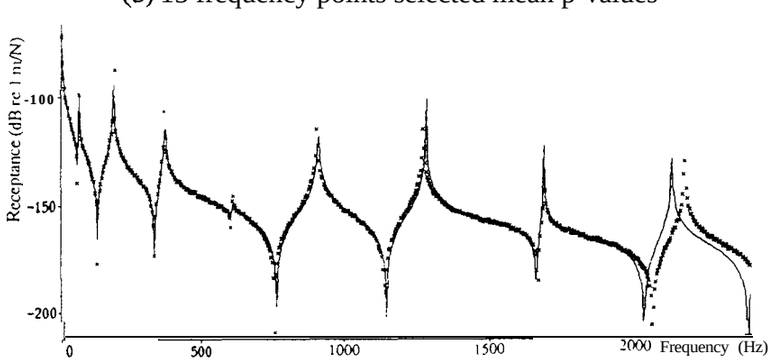


(c) 30 frequency points all mean p-values

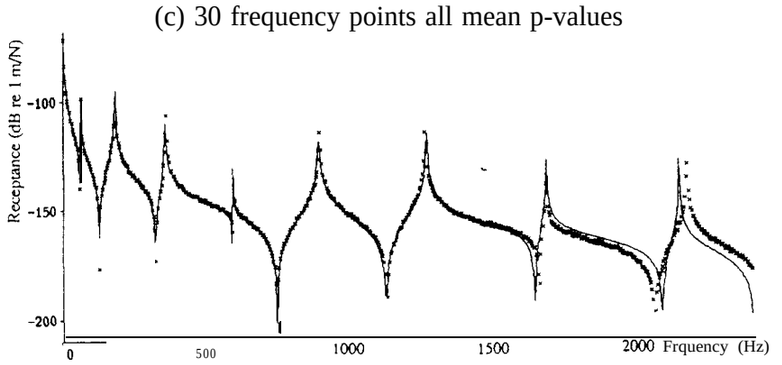


(d) 30 frequency points selected mean p-values

× × *experimental*
updated analytical

**Fig. 7.15:** ***Experimental*** and updated receptance curves using all- and selected p-value

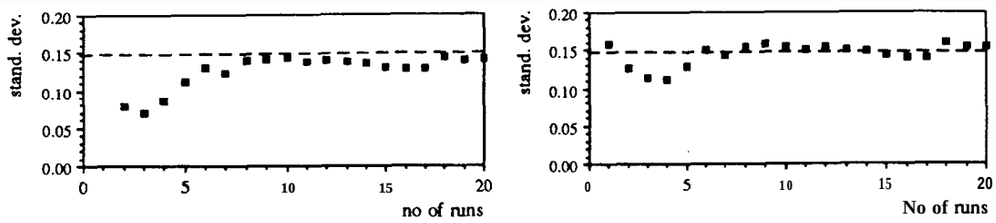


(a) standard deviation of all p-values (b) standard deviation of mean p-values with respect to the expected p-values

**Fig. 7.16:** Standard deviation against the number of runs for the beam example with 10% random noise

Let us also consider the error threshold used for error location; that is, the cut off value for mean p-value to standard deviation ratio above which the elements are considered to be in error. Previously, an error threshold of 2 has been applied successfully, although it has also been suggested that for substantial standard deviations, a lower threshold might be more appropriate. For the beam example with 10% noise, the standard deviation was fairly large and both error thresholds were applied and compared to the 10 true modelling errors ( **Fig. 7.17).** For an error threshold of 2, additional elements were identified as being in error only when the number of RFM runs was less than 4. When the number of RFM runs was more than 3 between 60-80% of the true erroneous elements were identified. There was no significant improvement by conducting more RFM runs. Reducing the error threshold to 1 identified all erroneous elements correctly independent of the number of RFM runs. However, all cases using less than 18 RFM runs also identified additional errors. The mean p-values for the additional errors were small and decreased as the number of runs increased. The updated receptance curves, using an error threshold of 2, are compared with their experimental counterparts in **Fig. 7.18.**

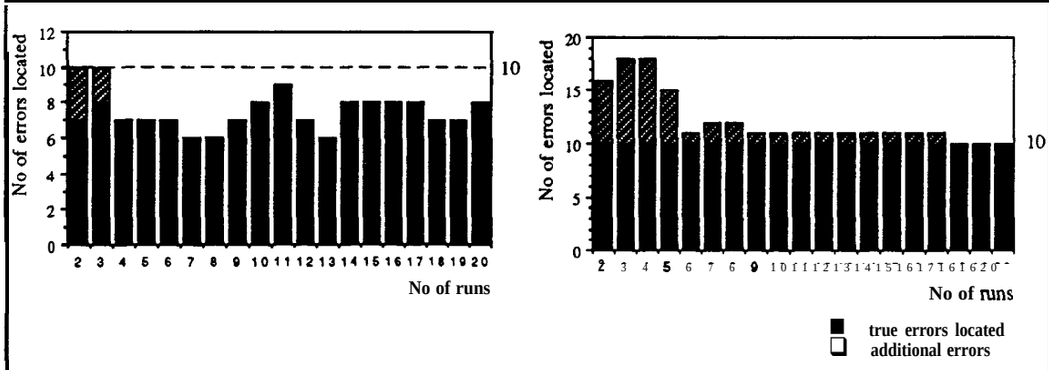


(a) error threshold = 2 (b) error threshold = 1

**Fig. 7.17:** Number of modelling errors located for the beam example with 10% random noise. for an increasing number of RFM runs

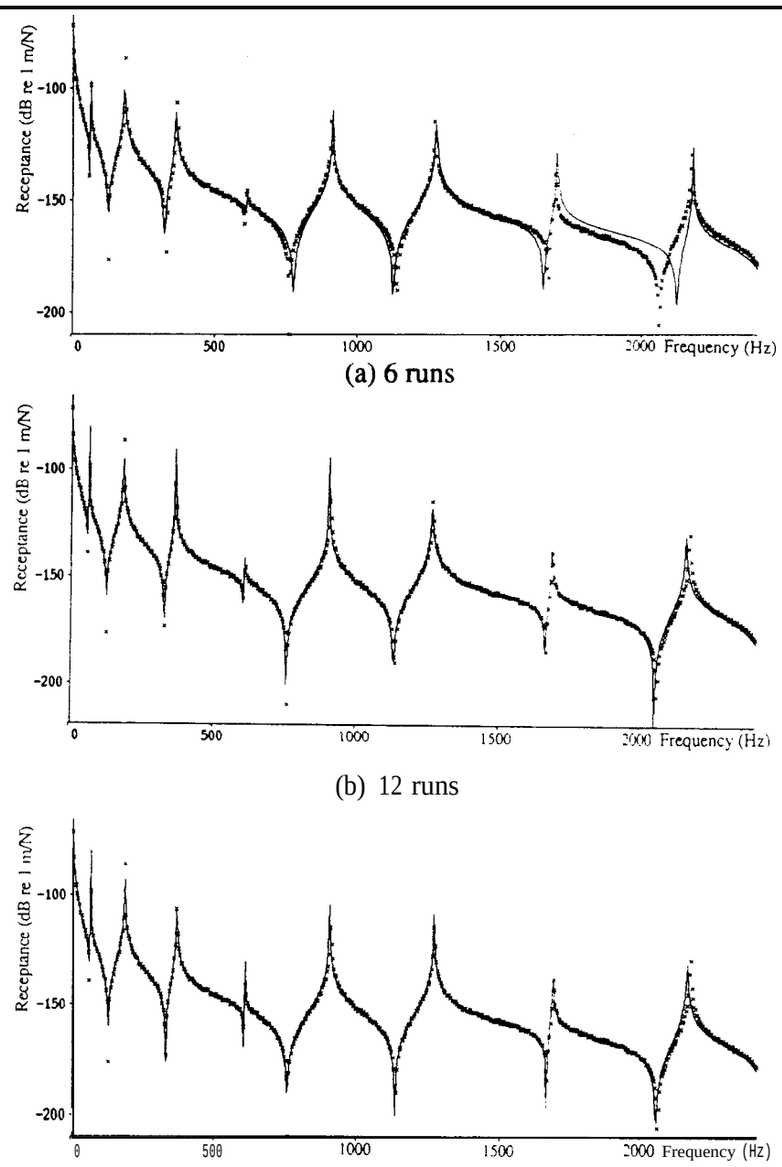


**Fig. 7.18:** Updated and ***experimental*** receptance curves, for an increasing number of RFM runs

Fig.7.18 shows that for the frequency range of interest all examples regenerated the ***experimental*** **FRFs** well. Above 1600 Hz, using more frequency point sets improved the comparison, as was to be expected from the previous results. Increasing the number of RFM runs is more beneficial than increasing the number of frequency points used per run, but increases the CPU time. Again the requirements of the updated model need to be assessed together with the available computational facilities. If the model is to be used for further analysis it is of more interest to locate and understand the modelling errors

identified so that these can be inspected. Physical understanding should be preferred to visual and numerical correctness obtained by comparing measured and updated FRF data, especially as the modelling errors can also be due to incorrect measurement set-up.

Another possibility to obtain a unique answer is by introducing additional constraints. Additional constraints in the form of reducing the number of unknowns, as mentioned in chapter 5, can be applied by (i) updating material properties rather than each element or (ii) by grouping elements together to form macro elements. This might be appropriate to identify a damping matrix but not necessarily for updating mass end stiffness matrices. However, in the opinion of the author, although the computational effort of the RFM will be reduced, to a large extent the error location capability of the RFM will be lost and the resulting p-values will be a further approximation of local errors. Thus the results become artificially unique rather than approaching the correct model. A priori knowledge of correct parts of the analytical model can be incorporated in the RFM without any difficulty, but care must be taken that so-called engineering judgement does not include sweeping assumptions because it can lead to numerical instability and/or correct elements being changed to represent the modelling errors.

Alternatively, extra constraints can be introduced in the form of:

$$[Z_X]\,[\,\alpha_X\,] = [Z_A + \Delta Z\,]\,[\,\alpha_X\,] = [\,I\,] \qquad (9)$$

This can be formulated in a similar way to the RFM and can be compared to an equation error optimisation method. As such, it could be an updating method in its own right, as has recently been suggested [105-107]. The advantage of this approach over the RFM is that the analytical and subsequently updated receptance matrices are not required. However, the benefits of including equation (9) as an additional constraint within the RFM is doubtful as the above equation is implicitly incorporated within RFM.

An updating algorithm based on equation (9) can be beneficial if used in parallel with the RFM. Updating using a combination of techniques increases the confidence in the obtained results, which is especially useful for updating using modal data where all experimental data are used at once and the procedure cannot be repeated for other data sets. For the RFM, the need is not so great as there are usually enough experimental data available. For example, in the beam test case only 15 frequency points are necessary while typically 801 points are measured. The RFM can therefore, in theory, be repeated, avoiding frequencies below the first resonance and in the direct vicinity of experimental resonances, over 40 times.

### 7.4.4 Recommendations

To obtain a least-squares solution the SVD technique should be used wherever possible as it gives a direct indication of the rank and condition of the solution matrix. If space and CPU time are limited then the generalised inverse provides a good alternative. In that case, it is recommended to include a check on inversion. In most cases it is more cost effective to calculate the full receptance matrix using modal summation, only a partial eigensolution being required for large analytical systems.

Numerical studies on a beam example with 10% noise showed the benefits of including more frequency points for each RFM run and conducting more runs. One should always consider the requirements from the updated model and the resources available. If updated FRFs only are required one RFM run using many frequency points is sufficient. For error location purposes more runs and subsequent statistical analysis of the results are necessary. As expected, increasing the number of runs improves the final results.

## 7.5 CONCLUDING REMARKS

Although the RFM is case-dependent and it is difficult to generalise from the simple cases investigated in this chapter, some specific trends were observed in the RFM, in particular concerning: solution stability, frequency point selection, measurement sites and statistical aspects.

It has been shown that balancing the matrices both towards element type and frequency point selection is beneficial for the convergence of the solution. It is therefore recommended that such a procedure should be included in the solution process.

The success of the RFM depends on the frequency points used. The effect varies along the frequency range and it also depends on the modelling errors. Measurements taken directly at the point(s) of error will identify a modelling error more easily. It is recommended that frequency points below the first mode should be avoided in the frequency point selection. In general, better results are obtained for frequency points with larger differences between experimental and analytical receptance values, as the effect of the noise on the experimental data becomes less dominant for larger differences. Equally, frequencies in the direct vicinity of the experimental resonances should be avoided.

The adverse effect of the substitution of the unmeasured FRF values by their analytical counterparts is indicated. During a preliminary assessment on the use of expanded data is it is observed that, assuming an expanded set for all unmeasured coordinates can be obtained, the estimated values of the unmeasured coordinates should be used to substitute missing coordinates in the rows retained in the RFM and not to increase the number of linear equations for each frequency point selected. Thus the rows of $\Delta\alpha$ corresponding to unmeasured degrees of freedom should still be deleted.

Numerical studies on a beam example with simulated 10% simulated noise show the benefits of increasing the number of frequency points included in each RFM run and of conducting an increased number of runs as compared to the 6 runs used previously. One should always consider the requirements of the updated model and the resources available, if updated FRFs only are required one RFM run using many frequency points is sufficient. For error location purposes, more runs and subsequent statistical analysis of the results are necessary. As expected, increasing the number of runs improves the final results.

# CHAPTER 8

# COORDINATE INCOMPATIBILITY

## 8.1 INTRODUCTION

One of the major problems in most practical model updating applications is the coordinate incompleteness of the experimental model when compared with the Finite Element model. As discussed in previous chapters, experimental coordinate incompleteness with respect to the FE model can be due to:

(i) coordinates being to difficult to measure (e.g. rotations);
(ii) physically inaccessible (e.g. internal) coordinates; or
(iii) expense of measurements at all FE coordinates.

There are two possible avenues to overcome coordinate incompatibility: (a) reducing the Finite Element model to the measured degrees of freedom or (b) expanding the measured data to the full size of the FE model.

In previous chapters an iterative process has been applied to overcome the problem of coordinate incompleteness whereby unmeasured values are estimated from the corresponding FE data. It has been suggested in chapter 7 that expanding the experimental FRF receptance column to include all FE coordinates might improve the updating process. The possible benefits have been illustrated in section 7.4.5 on a 2 DOF example assuming that expanded coordinates can be obtained with some accuracy. Unlike mode shape coordinate expansion, which is commonly used in updating procedures based on modal data, expansion of FRF data has not been attempted before. In this chapter two methods are proposed to expand an incomplete column of receptances to the size of the full FE model.

## 8.2 RECEPTANCE COLUMN COORDINATE EXPANSION METHODS

### 8.2.1 The inverse-reduction method

The first proposed expansion technique for a column of experimental receptance data is a 'physical' interpolation which makes use of the analytical system matrices. It is an inverse procedure of model reduction and is similar to the approach employed for the expansion of modal data (section 4.2.1). One disadvantage of this technique is that the expansion depends on the knowledge and the validity of the original FE model, while an advantage is that by using the partitioned analytical system matrices the physical connectivity properties are imposed directly.

Starting from the basic equation, at an excitation frequency $\omega$:

$$\left\{ \begin{bmatrix} K_{11} & K_{12} \\ K_{21} & K_{22} \end{bmatrix}_A - \omega^2 \begin{bmatrix} M_{11} & M_{12} \\ M_{21} & M_{22} \end{bmatrix}_A \right\} \begin{Bmatrix} \alpha_1(\omega) \\ \alpha_2(\omega) \end{Bmatrix}_X = \begin{Bmatrix} u_1 \\ u_2 \end{Bmatrix} \tag{1}$$

where $\{\alpha_1\}_X$ is the measured part of the receptance column while $\{\alpha_2\}_X$ is the unknown part, $\omega$ the frequency of interest and $u_i = 1$ at the point receptance coordinate while $u_i = 0$ at all other coordinates. If one assumes that the modelling errors are predominantly in the measured coordinates, the lower matrix equation will be more correct. Rearranging the lower matrix equation, gives:

$$\{\alpha_{2_X}(\omega)\}_{(N-n)x1} =$$

$$- [[K_{22_A}] - \omega^2[M_{22_A}]]^{-1}_{(N-n)x(N-n)} [[K_{21_A}] - \omega^2[M_{21_A}]]_{(N-n)xn} \{\alpha_{1_X}(\omega)\}_{nxl} \tag{2}$$

### 8.2.2 Using analytical mode shapes

The second method proposed assumes that each column of experimental receptance data, i.e. a forced response shape for a certain excitation frequency, can be expressed as a linear combination of the analytical mode shapes. This is a valid assumption if the mode

shapes of the analytical model span the same subspace as the true structure, which is an acceptable supposition if there are enough degrees of freedom used.

Thus, it is possible to expand the experimental receptance column on the strength of the analytical mode shapes:

$$\{\alpha\}_X = [\phi]_A \{\gamma\} \tag{3}$$

The matrices can be rearranged such that the known measured coordinates are contained in the top part of the matrix equation:

$$\begin{Bmatrix} \alpha_1 \\ \alpha_2 \end{Bmatrix}_{X_{Nx1}} = \begin{bmatrix} \phi_{11} & \phi_{12} \\ \phi_{21} & \phi_{22} \end{bmatrix}_{A_{NxN}} \begin{Bmatrix} \gamma_1 \\ \gamma_2 \end{Bmatrix}_{Nx1} \tag{4}$$

Assuming the analytical mode shapes away from the excitation frequency of interest have a negligible contribution to the forced response shape at that excitation frequency, then equation (4) can be partitioned accordingly, including m appropriate modes. Hence:

$$\begin{Bmatrix} \alpha_1 \\ \alpha_2 \end{Bmatrix}_{X_{Nx1}} \cong \begin{bmatrix} \phi_{11} \\ \phi_{21} \end{bmatrix}_{A_{Nxm}} \{\gamma_1\} \tag{5}$$

Thus $\{\gamma_1\}$ can be found from the known coordinates:

$$\{\gamma_1\}_{mx1} = [\phi_{11}]^+_{A_{mxn}} \{\alpha_1\}_X \tag{6}$$

So that:

$$\{\ \}_{E_a}{}_{X_{Nx1}} = \begin{bmatrix} 911 \\ \$21 \end{bmatrix}_A [\phi_{11}]^+_{A_{mxn}} \{\alpha_1\}_{X_{nx1}} \tag{7}$$

Where: N = total number of analytical coordinates
n = number of measured coordinates
m = number of modes selected.

Choosing n to be greater than m, equation (7) is overdetermined and either the generalised inverse or the SVD inversion technique can be used to invert $[\phi_{11}]$. The expanded forced response shape is a smoothed version of the measured receptance column. Either the entire smoothed expanded receptance column can be used or the expanded coordinates only can be used for substitution while the regenerated measured coordinates are used to verify the quality of expansion. Notice that the analytical modes selected must be such that $[\phi_{11}]$ can be inverted, therefore the mode shapes selected must be linearly independent for the subset of measured coordinates. Care must be taken that coordinate aliasing does not occur.

One advantage of this technique is that it involves only one inversion for all frequency points, if suitable analytical mode shapes are selected for the entire frequency range. The main disadvantage of the expansion procedure using analytical modal data is that a choice of suitable modes is required in contrast to the inverse reduction technique which can be used directly. This modal based receptance column expansion technique is similar to the modal transformation method for the expansion of modal data as described in section 4.2.2.

## 8.3 COMPARISON OF COORDINATE EXPANSION METHODS

The two expansion methods were explored on the free-free beam test cases of the previous chapters. Firstly, the experimental data were assumed to consist of 15 out of 90 noise-free *measured* coordinates, i.e. a correspondence factor of 16.7%, for excitation in the y direction at node 5. Due to the decoupling of the degrees of freedom in this theoretical example, only the cross receptances with the $\theta_z$ direction were of interest (other receptances for excitation in the y direction at node 5 were zero). Typical expanded receptance curves, obtained using both the inverse reduction technique and the analytical modal solution are shown in **Figs. 8.1** and **8.2** respectively, together with the corresponding analytical and true *experimental* receptance curves.

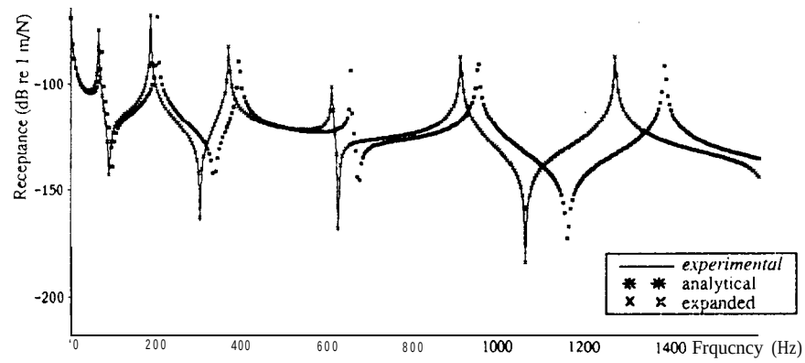


**Fig. 8.1:** Expanded cross receptance, $\alpha_{5y1\theta z}$, for a correspondence factor of 16.7% obtained from the inverse reduction expansion technique

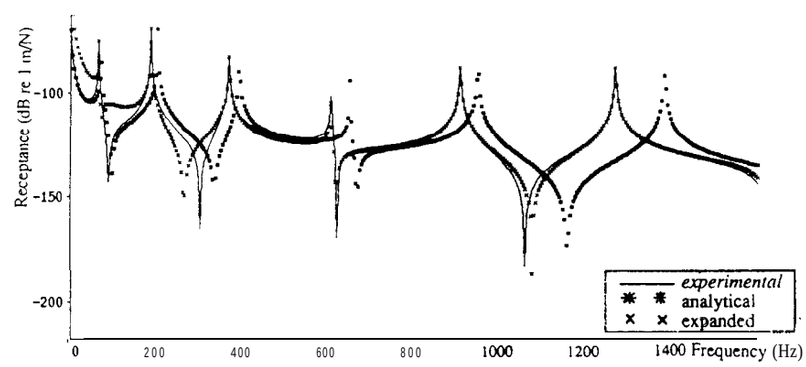


**Fig. 8.2:** Expanded cross receptance, $\alpha_{5y1\theta z}$, for a correspondence factor of 16.7% obtained from the modal exnansion technique

Around resonances both sets of expanded receptances compared very well with their expected ***experimental*** counterparts. Away from resonance the inverse reduction technique showed much better agreement with the correct response. The method using modal data requires a decision on how many and which mode shapes should be included in the selection used for the expansion and it has been found that best results are obtained using a few modes below and a few above the excitation frequency. In this case in-plane modes, i.e. modes with deflections in the y direction, were selected as the beam was excited in the y direction only.

The number of ***experimental*** coordinates was reduced to 7 and typical expanded receptance curves are shown in **Figs. 8.3** and 8.4. Again expansion was very successful around the ***experimental*** resonances. The effect of reducing the number of coordinates on the method using inverse reduction is not as significant as for the modal expansion method. Comparing **Fig. 8.2** and **Fig.** 8.4, the discrepancies were found

to increase significantly as the number of ***measured*** coordinates decreased. An advantage of the modal based approach is that the expanded receptance data can be checked by comparing the reproduced measured coordinates with their initial values. This option is not available for the inverse reduction technique. Advantages of the inverse reduction receptance column expansion technique are that it is successful for a much wider frequency range around each experimental resonance and it does not require decisions. The modal approach requires only one inversion for a wide frequency range while the inverse reduction method needs an inversion at each excitation frequency of interest. Hence, in comparison, the inverse reduction technique is more CPU-intensive.

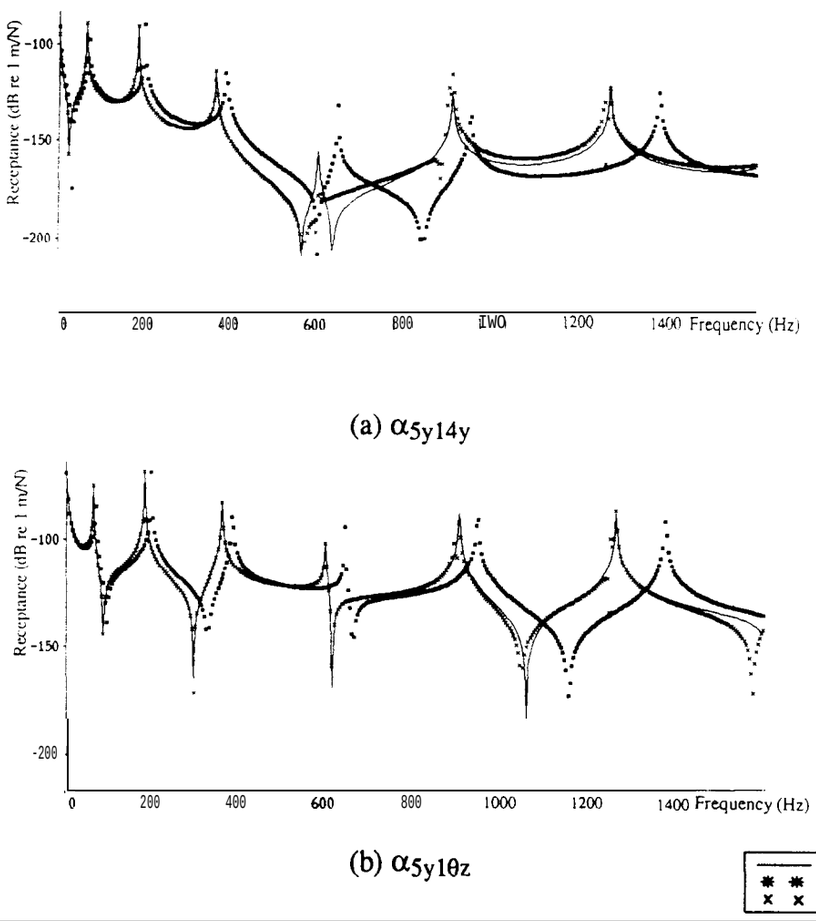


**Fig. 8.3:** Expanded receptances for a correspondence factor of 7.8% obtained from the inverse reduction expansion technique

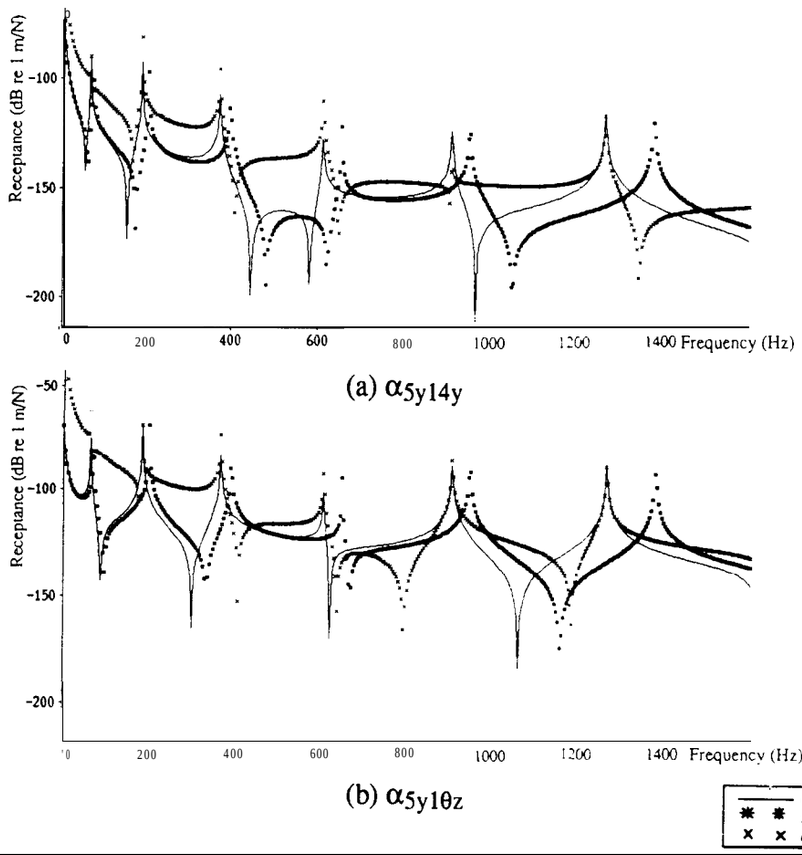


Fig. 8.4: Expanded receptances for a correspondence factor of 7.8% obtained from the expansion technique using modal data

As for the mode shape coordinate expansion methods, analytical modelling errors and a low ratio of measured to unmeasured coordinates have adverse effects on the success of the two receptance column expansion techniques. As is shown, both techniques can expand the receptance columns well around resonant frequencies but not so well around anti-resonances. This is a severe disadvantage if agreement over the entire frequency range is required. For each RFM run, a selected number of frequency points only is required and hence the use of expanded receptance columns is likely to be beneficial.

## 8.4 EXPANDED EXPERIMENTAL COORDINATES IN THE RFM

### 8.4.1 2 DOF test case

The two proposed expansion techniques were applied to the 2 DOF example with a 20% error in $k_2$ as used in section 7.2. As expected from the previous comparison, both

resonances but were not so accurate at off-resonance frequencies. This was reflected in the results obtained using the RFM. As previously, the RFM was repeated many times selecting each frequency point consecutively to find the p-values **(Fig.** 8.5). Comparing the p-values with those obtained substituting the missing ***experimental*** data with their analytical counterparts **(Fig. 7.5), the** results were found to have improved substantially for frequency points chosen around ***experimental*** resonances while, as expected, for frequency points selected between resonances the substitution using either set of expanded data was not so successful. The range of frequencies for which the RFM did not converge was substantially larger for the expansion technique employing analytical modal data than for the inverse reduction method.

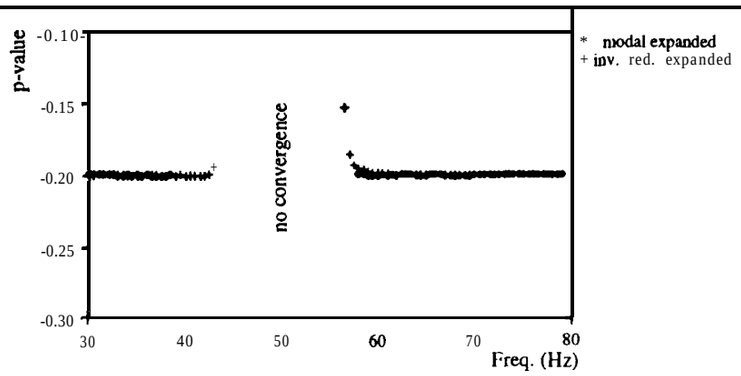


(a) p-values against frequency point selected

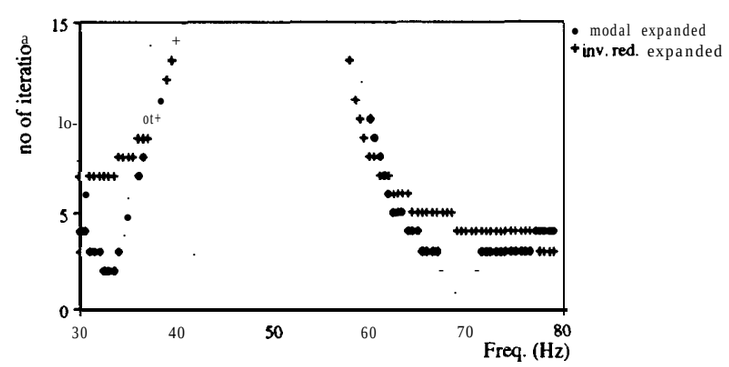


(b) number of iterations against frequency point selected

**Fig. 8.5:** RFM applied to update a 2 DOF system using expanded ***experimental*** data

Despite the existence of a frequency range between the resonances where the expansion was not successful, represented by wrong p-values and non-convergence of the RFM, the results were encouraging as the experimental resonances are at fixed frequency points, independent of measurement position while anti-resonances change with measurement location.

### 8.4.2 Beam test cases

As a 2 DOF lumped mass-spring system does not test expansion methods adequately, especially if there is only one measured coordinate, the investigation of the use of receptance column expanded data was continued on the beam example. Three cases were explored:

(i) replacing unmeasured coordinates with their analytical counterparts,
(ii) replacing unmeasured coordinates with inverse reduction expanded receptances,
(iii) replacing unmeasured coordinates with modal expanded receptances.

Assuming 15 noise-free experimental coordinates were *measured the RFM* was executed. Substituting the missing 75 coordinates with their (updated) analytical counterparts, 9 out of 10 consecutive runs converged in an average of 7 iterations. Replacing the missing coordinates with the expanded data only 4 out of 10 runs were successful for both expansion methods and the number of iterations to reach convergence was substantially increased. This can be explained as follows; due to calculating the updated system for each iteration the replacement updated analytical values become closer to their true *experimental* values while the expanded data remain constant throughout the iterative process.

The iterative procedure was changed to include expansion at each iteration. This, of course, has the disadvantage of increasing the CPU time per iteration, especially for the inverse reduction expansion technique which requires a matrix inversion for each frequency point selected within the RFM. The method using the analytical modal data was harder to implement as it involves a choice of how many and which modes to use for expansion. In this example, in-plane modes close to the frequency point selected produced well-expanded receptance columns. For the modal expansion method an additional inspection was implemented, for each iteration a surplus of receptance columns were expanded and only those reproducing the measured coordinates within a correlation bound of 0.95 were acceptable for use in the iterative RFM procedure. This is in contrast to the normal utilisation of the RFM where the frequency points selected remain the same throughout the iterative process.

The test cases were carried out for 10 randomly selected frequency point sets. In this case all three approaches (i-iii) located all erroneous elements correctly using an error threshold of 2. Both for the standard RFM and for the version employing expanded data using the analytical mode shapes, 9 runs out of 10 converged successfully and

approximately the same number of iterations to reach convergence were required. Thus there was no apparent additional benefit using the modal based expanded receptance data. Including the inverse reduction technique within the RFM gave an improvement over the standard procedure; all runs converged successfully in half the number of iterations as compared with the standard RFM. However, the CPU time was nearly doubled for each iteration due to the additional matrix inversions necessary for expansion. Thus, despite a great reduction in the number of iterations to reach convergence the total CPU time for each run was on average approximately the same as for the standard RFM. An advantage of employing expanded data for unmeasured coordinates is that it improves the stability of the solution process, especially during the first few iterations during which p-values can fluctuate erratically.

The same test cases were repeated for 5 measurement sites only, i.e. a correspondence factor of 5.6%. It was found that in this case including the modal-based expansion technique in the RFM resulted in non-convergence due to the very limited success of the expanded coordinates as a result of coordinate aliasing. With the standard RFM 3 out of 10 runs converged successfully while including the inverse reduction procedure resulted in 7 out of 10 runs converging. For the latter case, pre-selecting frequency points around resonances improved the solution stability. This is therefore a recommended procedure if receptance coordinate expansion is included in the RFM.

Adding 3% random noise to the experimental data reduced the speed and success rate of convergent solutions. Including the inverse reduction technique in the RFM resulted in 4 out of 10 runs converging in, on average, 25 iterations compared with 2 out of 10 for the standard RFM in an average of 36 iterations. However, the average CPU time per run was again approximately the same in both cases due to the additional matrix inversions for the inverse reduction approach. The standard deviation of the p-values using the inverse reduction expansion technique was reduced to 0.13 compared with 0.17 for the standard RFM, and 7 out of 10 elements in error were correctly identified compared with 6 out of 10. This showed that including expanded data is also beneficial for the RFM in the case of noisy experimental data.

For more complicated systems where the ratio of measured to unmeasured coordinates is small, there will be an even greater necessity for expansion, as was already shown in the beam example when reducing the number of coordinates to 5. If expanded data are required, the inverse reduction technique ought to be used as the modal based receptance coordinate expansion method deteriorates quickly as the number of measured coordinates decreases.

One ought to bear in mind that the RFM is case-dependent. This could be working to our disadvantage to illustrate the potential of coordinate expanded experimental receptance data. For example, it is likely that the use of expanded data is vital in the event of unstable p-values. In the beam case studies there are no distinctive unstable elements in the analytical model, although to a certain extent this is addressed by assuming less measurement sites resulting in a less stable RFM. Another area where expanded data are expected to be useful is the updating of joints when a more detailed local error description is required. Further investigation is therefore recommended on more complex and/or detailed structures.

## 8.5 REDUCED ANALYTICAL COORDINATES IN THE RFM

Reducing the size of the analytical model can be achieved by using matrix condensation techniques which rely on choosing a number of coordinates as masters and expressing the initial mass and stiffness matrices in terms of these coordinates only. The main disadvantages of condensation techniques have already been discussed in chapter 2, but a summary will be given here;

(i) the measurement points often are not the best points to choose as masters,
(ii) there may not be enough measurement coordinates to be used as masters,
(iii) the connectivity of the original model is lost,
(iv) the reduction introduces extra inaccuracies,
(v) the efforts in creating a detailed analytical model are compromised.

The main reason the author considers using condensation techniques unsuitable for the RFM because the connectivities of the full analytical system are lost. Since the RFM employs an element-by-element error location procedure it is imperative that the connectivities of the element system matrices are represented in the analytical system matrices.

Alternatively, one can delete the unmeasured coordinates from the analytical receptance matrix. The resulting reduced receptance matrix is fully representative of the dynamic behaviour of the full analytical system as there are no approximations made. For a deleted analytical receptance matrix, the basic RFM becomes:

$$[\alpha_A^D(\omega)]_{nxn}[\Delta Z^R(\omega)]_{nxn}\{\alpha_X(\omega)\}_{i_{nx1}} = \{\Delta\alpha(\omega)_i\}_{nx1} \tag{8}$$

where the error matrix, $[\Delta Z^R(\omega)]$, is reduced to the experimental coordinates, and superscript D denotes deleted.

Now that the experimental receptance column is fully known with respect to $[\Delta Z^R(\omega)]$, the results can be obtained directly without iteration. There are three variations in the definition of $[\Delta Z^R(\omega)]$:

(i) $$[\Delta Z^R(\omega)]_{nxn} = [[\Delta K^R] - \omega^2[\Delta M^R]]_{nxn} \tag{9}$$

Where $[\Delta K^R]$ and $[\Delta M^R]$ are obtained using standard condensation techniques with the aforementioned drawbacks.

A more appropriate approach using condensation techniques is proposed by Conti and Donley **[106]** in a recent publication on updating methods using response data. Both the complete system and the element system matrices are condensed using the same transformation prior to updating. This assures that the connectivity of the analytical model is retained and enables an element by element error location procedure. But the other disadvantages mentioned still apply.

(ii) $$[\Delta Z^R(\omega)]_{nxn} = [[\Delta K^D] - \omega^2[\Delta M^D]]_{nxn} \tag{10}$$

Where $[\Delta K^D]$ and $[\Delta M^D]$ are obtained by deleting the unmeasured coordinates from the full system. Equation (10) suggests that all modelling errors are at the measured coordinates only. This approach can be suitable for lumped parameter systems, but will not produce the required results if there are errors at the other degrees of freedom (see example in Appendix B). Thus for more realistic systems and for an element-by-element approach of error location, this deleting approach in the RFM will not produce satisfactory results.

(iii) An alternative approach to define $[\Delta Z^R(\omega)]_{nxn}$ has recently been suggested by Larsson **[105,120]**. Starting from the following definition of a reduced dynamically equivalent stiffness matrix,

$$[Z^D(\omega)]_{nxn} = [\tilde{Z}^D(\omega)]_{nxn} = [\alpha^D(\omega)]^{-1}_{nxn} \tag{11}$$

*Now* $$[Z][\alpha] = [I] \text{ and } [\tilde{Z}^D][\alpha^D] = [I] \tag{12}$$

From the product rule: $$\frac{\delta[Z]}{\delta p}[\alpha] + [Z]\frac{\delta[\alpha]}{\delta p} = 0 \tag{13}$$

and since: $$\frac{\delta[\alpha^D]}{\delta p} = \left[\frac{\delta[\alpha]}{\delta p}\right]^D \tag{14}$$

Substituting equations (12) and (14) into equation (13) and rearranging gives:

$$\frac{\delta[\tilde{Z}^D]}{\delta p} = -[\tilde{Z}^D]\frac{\delta[\alpha^D]}{\delta p}[\tilde{Z}^D] = -[\tilde{Z}^D]\left[[\alpha]\frac{\delta[Z]}{\delta p}[\alpha]\right]^D[\tilde{Z}^D] \tag{15}$$

Larsson uses (15) in a force balance, or equation error approach:

$$[\Delta Z^D(\omega)][\alpha_x(\omega)] = [I] - [Z^D(\omega)][\alpha(\omega)_x] \tag{16}$$

which is effectively the same as the RFM (pre-multiply both sides of equation (8) by the analytical receptance matrix). As mentioned in chapter 2 the advantage of this approach is that it is not necessary to calculate the entire analytical receptance matrix for each iteration if the system is fully known. If the missing coordinates are substituted by their analytical counterparts (as in the RFM), a full analytical system receptance matrix is still required and if Larsson's dynamic equivalent reduction technique is used, all analytical receptances are required for equation (15). Thus the equation error approach is only advantageous over the standard RFM if the experimental data is complete.

A disadvantage of Larssons' approach is the increased CPU time due to the additional matrix manipulations involved to relate a change in the analytical system matrices to changes in measured receptance data, although this will be offset by a reduction in CPU time due to the smaller system matrices involved. This approach appears to be very promising as there are no assumptions that all modelling errors should be in the measured coordinates only. A 2 DOF example (see Appendix B) showed that the dynamic equivalent by deletion approach is an approximation except in some special circumstances which will be case-dependent. For a particular 2 DOF system (also Appendix B) equation (16) is an equality if $\omega=0$ or if $p_2 = p_4$. These limitations are due to the first-

order truncation of the Taylor expansion defining the relationship between $[\tilde{Z}_X^D]$ and $[\tilde{Z}_A^D]$:

$$[\tilde{Z}_X^D] = [\tilde{Z}_A^D] + \frac{\delta[\tilde{Z}_A^D]}{\delta p} Ap + 0\,(\Delta p)^2 \qquad (17)$$

Thus the approach adopted by Larsson is equivalent to a perturbation theory based method and it has no obvious advantages over the standard RFM for the general case, although it may be that the solution process itself is more stable.

The derivation of the 2 DOF example in appendix B verifies the explanation by Larsson that at the natural frequencies of the system obtained using the unmeasured degrees of freedom, the resulting equation becomes invalid (in this case $k_2 - \omega^2 m_2 = 0$), Larsson states that the equations can only be used for frequencies up to the first natural frequency of the *measured* coordinates.

## 8.6 CONCLUDING REMARKS

This chapter focused on the coordinate incompatibility between experimental and analytical models within the RFM. Two techniques to expand the coordinates of a receptance column were proposed; (i) an inverse reduction procedure employing the analytical mass and stiffness matrices and (ii) a method based on the assumption that a forced response shape can be expressed as a linear combination of the analytical mode shapes.

Both expansion procedures give good expanded data for frequencies in the vicinity of resonances but are not so accurate between resonances. Generally the inverse reduction method produces better expansions. As for the mode shape expansion techniques, both receptance column expansion procedures depend on the ratio of measured to unmeasured coordinates and on the accuracy of the analytical model. In particular, the expansion technique employing analytical modal data deteriorates rapidly as the ratio of measured to unmeasured coordinates decreases.

To include an expansion procedure within the RFM it is recommended that the experimental data be expanded for each iteration using the newly-updated analytical model. This has the disadvantage of increasing the CPU time per iteration, especially if

the inverse reduction method is used which requires an inversion for each frequency point selected. A smoother solution process, especially during the first few iterations, is achieved when using expanded experimental data compared to analytical coordinate substitution. However, if the RFM converges easily by substituting with updated analytical counterparts, it does not warrant the extra CPU time required for a full expansion. For unstable solutions and few measured coordinates with respect to the number of unknown p-values, the use of expanded data obtained by the inverse reduction procedure is recommended. Including the inverse reduction expansion procedure in the RFM, selecting frequency points around resonances is preferable to selecting frequency points between resonances, due to the improved expansion of receptance columns at frequencies in the vicinity of resonances.

The reduction of the analytical model to the measured coordinates is not a recommended practice for the RFM. The condensation techniques used in practise loose the analytical model system connectivities and introduce additional inaccuracies and as such are unsuitable for the RFM. Using a dynamic equivalent reduction procedure by deleting rows and columns of the receptance matrix is an improvement over the standard condensation techniques. However, including this procedure within the RPM one also incorporates the (inherent) assumption that all modelling-errors are at the measured coordinates only. This is an invalid prerequisite for most realistic updating applications, and hence this type of reduction is also not advocated in general.

# CHAPTER 9

# UPDATING OF STRUCTURAL JOINTS

## 9.1 INTRODUCTION

In previous chapters the applicability of the RFM both for error location and updating of analytical models has been demonstrated. So far, the main emphasis of this thesis has been on analytical model updating without distinguishing between various sources of modelling errors. A major source of modelling errors is usually in structural joints and boundary conditions as these are the most difficult to model. It is much easier to model a complex but smooth 3 dimensional geometry than it is to represent a structural joint.

A wide variety of joints such as welded, bolted, adhesive joints are encountered in engineering structures (see **Fig.** 9.1). In general, certain industries tend to use specific types of joints more frequently than others:

Aircraft - lap joints, bolted and riveted joints, adhesive bonds
Automotive - spot-welded joints
Construction - bolted and welded I beams
Manufacturing - all
Marine - Stiffened plates, offset beams
Off-shore - welded tubular joints
Power / Nuclear - butt-welded, fillet-welded and bolted flanges

Although these are representative examples, a mixture of joints will be found in any one complex structure, a ***typical joint being the usual*** simplification of the analyst.

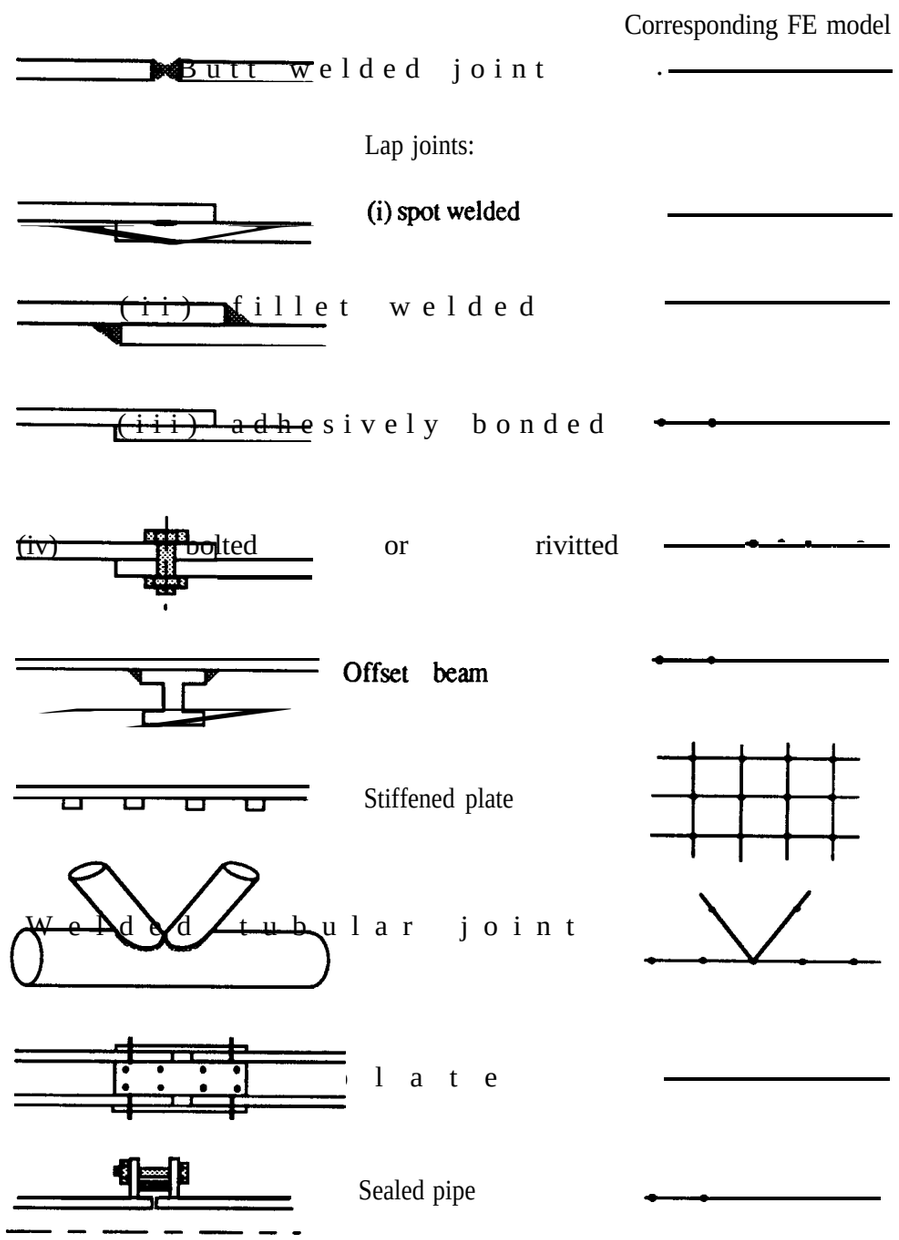


**Fig. 9.1:** Joint examples and typical FE models

Let us consider the FE modelling of these joints. A detailed model is usually set up for structures where accurate results are imperative, such as in the aerospace industry, or for structures with known high stress concentrations, e.g. pressure vessels and tubular joints. However, these models are primarily used to predict stress distributions, the joint model not necessarily being appropriate for a dynamic analysis. During a stress analysis,

the main load path is through the stiffest direction of the joint, while during a modal analysis the lowest modes are determined by the smallest stiffnesses of that joint which is often in the most ill-defined direction(s). This can result in inaccuracies in the dynamic analysis.

FE modelling of joints for dynamic analysis is usually very simple. The use of stick-models for modal analysis of large structures is very common. The joint is represented by one node at which adjacent elements are connected directly. Typical FE model representations of joints are also illustrated in **Fig.** 9.1.

In addition to flexibility, joints are also the main source of damping in a structure, especially if there are overlapping surfaces which introduce Coulomb damping (non-linear). The assumption of structural (material damping) is adequate for continuous parts of the structure, where one damping value is often sufficient to represent these parts: this presents no problem for model updating. However, it is essential to define damping due to structural joints in more detail. Therefore, the use of damping elements at, and in the direct vicinity of, joints will be necessary to produce a correct updated analytical model of many practical structures.

## 9.2 PROPOSED JOINT UPDATING PROCEDURE

In the light of these observations, updating of joints is not an easy task. Before applying the RFM to specific problems of structural dynamic joint updating, some general aspects of a joint updating strategy are considered.

There are several possibilities for representing the effects of structural joints for model updating purposes. Three suggestions are proposed: (i) the introduction of additional spring-damper elements between coincident nodes at the joint, (ii) to introduce only one additional element representing the entire joint and (iii) to introduce more than one element depending of the number of *brunches* being joined together. These three options are illustrated in **Fig. 9.2.**

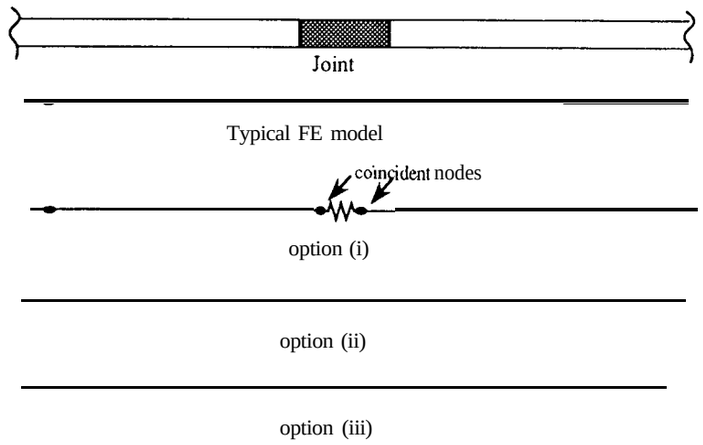


**Fig. 9.2:** Updating of joints, options.(i), (ii) and (iii)

Considering option (i), an example of which is shown in **Fig. 9.2,** there are two disadvantages, apart from increasing the number of degrees of freedom:

- by introducing additional springs in any one direction a large stiffness disparity across the joint is also introduced. This is not representative of the true interfacing at the joint and it will be kinematically inconsistent, which, due to the smearing effect of FE analysis in case of discontinuities, will result in an approximate solution.
- if a joint model is not stiff enough, an additional spring element cannot increase the stiffness as compared to fully connected nodes, unless an additional spring element across the joint is introduced. Thus if the joint is modelled too flexibly a spring element between adjacent nodes of the joint should be introduced while if a joint model is too stiff, an additional spring element between joint nodes has to be introduced (spring in parallel or series).

Therefore it will be more appropriate to introduce and/or to adjust elements around the joint which represent the area of the joint and slightly beyond, as in options (ii) and (iii). The latter, although introducing more unknowns, also gives greater versatility. Both options (ii) and (iii) can give additional versatility as different p-values can be assigned to any one joint, e.g. corresponding to various directions, provided experimental data is available for sufficient measurement sites. This is in contrast to option (i) which can just have one p-value for each joint stiffness element and additional flexibility is achieved by introducing more spring elements at the joint. Option (iii) is most versatile and is therefore considered to be the most appropriate. The additional joint elements can also be

used to obtain damping estimates of a joint by assuming the damping to be a linear combination of the stiffness elements of that joint.

These additional joint elements can be introduced either before or after a first error localisation process. Taking the original FE model as it is, a first error localisation procedure will indicate modelling errors by an averaged p-value smeared out over FE elements adjacent to the joint(s) in error. This is not as accurate but it keeps the initial error localisation problem down in size. Then additional joint elements can be introduced at the indicated erroneous joint(s). A subsequent second updating process will produce refined estimates for the joint correction values. This approach relies on the success of the initial error localisation process and also incurs additional costs due to setting up two FE models.

If the additional joint elements are introduced at the start of the updating problem, the problem size increases but a direct estimate of the joint p-value is obtained. An additional advantage of introducing the joint elements at an early stage is that in that case a *priori* knowledge of the joint can readily be included in the original model before error location. Therefore the author considers introduction of (additional) joint elements at the initial FE stage more appropriate.

Thus the proposed model updating strategy for a structure with joints is to introduce additional joint elements in the initial set-up of the FE model. One joint element for each *branch* of the joint is recommended and any a *priori* knowledge of the joint should be included. To reduce the possibility of modelling disparities it is advised that the joint elements are of the same type as the elements used to model adjacent continuous parts of the structure under study. Error location using the RFM can then be carried out directly on the FE model.

## 9.3 CASE STUDIES ON A FRAME STRUCTURE

### 9.3.1 The 2D frame models

Some difficulties associated with joint updating were investigated on a 2D frame structure. The frame consisted of 21 elements and 20 nodes as shown in **Fig. 9.3. The** excitation point was at node 10 in the x direction, and a frequency range of O-1600 Hz is

considered. Sixty in-plane coordinates were *measured.* To focus attention on joint modelling errors only, noise-free *experimental* data was used.

### *9.3.2* Joint discontinuity

A complete break in one of the joints was considered as a most severe case of joint modelling error, the location of the fracture being indicated in **Fig 9.3a**. Both the experimental and analytical models consisted of 21 2D beam elements. Typical receptance curves for both models are shown in **Fig. 9.3b.** As can be seen the dynamic behaviour is significantly different.

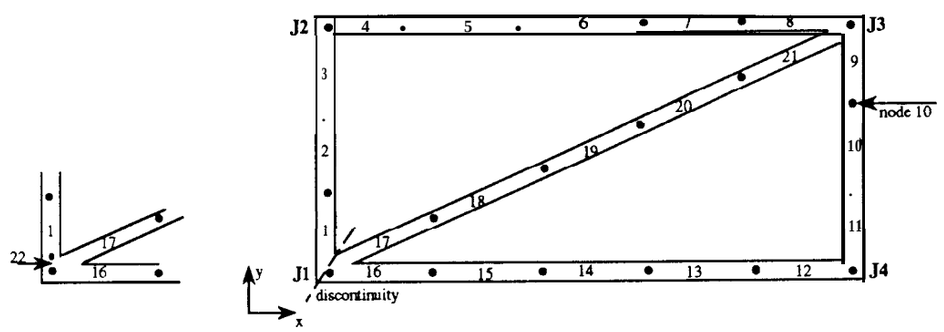


(a) Frame model with discontinuity

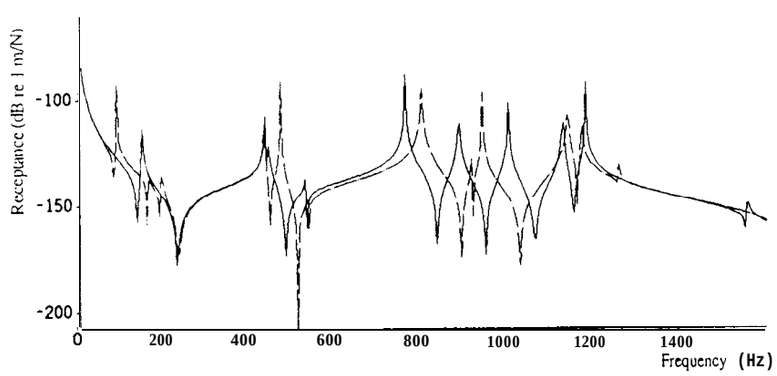


(b) Receptance FRF $\alpha_{10x10x}$ obtained from frame models with and without a joint discontinuity at **J1**

Fig. 9.3: 2D frame models

First, a discontinuity in the *experimental* model was investigated. Of six RFM runs none converged as in each run the matrix solution became rank deficient. As before, the sum of the squared percentages difference between *experimental* and updated receptance values for each iteration was calculated to monitor convergence. The p-values at the iteration where this scalar reaches its minimum were used to calculate the mean p-values and the mean-to-standard deviation ratio of the p-values. These are plotted for mass and stiffness elements in **Fig. 9.4.**

The stiffness modelling error was located at element 1, at the correct position (next to J1) with a mean to standard deviation ratio of 12.6 and a mean value of -0.97. A mean p-value of -0.97 meant that element should be deleted and this adequately represented the discontinuity in the *experimental* model. Three additional stiffness errors were also indicated with mean-to-standard deviation ratios between 2 and 3. There are 3 mass elements in error which were indicated with a maximum mean-to-standard deviation ration of 12.3 at element 1 and a mean p-value of -0.89. Despite the non converging solution and some spreading of errors over the entire structure, the results obtained pointed towards the true modelling error location .

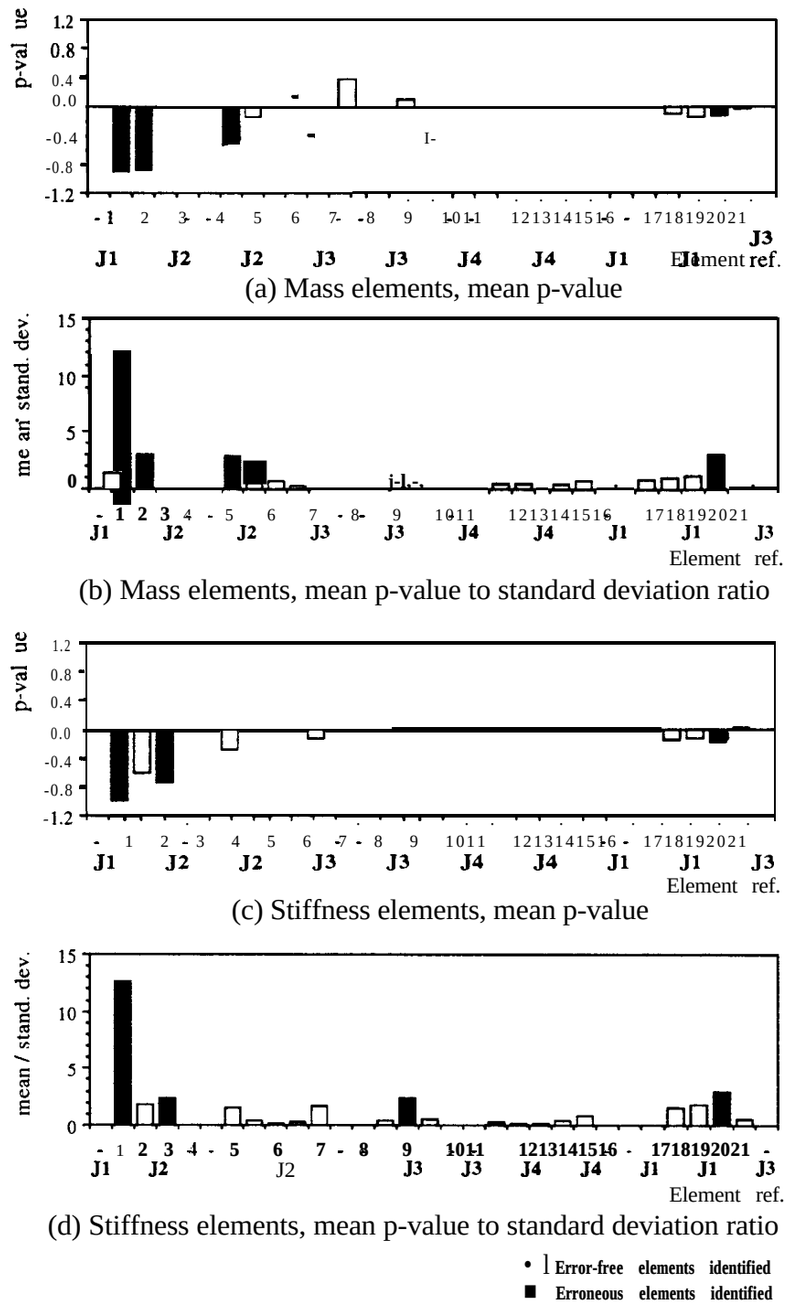


**Fig. 9.4:** RFM results for a discontinuity at joint Jl in the *experimental* model

Next a reversed scenario, a joint discontinuity in the analytical model, was considered. Again none of six RFM runs converged but in this case erroneous elements were indicated over the entire analytical frame model. Knowing that the joint discontinuity is at **J1,** one can see that stiffness modelling errors were indicated at all elements adjacent to this joint. However, the mean p-values associated with these elements were inconsistent

with the actual modelling errors and the maximum mass modelling error was indicated near J3 **(Fig.** 9.5).

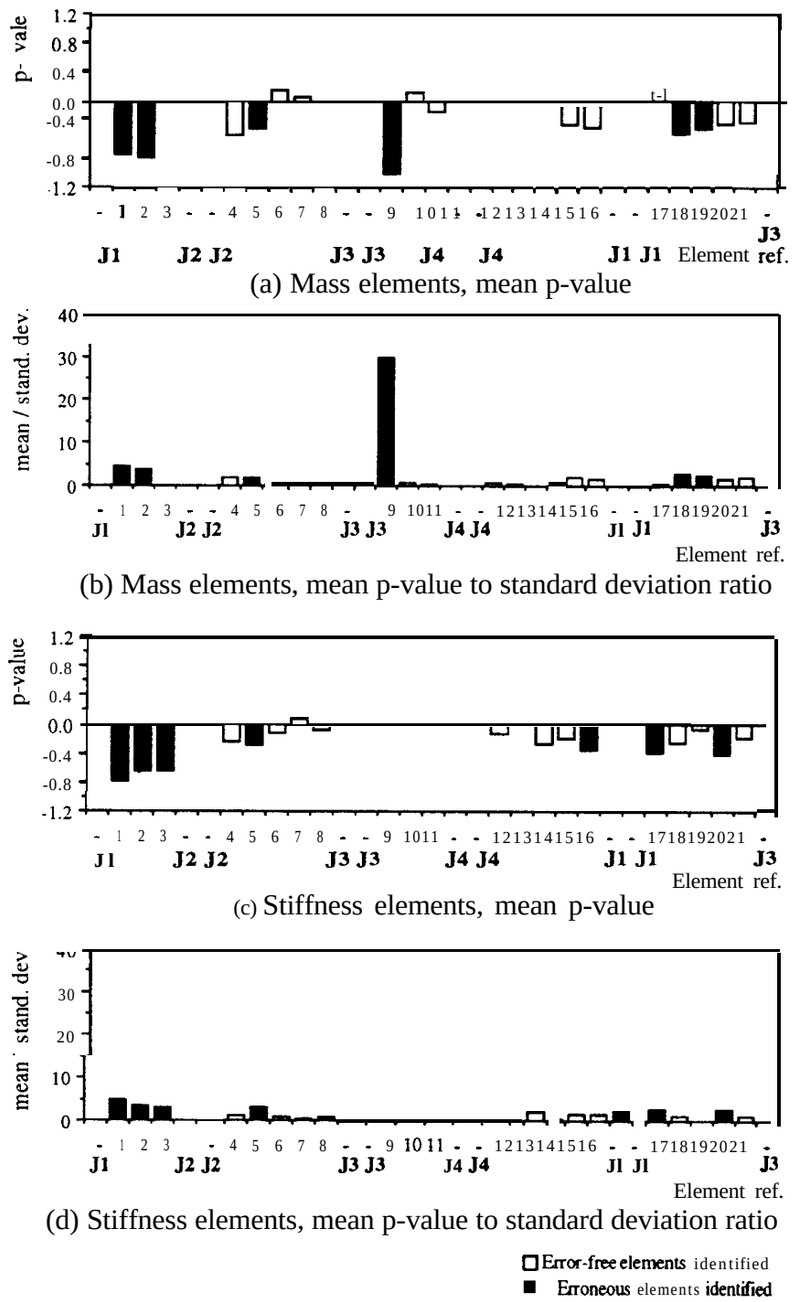


**Fig. 9.5:** RFM results for a discontinuity at joint J1 in the analytical model

The difference between this case and the previous one is clear: a connectivity in the analytical model can be broken by deleting the appropriate element while it is not possible to make a connection if the connectivity in the analytical model is not there in the first

place. This is to be expected as in the latter case there is no element to represent the connectivity and the p-values of the RFM are directly representative of element errors.

### 9.3.3 Joint stiffness modelling errors

A discontinuity is an extreme case of joint modelling error. The test cases in this section regard more realistic joint modelling errors where the analytical model had the correct connectivities but there were some discrepancies in joint properties e.g. due to the manufacture of the joint. Another *experimental* model was set up with an additional small joint element at the position of the joint **J1**. This element, number 22 (see **Fig. 9.3**), was created by reducing the length of element 1 by one tenth of its original length. The joint element had the same properties and dimensions as the other beam elements but the element stiffness matrix was multiplied by a constant factor, kj. A range of kj values between 0.0001 and 1000 is investigated (where kj=l is equivalent to no modelling error). The joint element mass matrix remained unchanged in all test cases although all mass elements are still retained in the updating process.

It is interesting to note that for these test cases, convergence was achieved for all runs with an increased joint stiffness (**kj>1**), while for a reduced joint stiffness (**kj<1**) no convergence was achieved. For the latter cases either the maximum allowed number of iterations (50) was reached without achieving convergence or the solution process became rank deficient due to complete elimination of stiffness element 1 and/or 2. This is probably because (i) the p-values expected for a decreased joint stiffness are close to -1 which makes it likely that during the iterative process a value of -1 is obtained and (ii) the change due to an increased joint stiffness on the receptance curves is small. Typical results of 6 RFM runs for reduced joint stiffness are shown **Figs. 9.6** and 9.7, for kj=O. 1 and kj=O.OO 1 respectively.

The results for **kj=0.1** were promising as the maximum mean p-value to standard deviation ratio is 5 14 and occurred at stiffness element 1. Additional fictitious modelling errors were also identified both for the mass and for stiffness elements but, in comparison, their maximum mean p-value to standard deviation ratio is much smaller (less than 10) and the associated mean p-values were also smaller. On decreasing the *experimental* joint stiffness (**kj=0.01** or **kj=0.001**), the picture became less clear. The maximum mean-to-standard deviation ratio still occurred at stiffness element 1 but the error location and mean p-values for wrongly identified erroneous elements became more significant in comparison with the values associated with stiffness element 1 (**Fig.** 9.7).

The additional erroneous elements identified were distributed over the entire analytical model again and their number increased for decreasing joint stiffness modelling error.

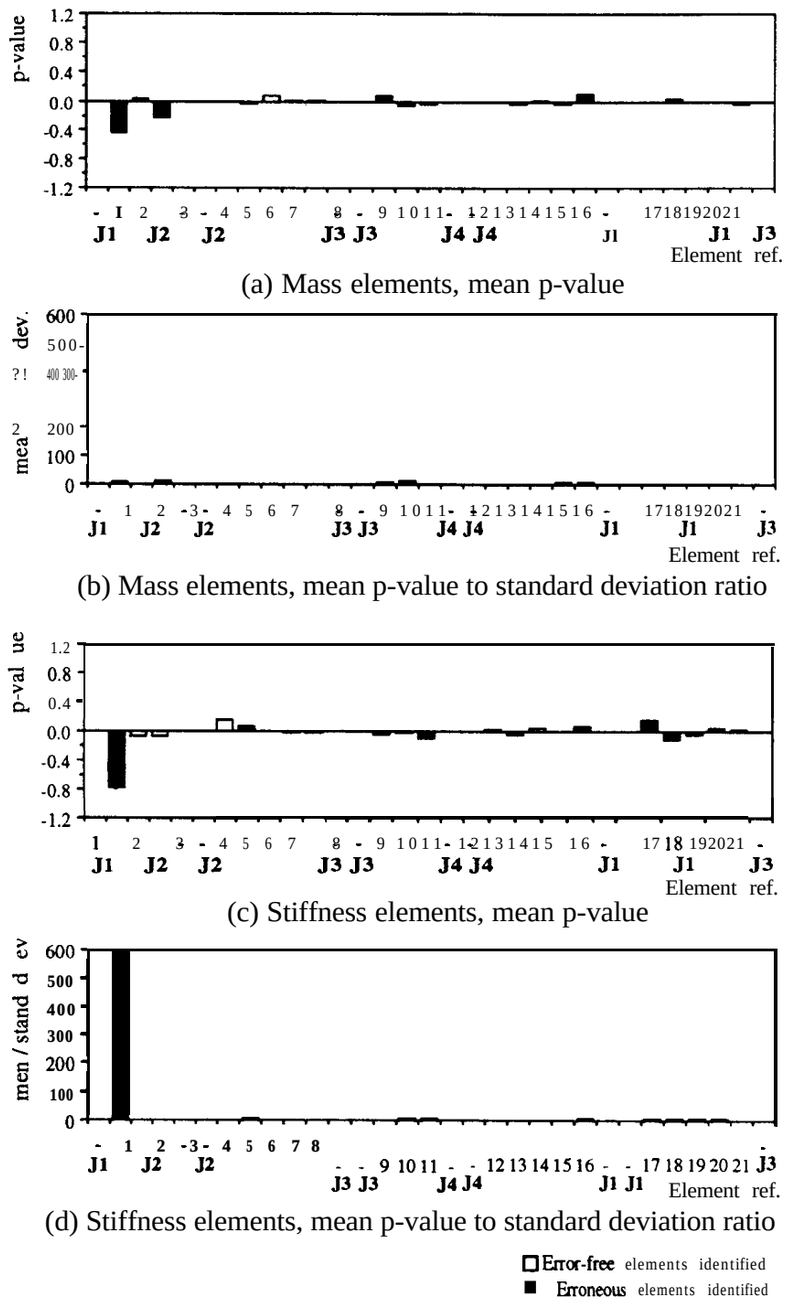


**Fig. 9.6:** RFM results for a joint modelling error, kj=O. 1, at joint **J1** in the experimental model

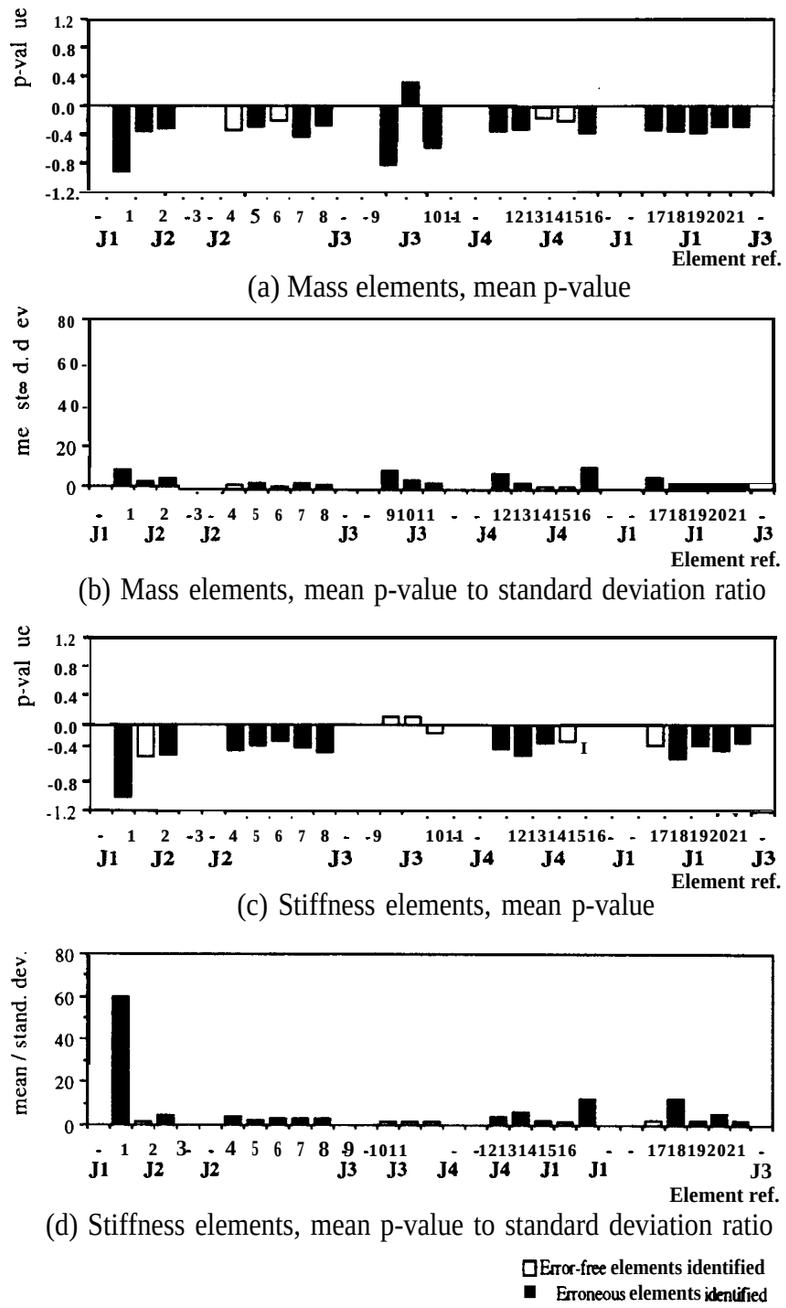


**Fig. 9.7:** RFM results for a joint modelling error, **kj=0.001,** at joint **J1** in the *experimental* model

The frame test cases for increasing joint stiffness modelling errors (kj=10, kj=100) showed only small changes in error location. Typical results for an increased *experimental* joint stiffness are given in **Fig. 9.8** (kj=lO). There was a considerable spread of wrongly identified elements in error but the maximum of their mean p-values is

only -0.12. For frame test cases with an increased *experimental* joint stiffness, reasonable results were achieved. Comparing RFM results for an increase in *experimental* joint stiffness **(Fig. 9.8)** with those for a decrease in *experimental* joint stiffness **(Fig. 9.6-9.7)**, improved convergence were observed and p-value estimates for wrongly identified erroneous elements were smaller.

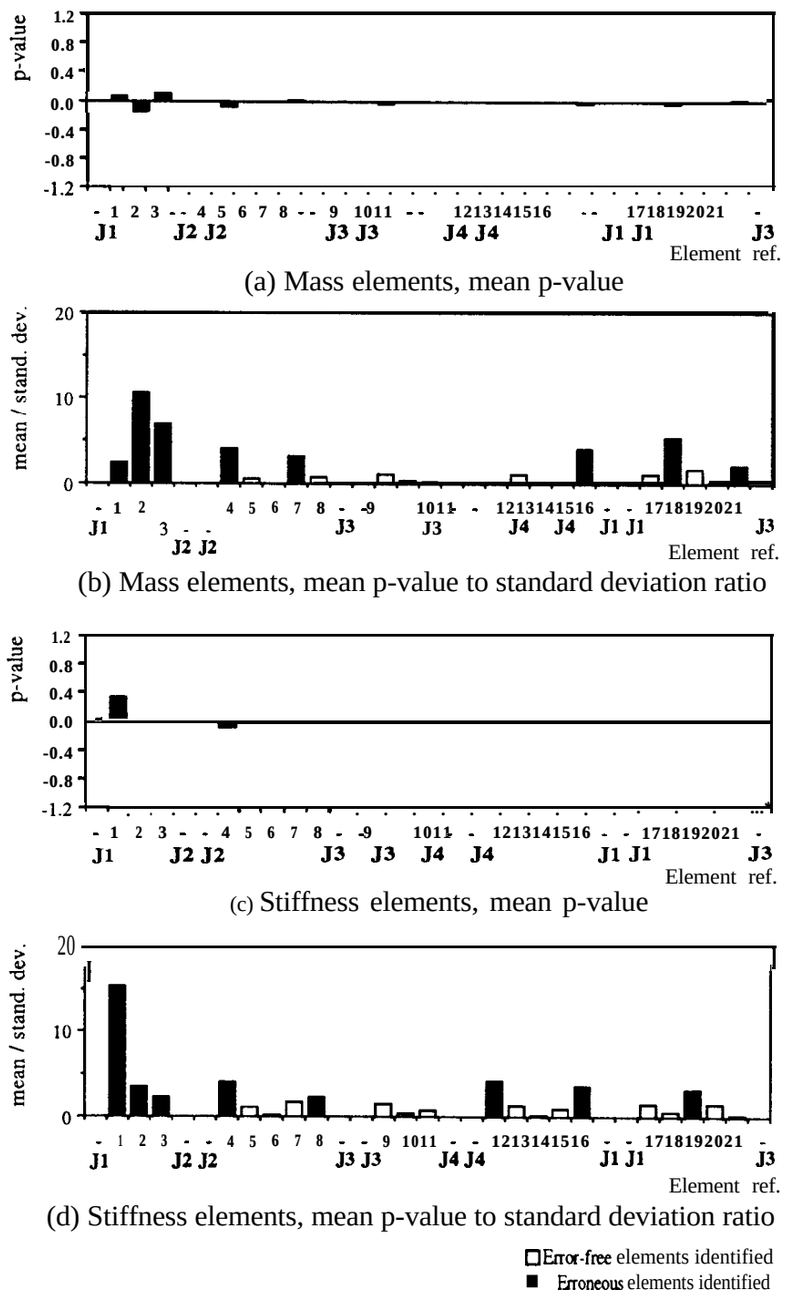


**Fig. 9.8:** RFM results for a joint modelling error, kj=lO, at joint **J1** in the *experimental* model

### 9.3.4 Discussion

For all cases except that of joint discontinuity in the analytical model, the erroneous stiffness element was located correctly. Hence the RFM can indicate joint error regions correctly if the connectivities between the analytical and experimental models are compatible. For most test cases, some additional mass and stiffness errors were indicated distributed over the entire structure. The mean p-values of these wrongly identified erroneous elements were generally less significant than those obtained for stiffness element 1. The updated receptance curves, using the mean p-values of the elements in error, reflected these promising results favourably. However, the updated model obtained was not an adequate reflection of the actual *experimental* structure as the joint modelling was approximated by a large element in comparison with the actual discrepancy. Also the error location results became less clear as the modelling error became more significant.

The spreading of wrongly-indicated erroneous elements over the entire analytical model and not just to elements adjacent to the actual joint modelling error indicated that the approach introducing additional joint elements after a first error location process is not advisable.

## 9.4 APPLICATION OF THE JOINT UPDATING PROCEDURE

### 9.4.1 The analytical frame model

In this section the frame joint modelling test cases were repeated using the proposed joint updating procedure by introducing additional joint elements prior to error location **(Fig. 9.2** option (iii)). The analytical FE model of the frame was changed to include small joint elements at each of the joint branches. The length of these joint elements was one fifth of the original element length. As suggested in the joint error location strategy, the additional joint elements covered the area of the joint and beyond. The new analytical model consisted of 31 elements and 30 nodes **(Fig. 9.9).** The *experimental* model used was the same as before, with joint elements of zero length and one tenth of the original beam element length **(Fig. 9.3).**

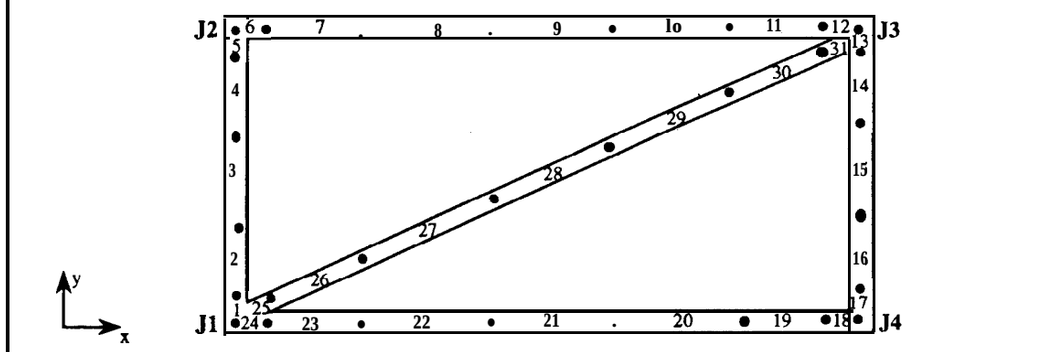


**Fig. 9.9:** The analytical frame model with additional joint elements.

### 9.4.2 Joint discontinuity

Discontinuities in both the *experimental* model and the analytical model were investigated. As before, none of the six RFM runs converged and the p-values from the minimum of the sum of the percentages difference squared between the *experimental* and updated models were used. Results for a discontinuity at **J1** in the *experimental* model are shown in **Fig. 9.10.** A distinct improvement on the error location results was obtained by employing the joint updating strategy. This is evident by comparing **Fig. 9.10** with the direct RFM results shown in **Fig. 9.4.**

For a discontinuity in the analytical model no such improvement was achieved as can be seen comparing **Fig. 9.11** with **Fig. 9.5.** Thus, as expected, the RFM cannot detect connectivities which are not there in the original FE model. Unfortunately the mean p-values, both for the original analytical model and for the model with the additional joint elements model, did not reflect the actual modelling error at all. This is in contrast to a discontinuity in the experimental model which can be represented by removing the appropriate element in the analytical model.

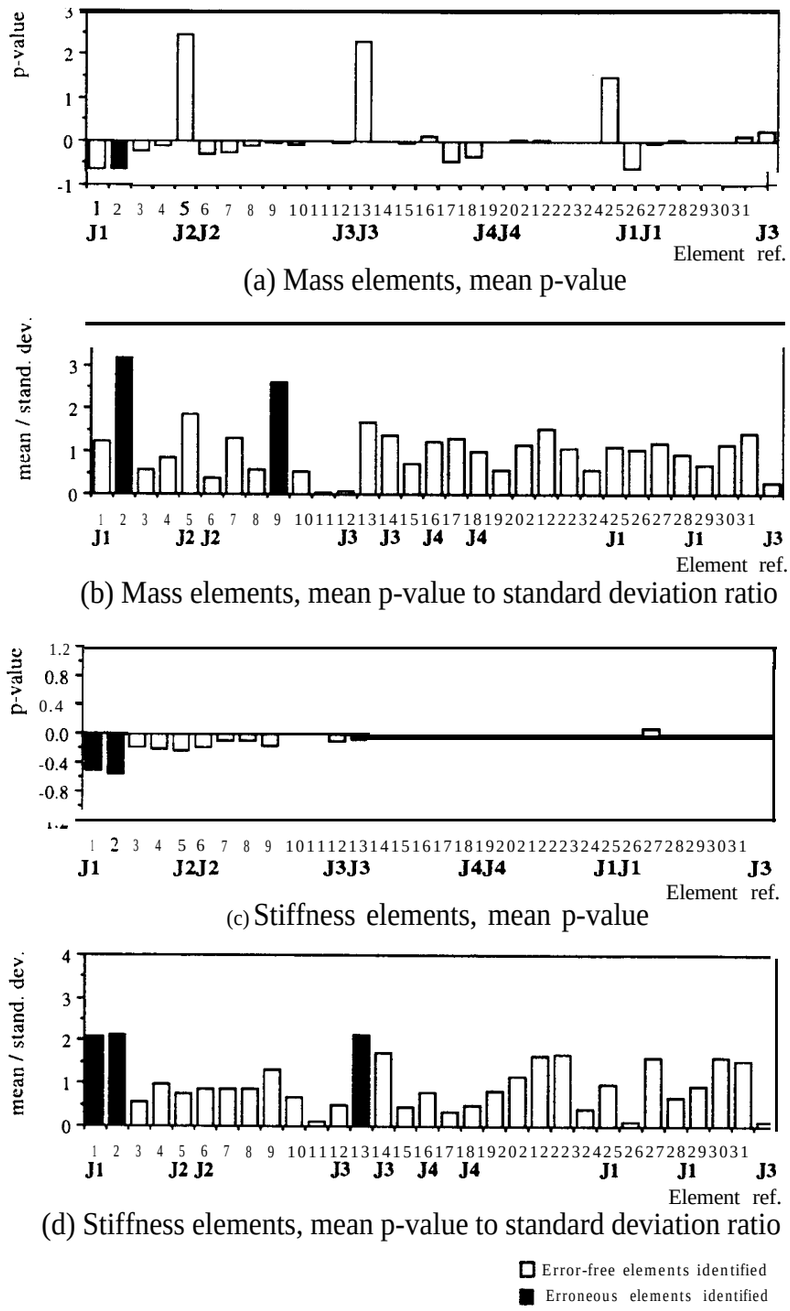


(a) Mass elements, mean p-value

(b) Mass elements, mean p-value to standard deviation ratio

(c) Stiffness elements, mean p-value

(d) Stiffness elements, mean p-value to standard deviation ratio

**Fig. 9.10:** RFM results using the proposed joint updating strategy for a discontinuity at joint J1 in the ***experimental*** model

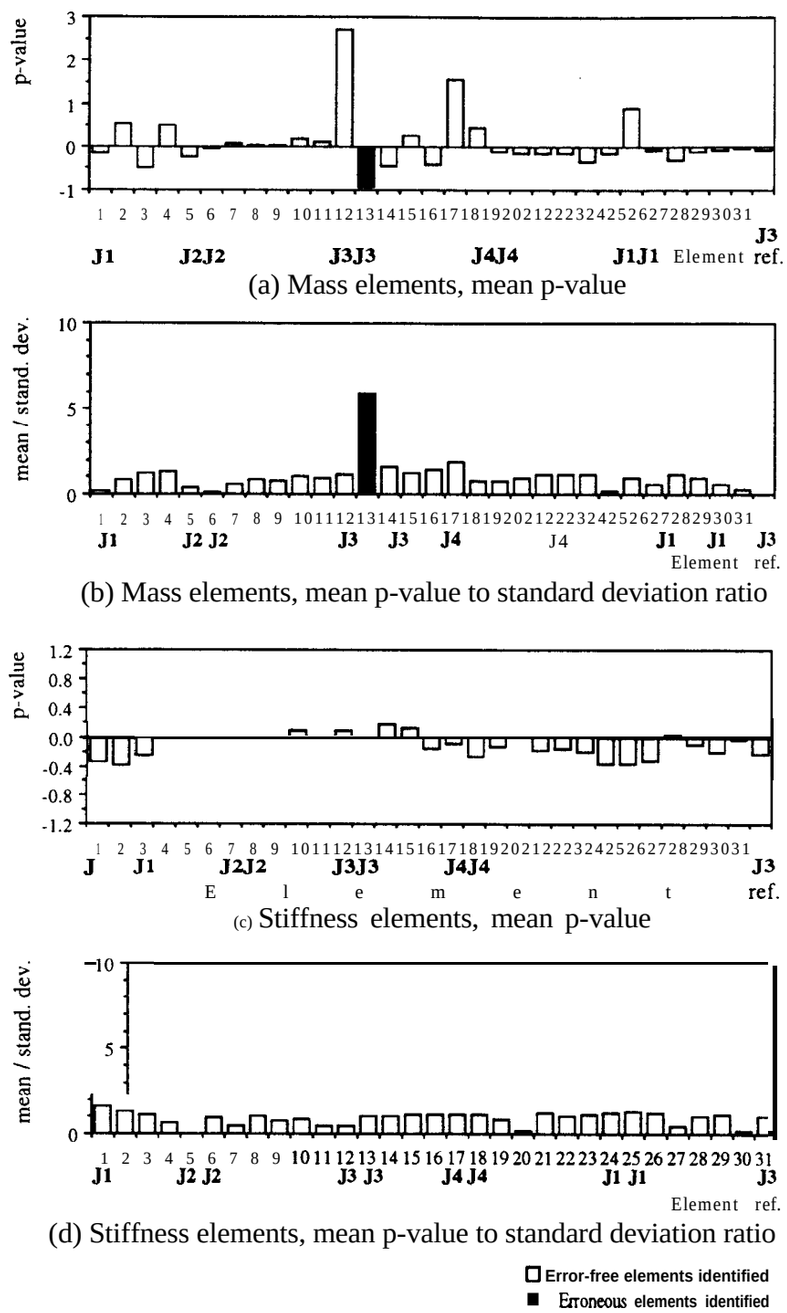


Fig. 9.11: RFM results using the proposed joint updating strategy for a discontinuity at ioint J1 in the analvtical model

### 9.4.3 Joint stiffness modelling errors

The test cases of section 9.4.2, with joint stiffness modelling errors introduced on element 22 of the *experimental* model for a range of kj values between 0.0001 and 1000 and an unchanged joint element mass matrix were investigated.

As in section 9.3.3, convergence was again achieved for all runs with an increased joint stiffness while for a reduced joint stiffness convergence was not achieved. Typical results of six RFM runs for reduced joint stiffness for kj=O.l, **kj=0.001** and kj=lO are shown **Figs. 9.12-9.14.**

Each of the test cases carried out showed a remarkable improvement using the analytical model with additional joint elements **(Figs. 9.12-9.14)** as compared with the earlier results for the original analytical model **(Figs. 9.6-9.8).** Stiffness error location was entirely focused on the actual joint modelling error and significantly fewer mass elements were indicated as being in error. Also, the resulting changes to the analytical model due to wrongly identified erroneous joint mass elements had only a small influence on the overall dynamic behaviour of the model.

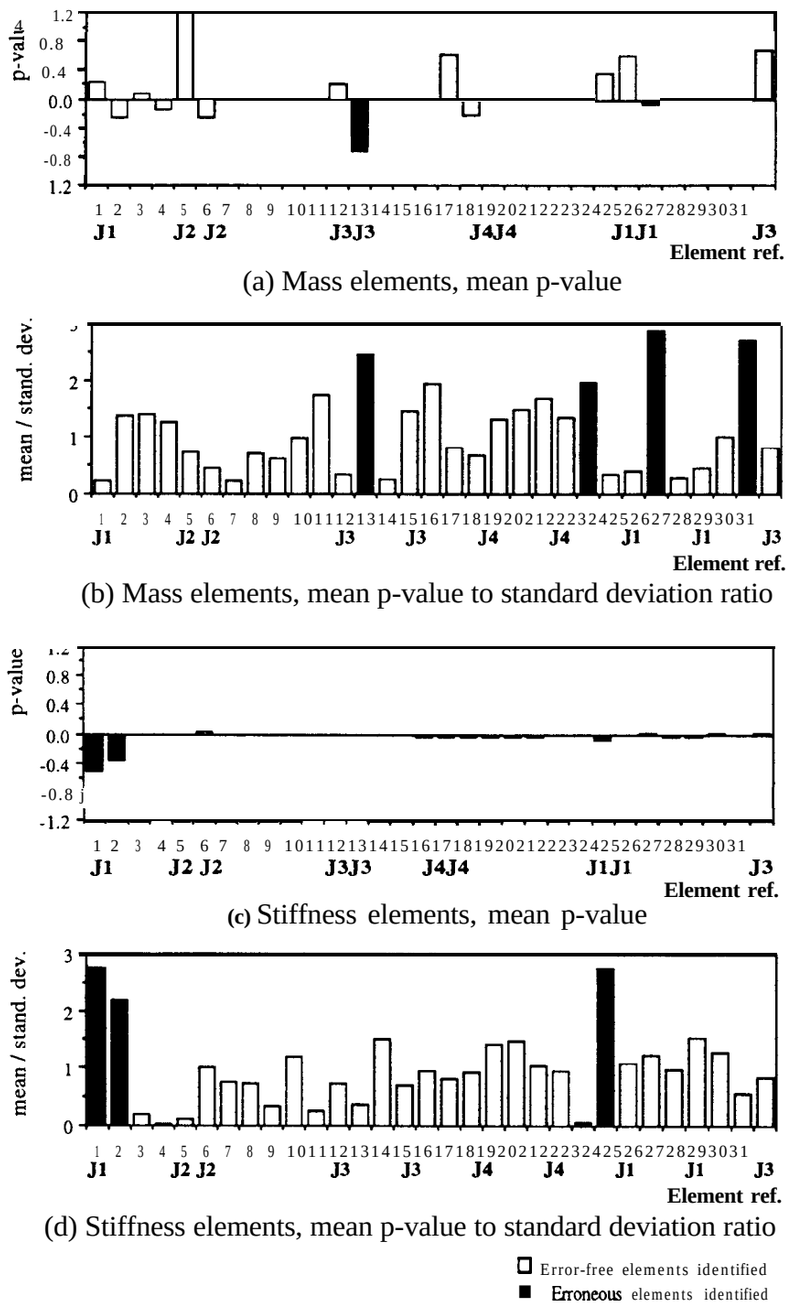


(a) Mass elements, mean p-value

(b) Mass elements, mean p-value to standard deviation ratio

(c) Stiffness elements, mean p-value

(d) Stiffness elements, mean p-value to standard deviation ratio

Fig. 9.12: RFM results using the proposed joint updating strategy for a joint modelling error, kj=O. 1, at joint J1 in the ***experimental*** model

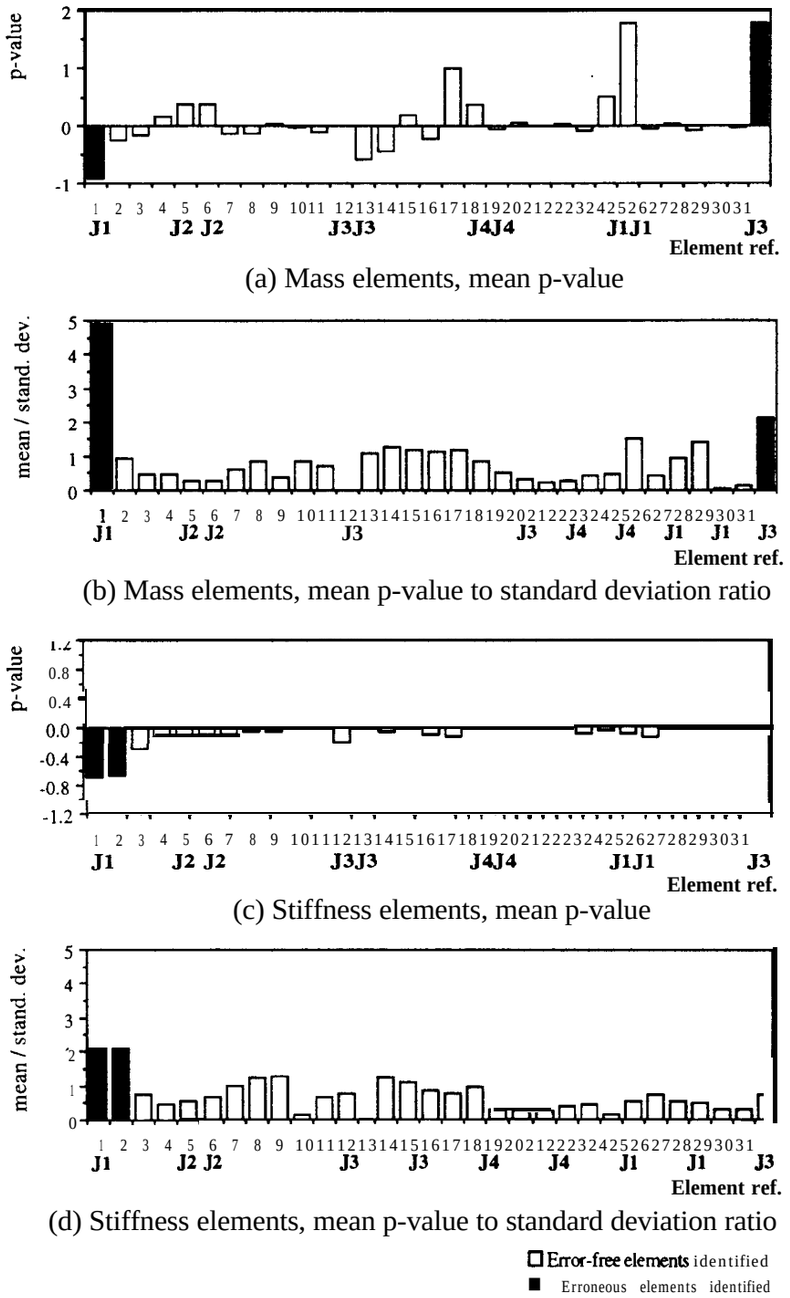


(a) Mass elements, mean p-value

(b) Mass elements, mean p-value to standard deviation ratio

(c) Stiffness elements, mean p-value

(d) Stiffness elements, mean p-value to standard deviation ratio

Fig. 9.13: RFM results using the proposed joint updating strategy for a joint modelling error, kj=O.OOl, at joint J1 in the *experimental* model

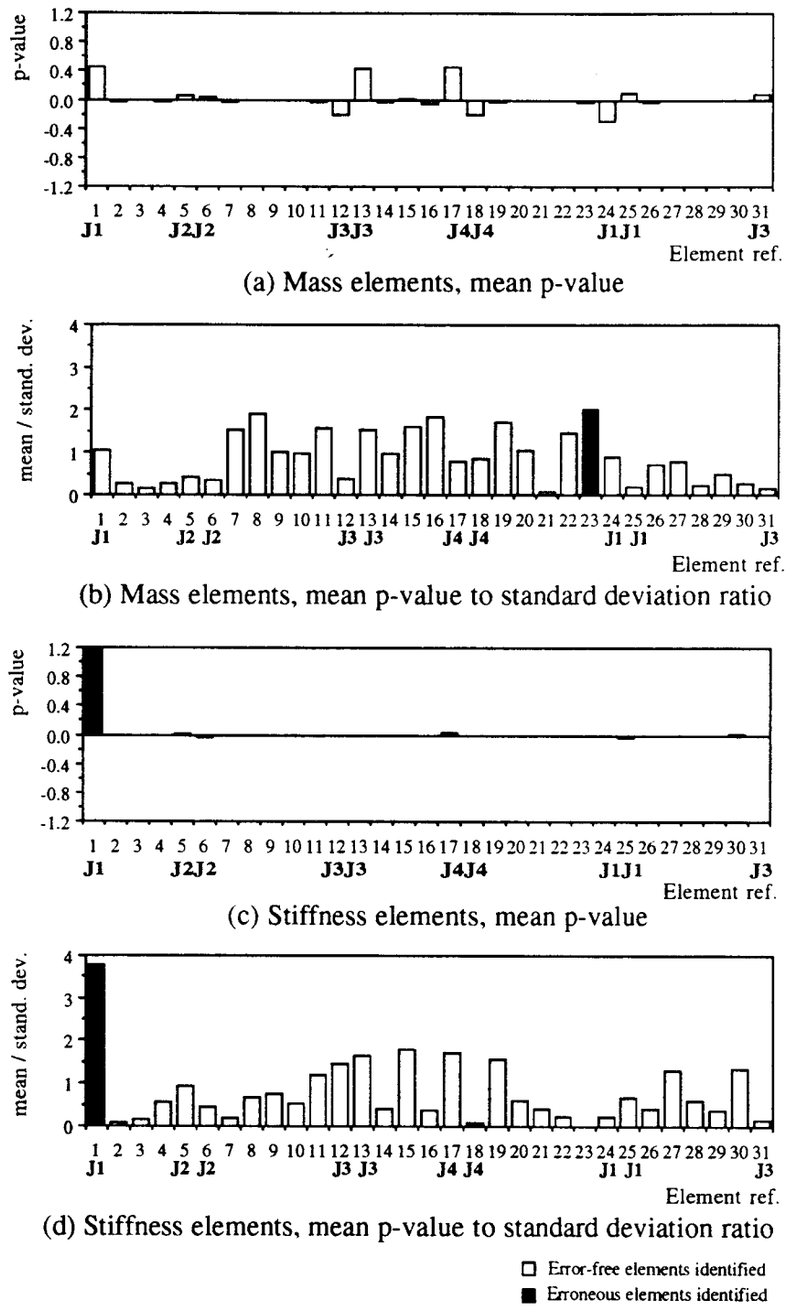


(a) Mass elements, mean p-value

(b) Mass elements, mean p-value to standard deviation ratio

(c) Stiffness elements, mean p-value

(d) Stiffness elements, mean p-value to standard deviation ratio

**Fig. 9.14**: RFM results using the proposed joint updating strategy for a joint modelling error, kj=10, at joint J1 in the *experimental* model

### 9.4.4 Discussion

From the frame test cases it is shown that the proposed modelling strategy for joint error location was clearly an improvement over error location in the original FE model as discussed in section 9.3. This reinforced the recommendation that additional joint elements ought to be introduced prior to a first error location procedure.

For the frame examples one joint modelling error only without any additional analytical modelling errors was considered. This can be justified in the light of the RFM results for the beam test cases of chapter 5. The beam examples had a combination of modelling errors in the analytical model. Using the RFM all elements in error were localised independent of size or nature in the case of noise-free *experimental* data. The smallest analytical modelling errors disappeared first from the error location results as the coordinate incompleteness increased and as the noise on the experimental data increased. Small modelling errors can also vanish due to model mismatch. Similar trends will be observed for joint modelling errors. The most significant modelling errors will feature most prominently in the error location results, depending on the accuracy of the experimental data and the closeness of the analytical model to the actual structure. For most practical applications it is likely that the joint modelling errors are more significant than modelling errors in continuous parts of the structure.

If several correction factors for each joint modelling error are desired, it is imperative to measure receptance columns for various excitation directions, especially if response directions in the analytical model are independent of one another. As mentioned in chapter 5, FRFs obtained from excitation at one coordinate only can locate modelling errors for each element if the analytical response model is sensitive to changes in the p-values selected for those elements.

It must be pointed out that it will always be difficult to locate errors in the analytical FE model if the assumed connectivity is wrong. If the connectivity is not in the analytical model in the first place, as shown in both analytical joint discontinuity test cases, it is unlikely that this error will be located.

If a joint (or the elements around a joint) has been identified as being in error, then a closer inspection of the connectivities in the FE model is recommended. Inspection of the experimental data is also suggested as the indicated discrepancies can also be due to

experimental set-up and equipment problems, such as added mass at measurement points and additional constraints due to supports and/or the excitation systems.

Although the examples used in this chapter were based on relatively easy joint modelling errors they can be considered representative case studies for the problems encountered during updating of structural joints. More case studies with variations on the theme of joint modelling errors will show similar trends to those demonstrated in the previous chapters and therefore will be of little added benefit. It is considered more useful to highlight difficulties encountered during a true to life updating problem. Hence, in the next chapter, updating of a fairly complicated structure with joints using experimental data is presented.

## 9.5 CONCLUDING REMARKS

In this chapter the problem of joint modelling errors, a primary cause of FE modelling errors, is addressed. Several ideas to update structural joints are discussed. The proposed joint updating strategy is to introduce additional joint elements for each ***brunch*** of the joint. These elements should cover the area of the joint and slightly beyond. It is recommended that the additional elements are incorporated into the FE model prior to a first stage of error location to include any ***a priori*** knowledge of the joint.

The success of the proposed strategy is demonstrated employing several representative test cases on a 2D frame structure. Reasonable results are achieved by applying the RFM to an FE model without implementing the suggested joint error updating strategy. The main drawback is that there is a considerable spread of additional erroneous elements indicated both for mass and stiffness elements, especially for more severe joint modelling errors. A marked improvement is achieved by introducing additional joint elements prior to updating. The identified erroneous stiffness elements are all focused on the actual joint in error and there are considerably less, and less significant, wrongly identified erroneous mass elements.

The significance of correct connectivities is emphasised. It is unlikely that the RFM can identify erroneous connectivities if the connectivities are not represented in the analytical model in the first place.

# CHAPTER 10

# EXPERIMENTAL CASE STUDY

## 10.1 THE 3-BAY TRUSS STRUCTURE

In this chapter the application of the RFM to a fairly complicated engineering structure with joints is investigated. For this purpose the 3-bay truss structure, shown in **Fig. 10.1,** was used. The structure is made of Dural (L105) and it consists of 18 cylindrical side-members and 3 ridge-members connected by 8 side-joints and 4 ridge-joints. Engineering drawings of the various parts are given in appendix C.

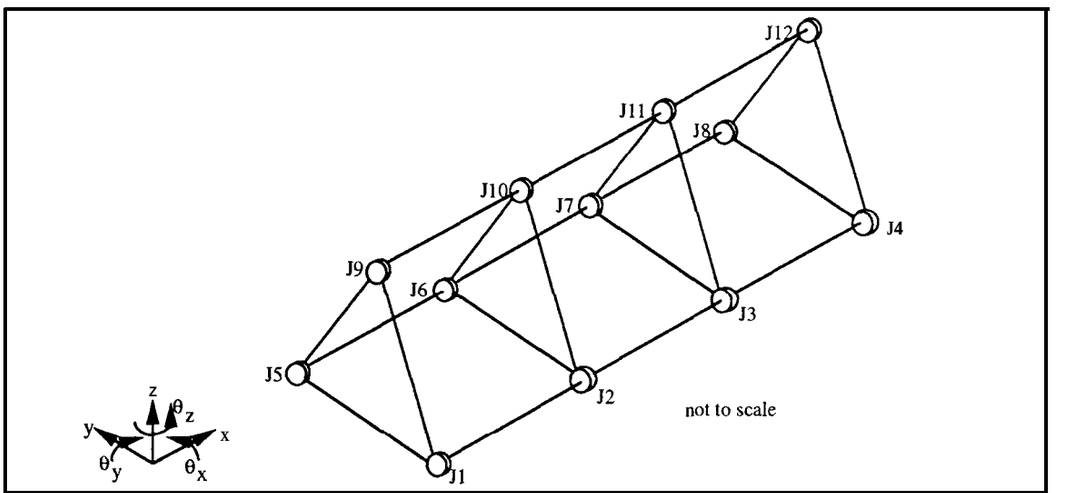


**Fig. 10.1:** The 3-bay truss structure

## 10.2 EXPERIMENTAL DATA

Experimental data were acquired at DRA, using a DIFA SCADAS 64 channel data acquisition unit and LMS Test and Modal software (version 2.4) running on an HP computer and employing a MIMO, multi-input multi-output, test procedure. The structure was freely suspended. Three-point simultaneous excitation in the form of bandlimited noise was applied by Ling Dynamics VP100 shakers at the following coordinates:

(i) in the x-direction, at joint J1;
(ii) in the y-direction, at joint J8; and
(iii) in the z-direction, at joint J4.

The force gauges, 2 of Entran type ELF TC500 5 and 1 PCB type 208B, were mounted at the 'wrong' ends of the pushrods, i.e. at the shaker end, to minimise cross-axis loading effects. Further details of the physical excitation system are also given in appendix C.

Thirty six response coordinates, namely three translational degrees-of-freedom at each joint, were measured using Entran type EGA 125F accelerometers. The accelerometers were attached to the structure using double sided tape so as to be as close to the centre of each joint as possible. Other hardware used included: 2 Vishay strain gauge bridge amplifiers, a PCB 483A02 conditioning unit, KEMO filters on excitation drive signals (bandpass 20- 156 Hz) and MAMA power amplifiers.

Each of the 108 FRF curves (3x36) was measured at 2048 frequencies for a baseband frequency range of 128 Hz. The number of averages was set to 16. The data were stored in universal file format and transferred to an IBM RISC 6000 workstation and an IBM compatible PC for subsequent analysis.

## 10.3 THE FINITE ELEMENT MODEL

ANSYS Finite Element models were set up in accordance with the updating strategy for structures with joints as proposed in chapter 9. To obtain a model which was neither under-defined nor over-defined several FE models were set up. In order to get these different models each of the cylindrical side and ridge trusses was modelled using various numbers of beam elements for the main, continuous, part of the strut (360 mm). 2 small beam elements represented the joint area of the cylindrical trusses. A length of 20 mm was selected for these joint beam elements, this being the length of the tapered section of the trusses. Part of each tapered section of a truss goes into a joint. The 12 joints of the 3-bay truss structure were modelled using lumped masses.

Each continuous part of a truss was alternately modelled using 4, 3, 2 and 1 beam elements resulting in models with 702, 576, 450 and 324 DOFs respectively. The natural frequencies and mode shapes for the first 40 modes were compared for all four models. The natural frequencies and mode shapes for the 3 models with 2, 3 and 4 beam elements between joint elements compared very well with each other, the maximum difference in natural frequency was 0.6%. The model with only 1 beam element between joint elements was notably stiffer and a maximum discrepancy in natural frequency of 13.9% was observed. For updating purposes the number of elements should be as small as

possible to keep the number of unknowns down while still adequately representing of the structure under study. Therefore, the model with 2 beam elements between joint elements was selected for updating.

The effect of the three excitation devices were also represented in the FE model. The pushrod was modelled using a beam element with lumped masses at the ends to represent the nuts, the threaded rod, the force gauge and the carrier, and torsional springs to represent the shaker constraint. Displacement constraints were applied to the shaker end of the pushrod which only allowed translation along the axis of excitation and 2 of the rotations were constrained by the torsional springs while the rotation about the axis of excitation was left free. The final FE model consisted of 105 mass elements and 90 stiffness elements resulting in a total of 462 DOFs (Fig. 10.2).

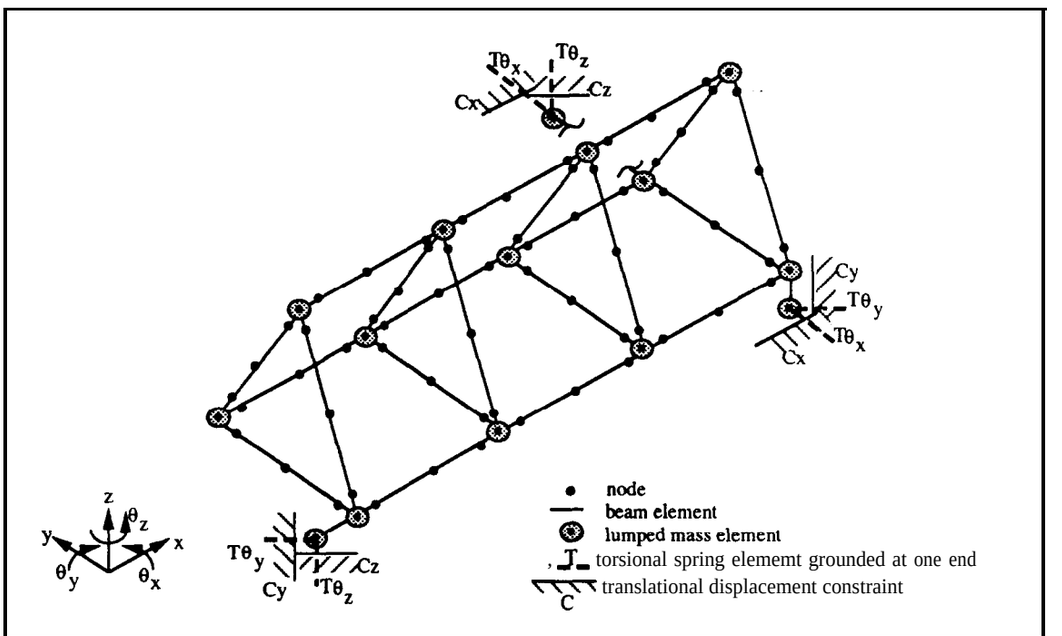


Fig. 10.2: The FE model of the 3-bay truss structure

## 10.4 CORRELATION BETWEEN EXPERIMENTAL AND FE DATA

Prior to updating the FE model, comparisons of the experimental and FE data sets were carried out. Firstly a straightforward comparison of the FRF data was carried out. For the lower frequency range, the FRF data matched reasonably, the discrepancies increasing as the frequency increased. The experimental model seemed to be stiffer than the analytical model. A typical comparison of an experimental receptance curve and its analytical counterpart is shown in Fig. 10.3.

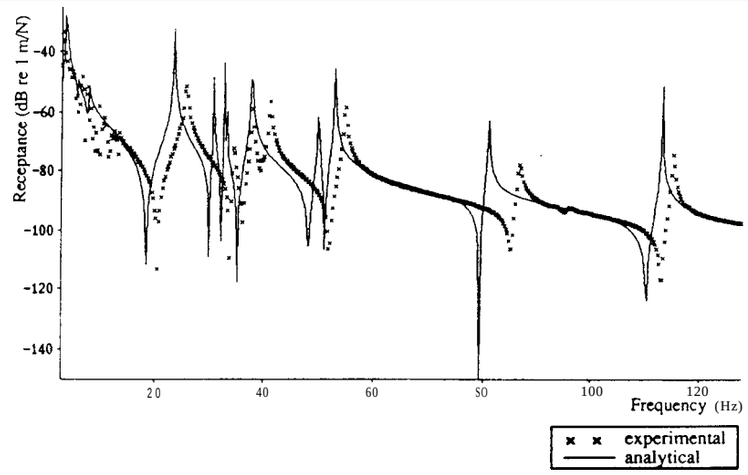


**Fig. 10.3:** 3-bay truss structure experimental and analytical receptance FRF $\alpha_{J4z\,J4z}$

The experimental FRF data were analysed using MODENT, a modal analysis package running on IBM compatible PCs. The modal analysis method used was GRF-M, a global multi-FRF analysis method. GRF-M is based on the rational fractional method and is an improvement of the standard method as the modal parameters are found a number of times and averaged to yield a single consistent set. The universal file containing the experimental data was separated into an FRF data set for each of the 3 excitation points. Each FRF data set contained 36 individual FRFs in appropriate file format for MODENT. The data sets were analysed by applying 20 GRF-M runs to consecutive limited frequency ranges covering the entire frequency range. The most consistent results were saved in a modal data set.

It was observed that some of the FRFs regenerated from the experimental modal data exhibited a sign (phase) change compared with the measured FRF. Closer inspection of the modal analysis results obtained via SDOF curve-fitting of the 3 available point receptances showed that 2 of these had negative modal constants for all the modes. This indicated a sign convention error in the data as the modal constants for a point receptance are always of positive sign. If one or more of the measured FRFs is of the wrong sign, the RFM cannot work.

As it is of vital importance to have a consistent sign convention throughout the acquisition of the experimental data and the updating process, it was necessary to resolve the observed inconsistency. This was achieved by comparing the phase of the experimental FRFs with their analytical counterparts for each of the 108 FRFs. It was found that not only the two point receptances were of wrong sign but all other FRFs for these excitation coordinates too. As each FRF was inspected, noisy parts of the measured data were also

monitored so that later during the frequency point selection of the RFM these frequency ranges could be avoided.

The signs of the input coordinates at joint 8 in the y-direction and joint 4 in the z-direction of the measured data were corrected accordingly and the 3 measured FRF data sets were analysed again. The 3 experimental data sets will from now on be referred to as XJ1x, XJ8y, XJ4z for experimental data obtained from excitation at J1 in the x-direction, J8 in the y-direction and J4 in the z-direction respectively. The various modal data sets were compared to verify that the analytical model resembled the actual structure under study. After a visual comparison the MAC values of experimental and analytical modal data were calculated.

MAC plots of the experimental modal data sets with one-another (Fig. 10.4) showed a lack of correlation between experimental modes 9,10 and 11. This could possibly mean that there was some inconsistent local dynamic behaviour which depended on the excitation direction and/or that the GRF-M method was unable to adequately identify these close local modes.

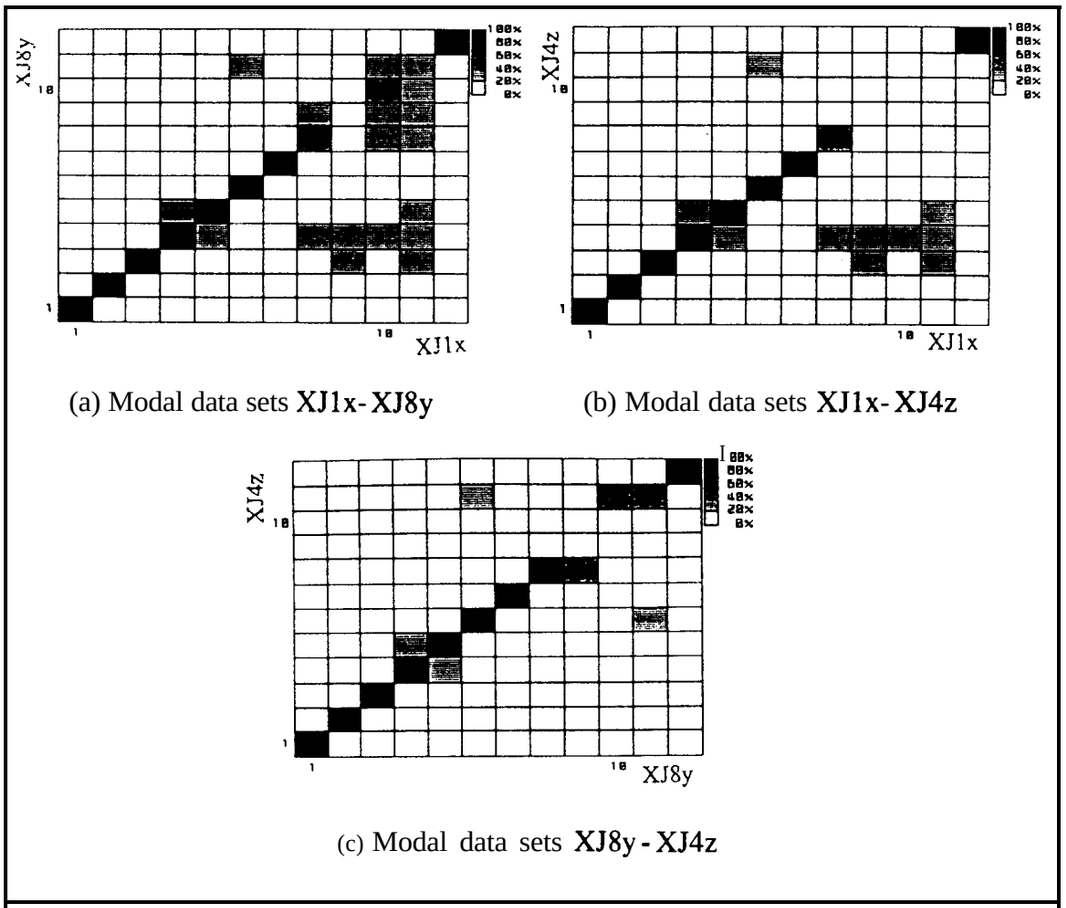


(a) Modal data sets **XJ1x-XJ8y**

(b) Modal data sets **XJ1x-XJ4z**

(c) Modal data sets **XJ8y-XJ4z**

**Fig. 10.4:** 3-bay truss structure MAC values between various experimental data sets

As can be seen from MAC plots of the experimental with the analytical modal data **(Fig. 10.5)** there were 9 correlated modes for the excitation at Jlx and **J8y** and 8 correlated modes for excitation at **J4z**. Experimental modes 9, 10 and 11, which were already seen to be inconsistent between the various experimental data sets **(Fig. 10.4**), were not correlated with any of the analytical modes **(Fig. 10.5).**

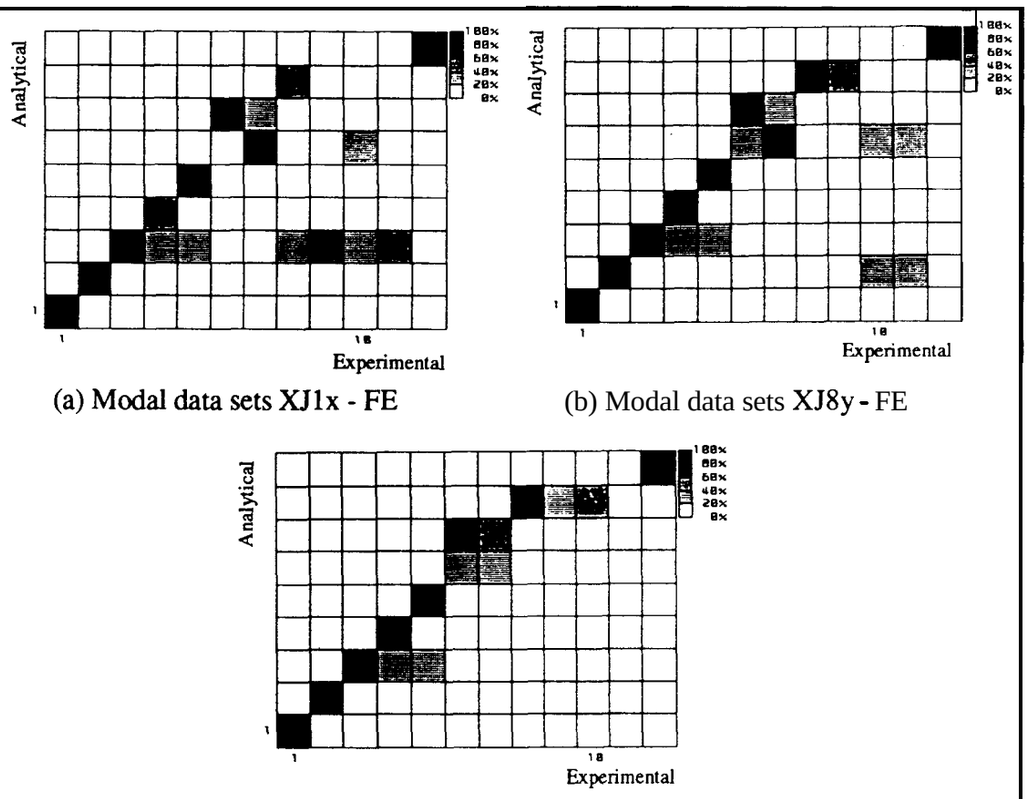


(a) Modal data sets XJ1x - FE

(b) Modal data sets XJ8y - FE

(c) Modal data sets XJ4z - FE

Fig. 10.5: 3-bay truss structure MAC values between experimental and analytical data

The natural frequencies of the 3 experimental modal data sets compared very well with one-another, the maximum discrepancy being less than 0.6%. A comparison of the natural frequencies of the correlated mode pairs for one of the three experimental modal data sets and the analytical modal data is presented in Fig. 10.6.

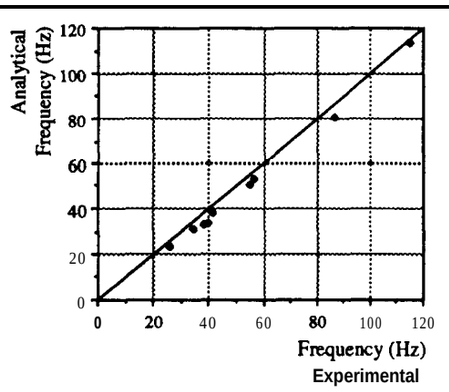


Fig. 10.6: Natural frequency comparison of the 3-bay truss structure

The COMAC values were calculated using 9 correlated mode shapes pairs of each of the experimental modal data set with the FE modal data set. Fig. 10.7 shows that the modelling errors indicated by COMAC were mainly at joint coordinates J1, J2, J3, J4, J9, J10, J11, J12 in the x-direction and J3 and possibly J4 and J8 in the y-direction.

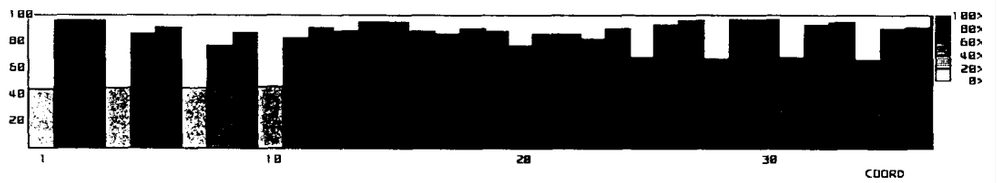


(a) Modal data sets XJ1x - FE

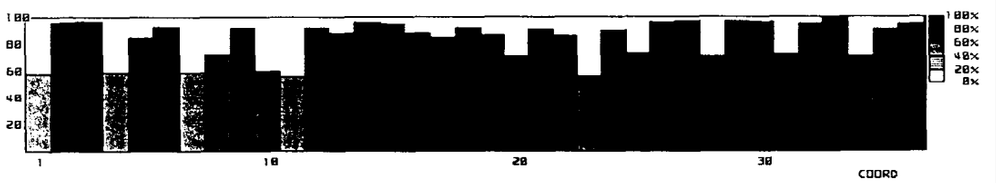


(b) Modal data sets XJ8y - FE

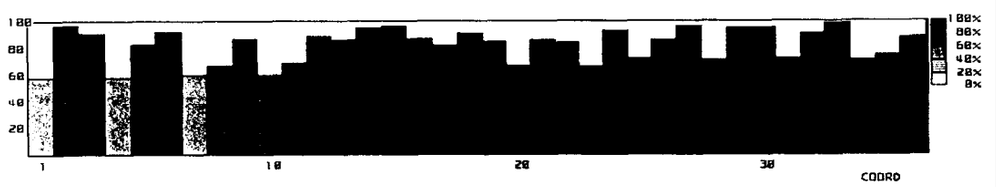


(c) Modal data sets XJ4z - FE

Fig. 10.7: 3-bay truss structure COMAC values between experimental and FE data

The COMAC values of the 3 experimental modal data sets with one-another were also of some interest (Fig. 10.8). Small COMAC values at some coordinates indicated lack of correlation at these points between the simultaneously-measured experimental data sets. This can be due either to experimental error or to errors in the modal analysis of the measured data. The coordinates with small COMAC values are at J1 J2 J3 in the x-direction, J4 in all 3 directions and J8 in the y direction. Note that these coordinates include all three excitation coordinates.

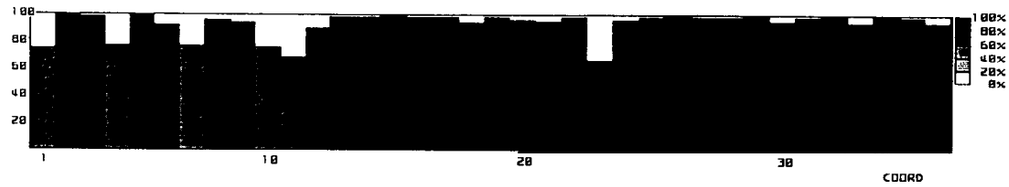


(a) Modal data sets XJ1x- XJ8y

(b) Modal data sets XJ1x- XJ84z

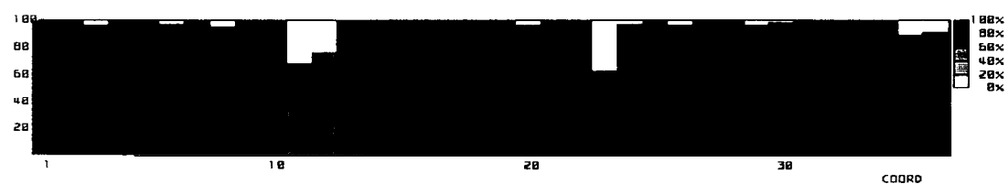


(c) Modal data sets XJ8y - XJ4z

**Fig.** 10.8: 3-bay truss structure COMAC values between various experimental data sets

## 10.5 SIMULATED UPDATING CASE STUDIES

To verify the feasibility of the proposed experimental updating exercise some simulated updating case studies were carried out using simulated *experimental* data with known modelling errors in one of the joints. The generated data were noise-free and, like the experimental data, consisted of 36 coordinates for each of the 3 excitation points. Several RFM runs for receptance columns for each of the excitation points indicated that the dynamic response was insensitive to changes in p-values for some elements. Hence the RFM did not converge. In particular, the mass elements of the little joint beams, mass elements at the shaker end of the excitation systems and the torsional spring elements of the excitation systems were found to be unstable.

The number of unknown p-values was reduced by assuming some elements to be correct and grouping some elements into macro elements. Mass changes in the small joint beam elements were considered to be insignificant. Should the mass in any of these elements

be wrong this could be compensated by the lumped mass elements representing the actual joint. Furthermore, single correction factors were assumed for the mass of the 2 beam elements between the joint beam elements representing each truss. And similarly the 2 stiffness elements of the same 2 beam elements were grouped together. This was considered appropriate as these macro-elements represent continuous parts of the 3-bay truss structure. The stiffness elements representing each of the excitation systems were also grouped into 3 macro elements. This reduced the total number of unknowns from 195 to 99.

For these 99 unknowns convergence was readily achieved for excitation in the y- and z-directions. The most significant p-values identified the joint in error correctly. There were some additional smaller p-values which were due to convergence being reached under the criterion of defined by the maximum allowed difference between experimental and updated receptance values rather than that of the maximum allowed incremental changes of the p-values between iterations. For excitation in the x-direction, convergence was not so easily achieved. As the mode shapes have significant deflections mainly in the y- and z-directions, the receptance curves for excitation in the x-direction have many resonant peaks which are less pronounced than those obtained for excitation in the y and z directions. By re-selecting frequency points to concentrate on regions where the response was significant, the RFM solution process improved but convergence was still not reached after 30 iterations. Therefore the number of unknowns was reduced further to 29 by selecting a single correction factor for each of the major parts of the 3-bay truss structure (see **Table 10.1).** In this case convergence was reached and again the most significant **p-values indicated the modelling errors correctly.**

## 10.6 MODEL UPDATING USING MEASURED FRF DATA

### 10.6.1 Direct use of the experimental data

The element groups used in the preliminary simulated test cases were also employed for the first test cases using the experimental data. At this stage, the modelling of damping had to be considered. The modal analysis of the experimental data showed that the modal damping was in the order of 0.5% for most modes and so a proportional damping factor of 0.005 was selected for each stiffness element. For the 3-bay truss structure the damping elements were grouped into 4 macro-elements: namely, (i) for ridge- and (ii) side-continuous trusses and (iii) ridge- and (iv) side-joint elements. These 4 damping macro-elements should give an adequately representation of the damping distribution in

the 3-bay truss structure without adding too many unknowns to be solved for in the RFM.

Frequency points were selected in accordance with the recommendations made in previous chapters, avoiding those from the noisiest frequency ranges, as detected by visual inspection. The ridge joint x-direction coordinates in FRF data set XJ8y were substantially different from their FE counterparts. Thus, these FRFs were eliminated from that data set and the number of coordinates employed from XJ8y was reduced from 36 to 32. Several RFM runs employing each of the 3 experimental data sets were carried out but, unfortunately, convergence was not achieved.

Next, the structure was assumed to be lightly damped such that a damping matrix was not required in the model and the imaginary part of the FRFs were set to zero. Again, no convergence was achieved. To overcome the difficulties in achieving a converging solution, the number of unknown p-values was reduced from 103 to 99, 31, 29, 10 and 8 unknowns for experimental data sets XJ8y and XJ4z and from 31 to 29, 10 and 8 unknown p-values for experimental data set XJ1x. Details of the different sets of unknown p-values used are presented in **Table 10.1.**

| el. type | part of 3-bay truss structure represented | test case reference | | | | | | |
|---|---|---|---|---|---|---|---|---|
| | | all | I | II | III | IV | v | VI |
| M | ridge truss beam elements | 6 | 3 | 3 | | | | |
| | side truss beam elements | 36 | 18 | 18 | 1 | 1 | 1 | 1 |
| | ridge joint beam elements | | | | | 1 | 1 | 1 |
| | side joint beam elements | | 0 | | 1 | 0 | 0 | 0 |
| | joint lumped masses | 28 | 0 | 0 | 0 | 0 | 0 | 0 |
| | excitation system lumped masses | 12 | 12 | 12 | 12 | 12 | 2 | 2 |
| | | 6 | 0 | 0 | 0 | 0 | 0 | 0 |
| K | ridge truss beam elements | 6 | 3 | 3 | 1 | 1 | | |
| | side truss beam elements | 36 | 18 | 18 | 11 | 11 | 1 | 1 |
| | ridge joint beam elements | | | | | | 1 | 1 |
| | side joint beam elements | 14 | 14 | 14 | 4 | 4 | 1 | 1 |
| | excitation system beam and spring elements | 28 | 28 | 28 | 8 | 8 | 1 | 1 |
| | | 9 | 3 | 3 | 1 | 1 | 0 | 0 |
| D | ridge and side beam elements | | | 0 | | 0 | | 0 |
| | ridge and side joint beam elements | 0 | 2 | 0 | 1 | 0 | 1 | 0 |
| | | 0 | 0 | 0 | 0 | 0 | 0 | 0 |
| | total number of unknown p-values | 195 | 103 | 99 | 31 | 29 | 10 | 8 |

**Table 10.1:** Number of p-values in the 3-bay truss structure case studies

Some inconsistent FRFs as indicated by the **COMAC** plots of experimental data sets with one another **(Fig. 10.8) were** eliminated from the experimental data sets to improve the general accuracy of the experimental data sets. Several RFM runs were carried out for each of these different sets of p-values. **However,** none of the runs converged. The results are summarised in 6 tables which are presented in appendix D.

### 10.6.2 Employing regenerated experimental data

**As the** previous results were unsatisfactory another approach was adopted: experimental FRFs were regenerated using modal analysis results instead of using the raw measured data. This should reduce the effects of the random noise on the experimental receptance curves and some of the inconsistencies between different receptance curves. However, it does not alleviate the problem of consistent bias errors in the experimental data.

One experimental data set, that for excitation at J4z which from now on will be referred to as RJ4z was regenerated and a typical FRF from the measured and regenerated data sets is plotted in **Fig. 10.9.** Data set RJ4z was employed in several RFM runs for the different numbers of unknown p-values as indicated in **Table 10.1.** However, again, convergence was not reached. It was observed that the standard deviation of the results was reduced as compared with the RFM results employing data set XJ4z, indicating that the RFM results employing RJ4z were more consistent.

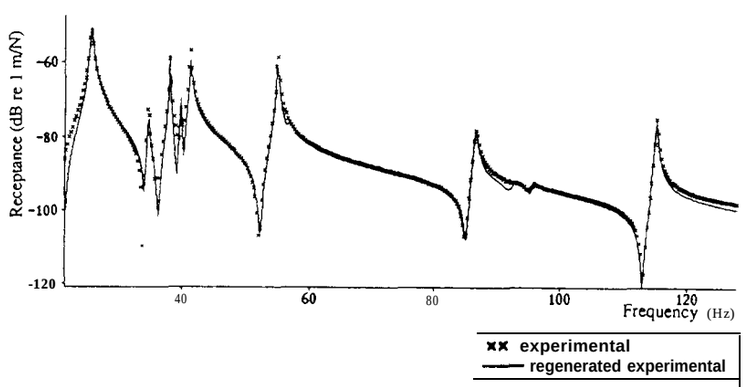


**Fig. 10.9:** Experimental and regenerated receptance FRF $\alpha_{J4z\,J4z}$ for the 3-bay truss structure

### 10.6.3 Error location using the RFM

Even if convergence is not reached it is still possible to locate modelling errors using the p-values of the iteration where the difference between experimental and updated receptance values used in the process reaches a minimum as demonstrated by the GARTEUR III exercise (section 5.7). It was observed that in some 3-bay truss structure RFM runs this difference increased directly at the first iteration and obviously, these results were not included in the statistical analysis. For each p-value reference set the indicated modelling errors and their mean p-values are presented in appendix D. An error threshold of mean-to-standard deviation ratios greater than 2 was used.

It was also observed that in some cases the natural frequencies of the iterative updated model within each RFM run diverged from the experimental model. The error location process was repeated selecting the p-values at the iteration where the difference between the first natural frequency of the experimental and the updated models reached a minimum while omitting runs with increasing natural frequency difference. These error location results are also presented in appendix D. There were numerous inconsistencies between all these error location results. This is not surprising considering the large standard deviations of the p-values. In most cases including 6 RFM runs gave standard deviations between 0.6-0.8 and 0.3-0.4 for RFM results obtained employing raw experimental data and regenerated experimental data respectively. The most consistent modelling errors are indicated in **Fig. 10.10.**

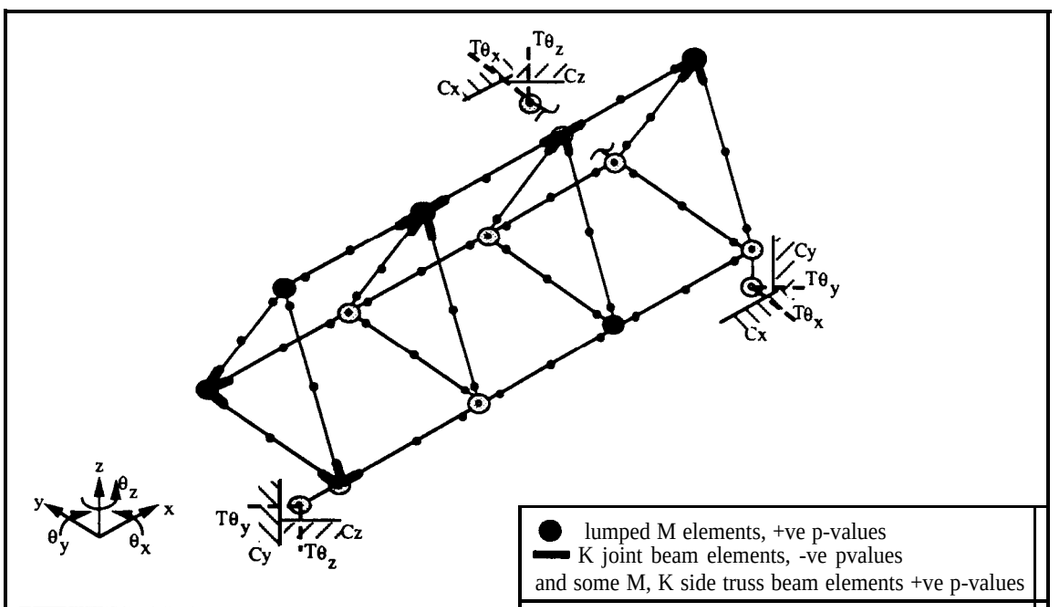


**Fig. 10.10:** Locations of modelling errors in the FE model of the 3-bay truss structure

### 10.6.4 Updating the FE model

Results of 12 RFM runs obtained by employing data set XJ4z were combined. The mean p-values of those elements indicated by Fig. 10.10 and having a mean-to-standard deviation ratio greater than 1 were used to update the FE model. These p-values are shown (in (italics)) in Fig. 10.11. However, the updated model showed no improvement on the original model, a typical comparison of experimental, analytical and updated receptance curves being shown in **Fig. 10.12.** The difference between the natural frequencies of the updated model and those measured was either the same or increased as compared with the difference between the original data sets. The same procedure was repeated for mean p-values obtained by employing data set RJ4z. The mean p-values of the located erroneous elements are also shown in Fig. 10.11.

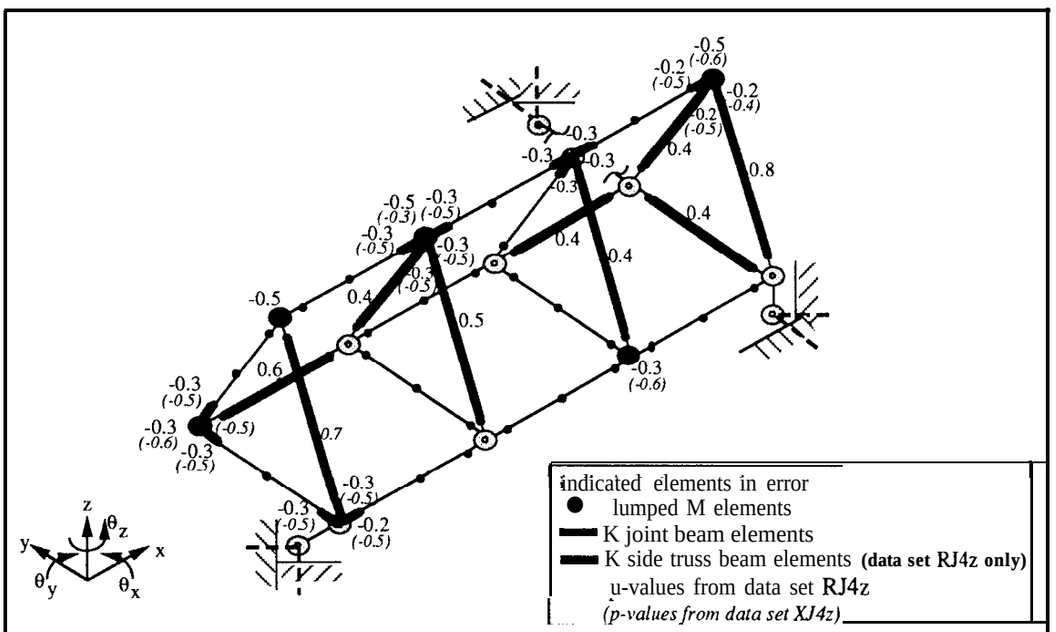


Fig. 10.11: Indicated modelling errors in the FE model of the 3-bay truss structure

The updated model obtained by employing the regenerated data was better than the previous one, obtained by employing raw experimental data. The updated model obtained by employing the regenerated data showed marginal improvements for some natural frequencies in the O-60 Hz range while other natural frequencies remained similar or became further away from the target experimental data. A typical comparison of experimental, regenerated experimental, analytical and updated receptance curves is plotted in Fig. 10.12.

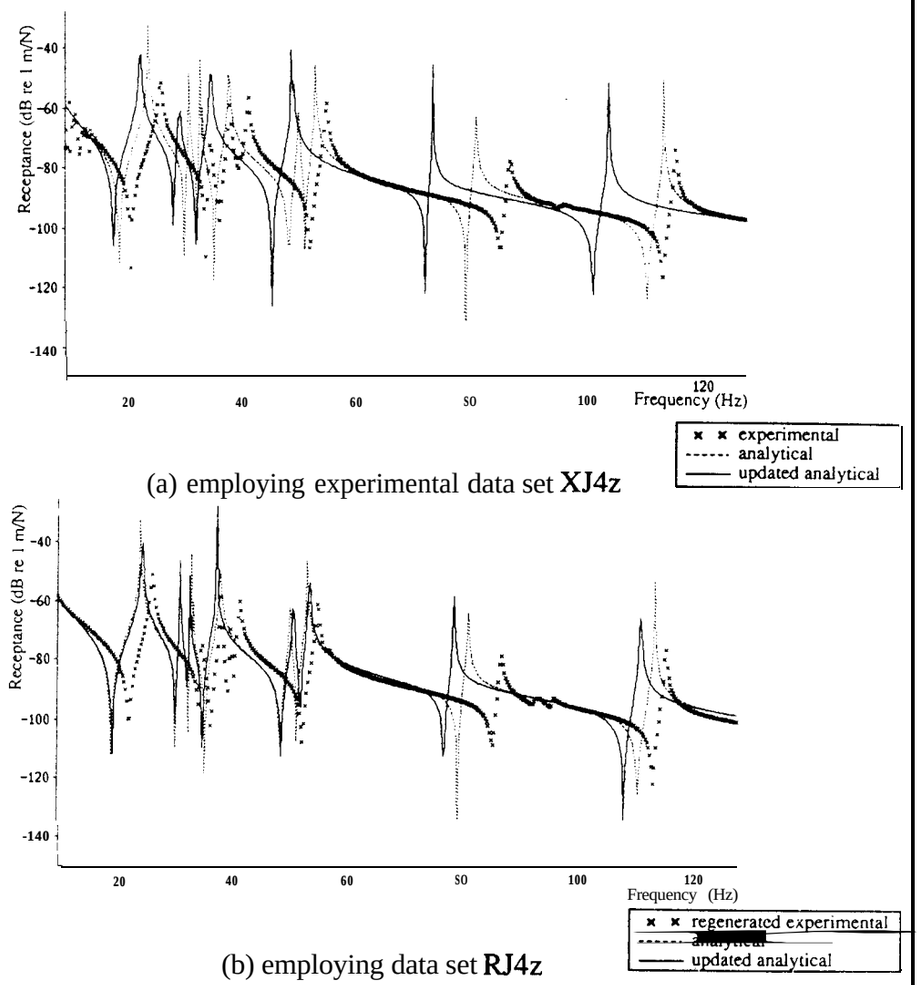


**Fig. 10.12:** 3-bay truss structure experimental, analytical and updated analytical receptance FRF $\alpha_{J4z\,J4z}$

Generally, the RFM results were far from conclusive and the updated model remained far from satisfactory.

### 10.6.4 Discussion

The RFM results for the 3-bay truss structure were far from satisfactory. As mentioned in previous sections, none of the RFM runs converged: some RFM runs started diverging at the first iteration, and the standard deviations of resulting p-values were large. There are various reasons which might explain the lack of success of the RFM to update the FE model of the 3-bay truss structure.

There appeared to be a significant amount of noise and a lack of consistency within the entire experimental data set. This was already indicated in section 10.4 and further illustrated in **Fig. 10.13** showing reciprocal receptance curves.

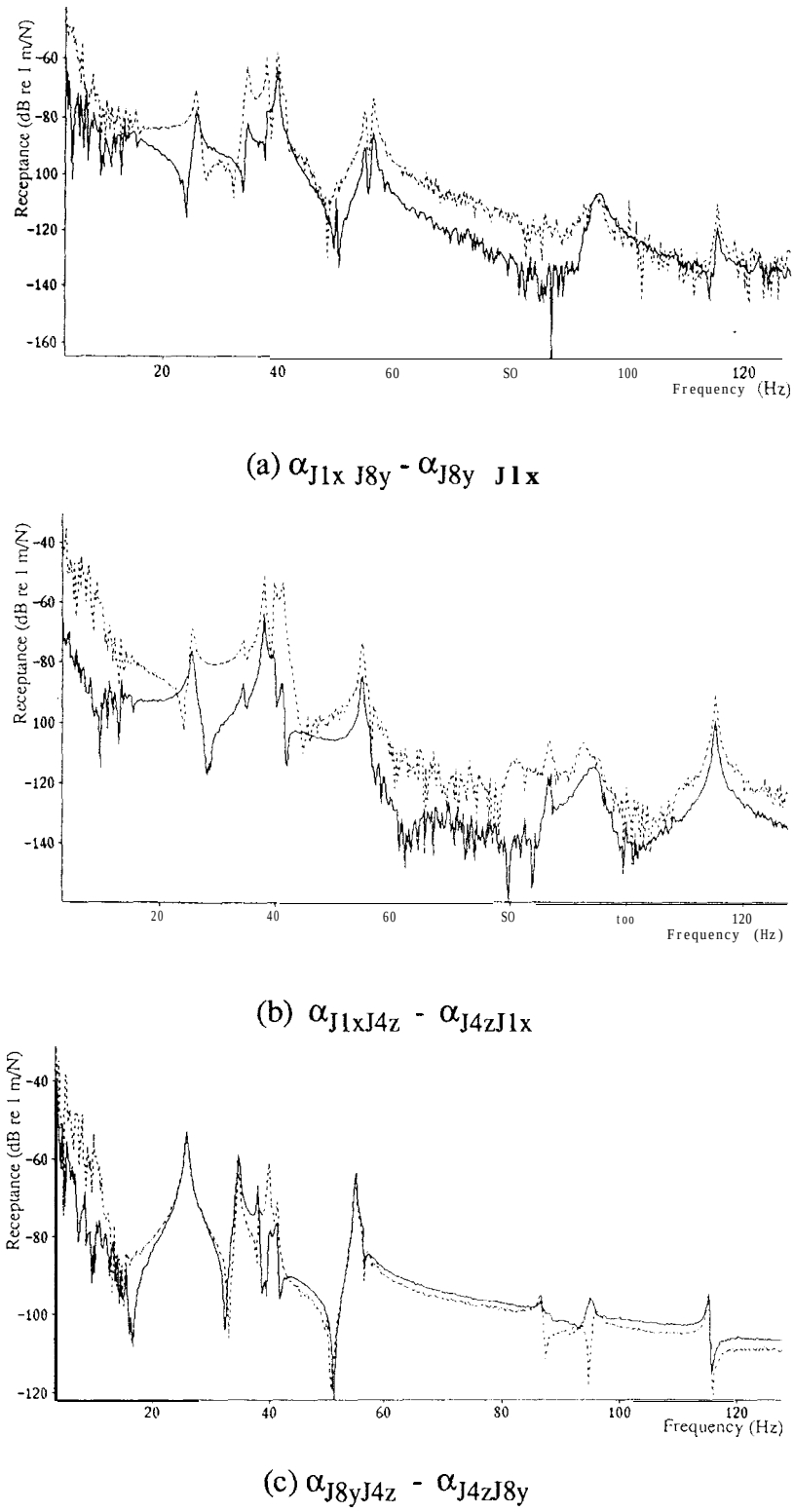


**Fig. 10.13:** Reciprocal experimental receptance curves of the 3-bay truss structure

Observation of such significant noise on a logarithmic scale suggested that experimental errors were of an order of magnitude at some frequencies. Some of the effects of the random noise could be overcome by careful selection of the frequency points used in the RFM and, at a later stage, by employing regenerated receptance data. Note that employing regenerated receptance data requires accurate modal analysis while one significant advantages of the RFM is its ability to make direct use of measured data and modal analysis results should merely be used to verify the consistency between experimental and analytical data.

During the course of the exercise the number of measured coordinates was decreased and therefore the simulated test cases for 99 unknown p-values were repeated employing the reduced number of measured coordinates. In the case of noise-free data, convergence was achieved in 17 iterations. The same simulated test cases were repeated for noisy simulated *experimental* data since there was obviously (Fig 10.13) significant experimental noise. As it should be possible to measure FRF data to within 5% of its actual value, 5% random noise was distributed over the simulated receptance data. In this case no convergence was achieved in 30 iterations. After 30 iterations the most significant mass related p-values indicated the mass modelling error correctly while the stiffness related p-values were not so successful. Note that this also indicated that, in this case, mass modelling errors can be located more easily than can stiffness modelling errors.

Despite the attempts to overcome some of the noise related problems, the overall effect of experimental noise was certainly not less than an equivalent of the 5% random noise applied during the simulated test cases. And since the simulated test cases with 5% random noise had convergence difficulties, it is not surprising that convergence was not reached while employing the actual experimental data.

Although the lack of convergence during the simulated 5% noise case study should not necessarily be detrimental to obtaining error location results, it did indicate the general instability of the RFM updating exercise using the given set of measured coordinates. In chapter 5, the recommendation was made that at least one coordinate per element should have an experimental FRF associated with it. This was certainly not the case for the 3-bay truss structure. Even by reducing the number of unknown p-values, a measured coordinate at each (macro-)element was not accomplished because of the positions of the actual measurement sites and the specific updating interests, namely the joints of the FE model.

During this case study there were also some adverse effects due to model mismatch as the measurement sites were not at the actual FE nodes, unlike during the simulated case studies. Again, this in itself is not necessarily detrimental to successful error location using the RFM but adds to the unfavourable state of affairs.

The overall RFM performance might have been improved by expansion of the experimental data to the full FE size during the first few iterations, as was demonstrated in chapter 8. However, due to limited available computing power, this option was not included in the RFM solution process for this case study.

In this case, the experimental data were externally provided prior to setting up the FE model. Simulated test cases demonstrated that for the 36 *measured* coordinates, even in case of noise-free data, convergence was not reached if all elements (195) were to have a single correction factor. Reducing the number of unknowns did overcome the problem but one must bear in mind that local modelling errors will now have to be represented over a coarser 'error location mesh'. For error location purposes a better approach to overcoming these difficulties would be to acquire an increased number of measurement coordinates. This, and the points discussed above, emphasise that, ideally, simulated updating test cases should be carried out prior to acquisition of the experimental data in order to indicate: (i) the number and location of measurement sites; and (ii) the required measurement accuracy.

## 10.7. CONCLUDING REMARKS

In this chapter the Response Function Method has been applied to a second experimental case study based on an existing physical structure with joints, the 3-bay truss structure. The RFM results obtained using externally-provided simultaneously-measured FRFs were far from satisfactory. This was mainly due to the amount of measurement noise, demonstrated by checking the reciprocity of some receptance curves, and because of the limited number of measured coordinates available by comparison with the number of DOFs in the FE model.

Simulated updating test cases indicate the feasibility of an updating exercise but should preferably be carried out before acquiring the measured data set in order to indicate experimental data requirements. Consistent experimental and analytical data sets are a prerequisite for successful updating.

Regenerating experimental FRF curves using modal analysis results might decrease the effects of random noise on the measured data. In this case study, employing regenerated data instead of raw experimental data reduced the standard deviation of the RFM results.

From this case study it is shown that in practice the two most significant factors for successful updating using the RFM are: (i) the accuracy of the measured data and (ii) the number of measured FRFs.

# CHAPTER 11

# CONCLUSIONS AND SUGGESTIONS FOR FURTHER WORK

## 11.1 CONCLUSIONS

This section presents a summary of the conclusions of the work presented in this thesis.

### 11.1.1 Introduction

Structural dynamics model updating has been defined as the adjustment of an existing analytical (Finite Element) model representing the structure under study, using experimental data, such that it more accurately reflects the dynamic behaviour of the structure. Although a considerable amount of research had been dedicated to the area of model updating, a detailed literature survey indicated that previously the problem remained largely unsolved and more work was needed. Potential difficulties which updating methods must address were identified, the major difficulties being due to incompleteness of and noise on the experimental data.

### 11.1.2 Updating using modal data

Most previous updating methods have been based on modal data. A new error matrix procedure, derived from a mathematical identity rather than perturbation theory, can give numerically better results for the unrealistic case of complete *experimental* models but for cases of incomplete experimental data, the improvements are negligible since there are inherent difficulties within the basic algorithm.

Coordinate expansion is one possible way of overcoming some of the limitations of the error matrix method which derive from the reduction process. Well-expanded modes can be obtained both by an inverse reduction technique and by a modal transformation method. This latter method, as compared with the inverse reduction technique, shows no discontinuities in the mode shapes, experimental noise can be smoothed out, the error is generally smaller although more spread out and it is less CPU-intensive. One advantage of the inverse reduction technique is that there are no decisions to be made, in contrast to

the modal transformation method where the analytical mode selection is of vital importance to the success of the method. For both expansion techniques, the expanded set is not orthogonal with respect to the experimental system matrices, discrepancies are case-dependent, and are mainly influenced by the closeness of the analytical model to the experimental model. Expanded experimental modes must satisfy the mass-orthogonality condition if employing an updating technique based on this property.

Despite numerical improvements to the error matrix procedure, updating using modal data remains far from satisfactory.

### 11.1.3 Updating **using frequency response data**

Advantages of employing FRF data, as compared to using modal data, are that (i) each individual FRF measurement contains information on the out-of-range modes as well as on those within the frequency range of interest, (ii) there is surplus of data and, (iii) the direct use of raw measured data eliminates lengthy modal analysis procedures.

#### (i) The response function method

The response function method (RFM), an updating technique employing frequency response data, can locate modelling errors in the realistic case of noisy and incomplete experimental data. The updated models are in good agreement with their measured experimental counterparts for both resonant and off-resonant response. In the general case, modelling errors cannot be expressed as linear combinations of the individual element mass and stiffness matrices: hence, any attempt to model the error(s) in each element by a single correction factor can only be an approximation. This technique is useful for error location but not necessarily for updating.

The consequences of the incompleteness of the experimental model can be overcome to some extent by substitution of the missing coordinates by their (updated) analytical counterparts. This problem can also be addressed on a statistical basis, made possible because of plentiful data, by considering several sets of solutions for various frequency point sets. More reliable estimates of the indicated modelling errors in the presence of noise can be achieved by judicious use of the ratio of mean to standard deviation of the correction factors determined in this way.

Complex FRF data with noise make the RFM convergence process slow and often numerically unstable. However, in the case of lightly damped structures, an acceptable solution can be found by setting the imaginary part of the FRF to zero. Good initial

assumptions about the damping present in the structure and accurate measured response data are required to identify a damping matrix successfully.

Structural joints are a primary cause of FE modelling errors. The joint updating strategy proposed in this work is to include additional joint elements for each ***branch*** of the joint. It is recommended that the additional elements are incorporated into the FE model prior to a first stage of error location. These elements should cover the area of the joint and slightly beyond and any ***a priori*** knowledge of the joint should be included. The proposed updating strategy gave a marked improvement as compared with updating FE models without additional joint elements. Correct connectivities are a prerequisite to successful model updating. It is unlikely that the RFM can identify erroneous connectivities if these are not represented in the analytical model in the first place.

### (ii) Computational aspects of the RFM

Noise on the measured FRF data, a reduced number of measurement sites and model mismatch all have adverse effects on error location since they tend to make the solution process unstable and to increase the scatter of results. The number of frequency points used for updating should be 4-8 times the minimum requirement; (i) to make the system of equations numerically stable and (ii) to reduce the adverse effects of noisy and incomplete experimental data.

Correction factors (the so-called p-values) can be unstable either because the system is insensitive to changes in particular elements, or because the solution process makes them unstable. The latter occurs especially when the number of measurement coordinates is too small in the vicinity of the corresponding element. These difficulties can be overcome by reducing the number of unknowns by grouping elements together into macro elements. Balancing the matrices both with respect to element type and frequency point selection is beneficial for stabilising the solution process and therefore the convergence of the solution.

Measurements taken directly at the point(s) of modelling error will identify these error(s) more easily. Frequencies in the direct vicinity of the experimental resonances make the RFM matrix equation singular and should therefore not be included in the frequency point selection. Frequency points below the first mode should also be avoided in the frequency point selection. The frequency points should be selected where the differences between experimental and analytical receptance values are significant.

If the only requirement of the updated model is to regenerate measured FRFs, one RFM run using many frequency points is sufficient. For error location purposes, more runs

and subsequent statistical analysis of the results are necessary. Increasing the number of runs improves the final error location results.

### (iii) Coordinate incompatibility

Some of the adverse effects of the substitution of unmeasured FRF values by their analytical counterparts can be overcome by the use of expanded data. The estimated values of the unmeasured coordinates should be used to substitute missing coordinates in the rows retained in the standard RFM and not to increase the number of linear equations for each frequency point selected.

Two techniques to expand an incomplete receptance column are proposed: (i) an inverse reduction procedure employing the analytical mass and stiffness matrices and (ii) a transformation method using the analytical mode shapes. Both expansion procedures can give good expanded data for frequencies in the vicinity of resonances but are not so accurate elsewhere. The success depends on the ratio of measured to unmeasured coordinates and on the accuracy of the analytical model. Generally, the inverse reduction method produces better expansions.

In order to include an expansion procedure within the RFM, the experimental data should be expanded for each iteration using the newly-updated analytical model. A smoother solution process, especially during the first few iterations, can be achieved when using expanded experimental data instead of analytical substitutions. Reduction of the analytical model to the measured coordinates is not a recommended practice for the RFM.

### (iv) Case studies

The RFM was successfully applied to analytically-generated test cases and experimental data for a free-free beam. However, the results from some case studies on the 3-bay truss structure, using externally-provided experimental test data, were not so satisfactory. The success of updating using the RFM depends on the quantity and quality, in terms of the measurement sites and measurement accuracy, of the experimental data.

## 11.2 RECOMMENDED UPDATING STRATEGY

In the view of the experience gained during the course of the research, and of the case studies presented in this thesis, the following strategy for updating analytical structural dynamics models is recommended.

### (i) The analytical model

The analytical model must be representative of the structure under study. The model should be detailed enough such that further refinements do not significantly change the predicted dynamic behaviour in the frequency range of interest but it should not be too detailed as in that case the number of elements to be updated becomes excessive and the ratio of measured to unmeasured coordinates will be too low. It is recommended that additional small elements for each ***brunch*** of a structural joint be incorporated into the FE model prior to a first stage of error location.

### (ii) Simulated test cases

It is advisable to check the feasibility of the proposed updating procedure by carrying out preliminary runs using simulated experimental data derived from the analytical model. This will indicate possible limitations, unstable elements and whether or not enough experimental coordinates will be available. One advantage of simulated test cases preceding measurements is that the results of these can be used to indicate which points to measure.

Modelling errors are expressed as linear combinations of the individual element mass and stiffness matrices. If there is no convergence, or if there are insensitive elements, several elements can be grouped together into macro-elements. It is advocated that elements representing continuous parts of a structure can be grouped together in this way and enough unknowns should remain to represent adequately regions of modelling errors, especially at, and in the vicinity of, structural joints.

### (iii) Experimental data

Bearing in mind standard practice and the general recommendations for good modal testing, the experimental data should be acquired as accurately as possible and measured at as many coordinates as possible. Experimental measurement sites should correspond, or be as close as possible, to points in the FE nodal grid and should have the same reference axes. It is beneficial to have measurement sites at points where modelling errors are more likely to be found. For solution stability, the recommended number of measurement points is at least one per element to be updated, but this is not essential.

### (iv) Preliminary comparisons

A preliminary comparison of the two data sets is of vital importance, firstly to see whether the two models show reasonable agreement and secondly to verify that consistent

data sets are being used. Although the second reason might appear obvious, it tends to be prone to mistakes and errors. Due care and good communication between analyst and experimentalist are of vital importance to achieve reliable updating results. Direct comparisons of natural frequency, mode shape and FRF curves comparisons, and MAC and COMAC calculations are suggested.

### (v) Damping estimates

At this stage, the modelling of the damping should also be considered. If the structure is lightly damped, acceptable results can be achieved by ignoring the damping and setting the imaginary part of the FRF to zero. For more complex structures, careful initial assumptions about the actual damping and the number of unknowns necessary for the damping (macro-)elements are of vital importance to achieving a representative updated system.

### (vi) Error location using the RFM

Several RFM runs using different sets of frequency points should be carried out bearing in mind the recommendations made in the previous section. Statistical analysis of the results, in particular the mean to standard deviation ratio, should be used to locate and evaluate the elements in error.

It is be possible that none of the RFM runs converge; for example due to the presence of measurement noise. There are then two options: (i) to repeat the runs for a reduced number of unknowns, by grouping elements together or assuming some elements to be error-free, or (ii) to use the correction factors at the iteration at which the sum of the percentages differences squared is a minimum. Results obtained via the latter option should be used with caution.

### (vii) Updating of the FE model

If regenerating the measured FRFs is the only objective, one RFM run using an increased number of frequency points is advised. Otherwise, the mean correction factors obtained for the located elements in error can be employed to update the model. Careful inspection of these correction factors is recommended as they can also indicate possible errors in the measurement set-up. Engineering judgement should also be used to review the validity and/or physical significance of the indicated errors. When using a set of correction factors to update a model and to regenerate FRFs, it must be borne in mind that it is possible that improvements only are achieved for certain response directions. For more

refined updating, a comparison of results obtained from various excitation points can indicate modelling errors due to linear element modelling errors, such as material properties, or modelling errors affecting the dynamic behaviour differently for different excitation directions, such as changes in thickness.

## 11.3 SUMMARY OF CONTRIBUTIONS OF PRESENT WORK

A brief overview of contributions made in this thesis to the area of 'Updating of Analytical Structural Dynamics Models using Experimental Response Data' is given here.

- Structural dynamics model updating was defined and 6 levels of correctness of increasing complexity and vigour which an updated model ought to satisfy were identified.

- A detailed literature survey was carried out and all the major state-of-the-art updating techniques were classified on the basis of their approach and were presented in a consistent notation.

- Problems encountered during model updating using modal data were illustrated using the error matrix method and a new improved error matrix procedure was proposed.

- Comparisons of existing modal data coordinate expansion methods showed that the success of the coordinate expansion is case-dependent. Mass-orthogonality was highlighted as an area of concern when employing expansion methods in modal-based model updating techniques using this property.

- An updating procedure using frequency response function data in the realistic case of noisy incomplete complex experimental data, the response function method (RFM), was developed to the point at which it can be used for practical applications.

- Advantages of using FRF-based updating techniques compared with modal based updating techniques were demonstrated.

- Different approaches for error location and regeneration of the measured FRFs were suggested.

- Two new methods to expand incomplete receptance columns were proposed and evaluated.
- Problems and inaccuracies arising from the use of reduced analytical systems were discussed and comparisons of various reduction approaches were presented.
- A new approach to facilitate updating of structural joints was proposed. The importance of correct connectivities was also emphasised.
- Problems encountered during updating using the RFM were demonstrated on two true experimental test cases.

## 11.4 SUGGESTIONS FOR FURTHER STUDIES

Whereas extensive research work on updating of analytical structural dynamics models has been carried out in this thesis, the study undertaken has revealed that some further development may be necessary and of interest. Areas for possible further studies are sumrnarised below.

The success of model updating depends on the quantity and quality of the experimental data and, specifically on the number and choice of measurement sites and the level of experimental noise, and hence further developments of experimental data acquisition technique are of considerable importance. Development of a smoothing technique to reduce the effect of experimental noise on the FRFs and a method which is able to indicate the accuracy of the measured FRF data such that the most reliable frequency points can be selected for use in the RFM are both required.

In general, the expectations of the model updating process in terms of maximum allowable discrepancies between the two models and the relationship to measurement accuracy need to be defined. The difficulty in establishing this relationship is compounded by the difficulty of assessing the measurement noise. As the randomly distributed noise on the simulated experimental data is an inadequate representation of the noise encountered in true experimental data this measure of noise cannot be used for this purpose.

In practical cases, sources of error are often to be found in boundary conditions and/or structural joints. Although the effectiveness of a new joint updating strategy and the RFM to locate joint modelling errors was demonstrated, further studies on the possibilities of the RFM for more detailed updating of joints will be of interest. A

strategy to indicate missing connectivities, which the RFM as it is at the moment cannot detect, will also be of benefit.

As the RFM is case-dependent and since using simulated experimental data in most cases produces satisfactory results, further studies using true experimental data will be useful to determine trends in success and failure of the method in full scale practical applications. In particular, further work on the 3-bay truss structure, will be of interest, especially: (i) the use of another, more accurate, experimental data set measured at more coordinates to see if improvements to the results can be achieved, and (ii) a more detailed investigation on updating of the damping matrix so that the damping distribution within the structure is reflected.

## 11.5 CLOSURE

The primary aim of this work was to develop a practical approach to update analytical structural dynamics models using experimental response data. This was achieved by critical investigation of existing methods and by exploring new techniques and a recommended updating strategy has been presented in this thesis.

A summary of conclusions and contributions showed the advances made to the area of model updating. Not surprisingly, however, there is still scope for further work and suggestions for further study to improve the success and accuracy of analytical model updating to increasingly complex practical structures have been made.

FRF-based updating techniques can update practical structural dynamics models and have several advantages over modal-based updating methods. However, success depends on the availability of better experimental data than is currently obtained in normal modal tests.

# APPENDIX A

# THE RESPONSE FUNCTION METHOD

In this appendix the step transforming the basic RFM (equation (Al)) into a set of linear equations where the LHS is expressed as a linear combination of the unknown p-values (equation(A2)) is illustrated using a 2 DOF example.

Starting from chapter 5 equation (4):

$$[\alpha_A(\omega)]_{NxN}\,[[\Delta Z(\omega)]]_{NxN}\,\{\alpha_X(\omega)\}_{i_{Nx1}} = \{\{\alpha_A(\omega)\}_i - \{\alpha_X(\omega)\}_i\}_{Nx1} \qquad \text{(A1)}$$

to chapter 5 equation (5): $[C(\omega)]_{NxNp}\,\{p\}_{N_p} = \{\Delta\alpha(\omega)\}_N$ (A2)

Consider a 2 DOF system and suppose the first receptance column of the experimental system is measured, then equation (Al) can be written as:

$$\begin{bmatrix} \alpha_{11}(\omega) & \alpha_{12}(\omega) \\ \alpha_{21}(\omega) & \alpha_{22}(\omega) \end{bmatrix}_A \begin{bmatrix} \Delta Z_{11}(\omega) & \Delta Z_{12}(\omega) \\ \Delta Z_{21}(\omega) & \Delta Z_{22}(\omega) \end{bmatrix} \begin{Bmatrix} \alpha_{11}(\omega) \\ \alpha_{21}(\omega) \end{Bmatrix}_X = \begin{Bmatrix} \alpha_{11}(\omega) \\ \alpha_{21}(\omega) \end{Bmatrix}_A - \begin{Bmatrix} \alpha_{11}(\omega) \\ \alpha_{21}(\omega) \end{Bmatrix}_X \qquad \text{(A3)}$$

Hence:

$$\begin{Bmatrix} \alpha_{11}\Delta Z_{11}\alpha_{11_X} + \alpha_{12}\Delta Z_{21}\alpha_{11_X} + \alpha_{11}\Delta Z_{12}\alpha_{12_X} + \alpha_{12}\Delta Z_{22}\alpha_{12_X} \\ \alpha_{11}\Delta Z_{11}\alpha_{11_X} + \alpha_{12}\Delta Z_{21}\alpha_{11_X} + \alpha_{11}\Delta Z_{12}\alpha_{12_X} + \alpha_{12}\Delta Z_{22}\alpha_{12_X} \end{Bmatrix} = \begin{Bmatrix} \Delta\alpha_{11} \\ \Delta\alpha_{12} \end{Bmatrix} \qquad \text{(A4)}$$

where, for simplicity, both references to the analytical system (subscript A) and to frequency $(\omega)$ are omitted. Unless a specific reference is made to the experimental system (subscript X) each symbol is related to the analytical system.

For each element: $\Delta Z_{ij} = \Delta K_{ij} - \omega^2 \Delta M_{ij}$, thus:

$$\begin{Bmatrix} \alpha_{11}\Delta K_{11}\alpha_{11_X} - \omega^2\alpha_{11}\Delta M_{11}\alpha_{11_X} + \alpha_{12}\Delta K_{21}\alpha_{11_X} - \omega^2\alpha_{12}\Delta M_{21}\alpha_{11_X} + \\ \alpha_{11}\Delta K_{12}\alpha_{12_X} - \omega^2\alpha_{11}\Delta M_{12}\alpha_{12_X} + \alpha_{12}\Delta K_{22}\alpha_{12_X} - \omega^2\alpha_{12}\Delta M_{22}\alpha_{12_X} \\ \\ \alpha_{21}\Delta K_{11}\alpha_{11_X} - \omega^2\alpha_{21}\Delta M_{11}\alpha_{11_X} + \alpha_{22}\Delta K_{21}\alpha_{11_X} - \omega^2\alpha_{22}\Delta M_{21}\alpha_{11_X} + \\ \alpha_{21}\Delta K_{12}\alpha_{12_X} - \omega^2\alpha_{21}\Delta M_{12}\alpha_{12_X} + \alpha_{22}\Delta K_{22}\alpha_{12_X} - \omega^2\alpha_{22}\Delta M_{22}\alpha_{12_X} \end{Bmatrix} = \begin{Bmatrix} \Delta\alpha_{11} \\ \Delta\alpha_{12} \end{Bmatrix} \tag{A5}$$

Assuming symmetric analytical and updated system matrices, i.e. $\Delta M_{12} = \Delta M_{21}$ and $\Delta K_{12} = \Delta K_{21}$, rearranging equation (5) gives:

$$\begin{bmatrix} -\omega^2\alpha_{11}\alpha_{11_X} & -\omega^2(\alpha_{12}\alpha_{11_X} + \alpha_{11}\alpha_{12_X}) & -\omega^2\alpha_{12}\alpha_{12_X} & \alpha_{11}\alpha_{11_X} & (\alpha_{12}\alpha_{11_X} + \alpha_{11}\alpha_{12_X}) & \alpha_{12}\alpha_{12_X} \\ -\omega^2\alpha_{21}\alpha_{11_X} & -\omega^2(\alpha_{22}\alpha_{11_X} + \alpha_{21}\alpha_{12_X}) & -\omega^2\alpha_{22}\alpha_{12_X} & \alpha_{21}\alpha_{11_X} & (\alpha_{22}\alpha_{11_X} + \alpha_{21}\alpha_{12_X}) & \alpha_{22}\alpha_{12_X} \end{bmatrix} \begin{Bmatrix} \Delta M_{11} \\ \Delta M_{12} \\ \Delta M_{22} \\ \Delta K_{11} \\ \Delta K_{12} \\ \Delta K_{22} \end{Bmatrix} = \begin{Bmatrix} \Delta\alpha_{11} \\ \Delta\alpha_{12} \end{Bmatrix} \tag{A6}$$

Equation (A6) is of the form: $[C]\{p\}=\{\Delta\alpha\}$ where [C] and $\{\Delta\alpha\}$ are fully known and the unknown {p} represents the location and the value of the modelling errors directly. In this case there are 6 unknown p-values, namely $\Delta M_{11}, \Delta M_{12}, \Delta M_{22}, \Delta K_{11}, \Delta K_{12}$ and $\Delta K_{22}$ and apart from assuming a symmetric system there are no further assumptions made.

Consider a typical 2 DOF system with the following system matrices:

$$[M] = \begin{bmatrix} m_1 & 0 \\ 0 & m_2 \end{bmatrix}, \; [K] = \begin{bmatrix} k_1+k_2 & -k_2 \\ -k_2 & k_2 \end{bmatrix} \tag{A7}$$

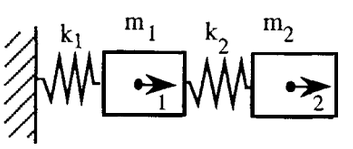


The 2 DOF svstem

Assuming that each element of the system matrices in error can be expressed as a linear function of the non-zero elements of the analytical system matrices, which is referred to as the Cl constraints in chapter 5, we can write:

$$\Delta M_{11} = p_1 m_1, \quad \Delta M_{12} = \Delta M_{21} = 0, \quad \Delta M_{22} = p_2 m_2,$$
$$\Delta K_{11} = p_3(k_1+k_2), \quad \Delta K_{12} = \Delta K_{21} = -p_4 k_2 \text{ and } \quad \Delta K_{22} = p_5 k_2.$$

Now {p} contains 5 unknowns and $[C(\omega)]$ becomes:

$$\begin{bmatrix} -\omega^2\alpha_{11}\alpha_{11_x}m_1 & -\omega^2\alpha_{12}\alpha_{12_x}m_2 & \alpha_{11}\alpha_{11_x}(k_1+k_2) & (\alpha_{12}\alpha_{11_x}+\alpha_{11}\alpha_{12_x})k_2 & \alpha_{12}\alpha_{12_x}k_2 \\ -\omega^2\alpha_{21}\alpha_{11_x}m_1 & -\omega^2\alpha_{22}\alpha_{12_x}m_2 & \alpha_{21}\alpha_{11_x}(k_1+k_2) & (\alpha_{22}\alpha_{11_x}+\alpha_{21}\alpha_{12_x})k_2 & \alpha_{22}\alpha_{12_x}k_2 \end{bmatrix} \tag{A8}$$

Assuming each element of the system matrices in error can be expressed as a linear function of the FE element system matrices (C2 constraints), i.e.

$$AM1_1 = p_1 m_1, \quad \Delta M_{12} = \Delta M_{21} = 0, \quad \Delta M_{22} = p_2 m_2,$$
$$\Delta K_{11} = p_3 k_1 + p_4 k_2, \quad \Delta K_{12} = \Delta K_{21} = -p_4 k_2 \quad \Delta K_{22} = p_4 k_2$$

in this case {p} contains 4 unknowns and $[C(\omega)]$ becomes:

$$\begin{bmatrix} -\omega^2\alpha_{11}\alpha_{11_x}m_1 & -\omega^2\alpha_{12}\alpha_{12_x}m_2 & \alpha_{11}\alpha_{11_x}k_1 & ((\alpha_{11}+\alpha_{12})\alpha_{11_x} + (\alpha_{11}+\alpha_{12})\alpha_{12_x})k_2 \\ -\omega^2\alpha_{21}\alpha_{11_x}m_1 & -\omega^2\alpha_{22}\alpha_{12_x}m_2 & \alpha_{21}\alpha_{11_x}k_1 & ((\alpha_{21}+\alpha_{22})\alpha_{11_x} + (\alpha_{21}+\alpha_{22})\alpha_{12_x})k_2 \end{bmatrix} \tag{A9}$$

For an incomplete experimental data set, say only $\alpha_{11_x}$ is measured, the RFM becomes:

$$[\,-\omega^2\alpha_{11}\alpha_{11_x}m_1 \;\; -\omega^2\alpha_{12}\alpha_{12_x}m_2 \;\; \alpha_{11}\alpha_{11_x}k_1 \;\; ((\alpha_{11}+\alpha_{12})\alpha_{11_x} + (\alpha_{11}+\alpha_{12})\alpha_{12_x})\,k_2\,] \begin{Bmatrix} p_1 \\ p_2 \\ p_3 \\ p_4 \end{Bmatrix} = \{\Delta\alpha_{11}\} \tag{A10}$$

The RFM is now changed from a direct method into an iterative process where $\alpha_{12_x}$, the unmeasured receptance value, is replaced by its updated analytical counterpart until convergence is reached.

# APPENDIX B

# ILLUSTRATIONS OF REDUCED COORDINATES IN THE RFM

In this appendix the consequences of using a reduced number of coordinates in the RFM are illustrated using a 2 DOF example. The various possibilities for dealing with this inevitable practical situation as discussed in chapter 8 are:

(i) replacing unmeasured coordinates with their analytical counterparts;
(ii) replacing unmeasured coordinates with values obtained from receptance expansion;
(in) applying condensation techniques to the full and to the element-system matrices;
(iv) deleting unmeasured coordinates from the analytical receptance matrix; and
(v) as (iv) and also using an equivalent dynamic reduction for derivatives.

For a 2 DOF system:

$$[\alpha_A(\omega)] = \frac{1}{Z(\omega)_{22}Z(\omega)_{11} - Z(\omega)_{12}^2}\begin{bmatrix} Z_{22}(\omega) & -Z_{12}(\omega) \\ -Z_{21}(\omega) & Z_{11}(\omega) \end{bmatrix} = \frac{1}{|A|}\begin{bmatrix} Z_{22}(\omega) & -Z_{12}(\omega) \\ -Z_{21}(\omega) & Z_{11}(\omega) \end{bmatrix} \tag{B1a}$$

$$[\alpha_X(\omega)] = \frac{1}{|X|}\begin{vmatrix} Z_{22_X}(\omega) & -Z_{12_X}(\omega) \\ -Z_{21_X}(\omega) & Z_{1\ 1_X}(\omega) \end{vmatrix} \tag{B1b}$$

and:

$$[Z_X(\omega)] = \begin{bmatrix} Z_{11_A}(\omega) + \Delta Z_{11}(\omega) & Z_{12_{A(\omega)}} + \Delta Z_{12}(\omega) \\ Z_{21_A}(\omega) + \Delta Z_{21}(\omega) & Z_{22_A}(\omega) + \Delta Z_{22}(\omega) \end{bmatrix} \tag{B2}$$

Throughout this appendix it is assumed that only $\alpha_{11_X}$ of the experimental system is measured. Again, for simplicity, both references to the analytical system (subscript A) and to frequency $(\omega)$ are omitted and unless a specific reference is made to the experimental system (subscript X), each symbol is assumed to relate to the analytical system.

### (i) Replacing missing coordinate(s) with their analytical counterpart(s)

Replacing missing coordinates with their analytical counterparts, the standard RFM becomes:

$$\alpha_{11}\Delta Z_{11}\alpha_{11_X} + \alpha_{12}\Delta Z_{21}\alpha_{11_X} + \alpha_{11}\Delta Z_{12}\alpha_{12_X} + \alpha_{12}\Delta Z_{22}\alpha_{12_X} = \alpha_{11} - \alpha_{11_X} \qquad \text{(B5)}$$

The unmeasured $\alpha_{12_X}$ is replaced by its analytical counterpart, i.e.:

$$\alpha_{11}\Delta Z_{11}\alpha_{11_X} + \alpha_{12}\Delta Z_{21}\alpha_{11_X} + \alpha_{11}\Delta Z_{12}\alpha_{12} + \alpha_{12}\Delta Z_{22}\alpha_{12} = \alpha_{11} - \alpha_{11_X} \qquad \text{(B6)}$$

To get an impression of the inaccuracies introduced by this substitution, equation (B6) is expanded to contain symbols referring to the analytical system only:

$$\frac{Z_{22}}{|A|}\Delta Z_{11}\frac{Z_{22} + \Delta Z_{22}}{|X|} + \frac{-Z_{12}}{|A|}\Delta Z_{21}\frac{Z_{22} + \Delta Z_{22}}{|X|}, \frac{Z_{22}}{|A|}\Delta Z_{12}\frac{-Z_{12}}{|A|} +$$

$$\frac{-Z_{12}}{|A|}\Delta Z_{22}\frac{-Z_{12}}{|A|} = \frac{Z_{22}}{|A|}\frac{Z_{22} + \Delta Z_{22}}{|X|} \qquad \text{(B7)}$$

Multiplying both sides by $|A|$ and $|X|$:

$$Z_{22}\Delta Z_{11}(Z_{22} + \Delta Z_{22}) - Z_{12}\Delta Z_{12}(Z_{22} + \Delta Z_{22}) - Z_{22}\Delta Z_{12}Z_{12}\frac{|X|}{|A|} +$$

$$Z_{12}\Delta Z_{22}Z_{12}\frac{|X|}{|A|} = Z_{22}|X| - (Z_{22} + \Delta Z_{22})|A| \qquad \text{(B8)}$$

**Now:** $Z_{22}|X| - (Z_{22} + \Delta Z_{22})|A| =$

$$Z_{22}\left((Z_{22} + \Delta Z_{22})(Z_{11} + \Delta Z_{11}) - (Z_{12} + \Delta Z_{12})^2\right) - (Z_{22} + \Delta Z_{22})(Z_{22}Z_{11} + Z_{12}^2) =$$

$$Z_{11}Z_{22}^2 + Z_{22}^2\Delta Z_{11} + Z_{11}Z_{22}\Delta Z_{22} + Z_{22}\Delta Z_{11}\Delta Z_{22} - Z_{12}^2Z_{22} - 2Z_{12}Z_{22}\Delta Z_{12} - Z_{22}\Delta Z_{12}^2$$

$$- Z_{11}Z_{22}^2 + Z_{12}^2Z_{22} - Z_{11}Z_{22}\Delta Z_{22} + Z_{12}^2\Delta Z_{22} =$$

$$Z_{22}^2\Delta Z_{11} + Z_{22}\Delta Z_{11}\Delta Z_{22} - 2Z_{12}Z_{22}\Delta Z_{12} - Z_{22}\Delta Z_{12}^2 + Z_{12}^2\Delta Z_{22} \qquad \text{(B9)}$$

and: $$\frac{|X|}{|A|} = 1 + \frac{Z_{22}\Delta Z_{11} + Z_{11}\Delta Z_{22} + \Delta Z_{11}\Delta Z_{22} - 2Z_{12}\Delta Z_{12} - \Delta Z_{12}^2}{Z_{22}Z_{11} - Z_{12}^2} \qquad \text{(B10)}$$

Substituting (B10) into the LHS of (B8), and comparing with the RHS of (B9), the **RFM** for a 2 DOF example with only 1 measured coordinate is exact if:

$$\left(\frac{Z_{22}\Delta Z_{11} + Z_{11}\Delta Z_{22} + \Delta Z_{11}\Delta Z_{22} - 2Z_{12}\Delta Z_{12} - \Delta Z_{12}^2}{Z(\omega)_{22}Z(\omega)_{11} - Z(\omega)_{12}^2}\right) Z_{11}Z_{22}\Delta Z_{12} +$$

$$\left(\frac{Z_{22}\Delta Z_{11} + Z_{11}\Delta Z_{22} + \Delta Z_{11}\Delta Z_{22} - 2Z_{12}\Delta Z_{12} - \Delta Z_{12}^2}{Z(\omega)_{22}Z(\omega)_{11} - Z(\omega)_{12}^2}\right) Z_{12}^2\Delta Z_{22} -$$

$$Z_{12}\Delta Z_{12}\Delta Z_{22} + Z_{22}\Delta Z_{12}^2 = 0 \qquad \text{(B11)}$$

As can be seen, all terms are all of order $\Delta^2$ and $\Delta^3$. For incomplete experimental data the standard RFM is applied iteratively and the discrepancies will decrease till convergence is reached.

### (ii) Replacing unmeasured coordinate(s) with expanded receptance value(s)

**The 2** DOF example is also expanded substituting the unmeasured receptance value with an expanded value using the inverse reduction technique, i.e.:

$$\alpha_{11}\Delta Z_{11}\alpha_{11_X} + \alpha_{12}\Delta Z_{21}\alpha_{11_X} + \alpha_{11}\Delta Z_{12}\alpha_{12_X}^E + \alpha_{12}\Delta Z_{22}\alpha_{12_X}^E = \alpha_{11} - \alpha_{11_X} \qquad \text{(B12)}$$

where: $$a_{12x}^E = \frac{-Z_{12}}{Z_{22}}\alpha_{11_X} = \frac{-Z_{12}}{Z_{22}}\frac{Z_{22} + \Delta Z_{22}}{|X|} = -\frac{-Z_{12}}{|X|} - \frac{Z_{12}\Delta Z_{22}}{Z_{22}|X|} \qquad \text{(B13)}$$

Substituting equation (B 13) into equation (B12), *gives:*

$$\frac{Z_{22}}{|A|}\Delta Z_{11}\frac{Z_{22} + \Delta Z_{22}}{|X|} + \frac{-Z_{12}}{|A|}\Delta Z_{21}\frac{Z_{22} + \Delta Z_{22}}{|X|} + \frac{Z_{22}}{|A|}\Delta Z_{12}\left(\frac{-Z_{12}}{|X|} - \frac{Z_{12}\Delta Z_{22}}{Z_{22}|X|}\right) +$$

$$\frac{-Z_{12}}{|A|}\Delta Z_{22}\left(\frac{-Z_{12}}{|X|} - \frac{Z_{12}\Delta Z_{22}}{Z_{22}|X|}\right) = \frac{Z_{22}}{|A|}\frac{Z_{22} + \Delta Z_{22}}{|X|} \qquad \text{(B14)}$$

Multiplying both sides by |A| and |X|:

$$Z_{22}\,\Delta Z_{11}(Z_{22} + \Delta Z_{22}) - Z_{12}\,\Delta Z_{12}(Z_{22} + \Delta Z_{22}) - Z_{22}\,\Delta Z_{12}\left(Z_{12} + \frac{Z_{12}\Delta Z_{22}}{Z_{22}}\right) +$$

$$Z_{12}\,\Delta Z_{22}\left(Z_{12} + \frac{Z_{12}\Delta Z_{22}}{Z_{22}}\right) = Z_{22}\,|X| - (Z_{22} + \Delta Z_{22})\,|A| \qquad \text{(B15)}$$

Comparing the LHS of equation (B15) to the expanded RHS of equation (B9), the discrepancies are:

$$-Z_{12}\Delta Z_{12}\Delta Z_{22} + \frac{Z_{12}^2}{Z_{22}}\Delta Z_{22}^2 + Z_{22}\Delta Z_{12}^2 = 0 \qquad \text{(B16)}$$

As for the standard RFM, discrepancies are of order $\Delta^2$, but in contrast to the standard RFM an exact solution is achieved in 1 iteration if the modelling errors are at $Z_{11}$ only. Comparing equation (B16) with equation (Bl 1), the standard REM, the number of terms showing the discrepancy are reduced, although numerical improvements during the first iteration will be case-dependent. Even using expanded data, it is recommended that the RFM be applied iteratively so that discrepancies will decrease till convergence is reached.

**(iii) The use of condensation techniques**

Conti and Donley [106] advocate the application of condensation techniques to both the full and to the element-system matrices to overcome the problem of incomplete experimental data. For this example the RFM becomes:

$$\alpha^R\,\Delta Z^R\,\alpha_{11_X} = \alpha_{11} - \alpha_{11_X} \qquad \text{(B17)}$$

where $\alpha^R$ is obtained using a condensation technique e.g. Guyan reduction, thus:

$$M^R = M_{11} - 2\,M_{12}\frac{K_{12}}{K_{22}} + M_{22}\left(\frac{K_{12}}{K_{22}}\right)^2 \quad \text{and} \quad K^R = K_{11} - \frac{K_{12}^2}{K_{22}} \qquad \text{(B18)}$$

To retain connectivity the same condensation is also applied to the element system matrices and:

$$\Delta Z^R = \sum_{i=1}^{n} \frac{\delta Z^R}{\delta p_i} p_i \tag{B19}$$

Consider a 2 DOF consisting of 2 masses and 2 springs as used in appendix A,

$$[M] = \begin{bmatrix} m_1 & 0 \\ 0 & m_2 \end{bmatrix}, [K] = \begin{bmatrix} k_1+k_2 & -k_2 \\ -k_2 & k_2 \end{bmatrix} \tag{B20a}$$

assuming the error to be a linear combination of the element system matrices i.e.:

$$\Delta m_1 = m_1 p_1 , \Delta m_2 = m_2 p_2 , \Delta k_1 = k_1 p_3 , \Delta k_2 = k_2 p_4 \tag{B20b}$$

and thus:

$$\frac{\delta Z^R}{\delta p_1} = m_1$$

$$\frac{\delta Z^R}{\delta p_2} = \left(\frac{0}{0}\right)^2 m_2 = ?$$

$$\frac{\delta Z^R}{\delta p_3} = k_1 = 0$$

$$\frac{\delta Z^R}{\delta p_4} = k_2 - \frac{k_2^2}{k_2} = 0 \tag{B21}$$

Without further derivations it is clear that for this particular 2 DOF example the RFM by condensation is unable to indicate errors in $m_2$ and $k_2$. Bearing in mind that (i) the condensation technique is case-dependent and is likely to behave better for more realistic structures and (ii) that there are several other condensation techniques available, this simple illustration might not reflect the benefits of the RFM using condensation but it does show that this approach should be used with caution.

Reducing analytical coordinates to the measured data set, such as in (iii)-(iv), the RFM becomes non-iterative and can be solved directly.

### (iv) Deletion of unmeasured coordinate(s) from the analytical receptance matrix

In this case $\alpha_{11}$ is obtained from a deleted set and hence represents the dynamic behaviour of the full analytical system (as in (i) and (ii) but not as in (iii)), and the RFM becomes:

$$\alpha^D \, \Delta Z^R \, \alpha_{11_X} = \alpha_{11} - \alpha_{11_X} \tag{B22}$$

and:

$$\frac{Z_{22}}{|A|} \Delta Z^R \frac{Z_{22} + \Delta Z_{22}}{|X|} = \frac{Z_{22}}{|A|} \frac{+ \Delta Z_{22}}{|X|} \tag{B23}$$

Multiplying both sides by $|A|$ and $|X|$ (see equation (B9)):

$$Z_{22}\Delta Z^R(Z_{22}+\Delta Z_{22}) = Z_{22}\,|X| - (Z_{22} + \Delta Z_{22})\,|A|$$

$$= Z_{22}^2\Delta Z_{11} + Z_{22}\Delta Z_{11}\Delta Z_{22} - 2Z_{12}Z_{22}\Delta Z_{12} - Z_{22}\Delta Z_{12}^2 + Z_{12}^2\Delta Z_{22} \tag{B24}$$

Assuming:

$$\Delta Z^R = [\Delta Z^D] = \Delta Z_{11} \tag{B25}$$

thus:

$$Z_{22}\Delta Z_{11}(Z_{22}+\Delta Z_{22}) = Z_{22}^2\,\Delta Z_{11} + Z_{22}\Delta Z_{11}\Delta Z_{22} - 2Z_{12}Z_{22}\Delta Z_{12} - Z_{22}\Delta Z_{12}^2 + Z_{12}^2\Delta Z_{22} \tag{B26}$$

and:

$$-2Z_{12}Z_{22}\Delta Z_{12} - Z_{22}\Delta Z_{12}^2 + Z_{12}^2\Delta Z_{22} = 0 \tag{B27}$$

Now, discrepancies are of order A and, as in this case the RFM as described by equation (B22) is non-iterative, correct results will be achieved <u>only</u> if **all** errors occur at $Z_{11}$.

## (v) As (iv) and using an equivalent dynamic reduction for derivatives

Applying equation (B22) and using an equivalent dynamic reduction of the dynamic stiffness matrix and its derivatives [105,120] (see equation (15) chapter 8) gives:

$$\Delta Z^R = [\Delta Z^D] = \tilde{Z}^D \left[[\alpha]\ [AZ]\ [\alpha]\right]^D \tilde{Z}^D =$$

$$\tilde{Z}^D \left[ \begin{bmatrix} \alpha_{11}\Delta Z_{11} + \alpha_{12}\Delta Z_{12} & \alpha_{11}\Delta Z_{12} + \alpha_{12}\Delta Z_{22} \\ \alpha_{12}\Delta Z_{11} + \alpha_{22}\Delta Z_{12} & \alpha_{12}\Delta Z_{12} + \alpha_{22}\Delta Z_{22} \end{bmatrix} [\alpha] \right]^D \tilde{Z}^D =$$

$$\tilde{Z}^D \left( \alpha_{11}^2 \Delta Z_{11} + 2\alpha_{11}\alpha_{12}\Delta Z_{12} + \alpha_{12}^2 \Delta Z_{22} \right) \tilde{Z}^D \qquad \text{(B28)}$$

where: $$\tilde{Z}^D = \frac{|A|}{Z_{22}}$$

Substituting (B26) into (B22):

$$\frac{1}{|A|^2}\left(Z_{22}^2\Delta Z_{11} - 2Z_{12}Z_{22}\Delta Z_{12} + Z_{12}^2\Delta Z_{22}\right)\frac{|A|}{Z_{22}}\frac{(Z_{22} + \Delta Z_{22})}{|X|} = -i\,x - \frac{Z_{22} + \Delta Z_{22}}{|X|} \qquad \text{(B29)}$$

Multiplying both sides by $|A|$ and $|X|$:

$$\frac{1}{Z_{22}}\left(Z_{22}^2\Delta Z_{11}(Z_{22}+\Delta Z_{22}) - 2Z_{12}Z_{22}\Delta Z_{12}(Z_{22}+\Delta Z_{22}) + Z_{12}^2\Delta Z_{22}(Z_{22}+\Delta Z_{22})\right) =$$

$$Z_{22}\,|X| - (Z_{22} + \Delta Z_{22})\,|A| \qquad \text{(B30)}$$

Expanding (B30):

$$Z_{22}^2\Delta Z_{11} + Z_{22}\Delta Z_{11}\Delta Z_{22} - 2Z_{12}Z_{22}\Delta Z_{12} - 2Z_{12}\Delta Z_{12}\Delta Z_{22} + Z_{12}^2\Delta Z_{22} + \frac{Z_{12}^2\Delta Z_{22}^2}{Z_{22}} =$$

$$Z_{22}^2\,\Delta Z_{11} + Z_{22}\Delta Z_{11}\Delta Z_{22} - 2Z_{12}Z_{22}\Delta Z_{12} - Z_{22}\Delta Z_{12}^2 + Z_{12}^2\Delta Z_{22}$$

gives: $$\frac{Z_{12}^2\Delta Z_{22}^2}{Z_{22}} - 2Z_{12}\Delta Z_{12}\Delta Z_{22} = -Z_{22}\Delta Z_{12}^2 \qquad \text{(B31)}$$

Hence: $$Z_{12}^2\Delta Z_{22}^2 - 2Z_{12}Z_{22}\Delta Z_{12}\Delta Z_{22} + Z_{22}^2\Delta Z_{12}^2 = 0 \qquad \text{(B32a)}$$

or: $$(Z_{12}\Delta Z_{22} - Z_{22}\Delta Z_{12})^2 = 0$$

$$Z_{12}\Delta Z_{22} = Z_{22}\Delta Z_{12} \qquad \text{(B32b)}$$

Again there are discrepancies for a non-iterative approach. This is surprising as no assumptions were made about the error locations and each equation used was an equality. Correct results will only be achieved for a 2 DOF system if all errors occur at $Z_{11}$ or in the special case that equation (B32) is true.

Substituting the particular 2 DOF example of equation (B20) into (B31):

$$(k_2 - \omega^2 m_2)(-k_2 p_4) = (-k_2)(k_2 p_4 - \omega^2 m_2 p_2)$$

or: $$\omega^2 m_2 k_2 p_4 = \omega^2 m_2 k_2 p_2$$

i.e.: $\omega = 0$ or $m_2 = 0$ or $k_2 = 0$ or $p_4 = p_2$

# APPENDIX C

# THE 3-BAY TRUSS STRUCTURE

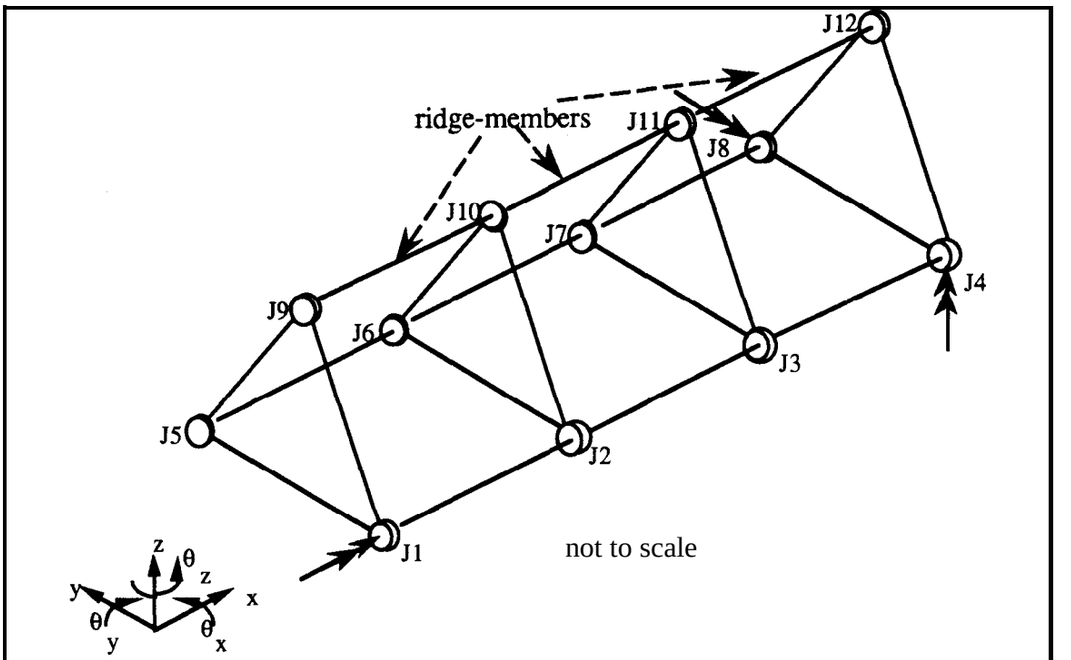


The 3-bay truss structure

The 3-bay truss structure consists of four types of components. Ridge members are indicated in the figure, all other trusses are side members. Joints J1-J8 are side-joints and joints J9-J12 are ridge-joints. Engineering drawings of the components are given on the next pages.

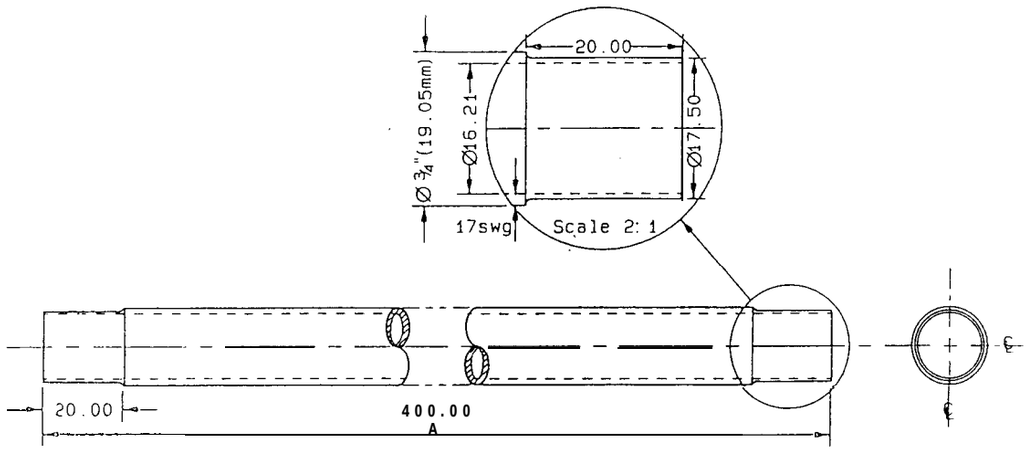


| | | | |
|---|---|---|---|
| | | | Drawn: S.M TOOLEY |
| | | | Date: 22/8/89 |
| | | | Title: RIDGE-MEMBER |
| | COMPONENT | PROPERTIES | Scale: |
| MATERIAL PROPERTIES | Centre-Sec$^n$ | End-Sec$^n$ | Material: DURAL (L105) |
| Density 2870 kgm$^{-3}$ | Area. 7 865x10$^{-5}$m$^2$ | Area: 3.415x10$^{-5}$m$^2$ | No. off. 3 |
| E 69 9x10$^9$ Nm$^{-2}$ | I. 3 075x 10$^{-9}$m$^4$ | I: 1.212x10$^{-9}$m$^4$ | All dimensions in mm unless |
| G 26 3x10$^9$ Nm$^{-2}$ | J: 6 151x 10$^{-9}$m$^4$ | J: 2.429x10$^{-9}$m$^4$ | otherwise stated |

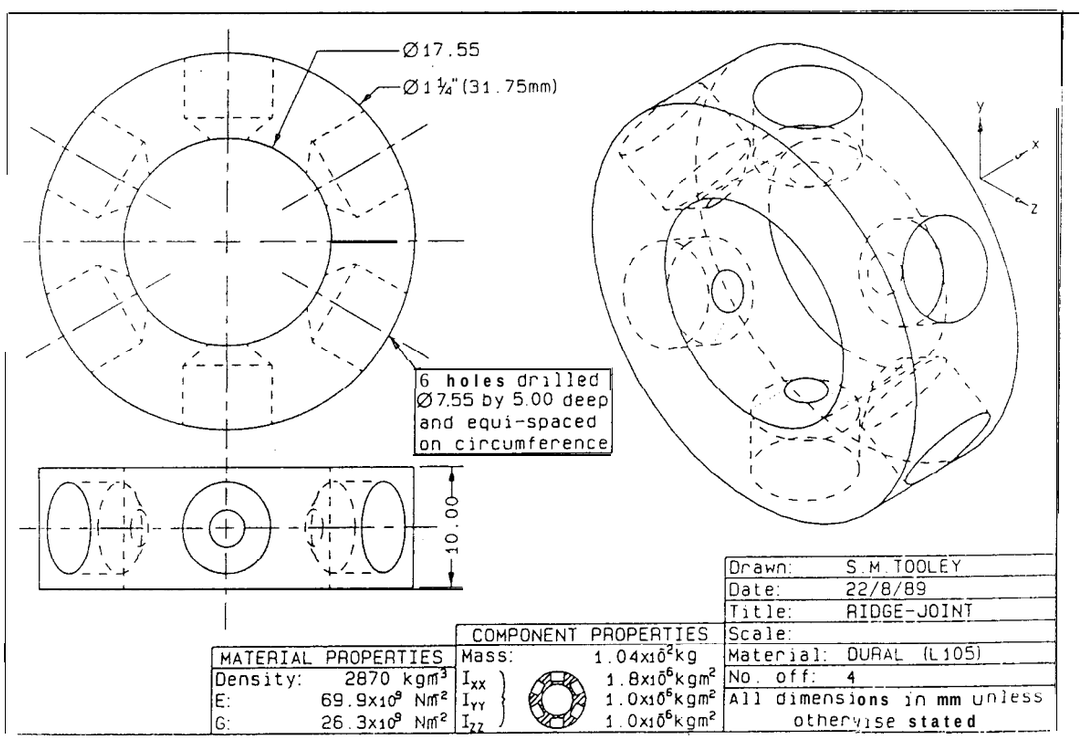


| | | | |
|---|---|---|---|
| | | | Drawn: S.M.TOOLEY |
| | | | Date: 22/8/89 |
| | | | Title: RIDGE-JOINT |
| | COMPONENT PROPERTIES | | Scale: |
| MATERIAL PROPERTIES | Mass: | 1.04x10$^2$kg | Material: DURAL (L105) |
| Density: 2870 kgm$^{-3}$ | $I_{xx}$ | 1.8x10$^6$kgm$^2$ | No. off: 4 |
| E: 69.9x10$^9$ Nm$^{-2}$ | $I_{YY}$ | 1.0x10$^6$kgm$^2$ | All dimensions in mm unless |
| G: 26.3x10$^9$ Nm$^{-2}$ | $I_{ZZ}$ | 1.0x10$^6$kgm$^2$ | otherwise stated |

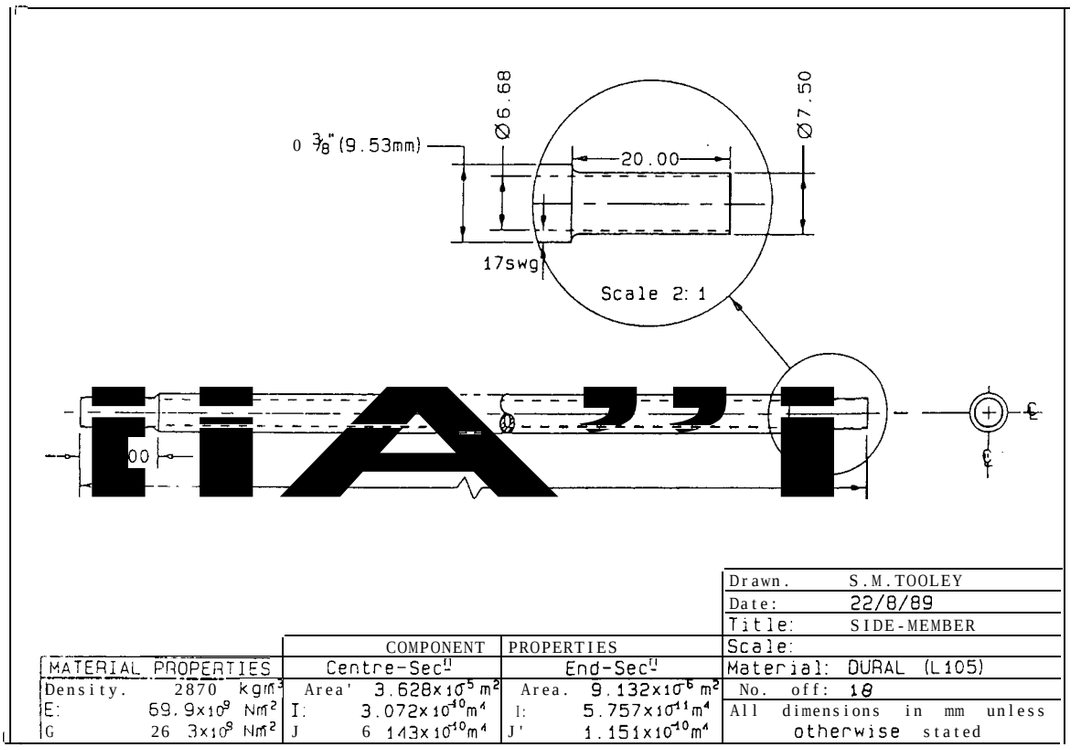
Ø6.68
Ø7.50
0 3/8" (9.53mm)
20.00
17swg
Scale 2: 1
00
Drawn. S.M.TOOLEY
Date: 22/8/89
Title: SIDE-MEMBER
Scale:
Material: DURAL (L105)
No. off: 18
All dimensions in mm unless otherwise stated
COMPONENT PROPERTIES
MATERIAL PROPERTIES
Centre-Sec
End-Sec
Density. 2870 kgm³
E: 69.9x10⁹ Nm⁻²
G 26 3x10⁹ Nm⁻²
Area' 3.628x10⁻⁵ m²
I: 3.072x10⁻¹⁰m⁴
J 6 143x10⁻¹⁰m⁴
Area. 9.132x10⁻⁶ m²
I: 5.757x10⁻¹¹m⁴
J' 1.151x10⁻¹⁰m⁴

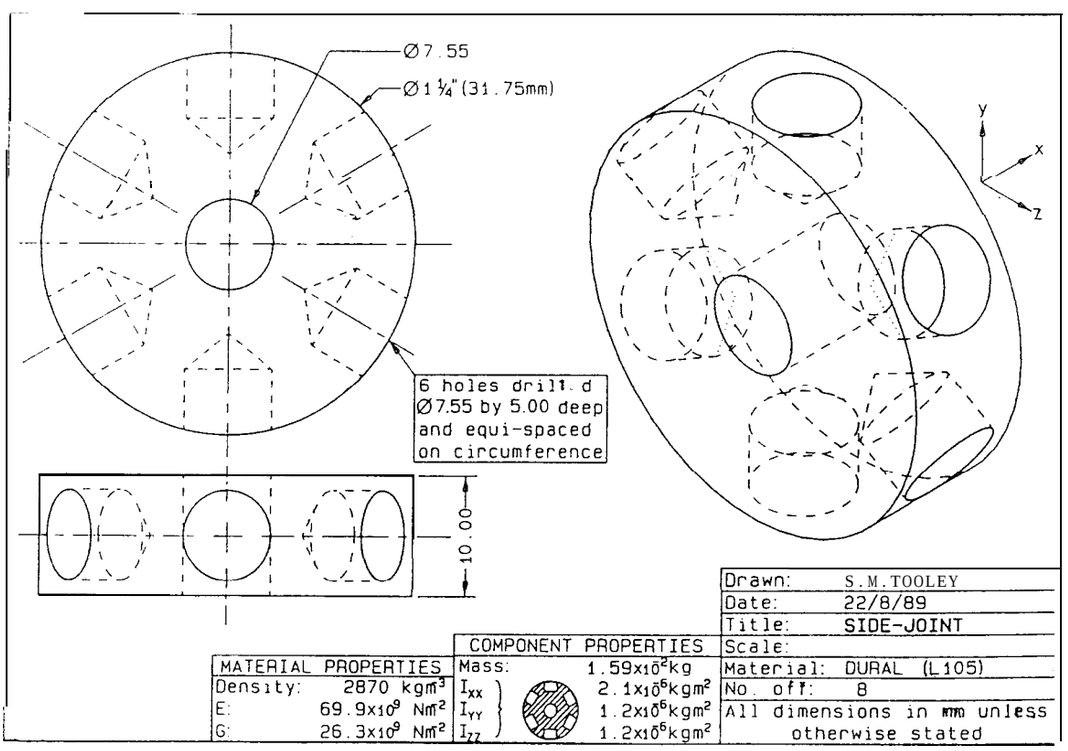
Ø7.55
Ø1 1/4" (31.75mm)
6 holes drill. d Ø7.55 by 5.00 deep and equi-spaced on circumference
10.00
y
x
z
Drawn: S.M.TOOLEY
Date: 22/8/89
Title: SIDE-JOINT
Scale:
Material: DURAL (L105)
No. off: 8
All dimensions in mm unless otherwise stated
MATERIAL PROPERTIES
Density: 2870 kgm³
E: 69.9x10⁹ Nm⁻²
G: 26.3x10⁹ Nm⁻²
COMPONENT PROPERTIES
Mass: 1.59x10⁻²kg
Ixx 2.1x10⁻⁶kgm²
IYY 1.2x10⁻⁶kgm²
IZZ 1.2x10⁻⁶kgm²

The following information about the physical excitation systems was supplied:

Excitation in the x-direction at joint J1:

| | |
|---|---|
| pushrod length | 81 mm |
| concentrated mass at structure end | 0.0021 Kg |
| concentrated mass at shaker end | 0.0041 Kg |
| torsional springs at the shaker ends of the pushrods about the y and z-axes | 0.566 Nm/rad |

Excitation in the y-direction at joint J8:

| | |
|---|---|
| pushrod length | 81 mm |
| concentrated mass at structure end | 0.0021 Kg |
| concentrated mass at shaker end | 0.0041 Kg |
| torsional springs at the shaker ends of the pushrods about the x and z-axes | 0.566 Nm/rad |

Excitation in the z-direction at joint J4:

| | |
|---|---|
| pushrod length | 106 mm |
| concentrated mass at structure end | 0.0023 Kg |
| concentrated mass at shaker end | 0.01129 Kg |
| torsional springs at the shaker ends of the pushrods about the x and y-axes | 0.566 Nm/rad |

Pushrods:

| | |
|---|---|
| cross-sectional area | $502 \times 10^{-9}$ $m^2$ |
| second moment of area | $2 \times 10^{-13}$ $m^4$ |
| torsional constant | $4 \times 10^{-13}$ $m^4$ |
| Young's modulus | $207 \times 10^9$ N/m* |
| Poison's ratio | 0.3 |
| density | 7850 Kg/m3 |

# APPENDIX D

# 3-BAY TRUSS STRUCTURE - RFM RESULTS

This appendix presents error location results for the 3-bay truss structure obtained using the RFM. The results are grouped into tables according to the number of unknown p-values. Error location was based on a mean-to-standard deviation ratio larger than 2. Each table presents the mean p-values of the identified erroneous elements and the details of how these results were obtained, namely:

(i) which experimental data set;

(ii) the number of experimental receptance curves used;

(iii) the number of runs out of the number of attempted runs given in brackets; and (iv) the criterion used for selecting the p-values: (a) where the sum of the squared percentage difference reached a minimum or (b) where the differences between the experimental and updated natural frequencies was a minimum.

In cases of 103 or 99 p-values and only 1 RFM run only the most significant p-values for a particular section of the FE model and the overall results of that section are presented.

| RFM details<br>(i)<br>(ii)<br>(iii)<br>(iv)<br>elements | XJ8y<br>32<br>2 (6)<br>a | XJ4z<br>36<br>4 (6)<br>a | RJ4z<br>29<br>2 (6)<br>a | RJ4z<br>29<br>1 (6)<br>b |
|---|---|---|---|---|
| ridge trusses<br>beam M els. | √ | √ | √ | √ |
| side trusses<br>beam M els. | 2 els. 0.18<br>2 els. 0.14<br>2 els. 0.11 | 4 els 0.1 | 2 els. -0.12<br>2 els. 0.21 | 2 els. -0.23<br>2 els. 0.46<br>2 els. 0.26<br>2 els 0.68 |
| ridge joints<br>lumped M els. | J11 0.17<br>J12 0.17 | √ | J12 -0.39 | J11 -0.58<br>J12 -0.34 |
| side joints<br>lumped M. els. | J1 0.12<br>J4 0.12 | √ | J2 -0.17<br>J5 -0.36<br>J6 -0.15 | J4 -0.58<br>J5 -0.20 |
| ridge trusses<br>beam K els. | √ | √ | 2 els. 0.18 | many els.<br>mostly +ve |
| side trusses<br>beam K els. | 2 els. 0.14<br>2 els. 0.30<br>2 els. 0.11 | 2 els 0.2 | 2 els. 0.29<br>2 els. 0.81 | |
| ridge joints<br>beam K els. | √ | √ | J1 2 els.<br>J3 2 els.<br>J4 1 els.<br>J5 3 els.<br>J6 4 els.<br>all ≈-0.14 | √ |
| side joints<br>beam K. els. | √ | √ | √ | J3 1 el.<br>-0.31 |
| excitation systems<br>K els. | J4z 0.12 | √ | √ | J1x 0.61 |
| trusses<br>beam D els. | √ | √ | √ | ridge √<br>side 0.61 |
| joints<br>beam D els. | √ | √ | √ | ridge √<br>side 0.55 |

where √ = acceptable

**Table D.l:** RFM results 3-bay truss structure, 103 p-values

| RFM details (i) (ii) (iii) (iv) / elements | XJ4z 36 4 (10) a | XJ4z 36 5 (10) b | RJ4z 29 4 (6) a | RJ4z 29 1 (6) b |
|---|---|---|---|---|
| ridge trusses beam M els. | √ | √ | √ | √ |
| side trusses beam M els. | 2 els. -0.45 | 2 els. -0.11 | 2 els. -0.14 | √ |
| ridge joints lumped M els. | √ | √ | √ | √ |
| side joints lumped M. els. | J2 -0.68<br>J8 -0.67 | J1 -0.15<br>J3 -0.21<br>J5 -0.10<br>J7 -0.10<br>J8 -0.18 | √ | J2 -0.25<br>J4 -0.24 |
| ridge trusses beam K els. | √ | √ | √ | √ |
| side trusses beam K els. | 2 els. 0.71 | 2 els. 0.10<br>2 els. 0.25 | √ | 2 els. 0.38<br>2 els. -0.27<br>2 els. 0.41<br>2 els. 0.22 |
| ridge joints beam K els. | √ | many els. mostly ≈-0.1 | Jll 1 el. -0.14 | √ |
| side joints beam K. els. | J1 1 el. -0.57 | | J3 1 el. -0.15 | J1 lel. -0.24<br>J3 1 el. -0.22 |
| excitation systems K els. | J8y -0.87 | √ | √ | Jlx 0.40<br>J8y 0.39 |
| trusses beam D els. | | | | |
| joints beam D els. | | | | |

where √ = acceptable
and - = not included

**Table D.2:** RFM results 3-bay truss structure, 99 p-values

| RFM details (i) (ii) (iii) (iv) / elements | XJ1x 29 6 (8) a | XJ1x 29 6 (8) b | XJ8y 25 6a (8) | XJ8y 25 6b (8) | XJ4z 29 6a (9) | XJ4z 29 5b (9) | RJ4z 29 6a (6) | RJ4z 29 3b (6) |
|---|---|---|---|---|---|---|---|---|
| ridge trusses beam M els. | √ | √ | √ | √ | √ | √ | √ | √ |
| side trusses beam M els. | √ | √ | √ | √ | √ | √ | √ | √ |
| ridge joints lumped M els. | J9 -0.88 | J9 -0.71 | J12 -0.94 | J12 -0.94 | √ | J12 -0.69 | J10 -0.73 | J9 -0.44 J10 -0.76 J11 0.64 |
| side joints lumped M. els. | J1-J8 all ≈-0.4 | J1,2,5 J7,9 all ≈-0.5 | J6 -0.5 | J1,2,4 J5,8 all ≈-0.3 | J8 0.68 | √ | √ | J4 0.42 J7 0.42 |
| ridge trusses beam K els. | 0.47 | √ | √ | √ | √ | √ | √ | √ |
| side trusses beam K els. | 2.81 | 1.76 | √ | √ | √ | √ | √ | √ |
| ridge joints beam K els. | all ≈-0.4 | all ≈-0.3 | √ | √ | √ | √ | √ | √ |
| side joints beam K. els. | | | √ | √ | √ | √ | √ | √ |
| excitation systems K els. | √ | √ | √ | √ | -0.76 | √ | √ | √ |
| trusses beam D els. | √ | √ | √ | √ | √ | √ | √ | √ |
| joints beam D els. | √ | 1.12 | √ | √ | √ | √ | √ | √ |

where √ = acceptable
and - = not included

**Table D.3:** RFM results 3-bay truss structure 31 p-values

| RFM details (i) (ii) (iii) (iv) / elements | XJ4z 29 6 (9) a | XJ4z 29 5 (9) b | RJ4z 29 6 (6) a | RJ4z 29 4 (6) b |
|---|---|---|---|---|
| ridge trusses beam M els. | √ | √ | √ | √ |
| side trusses beam M els. | √ | √ | √ | √ |
| ridge joints lumped M els. | √ | √ | J10 -0.54 | J10 -0.48 |
| side joints lumped M. els. | J1,2,3 -0.3<br>J4 -0.8<br>J5,6,7 -0.3 | J5 -0.31<br>J7 -0.23 | √ | √ |
| ridge trusses beam K els. | √ | √ | √ | √ |
| side trusses beam K els. | √ | √ | √ | √ |
| ridge joints beam K els. | J10 -0.29<br>Jll -0.33<br>J12 -0.36 | J11 -0.20 | √ | √ |
| side joints beam K. els. | J1 -0.27<br>J2 -0.2<br>J5 -0.29<br>J6 -0.21<br>J7 -0.24 | J5 -0.12 | √ | √ |
| excitation systems K els. | √ | √ | √ | √ |
| trusses beam D els. | | | | |
| joints beam D els. | | | | |

where √ = acceptable
and - = not included

**Table D.4:** RFM results 3-bay truss structure, 29 p-values

| RFM details (i) (ii) (iii) (iv) / elements | XJ1x 29 3 (3)) a | XJ1x 29 3 (3) b | XJ8y 25 2 (3) a | XJ8y 25 3 (3) b | XJ4z 29 3 (3) a | XJ4z 29 3 (3) b | RJ4z 29 5 (6) a | RJ4z 29 6 (6) b |
|---|---|---|---|---|---|---|---|---|
| ridge trusses beam M els. | √ | 0.08 | √ | √ | √ | √ | √ | √ |
| side trusses beam M els. | √ | √ | √ | √ | √ | √ | 0.08 | 0.07 |
| ridge joints lumped M els. | -0.93 | √ | √ | √ | √ | √ | -0.62 | -0.40 |
| side joints lumped M. els. | -0.96 | √ | √ | √ | √ | √ | √ | √ |
| ridge trusses beam K els. | √ | 0.12 | √ | √ | √ | √ | √ | √ |
| side trusses beam K els. | 1.91 | √ | -0.08 | √ | √ | √ | 0.53 | 0.32 |
| ridge joints beam K els. | -0.52 | √ | -0.05 | √ | -0.29 | √ | -0.21 | √ |
| side joints beam K. els. | -0.49 | √ | √ | √ | | √ | -0.16 | √ |
| excitation systems K els. | - | - | - | - | - | - | - | - |
| trusses beam D els. | √ | √ | 1.18 | √ | 2.33 | √ | √ | √ |
| joints beam D els. | √ | 0.94 | √ | √ | √ | √ | √ | √ |

where √ = acceptable
and - = not included

Table D.5: RFM results 3-bay truss structure, 10 p-values

| RFM details (i) (ii) (iii) (iv) / elements | XJ4z 29 1 (1) a + b | RJ4z 29 6 (6) a | RJ4z 29 3 (6) b |
|---|---|---|---|
| ridge trusses beam M els. | √ | √ | 0.15 |
| side trusses beam M els. | √ | √ | √ |
| ridge joints lumped M els. | -0.14 | -0.76 | -0.46 |
| side joints lumped M. els. | -0.50 | √ | √ |
| ridge trusses beam K els. | √ | √ | 0.11 |
| side trusses beam K els. | 0.18 | √ | 0.38 |
| ridge joints beam K els. | √ | √ | √ |
| side joints beam K. els. | √ | √ | √ |
| excitation systems K els. | | | |
| trusses beam D els. | | | |
| joints beam D els. | | | |

where √ = acceptable
and - = not included

**Table D.6:** RFM results 3-bay truss structure, 8 p-values

# REFERENCES


1 **Bishop, R. E. D. and Johnson, D. C.**
***The Mechanics of Vibration***
Cambridge University Press, 1960

2 **Den Hartog, J. P.**
***Mechanical Vibrations***
Mc Graw-Hill, 4th edition, 1984

3 **Timoshenko, S., Youngh, D. H., and Weaver, W.**
***Vibration Problems in Engineering***
John Wiley, 4th edition, 1974

4 **Blevins, R. D.**
***Formulas for Natural Frequency and Mode Shape***
Van Nostrand Reinfold Company, 1979

5 **Cook, R. D.**
***Concepts and Applications of Finite Element Analysis***
John Wiley and Sons, 2nd edition, 1981

6 **Bathe, K-L**
***Finite Element Procedures in Engineering Analysis***
Prentice-Hall, 1982

7 **Zienkiewicz, 0. C. and Taylor, R. L.**
***The Finite Element Method,***
McGraw-Hill 4th edition, 1986

8 **Ewins, D. J. and Imregun, M.**
***State-of-the-Art Assessment of Structural Dynamic Response Analysis Models (DYNAS)***
Shock and Vibration Bulletin, Vol. 56, Part 1, 1986

9 **Kennedy, C. C. and Pancu, C. D. P.**
**Use *of Vectors in Vibration Measurement and Analysis***
J. Aero. Sci., Vol. 14 No. 11, 1947

10 **Ewins, D. J.**
***Modal Testing : Theory and Practice***
Research Studies Press Ltd., 1984

11 **Ewins, D. J. and Griffin, J.**
***A State-of-the-Art Assessment of Mobility Measurement Techniques - Results for the Mid-Range Structures***
J. of Sound and Vib., Vol. 78 No. 2, pp 197-222, 1981

12 **Allemang, R. J. and Brown, D. L.**
***A Correlation Coefficient for Modal Vector Analysis***
***hoc.*** of the 1st Int. Modal Analysis Conf., pp 110-l 16, 1983

13 **Lieven, N. A. J. and Ewins, D. J.**
***Spatial Correlation of Mode Shapes, the Coordinate Modal Assurance Criterion (COMAC)***
Proc. of the 6th Int. Modal Analysis Conf., pp 690-695, 1988

14 **Targoff, W. P.**
*Orthogonality Check and Correction of Measured Modes*
AIAA Journal, Vol. 14, No. 2, pp 164-167, 1976

15 **Wada, B. K.**
*Correlation of Modal and Test Analysis*
Technical Report Jet Propulsion Laboratory, 1980

16 Chu, **D. F. H., Debroy, J. M. and Yang, J.**
*Pitfalls of Mass Orthogonality Check*
Proc. of the *7th* Int. Modal Analysis Conf., pp 822-829, 1989

17 **Bugeat, L. P. and Lallement, G.**
*Methods of Matching Calculated and Identified Eigensolutions*
Strojnicky Casopis, Vol. 32, No. 5, pp 162-167, 1976

18 **Dornier Systems**
*Procedures for Updating Dynamic Mathematical Models*
Technical Report Domier Systems, 1985

19 **Fisette, E., Stavrinidis, C. and Ibrahim, S.**
*Error Location and Updating of Analytical Dynamic Models Using a Force Balance Method*
Proc. of the 6th Int. Modal Analysis Conf., pp 1063-1070, 1988

20 **Chen, T. Y.**
*Finite Element Model Refinement Using Modal Analysis Data*
PhD Thesis, Univ. of Texas at Arlington, 1987

21 **Guyan, R.J.**
*Reduction of Stiffness and Mass Matrices*
AIAA Journal, Vol. 3, No. 2, pp 380, 1965

22 **Leung, A. Y. T.**
*An Accurate Method of Dynamic Condensation in Structural Analysis*
Int. J. of Num. Methods in Eng., Vol. 12, pp 17051715, 1987

23 **Paz M.**
*Dynamic Condensation Method*
AIAA Journal, Vol. 22, No. 5, pp 724-727, 1984

24 **Urgueira, A. P. V., Lieven, N. A. J. and Ewins, D. J.**
*A Generalised Reduction Methodfor Spatial Models*
Proc. of the 8th Int. Modal Analysis Conf., pp 22-27, 1990

25 **Kidder, R. L.**
*Reduction of Structural Frequency Equations*
AIAA Journal, Vol. 11, No. 6, pp 892, 1973

26 **O'Callahan, J. C., Avitabile, P. A. and Riemer, R.**
*System Equivalent Reduction Expansion Process (SEREP)*
Proc. of the *7th* Int. Modal Analysis Conf., pp 29-37, 1989

27 **Freed, A. M. and Flanigan, C. C.**
*A Comparison of Test-Analysis Model Reduction Methods*
Proc. of the 8th Int. Modal Analysis Conf., pp 1344-1351, 1990

28 **O'Callahan, J. C.**
*Comparison of Reduced Model Concepts*
Proc. of the 8th Int. Modal Analysis Conf., pp 442-430, 1990

29 **O'Callahan, J. C., Lieu, I. W., Avitabile, P. and Madden, R.**
***An Efficient Method of Determining Rotational Degrees of Freedom from Analytical and Experimental Modal Data***
Proc. of the 4th lnt. Modal Analysis Conf., pp 50-58, 1986

30 **Lipkins, J. and Vandeurzen, U.**
***The Use of Smoothing Techniques for Structural Modification Applications***
Proc. of the 12th lnt. Modal Analysis Seminar at the K.U. Leuven, Sl-3, 1987

31 **Gysin, H. P.**
***Comparison of Expansion Methods for FE Modelling Error Localisation***
Proc. of the 8th lnt. Modal Analysis Conf., pp 195-204, 1990

32 **Brown, T.A.**
***A Unified Approach to the Identification of Dynamic Behaviour Using the Theory of Vector Spaces***
PhD Thesis, Univ. of Bristol, 1985

33 **Williams, E. J. and Green, J. S.**
***A Spatial Curve Fitting Techniques for Estimating Rotational Degrees of Freedom***
Proc. of the 8th lnt. Modal Analysis Conf., pp 376- 381, 1990

34 **Lieven, N. A. J. and Ewins, D. J.**
***Expansion of Modal Data for Correlation***
Proc. of the 8th lnt. Modal Analysis Conf., pp 605-609, 1990

35 **Ojalvo, I. U.**
***Contrasts in Two Classes of Structural Dynamic Correlation Procedures***
Proc. of the 4th lnt. Modal Analysis Conf., pp 81-87, 1986

36 **Heylen, W.**
***Optimisation of Model Matrices by Means of Experimentally Obtained Dynamic Data***
Proc. of the 8th lnt. Modal Analysis Conf., pp 32-38, 1990

37 **Ibrahim, S.R. and Saafan, A.A.**
***Correlation of Analysis and Test in Modelling of Structures Assessment and Review***
Proc. of the 5th lnt. Modal Analysis Conf., pp 1651-1660, 1987

38 **Caesar, B.**
***Updating System Matrices Using Modal Test Data***
Proc. of the 5th lnt. Modal Analysis Conf., pp 453-459, 1987

39 **Heylen, W. and Sas, P.**
***Review of Model Optimisation Techniques***
Proc. of the 5th lnt. Modal Analysis Conf., pp 1177-l 182, 1987

40 **Baruch, M.**
***Optimisation Procedure to Correct Stiffness and Flexibility Matrices Using Vibration Tests***
AIAA Journal, Vol. 16, No. 11, pp 1208-1210, 1978

41 **Berman, A. and Nagy, E. J.**
***Improvement of a Large Analytical Model Using Test Data***
AIAA Journal, Vol. 21, No. 8, pp 1168-l 173, 1983

42 **Caesar, B.**
***Update and Identification of Dynamic Mathematical Models***
Proc. of the 1st lnt. Modal Analysis Conf., pp 394-401, 1983

*43* **Wei., F. S.**
***Structural Dynamic Model Modification Using Vibration Test Data***
Proc. of the 7th Int. Modal Analysis Conf., pp 562-567, 1989

*44* **O'Callahan, J. C. and Chou, C. M.**
***Localisation of Model Errors in Optimised Mass and Stiffness Matrices Using Modal Test Data***
Proc. of the *6th* Int. Modal Analysis Conf., pp 49-55, 1988

*45* **To, W. M., Lin, R. M. and Ewins, D. J.**
***A Criterion for the Localisation of Structural Modification Sites Using Modal Data***
Proc. of the 8th Int. Modal Analysis Conf., pp 961-967, 1990

*46* **Smith, S. W. and Beattie, C. A.**
***Secant Method Matrix Adjustments for Structural Models***
*AIAA* ASME ASCE AI-IS Proc. 30th Structures, Structural Dynamics and Materials Conf., 1989

*47* **Smith, S. W. and Beattie, C. A.**
***Optimal Identification Using Inconsistent Modal Data***
*AIAA* ASME ASCE AHS Proc. 32th Structures, Structural Dynamics and Materials Conf., 1991

*48* **Smith, S. W. and McGowan, P.E.**
***Locating Damaged Members in a Truss Structure using Modal Data: a Demonstration Experiment***
NASA Technical Memorandum 101595, 1989

*49* **Chen, J. C., Kuo, C. P. and Garba, J. A.**
***Direct Structural Parameter Identification by Modal Test Results***
AIAA/ASME/ASCE/AMS Proc. of the 24th Struct. Dyn. and Mat. Conf., pp 44-49, 1983

*50* **Sidhu, J. and Ewins, D. J.**
***Correlation of Finite Element and Modal Test Studies of a Practical Structure***
Proc. of the 2nd Int. Modal Analysis Conf., pp 756-762, 1984

51 **He, J. and Ewins, D. J.**
***Location of Damping Elements in a Vibration Structure***
Proc. of the 1 lth Int. Sem. on Modal Analysis, A-2, K.U.Leuven, 1986

*52* **Ewins, D. J., He. J. and Lieven, N. A. J.**
***A Review of the error Matrix Method (EMM) for Structural Dynamic Model Comparison***
Proc. ESA, the Netherlands, 1988

*53* **Gysin, H. P.**
***Critical Application of the Error Matrix Method for Localisation of Finite Element Modelling Inaccuracies***
Proc. of the 4th Int. Modal Analysis Conf., pp 1339-1351, 1986

*54* **Lawrence, C.**
***Identification of Differences between Finite Element Analysis and Experimental Vibration Data***
Proc. of the 5th Int. Modal Analysis Conf., pp 1681-1691, 1987

*55* **Park, Y.S., Park, H.S. and Lee, S.S.**
***Weighted-Error-Matrix Application to Detect Stiffness Damage by Dynamic Characteristic Measurement***
Int. Journal of Anal. and Exp. Modal Analysis, Vol. 3, No. 3, 1988

*56* **Lieven-Lieven, N. A. J.**
***Validation of Structural Dynamic Models***
PhD thesis, Imperial College, London, 1990

57 **Lieven, N. A. J. and Ewins, D. J.**
***Error Location and Updating of Finite Element Model Using Singular Value Decomposition***
Proc. of the ***8th*** Int. Modal Analysis Conf., pp 769-773, 1990

58 **Maia, N. M. M.**
***An Introduction to the Singular Value Decomposition Technique (SVD)***
Proc. of the 7th Int. Modal Analysis Conf., pp 335-339, 1989

59 **Gaukroger, D. R.**
***A Note on Using Measured Vibration Modes to Modify an Analytical Model of a Structure***
Technical Memo MAI/SIR 1018, 1984

60 **Brown, T. A.**
***A Matrix Cursor for Dynamic Model Improvement Using Experimental Modes of Vibration***
GEC Journal of Research, Vol. 6, No. 3, pp139-146, 1988

61 **Link, M.**
***Identification of Physical System Matrices Using Incomplete Vibration Test Data***
Proc. of the ***4th*** Int. Modal Analysis Conf., pp 386-393, 1986

62 Caesar, **B.**
***Updating System Matrices Using Modal Test Data***
Proc. of the 5th Int. Modal Analysis Conf., pp 453-459, 1987

63 **Berger, H., Chaquin, J. P. and Ohayon, R.**
***Finite Element Modal Adjustment Using Experimental Modal Data***
Proc. of the 2th Int. Modal Analysis Conf., pp l-5, 1984

64 **Berger, H., Ohayon, R., Barthe, L. and Chaquin, J. P.**
***Parametric Updating of FE Model Using Experimental Simulation: A Dynamic Reaction Approach***
Proc. of the 8th Int. Modal Analysis Conf., pp 180-186, 1990

65 **Link, M.**
***Comparison of Procedures for Localising and Correcting Errors in Computational Models Using Test Data***
Proc. of the 9th Int. Modal Analysis Conf., pp479-485, 1991

66 **Link, M., and Zhang , L**
***Experience with Different Procedures for Updating Structural Parameters of Analytical Models Using Test Data***
Proc. of the 10th Int. Modal Analysis Conf., pp 730-738, 1992

67 **Fisette, E., Stavrinidis, C., Ibrahim, S.**
***Error Location and Updating of Analytical Dynamic Models Using a Force Balance Method***
Proc. of the 6th Int. Modal Analysis Conf., pp 1063-1070, 1988

68 **Ibrahim, S. R., Stravinidis, C., Fisette, E. and Brunner, 0.**
***A Direct Two Response Approach for Updating Analytical Dynamic Models of Structures With Emphasis on Uniqueness***
Proc. of the ***7th*** Int. Modal Analysis Conf., pp 340-346, 1989

69 Sayettat, **A.**
***Model Updating Using Sensitivity and Normal Mode Techniques***
MSc thesis, Imperial College, London,1990

70 **Berman, A. and Flanelly, W. G.**
***Theory of Incomplete Models of Dynamic Structures***
AIAA Journal, Vol. 9, No. 8, pp 1481, 1971

71 **Niedbal, N., Klusowski, E. and Luber, W.**
***Updating a Finite Element Model by Means of Normal Mode Parameters***
Proc. of the 13th Int. Sem. on Modal Anal., K.U.Leuven, I-15, 1988

72 **Nobari, A. S. , Robb, D. A. and Ewins, D. J.**
***A New Modal-Based Methodfor Structural Dynamic Model Updating and Joint Identification***
Proc. of the 10th Int. Modal Analysis Conf.,1992

73 **Creamer, N. G. and Junkins J. C.**
***Identification Methodfor Lightly Damped Structures***
AIAA Journal of Guidance, Vol. 11, No. 6, pp 571-576, 1988

74 **Collins, J. D., Hart, G. C., Hasselman, T. K. and Kennedy, B.**
***Statistical Identification of Structures***
AIAA Journal, Vol. 12, No. 2, pp 185-190, 1974

75 **Cben, J.C. and Wada, B.K.**
***Criteria for Analysis - Test Correlation of Structural Dynamic Systems***
Journal of Applied Mechanics,pp471-477, 1975

76 **Kim, K. O., Anderson, W. J. and Sandstrom, R. E.**
***Non-linear Inverse Perturbation Method in Dynamic Analysis***
AIAA Journal, Vol. 21, No. 9, PP 1310-1316, 1983

77 **Lallement, G. and Piranda, J. P.**
***Localisation Methods for Parametric Updating of FE Models***
Proc. of the 8th Int. Modal Analysis Conf., pp 579-585, 1990

78 **Jung, H.**
***Structural Dynamic Model Updating Using Eigensensitivity Analysis***
PhD thesis, Imperial College, London, 1992

79 **Zhang, Q., Lallement, G., Fillod, R. and Piranda, J. P.**
***A Complete Procedure for the Adjustment of a Mathematical Model from the Identified Complex Modes***
Proc. of the *5th* Int. Modal Analysis Conf., pp 1183-l 190, 1987

80 **Janter, T., Heylen, W. and Sas, P.**
***QA- Model Updating***
Proc. of the 12th Int. Sem. on Modal Analysis, K.U.Leuven, 1987

81 **Wei, J. J. C., Zhang, Q., Allemang, R. J. and Wei, M. L.**
***Correction of Finite Element Model Via Selected Physical Parameters***
Proc. of the 13th Int. Sem. on Modal Analysis, K.U.Leuven, C-12, 1988

82 **Lallement, G. and Zhang, Q.**
***Inverse Sensitivity Based on the Eigensolutions: Analysis of Some Difficulties Encountered in the Problem of Parametric Correction of Finite Element Models***
Proc. of the 13th Int. Sem. on Modal Analysis, K.U.Leuven, I-16, 1988

83 **Janter, T. and Heylen, W. and Sas, P.**
***A Comparison Between Model Optimisation Procedures Based on the Model Optimisation Parameter Set***
Proc. of the 6th Int. Modal Analysis Conf., pp 87-92, 1988

84 **Heylen, W. and Janter, T.**
***Applications of the Modal Assurance Criterion in Dynamic Model Updating***
Proc. of the 13th Int. Sem. on Modal Analysis, K.U.Leuven, I-18, 1988

85 **Filiod, R., Lallement, G., Piranda, J. P. and Zbang, Q.**
***Parametric Correction of Regular Non-Dissipative Finite Element Models***
Proc. of the 11th Int. Sem. on Modal Analysis, K.U.Leuven, 1986

86 **Wei, M. L. and Janter, T.**
***Optimisation of Mathematical Model via Selected Physical Parameters***
Proc. of the 6th Int. Modal Analysis Conf., pp 73-79, 1988

87 **Janter, T., Heylen, W. and Sas, P.**
***QA-model Updating***
Proc. of the 13th Int. Sem. on Modal Analysis, K.U.Leuven, C-13, 1988

88 **Janter, T., Heylen, W. and Sas, P.**
***Practical Applications of the UA Model Updating Scheme***
Proc. of the 8th Int. Modal Analysis Conf., pp 173-179, 1990

89 **Dascotte, E. and Vanhonacker, P.**
***Development of an Automatic Model Updating Program***
Proc. of the 7th Int. Modal Analysis Conf., pp 596-602, 1989

90 **Dascotte, E.**
***Practical Applications of Finite Element Tuning Using Experimental Modal Data***
Proc. of the 8th Int. Modal Analysis Conf., pp 1032-1037, 1990

91 **Slater, J.C., Johnson, A.R., Fatemi, B. and Wiederrich, J.L.**
***Model Refinement Through a Statistical Analysis of a Mode Shape Difference Vector***
Proc. of the 6th Int. Modal Analysis Conf., pp 93-99, 1988

92 **Roy, N. A. and Girard, A.**
***Updating Dynamic Finite Element Models: A Direct Energy Approach***
Proc.StruCoMe, pp 214-229, 1990

93 **Roy, N. A., Girard, A. and Dupuis, P. E.**
***A Direct Energy Approach for Updating Dynamic Finite Element Models***
Proc. of the 9th Int. Modal Analysis Conf., pp 51-57, 1991

94 **Ladeveze, P. and Reynier, M.**
***A Localisation Method of Stiffness Errors for the Adjustment of FE Models***
Special Tech. Corn. Handbook, 12 ASME Mech. Vib. and Noise Conf., Montreal, 1989

95 **Inman, D. J. and Minas, C.**
***Matching Analytical Models with Experimental Modal Data in Mechanical Systems***
Control and Dynamic Systems, Vol. 37, pp 327-363, 1990

96 **Minas, C. and Inman, D. J .**
***Matching Finite Element Models to Modal Data***
ASME J. of Vibration and Acoustics, Vol. 112 No. 1, pp84-92, 1990

97 **Starek, L. and Inman, D. J.**
***Solution to the Model Correction Problem via Inverse Methods***
Proc. of the 9th Int. Modal Analysis Conf., pp 352-355, 1991

98 **Zimmerman, D. C., and Widengren, M.**
***Correcting Finite Element Models Using a Symmetric Eigenstructure Assignment Technique.***
AIAA Journal, Vol. 28 No 9, pp 16700-1676, 1990

99 **Lin, R. M. and Ewins, D. J.**
***Modal Updating Using FRF Data***
Proc. of the 15th Int. Sem. on Modal Analysis, K.U.Leuven, 1990

**100 Natke, H. G.**
***Updating Computational Models in the Frequency Domain Based on Measured Data: a Survey***
Probabilistic Engineering Mechanics, vol. 4 No.1, pp 28-35, 1988

**10 1 Mottershead, J. E.**
***Theory for the Estimation of Structural Vibration Parameters from Incomplete Data***
AIAA Journal, Vol. 28, No. 3, pp 559-561, 1990

**102 Foster, C. D. and Mottersbead, J. E.**
***A Method for Improving Finite Element Models by Using Experimental Data: Application and Implications for Vibration Monitoring***
Int. Journal of Mech. Sci., Vol. 32, No. 3, pp 191-203, 1990

**103 Frisweii, M. I. and Penny, J. E. T.**
***Updating Model Parameters from Frequency Domain Data via Reduced Order Models***
Mechanical Systems and Signal Processing, Vol. 4No.5, pp 377-391, 1990

**104 Frisweil, M. I.**
***Candidate Reduced Order Models for Structural Parameter Estimation***
ASME Journal of Vibration and Acoustics, Vol. 112, 1990

**105 Larsson, P.-O. and Sas, P.**
***Model Updating Based on Forced Vibrations***
Proc 4th Int. Conf. on Rec. Adv. in Struct. Dyn., pp 95-108, 1991

**106 Conti, P. and Donley, M.**
***Testlanalysis Correlation Using Frequency Response Functions***
Proc. of the 10th Int. Modal Analysis Conf., pp 724-729, 1992

**107 Ibrahim, S. R., D'Ambrogio, W., Saivini, P. and Sestieri, A.**
***Direct Updating of Non-Conservative Finite Element Models Using Measured Input-Output***
Proc. of the 10th Int. Modal Analysis Conf., pp 202-210, 1992

**108 Berman, A.**
***Non-Unique Structural System Identification***
Proc. of the 7th Int. Modal Analysis Conf., pp 355-359, 1989

**109 Janter, T. and Sas, P.**
***Uniqueness Aspects of Model-Updating Procedure***
AIAA Journal, Vol. 28, No. 3, pp 538-543, 1990

**110 Baruch, M. and Itzhack, T.**
***Optimal Weighted Orthogonalization of Measured Modes***
TAE Report No. 297, 1977

**111 Ibrahim, S.R.**
***Computation of Normal Modes from Identified Complex Modes***
AIAA Journal, Vol. 21, No. 3, pp 446-451, 1983

**112 Niedbal, N.**
***Analytical Determination of Real Modes from Measured Complex Responses***
Proc. of the 25th Structures, Struct. Dyn. and Mat. Conf., pp292-295, 1984

**113 Berman, A.**
***Limitations on the Identification of Discrete Structural Dynamic Models***
Proc. of the 2nd Int. Conf. on Recent Adv. in Struct. Dyn., pp 427-435, 1984

**114 Visser, W. J.**
***Expanding Measured Mode Shapes***
Internal report No 90018, Dynamics Section, Dept. of Mech. Eng., Imperial College, 1990

**115 Mottershead, J. E.**
***Finite Element Tuning Using Measured Vibration Data***
presented at Effective Validation of Numerical Results for Stress and Vibration Analysis,Institute. of Physics, 1991

**116 Burden, R. L. and Faires, J. D.**
***Numerical Analysis***
PWS_Kent Publishing **Company, 4th edition, 1989**

**117 Brandon, J. A.**
***On the Robustness of Algorithms for the Computation of the Pseudo-Inverse for Modal Analysis***
IMAC VI, Vol. I, pp 397-400, Florida, 1988

**118 To, W. M.**
***The Role of Generalised Inverse in Structural Dynamics***
Internal report No 90016, Dynamics Section, Dept. of Mech. Eng., Imperial College, 1990

**119 Press, W. H., Flannery, B. P., Teukolsky, S. A. and Vetterling, W. T.**
***Numerical Recipes: the Art of Scientific Computing***
Cambridge University Press, 1986

**120 Larsson, P.-O. and Sas, P.**
***Model Updating Based on Forced Vibrations using Numerically Stable Formulations,***
IMAC X, pp 966974, 1992